8-2013

Effective Thermal Conductivity of Carbon Nanotube-Based Cryogenic Nanofluids

Lucas Samuel Anderson
Utah State University

EFFECTIVE THERMAL CONDUCTIVITY OF CARBON NANOTUBE-BASED CRYOGENIC NANOFLUIDS

by

Lucas S. Anderson

A thesis submitted in partial fulfillment
of the requirements for the degree

of

MASTER OF SCIENCE

in

Mechanical Engineering

Approved:

_____	_____
Dr. Heng Ban Major Professor	Dr. Byard Wood Committee Member
_____	_____
Dr. Christine Hailey Committee Member	Dr. Mark R. McLellan Vice President for Research and Dean of the School of Graduate Studies

UTAH STATE UNIVERSITY
Logan, Utah

2013

ABSTRACT

Effective Thermal Conductivity of Carbon

Nanotube-Based Cryogenic Nanofluids

by

Lucas S. Anderson, Master of Science

Utah State University, 2013

Major Professor: Dr. Heng Ban
Department: Mechanical and Aerospace Engineering

Nanofluids consist of nanometer-sized particles or fibers in colloidal suspension within a host fluid. They have been studied extensively since their creation due to their often times anomalous and unique thermal transport characteristics. They have also proven to be quite valuable in terms of the scientific knowledge gained from their study and their nearly unlimited industrial and commercial applications. This research has expanded the science of nanofluids into a previously unexplored field, that of cryogenic nanofluids. Cryogenic nanofluids are similar to traditional nanofluids in that they utilize nanometer-sized inclusion particles; however, they use cryogenic fluids as their host liquids. Cryogenic nanofluids are of great interest due to the fact that they combine the extreme temperatures inherent to cryogenics with the customizable thermal transport properties of nanofluids, thus creating the potential for next generation cryogenic fluids with enhanced thermophysical properties. This research demonstrates that by combining liquid oxygen (LOX) with Multi-Walled Carbon Nanotube (MWCNT) inclusion particles, effective thermal conductivity enhancements of greater than 30% are possible with nanoparticle volume fractions

below 0.1%. Three distinct cryogenic nanofluids were created for the purposes of this research, each of which varied by inclusion particle type. The MWCNT's used in this research varied in a number of physical characteristics, the most obvious of which are length and diameter. Lengths vary from 0.5 to 90 microns and diameters from 8 to 40 nanometers. The effective thermal conductivity of the various cryogenic nanofluids created for this research were experimentally determined by a custom made Transient Hot Wire (THW) system, and compared to each other and to more traditional nanofluids as they vary by type and particle volume fraction. This work also details the extensive theoretical, experimental, and numerical aspects of this research, including a rather detailed literature review of many of the salient sciences involved in the study of cryogenic nanofluids. Finally, a selection of the leading theories, models, and predictive equations is presented along with a review of some of the potential future work in the newly budding field of cryogenic nanofluids.

(383 pages)

PUBLIC ABSTRACT

Effective Thermal Conductivity of Carbon Nanotube-Based Cryogenic Nanofluids

Lucas Anderson

Heat removal and management is a concern for any technology that deals with high power, small size, or a lack of convenient thermal transport methods. A potential solution to this heat crisis lies in the field of nanofluids, which consist of colloidal suspensions of nanometer (one billionth of a meter) sized particles within a host fluid. Nanofluids have been of particular interest since their creation due to their exciting, unique, and often times anomalous thermal transport behavior. In many cases, a nanofluid can be custom made to fit a particular need and can act as a flexible cooling method, adapting to the requirements of a specific system. In essence, they have the potential to become the world's first smart/adaptable coolants. This research investigated the thermal behavior and transport phenomena of an, until now, unexplored area of nanofluid science, that of cryogenic nanofluids. Cryogenic nanofluids are similar to traditional nanofluids; however, they utilize cryogenic liquids as their host fluids. This enables them to use the extreme temperature gradients inherent to cryogenics in conjunction with the customizable and anomalous behavior of nanofluids. This thesis focused on the creation of three distinct multi-walled carbon nanotube based cryogenic nanofluids with liquid oxygen acting as the matrix fluid. A custom-made, transient hot wire system was used to measure the effective thermal conductivity of these unique cryogenic nanofluids as they vary with particle type and volume fraction. This thesis also included the details of the experimental, theoretical, and numerical methodologies that formed the foundation of this research, along with discussions on the various aspects of nanofluid science,

thermal conductivity, and the measurement of cryogenic nanofluids. Finally, the possible future research and real world applications of cryogenic nanofluids was explored.

DEDICATION

This thesis is the culmination of over three years' worth of work, none of which would have happened without the wonderful, family, friends and colleagues that I have been blessed with.

This research would not exist without my major professor Dr. Heng Ban, whose vision and knowledge made all of this possible. Throughout the years his advice, support, and encouragement has seen me through, and made this a reality.

I have been lucky to work with some of the finest men and women at USU in the Multi-Scale Thermo-Physics Laboratory. They have injected a degree of humor, and camaraderie into the workplace, and made it a truly delightful environment. In addition, during the hard times when all seemed lost, their support and help was invaluable. They have all become good friends.

Finally, my family is the pillar on which everything has been built. Without my loving family this would have simply been an unrealized dream. I will not even try to encompass, nor describe the value of my family, and what they have given to me over the years. It would simply be impossible.

Thank you.

Lucas Samuel Anderson

ACKNOWLEDGMENTS

I would like to thank Utah State University and the Space Dynamics Laboratory for their funding, support, and belief.

Lucas Samuel Anderson

FOREWORD

It is in the nature of humanity to explore, learn, and expand our universe and through this process to hopefully gain some amount of knowledge and wisdom. It is the greatest hope of any man's work, that it will somehow help the world as a whole and aid the human condition. With that being said, I hope, as the author, that this work can and will be a starting point for future research into the properties and behavior of cryogenic nanofluids. I envy those who will come after for they will have the opportunity to explore a new science, and through it, a glimpse at a before now unseen world. Theirs will be an exciting adventure.

This thesis has been written so that a basic understanding of nanofluids, along with the newly budded field of cryogenic based nanofluids can be understood by anyone and that perhaps it can guide some future work. However, this particular field of science is truly vast and is built upon an even vaster expanse of work and knowledge. A truly all-encompassing review would simply be unreasonable. Therefore, I haven't even tried. It will be up to the reader to take what he can from this work, and to let his curiosity explore even further.

I hope that this thesis will be enjoyable to anyone who reads it, and will offer some useful insight and knowledge.

Good Luck,

Lucas Samuel Anderson

CONTENTS

Page

LIST OF TABLES

LIST OF FIGURES

ACRONYMS

ANOVA	Analysis of Variance
BC	Boundary Condition
CATS	Center for Applied Thermodynamics
CN	Cryogenic Nanofluid
CVD	Chemical Vapor Deposition
DAQ	Data Acquisition
DWCNT	Double Walled Carbon Nanotube
EM	Electro magnetic
IC	Initial Condition
MWCNT	Multi-Walled Carbon Nanotubes
NIST	National Institute of Standards and Testing
NPL	National Physics Laboratory
ODE	Ordinary differential equation
PGM	Precious Metal Database
PRT	Platinum Resistive Temperature
RTD	Resistance Temperature Diode
SEM	Scanning Electron Microscopy
SWCNT	Single Walled Carbon Nanotube
TC	Thermocouple
THD	Transient Hot Disk
THS	Transient Hot Strip
TEM	Tunneling Electron Microscopy
USU	Utah State University

USU #1	MWCNT’s provided by Dr. T. C. Shen

NOMENCLATURE

A	Area over which thermal gradients act (m^2)
A_w	Area of THW wire (m^2)
A_{HW}	Numerical THW surface area (m^2)
A_0	ODE Solution constant
B	Length constant: equal to half the wire length (m)
B_0	Integration constant
Ch0	Numerical THW voltage channel variable (A)
Ch1	Numerical THW voltage channel variable (A)
Ch2	Numerical THW voltage channel variable (A)
F	ANOVA variance value
$F_{critical}$	ANOVA critical variance value
I_w	Current (A)
I_{HW}	Numerical THW current (A)
L_w	Length of wire (m)
L_{HW}	Numerical hot wire length (m)
N	The number of individual measurements of X_i
P_{HW}	Numerical THW Power (W)
Q	Source strength per unit length of the heat source ($m^2 \cdot K$)
Q'	Source strength per unit length per unit time ($m^2 \cdot K/s$)
R_w	Resistance of wire (Ω)
R_{HW}	Numerical THW Resistance (Ω)
R-Length	Regular Length

S-Length	Short Length
T	Temperature based upon cylindrical location and time (K)
T_1	Temperature based upon cylindrical location at t_1 (K)
T_2	Temperature based upon cylindrical location at t_2 (K)
T_0	Temperature based upon cylindrical location at t=0 (K)
T.C. Shen	MWCNT's created by Dr. T.C. Shen
V_{Total}	Total CN volume (m^3)
VHC_f	Volumetric heat capacity of a given medium ($J/m^3 \cdot K$)
X	Arbitrary variable
X_i	Uncertainty ith variable
X_{exp}	Uncertainty variable of expected value
$\bar{X}$	Uncertainty variable containing an average value
a	Elliptic semiaxes
b	Elliptic semiaxes
c	Elliptic semiaxes
c_p	Heat capacity of a material (J/K)
c_{pf}	Heat capacity of fluid of interest (J/K)
k	Thermal conductivity of a material (W/m·K)
k_e	Effective thermal conductivity (W/m·K)
k_f	Thermal conductivity of a fluid (W/m·K)
k_m	Host material thermal conductivity (W/m·K)
k_p	Nanoparticle thermal conductivity (W/m·K)
k_{calc}	Calculated effective thermal conductivity

k_{lox}	Reported effective thermal conductivity of LOX (W/m·K)
n	The total numerical number of averaged data points
q	Power (W)
q_f	Heat flux density of fluid (W)
q_w	Power of wire (W)
q'_w	Power per unit length of wire (W/m)
q'	Heat liberated per unit length (J/m·s)
$\dot{q}$	Body heat generation term (W/m^3)
r	Radial position variable (m)
r_w	Radius of wire (m)
r'	Arbitrary radial location (m)
s_x	Uncertainty based standard deviation of experimental data
t	Time variable (s)
t_1	Time point one (s)
t_2	Time point two (s)
t_{95}	Student-T coefficient
u	Arbitrary variable
v_p	Particle volume concentration
x	Error function argument
x	Elliptic geometry parameter
y	Elliptic geometry parameter
z	Elliptic geometry parameter
z	Vertical location variable (m)
z'	Arbitrary axial location (m)

ΔT	Temperature gradient based upon cylindrical location and time (K)
ΔT_1	Temperature gradient based upon cylindrical location at t_1 (K)
ΔT_2	Temperature gradient based upon cylindrical location at t_2 (K)
Δr	Radial difference between cylindrical position of interest and the wire radius (m)
ΔV_{HW}	Numerical voltage drop across THW (V)
ϕ	Azimuthal location variable (m)
Φ	First order dimensionless variable
α	Thermal diffusivity of a material (m^2/s)
α_f	Thermal diffusivity of fluid of interest (m^2/s)
γ	Euler' constant
η	Dimensionless similarity variable
μ	Experimental confidence interval
μ_{total}	Total experimental confidence interval
ρ	Density of a material (kg/m^3)
ρ_f	Density of fluid of interest (kg/m^3)
ρ_{ew}	Electrical resistivity ($\Omega \cdot m$)
ρ_{HW}	Numerical hot wire resistivity ($\Omega \cdot m$)

CHAPTER 1

INTRODUCTION

1.1. Cooling Challenge

Our modern world is based upon science, and the technology born from it.

As our world grows and evolves, it is becoming ever more complex, and as this occurs, the boundaries of our knowledge are defined not only by our imagination but by the physical limitations of our current technology. These boundaries come in many forms, span each discipline, and define the outer limits of what is currently possible. One of these limitations is that of the power challenge. Our technology is changing at an exponential rate, and our power requirements are growing to match. Whether it be from high power loads, temperatures, or fluxes, the ability to efficiently remove heat is proving to be one of our primary obstacles. Traditional methods of thermal management rely upon the various types of heat transport which include conduction, convection, and radiation. However, with today's substantial cooling requirements, many of the traditional methods are proving to be insufficient or simply too troublesome to implement. Liquid cooling is a prime example of this. Liquids have long been used for cooling purposes; however their inherently low thermal conductivity, along with other undesirable characteristics has resulted in a literal roof in terms of their usefulness for high performance cooling applications. For many years, scientists have sought to remedy this problem by adding millimeter to micrometer sized solid particles. This has proven to be effective in a limited sense. However, relatively small increases in thermal transport properties, highly unstable suspension characteristics, large pumping requirements, and abrasive nature limit millimeter to micrometer fluids usefulness as coolants. Therefore, a new approach needed to be devised to enhance the physical and thermal properties of fluids to allow them to handle the ever increasing cooling needs of our modern world. The answer would lie in the nanoworld [1, 2, 3, 4].

1.2. Nanoworld Background

On December 29th, 1959, the acclaimed physicist Richard Feynman presented a talk titled "*There's Plenty of Room at the Bottom,"* to assembled scientists and engineers of the American Physical Society at Caltech. The lecture proclaimed an invitation for the entire world to enter into and enjoy a new era of discovery, and understanding [5]. This world that Dr. Feynman spoke of was that of the very small. The microscopic world exists all around us and has done so for time interminable. However, our ability to perceive, much less explore and utilize this world is relatively new.

Interest and research into the microscopic has seen a tremendous amount of growth over the past few decades and is continuing in full force today. This is entirely due to the fact that a great deal of potential exists for both scientific advancement and applications in the nanoworld. Indeed, the ability to interact and manage at the nanolevel would allow for unparalleled control over almost every aspect of our world. The ability to understand and manipulate on the nanoscale is without a doubt one of mankind's next great evolutionary steps. Numerous aspects of the behavior and nature of the nanoworld have been studied, and many new forms of science and engineering have been born from this curiosity. This research focuses on another facet of this ongoing work, that of nanofluids.

1.3. Nanofluids Background

Nanofluids, coined in 1995 by Dr. Choi, are multi-phase systems with a base matrix host fluid, and a stable colloidal suspension of nanometer sized nanoparticles [1]. They can be produced in a one step process by creating the host fluid and nanoparticles together, or created separately and mixed in a two-step process. Traditional nanofluids consist of any type of fluid or fluid mixture and can have one or more of a wide variety of nanoparticles, dispersants, etc. acting as the inclusion phase. The variety of nanofluids is truly staggering, and indeed, a new nanofluid

can be created by simply mixing different base fluids or nanoparticle together. Even slight changes in the creation methodology of nanofluids can lead to significant changes in the end result.

Nanoparticles are solid particles of any material with sizes less than 100 nm that act as a whole unit in terms of their physical and thermal transport properties. Nanoparticles are of particular interest because materials below the critical length scale of 100 nm exhibit physical characteristics that differ from their bulk counterparts. Fundamentally, this is caused by the high proportion of constituent atoms residing at grain boundaries and the physics of the nanoworld taking over from that of the macro-world [1]. Nanoparticles can be created by either chemical or physical processes, and are unique in that due to their small size, they have surface to volume ratios on the order of 1000. This greatly enhances their surface thermal conductivity, and their small size allows them to be suspended with a great deal of stability. They also exhibit reduced physical erosion and required pumping power. These features along with their sub-micro size make them ideal for use with nanofluids.

Nanofluids are of great scientific curiosity and value due to their remarkable and often anomalous physical and thermal transport properties, which make them highly desirable from an industrial and commercial standpoint. Nanofluids are considered to have anomalous properties, because many of their properties, and subsequent behavior, cannot be anticipated or modeled with current theories. This could be due to some unique aspect of nanofluids, or to a lack of fundamental understanding in terms of the current models and theories. The ability to custom make fluids with specific characteristics in mind is truly staggering, and almost unlimited in terms of applications. The studied thermal transport properties of nanofluids include metallic based nanofluids with unusually high effective thermal conductivities, nonlinear relationships between particle volume fractions and effective thermal conductivity, strongly temperature and

size dependent thermal conductivity, enhanced laminar and turbulent convective heat transfer coefficients, a decrease in the natural convection heat transfer coefficient, and increases in the boiling heat transfer coefficient. Ultimately, the study of nanofluids fabrication, mixing, stabilization, behavior, properties, and uses has been extensive and are truly just a few of the many topics currently under consideration. However, due to the sheer size and complexity of nanofluids as a science, all of the work done to date is simply a first step into the much larger work that remains to be explored.

Nanofluids exhibit an ability to modify their properties based upon the situation or given need. For example, research has indicated that their ability to transfer heat through conduction increases with temperature, thus allowing them to act as a variable heat conductor for cooling applications. This, combined with their other favorable thermal transport properties, could allow nanofluids to become next generation customizable smart coolants. Because of their size, they also have great potential as fluids for micro-channel flow. In addition, the knowledge gained from their study could lead to a better understanding of the physical and thermal interactions of small scale, multi-phase dynamic systems, and could potentially lead to future work and the creation of new theories and models as well as offering a glimpse into how the physics of the very small and the very large come together to govern the natural world that surrounds us [1, 6, 7, 8].

1.4. Cryogenic Nanofluids Research Objectives

This research will introduce a new area of study to the field of nanofluid science, that of cryogenic nanofluids. In addition, it will expand the already vast field of nanofluids in another important and logical direction that of enhancing the thermo transport properties of cryogenics, via nanoparticles, in the hope of creating improved next generation cryogenic coolants. By combining the extreme temperature gradients found within cryogenics with the enhanced thermal

transport properties of nanofluids, a truly impressive and important new type of coolant has been created.

This research studied how the effective thermal conductivity of a variety of custom made cryogenic nanofluids vary with both inclusion particle type and particle volume fraction. Liquid oxygen (LOX) was used as the host fluid, and was combined with three distinct Multi-Walled Carbon Nanotubes (MWCNT's). This thesis details the extensive theoretical, experimental, and numerical methodologies involved in the measurement of a cryogenic nanofluid, the creation process of the world's first cryogenic nanofluids, along with the specific results of the effective thermal conductivity enhancement of each MWCNT based cryogenic nanofluid as they varied with particle volume fraction and type. In addition, a review of some of the constituent literature involved in this research is presented along with the authors opinions on what future research might look like in the newly created field of cryogenic nanofluids.

Specifically, the objectives of this research are:

- To obtain a working understanding of the current research and theories of nanofluid science, along with any additional knowledge required for their study.
- To construct a theoretical predictive structure for the experimental behavior of LOX, and LOX based CN's.
- To design, create and validate an effective thermal conductivity testing system that would be appropriate for a cryogenic nanofluid.
- To design and create a series of numerical modeling programs capable of the data analysis and post processing inherent in the study of CN's.
- To create well dispersed MWCNT based cryogenic nanofluids with LOX acting as the host fluid.
- To determine the effective thermal conductivity of several unique MWCNT based CN's as they vary with inclusion particle type, characteristics morphology, and volume fraction.

The secondary research objectives are:

- To make comparisons between the current results, and more traditional nanofluid data theories, models, and equations.

- To explore the physics or phenomena that might cause these measured effective thermal conductivity values.

Each of the objectives listed above, was achieved by a comprehensive theoretical, computational, and experimental research program. The following chapters will detail, in short, how each of the above research goals were accomplished.

CHAPTER 2

LITERATURE REVIEW

2.1. Introduction

Before any project can be undertaken a thorough and well-studied review of the current state of the science must be completed. This review by necessity includes any and all pertinent sciences upon which the current work is based. For this particular research, the following literature review will briefly explore the following fields.

- Thermal Conductivity Measurement Techniques
- Selected MWCNT Properties
- Nanofluid Science
- Cryogenic Science
- Cryogenic Nanofluids

2.2. Thermal Conductivity Measurement Techniques

2.2.1. Thermal Conductivity Background

Thermal conductivity is the ability of a material to transport energy in the form of heat (energetic vibrations). For the case of solids, it is the direct energy exchange through atomic level lattice vibrations and free electron diffusion, whereas for fluids/gases it takes the form of direct molecular contact and molecular diffusion. It is a fundamental and natural property of any physical material, and is defined as energetic power per unit temperature and per unit length over which the thermal conductivity is acting. Ultimately, a material's thermal conductivity is based upon the physical structure of the material, and its current state.

Thermal conductivity is one of the more important thermal transport characteristics of a material, and plays an important role in many design problems. Therefore, a great deal of effort

has gone into characterizing, and measuring thermal conductivity over the last few centuries. This literature review briefly discusses some of the more common methods of measuring a material's thermal conductivity. In addition, a brief history of the understanding of thermal conductivity, and how this lead to its eventual measurement and classification is included. Finally, the reasoning behind choosing the transient hot wire (THW) thermal conductivity measurement method for this research is discussed, along with some examples of how THW's are used in the measurement and classification of the thermal transport properties of nanofluids.

2.2.2. The History of Thermal Conductivity Measurement

The concept of thermal conductivity did not come about at a specific time, nor did it simple erupt from the conscious minds of scientists of a certain era. Instead, it was the gradual accumulation of knowledge, ideas, and discoveries ranging over more than three hundred years. The concept of how heat moves between and inside materials had long been speculated at, however, without the proper instrumentation, or knowledge of key concepts, anything but a crude understanding of how bodies transport heat was impossible. The first step in the evolutionary process of thermal conductivity was the development of the first rudimentary thermometer by Galileo in 1597. With an ability to measure the relative changes in temperature, the problem of quantifying heat flow, and the relative changes in a body's temperature could finally be tackled.

The use of thermometers in science was a slow and disjointed process. Hooke in 1664-84, among others, established rough estimates of the boiling and freezing points of water. The first true attempt at understanding the flow of heat was done by Mariotte in his examination of radiation in 1683. Newton worked on the concept of improving the thermometric scale in his piece "Scala Graduum Caloris et Frigoris" in 1701. Shortly after, Fahrenheit performed his work on the temperature scale, and established the method of temperature classification used today.

From this point on, numerous scientists and scholars published works on the relative temperatures of bodies, and the heating, cooling, and radiation of materials.

During this period the concept of convection was first detailed, along with the correlation of electrical energy and the heat energy derived from it. In fact, quite a bit of attention was devoted to the correlations and similarities between these two phenomena. The concept of electricity which was cemented in 1720 by Stephen Gray, and was later explored in detail by Benjamin Franklin, who would introduce some of the first experimental methods for measuring both electricity and thermal conductivity. The concept of thermal conductors was well encapsulated by professor Simson, and lead to the first experimental measurements of thermal conductivity by Franklin, which would later be greatly expanded upon by Dr. Ingenhousz in 1780. During this same period Black proposed his theories on the thermal transport properties of materials. He established the difference between heat and temperature, thermal equilibrium, the latent and specific heats of bodies, developed his method of mixtures, and invented the calorimeter.

At this point in history, the scientific world was finally able to measure the thermal conductivity of physical materials. Great strides were made by Rumford, and La Place, among others. The concept of convection was finally beginning to be fully understood, and could join conduction and radiation as the primary modes of heat transfer. Eventually, after nearly three hundred years, the mathematical foundation of thermal conductivity was laid down by Fourier in his “Magnum Opus”. In this work, he presented the exact scientific definition of thermal conductivity along with the differential equations and integrals used. Based upon this work thermal conductivity could be reliably computed from experimental data, namely the power transferred and temperature gradient. Finally, the ground was set for modern scientists armed with a complete understanding of thermal conductivity to create the numerous and widely varied methods of determining thermal conductivity used today [9].

2.2.3. Experimental Measurement of Thermal Conductivity

Experimental measurement methods for the determination of thermal conductivities are highly varied, but are generally broken into two broad categories. The first is that of steady state experimental methods, where any phenomena that vary with time are allowed to reach a state of thermal equilibrium. The second is that of transient experimental methods. In the case of transient analysis, the change of a material's properties with time are taken into account mathematically. In general, steady state methods are simple and more direct. However, they can tend to lack accuracy, and require extensive and highly complex experimental setups and procedures. Transient methods, on the other hand, are more accurate and far simpler in their implementation. Some of the factors that contribute to what type of testing methodology should and can be used are those of the materials:

- Sample geometry
  - Size
  - Shape
  - Fabrication specifics
  - Etc.

- Sample properties
  - Expected sample phase
  - Sample structure
  - Sample homogeneity
  - Expected sample thermal conductivity
  - Expected sample electrical conductivity
  - Expected sample density
  - Expected sample specific heat
  - Etc.

- Experimental
  - Experimental temperature range
  - Experimental temperature gradient
  - Desired accuracy.
  - Total testing time

- Etc.

This review will also create a distinction between standard methods, and custom methods. For the purposes of this discussion, standard methods will be those presented by the American Society of Standards and Testing (ASTM), while custom methods will refer to any experimental technique that is either not specifically condoned by ASTM or is a modified departure from the ASTM standards. The following discussions will focus on only a few of the more common methods used in the analysis and experimental determination of thermal conductivity. Indeed, an in depth review of all the available thermal conductivity testing techniques would require far more time and space than is presently provided for.

It should also be noted that some of these thermal conductivity measurement techniques are specified for use with either solids, fluids, or other material and phase types. This review simply focuses on some of the more common thermal conductivity measurement methods and techniques regardless of their specifics. However, those specifics play a paramount role when deciding which method best fits a given testing situation. In addition, many methods can be modified such that their general usefulness is expanded beyond their original specifications. It should finally be noted, that a great deal of the key concepts, knowledge and working theories for thermal conductivity and its measurement were taken from the works of the Compendium of Thermophysical Property Measurement Methods [10, 11].

2.2.4. Transient Thermal Conductivity Methods

The following standards are just a few of the numerous methods available for the determination of thermal conductivity. Some utilize a direct measurement of the thermal conductivity, while others calculate related values such as specific heat capacity or thermal diffusivity and use these along with some required previous knowledge to calculate the thermal

conductivity. For this research, the following techniques were used as beginning models for the design and validation of a cryogenic fluid specific system.

2.2.4.1. Standard Transient Thermal Conductivity Measurement

For the purposes of this research, standard testing methods for thermal conductivity will refer to those defined by ASTM.

2.2.4.1.1. *Line Heat Source Methods*

The Transient Hot Wire (THW) method is based upon using a long, thin platinum wire as a dual line heat source and temperature sensor. This is possible due to the relatively unique relationship between the temperature and thermal characteristics of platinum. The platinum filament is fully submerged within the fluid for which the thermal conductivity is to be determined, and a step increase in the electrical power supplied to the wire is introduced. This allows the platinum wire to heat up due to resistive heating. The excess heat from the hot filament is rejected to the surrounding fluid through conduction. Simultaneously, while this heating is occurring, the relative change in resistivity of the wire is being measured through a two or four wire resistive measurement system. The surface temperature of the hot wire and therefore the temperature of the immediate surrounding fluid can be calculated based upon this approach. The measured value of total input power, and power lost to the surrounding fluid, combined with the overall change in resistivity of the platinum wire due to electrical heating are collected; these values, in conjunction with the measured experimental time and dimensional parameters of the hot wire setup, can be used to back calculate the thermal conductivity of the fluid of interest [1, 12-24].

Several distinct ASTM transient line heat source standards exist. Their exact uses vary from the measurement of materials such as ceramics, fluids, porous media, polymers, and plastics, thus

making them truly versatile and applicable thermal conductivity measurement techniques. The following are a selection of the THW ASTM standards used in this research.

ASTM standard D2717-95 is a transient absolute method for directly determining the thermal conductivity of a wide variety of liquids by the hot wire technique. Thermal conductivity measurements can be made for chemically compatible liquids with thermal conductivity values up to, but excluding liquid metals. Fluid vapor pressures must be kept below 50 psia. The testing temperature of the fluids can vary over a wide range, and are only restricted by the experimental setup, materials, and the fluid itself. For this particular THW standard, the long thin platinum filament is connected to a series of platinum springs (to maintain a constant tension, and therefore a known length) and platinum connector studs. The hot wire assembly and the fluid of interest are sealed in a two-arm, borosilicate glass container which is in turn submerged within a temperature conditioning bath. The exact specifics of the setup, materials, and electronic power and measurement equipment used can be reviewed in detail within the literature [25].

An additional, ASTM hot wire standard that was used for this research is that of ASTM-C-1113. This standard refers specifically to the use of the transient hot wire for the determination of thermal conductivity for isotropic homogeneous dielectric refractory bricks. The test specifies an operating ambient temperature of up to 1500 °C, and low (less than 15 W/mK) thermal conductivity values. This version of the transient hot wire technique operates on the same principle of utilizing a long, thin platinum wire as dual temperature source and sensor. However, this particular standard utilizes a modification to the sample material, in the form of long, thin right angle cutouts, in which the hot wire lies between. Once again, the thermal conductivity is calculated by measuring the change in resistance over the length of the powered hot wire and the inputted power to the wire [26].

2.2.4.1.2 Thermal Probe

ASTM D-5334-08 Standard Test Method for Determination of Thermal Conductivity of Soil and Soft Rock by Thermal Needle Probe Procedure [27].

This test method refers to the use of the standard thermal probe method for the determination of the thermal conductivity of both undisturbed and remolded isotropic soil and soft rock samples. The test method applies for a wide ambient temperature range 0 °C - 100 °C. The method can also be used for samples containing moisture, although for that particular case, care should be taken such that large thermal gradients do not occur within the sample, and that a significant phase change does not occur for the inhibiting fluid. The thermal probe method is based upon a variation of the transient line heat source technique in that the thermal probe utilizes a very long and relatively thin heating element. A resistive element within the probe is energized and generates a thermal flux which is transferred through the thin wall of the probe body into the material of interest. The change in temperature is measured by a separate temperature sensor within the probe body. The heat flux into the surrounding medium along with the relative change in temperature and the input power is used to calculate the thermal conductivity of the material of interest.

The probe itself is composed of a thin-walled, stainless steel tube containing a wire resistive element and a separate temperature sensor. The resistive materials used for thermal probes vary, but in general are thermally stable and highly resistive metallic materials. The wire resistive element is doubled over and inserted into the stainless steel probe body, and sealed in place with a reservoir of thermal epoxy primer. A single or series of temperature sensors are placed inside the probe body, along with the wire resistive heating element. These temperature sensors are often placed in the geometric center of the actual probe body. Generally, thermocouples are used as the primary temperature sensor for the thermal probe method simply because they are small,

accurate, and easily placed. The thermal probe method can be used for a wide variety of testing, and in fact is fairly similar to the transient hot wire in its versatility. Just like many other test methods, a large variety exists in terms of custom designs and applications [28, 29].

2.2.4.1.3 Calorimeter

ASTM E 1952-06 Standard Test Method for Thermal Conductivity and Thermal Diffusivity by Modulated Temperature Differential Scanning Calorimetry [30].

ASTM standard E 1952 is a non-direct technique used to determine the thermal conductivity of homogeneous, nonporous solid materials with inherent thermal conductivity ranges of approximately 0.10 to 1.0 W/mK. For this particular standard, the recommended surrounding medium temperature is allowed to vary from 0 °C to 90 °C. This test method is used primarily for polymers, glasses, and ceramic materials.

Calorimetry relies upon measuring the heat capacity and thermal diffusivity of a particular material. These values can be related through the definition of thermal diffusivity which relates the heat capacity, thermal conductivity, and density of any given material. Modulated differential scanning calorimetry relies on the application of oscillatory temperature distributions on two geometrically distinct samples. A periodically or oscillatory repeating temperature profile is imposed upon specimens with known properties, which causes a related temperature response within the samples being studied. The thermal capacity is determined from measuring the amplitude of the resultant heat flow divided by the amplitude of the oscillatory or periodic temperature profile which created it. This value can then be converted to the specific heat capacity by normalizing it with the sample mass. This ASTM technique utilizes a thermally stable heating furnace, which maintains environmental stability through the use of feedback differential temperature sensors and temperature controllers, along with highly thermally conductive geometrically appropriate sample pans.

A thin/small specimen, or specimens with relatively small sizes and volumes, is enclosed within the testing pan, and a periodic temperature profile with a very small frequency (or long period) is imposed upon the sample. After a suitably long period of time and subsequent thermal stabilization, the test specimen is assumed to have a uniform temperature distribution. At this point, the sample has a measured heat capacity which is comparable to other methods and is considered to be precise and accurate. Another thick or geometrically large specimen is placed in an identical sample pan, and is exposed to a temperature profile with a relatively large frequency (short period) at one end. For this case, the material specimen obtains a temperature distribution over its length which is related to its thermal diffusivity. This measured heat capacity is smaller than the heat capacity measured with the thin sample, and is proportional to the square root of the thermal conductivity of the specimen materials. Therefore, the modulated differential scanning calorimetry method can calculate the thermal conductivity of a material based upon the apparent heat capacity of a relatively large specimen, the actual heat capacity of a small one, and a series of specific geometric and experimental constants.

The modulated temperature differential scanning calorimetry technique calculates the thermal diffusivity of a given material. The thermal diffusivity is the ratio of a materials thermal conductivity to its density and specific heat. Therefore, with some prior knowledge about the materials physical and thermal properties the thermal conductivity can be calculated from ASTM 1952-06.

This particular technique is commonly used for the determination of thermal properties of a wide variety of materials in multiple phases. It is fundamentally related to the basic method of calorimetry (measuring energy), and therefore is one of the bedrock methods of thermal property determination. However, due to its relative complexity, expense, and the difficulty in modifying it

for cryogenic and nanofluid conditions, it was not considered suitable for use in this research [31-36].

2.2.4.1.4 Laser Flash

ASTM E 1461 Standard Test Method for Thermal Diffusivity by the Laser Flash Method [37].

This particular ASTM standard refers to the ability to optically measure the thermal diffusivity of an opaque, isotropic, homogenous, small thin sample, of a given material. The material can have a wide range of thermal diffusivity values (10^{-7} to 10^{-3} m^2/s) and an equally wide range of applicable temperatures (75 to 2800 K). The laser flash method has many variations and is one of the more highly customizable thermal property experimental techniques. The fundamental operating principle is that a high intensity energy pulse generated by either a laser, flash lamp, or other energy producing device is deposited on the opaque surface of a relatively thin sample. This light/energy pulse produces a detectable temperature increase, which is measured on the opposite face of the thin sample. This thermogram is recorded and is used in conjunction with the sample geometry, energy pulse power, temperature rise, and time to calculate the thermal diffusivity. Thermal diffusivity is a measure of a materials thermal inertia, and by itself, is not enough to calculate the thermal conductivity. The heat capacity and density must also be known according to the definition. The laser flash method has the flaw that it only measures the thermal diffusivity, and a more complicated procedure must be followed to determine the thermal conductivity. Many modern laser flash experimental setups now use a dual measurement system, which allows them to measure two separate samples simultaneously. The principle behind the dual measurement system is simple. Two samples are characterized with the laser flash system simultaneously. The sample of interest with the unknown thermal capacity is measured while a sample with well-known thermal properties is simultaneously measured. If the

samples are measured separately, and at different times, then a great deal of error can be introduced into the system from time dependent variations in the experimental procedure and setup. Therefore, by measuring the materials at the same time, all of the required thermal properties can be measured both directly and comparatively, and the thermal conductivity of the sample can be determined.

Although, this particular ASTM standard refers exclusively to solid materials, the laser flash technique in general can be modified for use with fluids. An example of this was done by Shaikh and Lafdi et al. [38]. The fluid sample must be opaque and once again thin. Aside from these details, the fluid sample must be contained within materials which will not interfere with the energy pulse or temperature measurements, and the effect of the experimental system must be known or measureable and be taken into account [31, 37-41].

The laser flash technique is a versatile, comprehensive, accurate, and useful thermal property technique. However, for the case of nanofluids, the time dependent agglomeration and dynamic behavior of the fluid can cause the surface features, homogeneity, and isotropy of the material to vary, thus causing errors which can be extremely difficult to account for. Therefore, the laser flash method was not considered to be appropriate for this experimental research.

2.2.4.2. Non-standard Transient Methods

This section will detail some of the more common thermal conductivity measurements that are not currently defined by ASTM standards.

2.2.4.2.1. *Hot Strip Method*

The Transient Hot Strip (THS) method is a variation of the transient plane source method. The hot strip method utilizes a long, thin resistive planar heating strip with a substantial width to be backed on either side by the electrically insulating specimen of interest. As in the transient line

source methods, the transient hot strip acts as a dual heater and temperature sensor. A constant, measureable direct current is applied to the resistive heating element of the hot strip which is used to heat the sample backing materials. While this is occurring, the change in the voltage, and thus the electrical resistivity of the heating element is measured, and the temperature of the hot strip, and thus the immediate surface temperatures of the samples are inferred from this value. As with the transient line source, the transient hot strip technique requires that the temperature-to-resistance coefficient of the heating element be measured prior to experimentation, and the hot strips width must be substantially smaller than its length. The exact dimensions of the THS depend greatly on the physical and thermal properties of the material which is being measured. The energizing power and the heater insulating material, if any, also depend upon the specifics of the current application. The THS method has distinct advantages over other methods in the transient planar family, primarily because the hot strip has better surface contact for certain types of specimens. However, for the case of this work, the THS method was more complicated and did not provide sufficient advantages over the THW to warrant its use [42-47].

2.2.4.2.2. *Hot Disk Method*

The Transient Hot Disk (THD) is once again a variation on the transient planar technique. However, this method utilizes a thin circular disk as the working heater and temperature sensor. The advantages of this method are that a variety of materials can be tested within a surprisingly wide range of temperatures and thermal conductivities. The hot disk can use a variety of heater designs; however, one of the more common designs is based upon a double spiral geometry. The dual spirals are often metallic and extremely precise in their geometry, radii, number of spirals, and interlocking shape. The spirals are sandwiched between sheets of an inert, electrically insulative material to give the heating spirals a firm shape and mechanical strength. This thin disk is then inserted into or sandwiched between samples for which the thermal conductivity or other

properties are two be measured. A constant power is then applied to the heating spirals, and the change in resistivity of those spirals is measured to determine their temperature. Once again, this value is assumed to closely approximate the immediate surface temperature of the sample. The inputted power, time, and change in resistance of the heating/temperature probe are measured and used to calculate the thermal conductivity. The transient hot disk has many advantages that set it apart from other techniques; these include an extensive selection of materials which can be tested, high accuracy, and a wide range of applicability in terms of material thermal conductivity, ambient temperature, and sample geometry. Despite the obvious benefits of the transient hot disk, the necessary complexity of building a hot disk setup outweighed the benefits. In addition, many commercially available systems do not have the low end temperature ranges required for this research or are too expensive [48, 49].

Many variations exist within the transient planar techniques; including probes with almost every conceivable geometry. However, the fundamental essence behind each method is that a dual heating element and temperature sensor is used to produce a measurable temperature response within a sample. The exact variations within this method depend simply on what would fit the specific experimental and application needs best.

2.2.4.2.3. *3-ω Method*

The 3-ω method also known as the 3-ω thermal probe method is once again a transient test method for the simultaneous determination of the thermal diffusivity and thermal conductivity of a wide variety of materials and their phases. This technique is similar to many line heat source methods, in that it utilizes a long thin, electrically conducting element as a dual heater and temperature sensor. However, at this point the similarities stop. The 3-ω system relies on the periodic sinusoidal AC excitation heating of a long thin element that is submerged or surrounded by the material for which the thermal properties are to be measured. This particular technique is

based on the fact that when a known, uniform periodic thermal signal is introduced into an infinite medium by an infinitely long and thin electrically conducting wire, the Joule Thomson heating effect generates a corresponding thermal wave. This wave then induces subsequent variations in the temperature of the adjacent material. The third harmonic, or 3-ω signal, of this generated thermal wave is proportional to the specific thermal impedance of the host medium. The third harmonic signal is measured in terms of its phase, frequency, and amplitude. To accurately and repeatable detect both the original electrical signal, and the subsequent thermal signal, the experiment requires the use of a lock-in amplifier for signal detection, a balanced Wheatstone bridge, an accurate stable and repeatable AC power supply, as well as traditional voltage detection and experimental equipment. In addition to the physical experimental setup, this method utilizes a series of elaborate, complex, and complete heat transfer models for cylindrical geometry, which must be solved either analytically or numerically to determine the mathematical models for the temperature behavior and distribution within the hot wire and the surrounding material. The real and imaginary parts of these governing equations allow for the simultaneous measurement of both the thermal conductivity and the thermal diffusivity of the host material. Because this method relies on the detection of a primary signal, and its harmonics, the first harmonic of the measured signal is dominant, and must be canceled out. Once this is done, the third harmonic becomes much clearer and can be accurately measured. There exists an optimum frequency range for which the experimental signal detection sensitivity is at a maximum. This range has been determined from numerous experimental studies on the relative sensitivity of frequencies, phase, and signal amplitudes, and it can be used to predict an ideal range of settings for the periodic heating signal. Asymptotic heating often causes a limiting frequency for the 3-ω method with a low required modulation on the order of a few hertz. However, several researchers

have extended this range up to several decades above the theoretical ideal, and still maintained accuracy and performance [50-55].

The 3-ω technique is often a highly accurate and versatile experimental thermal property test. It is especially suited for the measurement of fluids, due to the fact that the method is highly insensitive to errors originating from black body radiation and improves the estimation of thermal conductivity by minimizing the errors caused by fluid convection. This is due to the fact that the relatively small temperature variations imposed upon the host fluid by the periodic temperature oscillations are small, often on the order of a few degrees, therefore changes in fluid momentum can be considered negligible. Despite the fact that this technique can and often is utilized in the determination of the thermal conductivities of nanofluids, it was deemed less appropriate for this research due to its extensive experimental setup requirements and relatively complex nature. However, it is one of the best thermal conductivity testing techniques available today.

2.2.5. Steady State Thermal Conductivity Measurement Methods

The following standards are just a few of the numerous methods available for the determination of thermal conductivity based on a steady state measurement system. Some utilize a direct measurement of the materials of interest thermal conductivity, while others calculate related values such as specific heat capacity, or thermal diffusivity and use these along with some required previous knowledge to calculate the thermal conductivity. It should also be noted that most of the following standards are originally designed to measure solids, or other non-fluid materials. However, these can be used as beginning models for design and validation of custom fluid specific models.

2.2.5.1. Standard Steady State Methods

For the purposes of this research standard testing methods for thermal conductivity will refer to those defined by ASTM.

2.2.5.1.1. *Guarded Hot Plate*

The guarded hot plate is an absolute, steady state, thermal heat flux and thermal conductivity measurement technique. It is primarily designed for long thin flat samples and can be utilized for a wide range of specimens, temperatures, and conditions. Although this method theoretically has no set limit to its measureable thermal conductivity range, sample conductivities are traditionally kept well below that of most metals. The guarded hot plate method is a general type of measurement and encompasses a wide range of experimental setups and measurement techniques. For a test method to be considered a guarded hot plate, it simply must have a few key characteristics; these include steady state, one dimensional heat flow through either one or a series of specimens, and these specimens must be bounded by temperature controlled surfaces which will restrict and direct the heat flows within the samples.

The guarded hot plate technique can either be setup in a single sided or double sided mode. For the case of the double sided mode, the heat flow from the temperature controlled meter plate is divided equally between two identical samples. Whereas, for a single sided design, all of the generated heat flux is shunted directly into a single specimen. Additionally, auxiliary insulation and cold plates are used along with individually controlled temperature plates to directionally shunt all available heat flux into the lone sample. For the double sided method, the specimen properties are averaged between the two samples, while for the single sided, the properties are directly measured from the individual sample. The guarded hot plate setup generally consists of a series of stacked sections. The first is a metered hot plate, one or two identical specimen samples, a series of concentric primary heating guards, and boundary cold guards. The centralized metered

hot plate is powered, thus allowing electrical energy to be dissipated through Joule heating, creating an elevated temperature which will cause a measureable unidirectional heat flux to dissipate into the adjacent samples. This central metered heating plate can either be formed from a single flat heater or from a guarded hot disk with circular line heat sources embedded at defined and constant radii. The heat generated either from the thin flat heater, or from the circular line sources, flows radially throughout the plate creating an adiabatic hot plate which can then directly shunt one dimensional heat flux into the adjacent samples. The sample or samples form a double layer backing the central hot plate. Primary heat guards are placed axially adjacent to the hot plate with small gaps. Cold surface boundaries are placed bordering the opposing sides of the samples. These maintain a temperature gradient within the specimens and act as isothermal heat sinks for the generated heat flux. The thermal guards specified for this technique are primarily meant to provide the proper thermal environment, to prevent lateral heat flow, and to control the direction and amount of heat flux into the sample/samples. To achieve this, they are designed to achieve as close to isothermal contact as possible. The metered hot plate, primary hot guards, and cold guards should be made from materials with significantly higher thermal conductivities than the samples being tested. This will ensure that no radial or in-plate transient temperature variations will persist for long, and that thermal equilibrium will be obtained quickly. Finally, a series of secondary guards are placed at the axial ends of the primary guards, samples, and cold plates. The entire setup is than surrounded by insulation and an environmental enclosure.

The actual thermal conductivity is calculated from the measured thermal heat flux and the general Fourier equation. The calculation requires accurate and detailed knowledge of the total test time, measured hot plate power, heat flux, as well as temperature gradients throughout the specimens, guard plates, and cold plates along with the physical and thermal details of the specimens. Because of the inherent experimental complexity of the guarded hot plate technique,

the specifics of the construction and materials used in the design of a guarded hot plate setup along with the measurement precision, bias, and accuracy are highly dependent upon the given situation. In addition, for any modified or new design, calibration on several known samples is required. While the guarded hot plate technique is very common and possesses quite a few appealing characteristics, the fact that it is steady state and experimentally complex limits its usefulness for this particular research [31, 56-58].

2.2.5.1.2 Heat Flow Meter

The heat flow meter is a steady state conductivity measurement system that relies on the accurate measurement of one dimensional heat flow within a material. It is similar to the guarded hot plate method in that the measureable heat flow is initiated by a hot plate and is sunk into a cold plate. This technique is primarily meant for temperatures in the range of borderline cryogenic (~123 K) to roughly 600 K. The recommended materials are solid, thin, opaque, and can have a relatively wide range of thermal conductivities. This test relies on the use of a flat specimen, sandwiched between a hot and cold plate. A heat flux transducer, which accurately measures the heat flow in terms of flux through the material, is placed directly in the path of the heat flow. Therefore, heat is generated at the top of the specimen by the hot place and flows down through the sample and heat flux transducer to the cold plate. The upper plate, which is often designated as the hot plate, is temperature controlled with a direct feedback system utilizing embedded temperature sensors. The hot plate is designed to have as near to homogeneous heating as possible. The heat flux transducer is a device which creates a voltage signal, which is proportional to the heat flux flowing through the meter. The cold plate is backed with insulation, and is in direct contact with a highly stable cold environment which provides the cold sink for the entire system. Additional, temperature controlled guards may be placed throughout and around the entire test setup, to ensure the heat flows are accurately directed, controlled, and measured.

Each temperature controlled plate, may have an additional thin highly conductive plate attached to it, to ensure that the various generated temperatures are smoothed out and homogenized before contact with the sample. Contact resistance between the various layers of the test setup is minimized by introducing a reproducible compression load axially through the flat surfaces of the various layers. In addition to the voltage output of the heat flux transducer, temperature sensors are embedded within the direct surface of the sample and the temperature controlled plates. As with most techniques, calibration is required and is done with a sample of similar physical and thermal properties as the desired specimen. In addition, similar test and environmental parameters are maintained. The calculation of the samples' thermal conductivity is done in a manner very similar to that of the guarded hot plate. The heat flux is measured, as well as the temperature gradients within the sample. These factors combined with the specific geometry of the sample, and the known heating power can be used in conjunction with Fourier's model to directly calculate the thermal conductivity of the unknown sample. While this method can be modified for use with cryogenic nanofluids, it is not as appealing as other test methods for the current research [59-62].

2.2.5.1.3 Temperature Oscillation

The temperature oscillation method is based upon the principle of thermal propagation and temperature oscillation within a cylindrical volume of material. The material can vary in its phase but must be isotropic and maintain uniform properties over a long period of time and throughout the specimen volume. The cylindrical sample is placed between two heating surfaces, which vary their heating according to the angular velocity equation. The two heating surfaces can have different temperatures, heating frequencies, phases, and amplitudes. However, the two heating signals must be periodic in nature. The method begins with measuring both the phase and amplitude of temperature oscillations at the two cylindrical end surfaces as well as the center

surface of the sample. From these values, the thermal diffusivity can be determined. To fully measure the thermal conductivity directly from the experiment, the temperature oscillations at the reference layer that borders the sample cell must be considered. The temperature oscillations in this layer are measured directly by utilizing a Peltier element, which converts the periodic thermal waves into corresponding voltage values. These voltage signals are converted and modeled using Fourier analysis. Finally, the thermal conductivity can be calculated from knowledge of the material density and specific heat according to the governing equation of thermal diffusivity. It should be mentioned again, that the temperature oscillation method is a steady state technique, therefore any temperature oscillations would occur after a steady state ambient temperature has been reached. The exact experimental setup and specifics of the temperature oscillation method can be reviewed further in the literature. Due to the fact that this technique is steady state, thus causing concern with respect to convection in fluids, and due to the fact that it is relatively complex, requiring a sealed and insulated container, it was not considered a good fit for the current research [63].

2.2.5.1.4. Absolute Radial/Axial Heat Flux and Cut Bar

The term radial/axial heat flux defines a type of thermal conductivity method in which the governing thermal parameter, that of heat flux, is forced to be unidirectional. This specifies that thermal guards are used to direct the flow of heat in a single spatial direction through: sources, references, and samples. The system utilizes a heat flux source, often a constant power heater along with thermal guards, reference materials, thermal sinks, temperature sensors, and well defined experimental setup and sample geometries to calculate the various components of the basic Fourier equation, to back calculate the effective thermal conductivity.

Whether a system is axial or radial in nature simply depends upon the physical and thermal characteristics of the sample being measured. Typically, high conductivity samples are tested, if

possible, with axial systems. If the samples have a relatively lower thermal conductivity, they are generally measured using a radial system. The reasoning behind this is based upon the generated heat fluxes, the comparative surface and directional losses of said heat fluxes, and the temperature gradients produced within the samples. In addition, the sample thermal conductivity compared to the experimental setup material conductivity and the overall environmental temperature play a significant role in the design of axial/radial systems. Ultimately, great many other parameters define what type of system is used in the measurement of thermal conductivity.

Axial/radial conductivity measurement systems have long been established as some of the most consistent and accurate experimental methods available. In addition, they are often the methods of choice for cryogenic conductivity measurements.

The cut bar method is simply a type of axial system. It is very common, and relies upon the principle of flowing a well-defined heat flux through a series of reference samples, and the sample for which the effective thermal conductivity is to be measured. The thermal conductivity can then be back calculated from the respective thermal gradients. The cut bar method often sandwiches the unknown sample between the two reference materials. This helps to eliminate minor heat losses.

The axial/radial heat flow methods are common, accurate, and have consistently been used throughout the years. However, due to the intrinsic nature of CN's, they were not deemed appropriate for use with the current research [10, 11, 64-66].

2.2.6. Thermal Conductivity Conclusions

The measurement of thermal conductivity depends only upon correctly interpreting the general equation for thermal conductivity for a given situation, and then creating an experimental environment which simulates the theoretical model. Therefore, many different experimental measurement techniques exist, and within these discrete methods, many more variations and

custom setups have been created. It is up to the researcher to choose which of the many systems available best fits the requirements of the research at hand.

2.2.7. Thoughts Behind The Transient Hot Wire

The literature review above proves that there are many different approaches to the determination of thermal conductivity. While each of the setups listed had aspects to their design which made them appealing for use in this research, the THW system was ultimately used due to its common use in current nanofluid research, as well as its simplicity, versatility, accuracy, ease of use, transience, and the fact that the basics of the system could easily be modified for use with a cryogenic nanofluid.

2.3. Nanoparticles Literature Review

2.3.1. Nanoparticle Background

Nanoparticles are defined as an object with a size on the order of 1-100 billionths of a meter. These particles exist as an individual and coherent unit in terms of their physical properties and thermal transport characteristics. Nanoparticles are the key to nanofluids and without them the entire science would simply not exist. Therefore, a basic understanding of their nature is prudent when their use plays such a prominent role in the current research.

While numerous nanoparticles have been used and subsequently tested in a variety of nanofluids, MWCNT's are of particular interest due to their own unique properties. For this reason, among a variety of others which will be discussed later, MWCNT's were chosen to be the inclusion phase of these CN's. Therefore, for the purposes of this review they will be the only type of nanoparticle under scrutiny. The specific thermo-physical properties of nanoparticles play a very important role in the behavior of nanofluids, and therefore must be studied with the same intensity as the nanofluids themselves. However, for the purposes of this research, the effective

thermal conductivities of the specified CN's are simply being measured and compared to the base host fluid values. Therefore, the physics behind, and the causes of, these measured effective thermal conductivity values is left to be investigated by future researchers. Because of this, only a limited amount of information is required for this particular research as to the thermo-physical nature of MWCNT's. Specifically, the directional thermal conductivity of single, multiple, and intertwined carbon nanostructures is required. These values will be used, later in this research, in conjunction with a sampling of some of the leading static models for nanofluid behavior. To this end, the following review is simply a small selection of the literature that focuses on the thermal conductivity of CNT's. The actual thermo-physical characteristics of the nanoparticles used in this research are not discussed in this chapter. Instead, they were determined based upon the manufacturer's specifications and can be viewed in the nanoparticle profile chapter [1].

The following literature will cover a variety of topics in terms of nanoparticle thermal conductivity and have been reviewed with four specific goals in mind. The first is to determine the author's research objectives. The second is to investigate the theoretical, numerical, or experimental details of how these objectives were satisfied. The third determines the final results and discussions of the work. The final goal describes how each of these works impacts the current research. The ultimate goal of this review is to pinpoint a rough estimate of the expected thermal conductivity of a MWCNT, and to gain a more comprehensive understanding of MWCNT's.

2.3.2. Nanoparticle History

Nanoparticles are generally considered to be a discovery of modern science; however their history is long and rich. Naturally occurring nanoparticles and nanostructures of all types are as common as the macro-sized objects that surround us. Indeed, the universe itself was built from the bottom up, and that by necessity, dictates that an astoundingly complex micro-world exists. Nanoparticles are common in nature as trace metals, organics, and non-organics formed through

varied natural processes. These include the production of carbon structures such as fullerenes, through the combustion of any complex carbon molecule, and the creation of organic, non-organic, and metallic nanostructures through thermal, chemical, biological, and physical processes. Truly, the collection of naturally occurring nanoparticles is noteworthy and can be reviewed further in the literature [67, 68].

The use and discovery of nanoparticles by humans dates back hundreds of years. Nanoparticles were employed in the 9th century as additives to paintings and pottery to add luster. They were also used as pigments in the alveoli of mummies which date back more than 5000 years and as coloring agents for stain glass windows and tattoos. Although humanity did not fully realize the impact or importance of their discoveries, their ability to manipulate and utilize nanoparticles at such an early date is impressive. Further investigation of the historical uses of nanoparticles can be reviewed in [69, 70].

The first truly scientific study of nanoparticles was done by Michael Faraday in 1857 when he discussed the optical properties of nanoscale metals [71]. Since that time, a great deal of scientific research has focused on the physical and transport properties of nanoparticles. Indeed, the entire field of nano-science and nanoparticles has blossomed along with their applications and potential.

2.3.3. Thermal Conductivity of Carbon Based Nanoparticles

Nihar R. Pradhan [72] in his doctorate dissertation provides a thoughtful and detailed review of the history of nanowires and nanotubes, the most common synthesis techniques used in their production, the theoretical and experimental methodologies utilized in their study, and their resultant measured thermal properties. The author reports that based upon his own literature review, thermal conductivities of 3000 W/mK for MWCNT's and greater than 6600 W/mK for SWCNT's in their axial direction were reported. He also notes that according to current

experimental results, carbon nanotubes of both types lose the vast majority of their conductivity when measured in large groups. Pradhan attributes this loss of effective thermal conductivity to the relatively large thermal contact resistances that exist between individual carbon nanofibers. Pradhan utilizes an AC Calorimeter to measure the specific heat and thermal conductivity of nanocomposites and provides the experimental and numerical background upon which their study was based. Pradhan provides his own study of the thermal properties of anisotropic MWCNT's, randomly oriented MWCNT's, and SWCNT's as they vary with temperature from 300-400 K. The research done by Pradhan is quite extensive and fascinating. Indeed for the current work, this review provided a great deal of background into the creation, use, and properties of carbon based nanotubes.

Zhidong Han and Fina [73] in both a doctorate dissertation and a peer-reviewed paper focused on the effective thermal conductivity of CNT's and their potential applications as fillers for carbon based polymers. This review presented a rather in depth discussion of some of the current work on the thermal conductivity of SWCNT's and MWCNT's, specifically, the effects of a variety of factors such as carbon lattice structure, atomic structure, topological defects, dimensions, morphology, purity, etc. They concluded that based upon the current literature, the exact effective thermal conductivity of any type of carbon nanotube is based upon a dizzying variety of factors and requires a great deal more knowledge to truly pinpoint. However, they noted that an effective thermal conductivity of greater than 3000 W/mK for MWCNT's and 2000 W/mK for SWCNT's is consistently reported in the literature. The authors note that because of the difficulties intrinsic in the experimental determination of the thermal conductivity of individual carbon nanotubes, a conductivity range of 2000-6000 W/mK is not unreasonable. This particular article helped pinpoint the relative range of thermal conductivity that could be expected for a variety of carbon nanotubes and what possible factors influence said conductivity.

P. Kim et al. [74] detailed the design and use of a micro-fabricated suspension device to measure the thermal conductivity of individual MWCNT strands as they vary with temperature. The authors found conductivities greater than 3000 W/mK, and a peak value of the effective thermal conductivity of a MWCNT at 320 K. This particular paper was of significant value due to the fact that the MWCNT studied had a diameter of 14 nm and was measured with temperature variations well within the cryogenic ranges being studied in the current work.

J. Hone [75] from Columbia University concluded a study on the thermal transport properties of carbon nanotubes. Specifically, the authors studied the phonon bandstructure of a variety of carbon nanotubes, and their interactions/coupling behavior. They also provided a brief review of the current literature on the effective thermal conductivity of MWCNT's and SWCNT's. In addition, the authors experimentally studied the specific heat and thermal conductivity of said carbon nanotubes. This research was extremely useful to the current research due to their study and subsequent graphical representation of the effective thermal conductivity of individual MWCNT's with respect to temperature at and near the cryogenic temperature range being utilized for this research.

Hisataka Murayama et al. [76] studied the thermal conductivity of a single carbon nanotube in a liquid suspension with the use of a quantum dot hydrogel sensor. Murayama, using this unique experimental method, measured the thermal conductivity of a single carbon nanotube suspended within a liquid to be approximately 412 W/mK. This research was of particular interest due to the fact that it studied the effective thermal conductivity of carbon nanotubes in fluid suspension, which is similar to the circumstances of the current work.

Natnael Behabtu et al. [77] provided a fascinating work in terms of the design, creation, and testing of a truly exciting synthesis method for the creation of carbon nanotube based fibers. The authors report fiber specific strength, stiffness, and thermal/electrical conductivities consistent

with current research and values that are similar to properties found in metals. Behabtu et al. created a high throughput wet spinning process that is potentially scalable to industrial requirements. They also studied the electrical and thermal conductivities of a variety of their fibers as they varied with temperature. Fiber thermal conductivity values of greater than 700 W/mK were measured. This work provided an understanding of the behavior of combined and interactive carbon nanotubes, which for any real world application would exist.

Tae Y. Choi et al. [78, 79] published two separate works on the experimental measurement of the thermal conductivity of individual MWCNT's with the 3-ω method, and the four wire 3-ω method. The authors in the standard 3-ω paper utilized a self-heating micro-fabricated experimental setup to individually measure two MWCNT samples. The authors found that for samples with inner and outer diameters of roughly (27-46 nm) and lengths of roughly (1.0 μm), the effective thermal conductivity varied from 650-830 W/mK. The authors note that the large variations in thermal conductivity could be due to carbon nanotube size variations. The same authors expanded this work into their subsequent paper which utilized an experimental setup composed of four micro-fabricated electrodes which suspended a single MWCNT over trench dug by a deep ion beam. The authors measured the thermal conductivity of the MWCNT to be 300 ± 20 W/mK at room temperature under vacuum conditions. Choi's research provided a valuable insight into how individual MWCNT's can be measured with a great deal of accuracy.

In a report by Motoo Fujii et al. [80], a method that can reliably measure the thermal conductivity of a single carbon nanotube with a suspended sample-attached T-type nanosensor was presented. Their experimental results show an inverse trend between the thermal conductivity and nanotube diameter at room temperature. The authors report a thermal conductivity in excess of 2000 W/mK for a nanotube diameter of 9.8 nm. They also found an asymptotic relationship between the magnitude of the thermal conductivity and the temperature for a 16.1 nm carbon

nanotube at roughly 320 K. This article once again provides insight into the nature and behavior of a variety of carbon based nanotubes and structures. This provides information of how the CNT might behave in terms of the current research.

2.3.4. Nanoparticle Review Conclusions

This particular review has focused on the effective thermal conductivity of carbon nanotube fibers, MWCNT's, SWCNT's, and interconnected carbon nanotube structures. It is certainly not a completely inclusive review, nor does it encompass the majority of the carbon nanoparticle scientific field. Considering that the current research requires only a rough idea of the thermal conductivity of MWCNT's at cryogenic temperature ranges, it was more than sufficient. If the readers wish a broader and more detailed discussion of the current field of nanoparticle research, they need to investigate further outside of this work. A broad review of how nanoparticles are used in nanofluid science can be found in Sarit K. Das et al. [1].

2.4. Nanofluid Literature Review

2.4.1. Nanofluid Background

This thesis is investigating the effective thermal conductivity enhancement of cryogenic nanofluids. Because no cryogenic nanofluids have been created or studied up to this point, a review of more traditional nanofluids is necessary. As with any work of science, a thorough and well-rounded review of the current work being done in the field is essential, therefore, the following literature review will present some, but certainly not all of the current scientific works in the field of nanofluids.

One of the most important aspects of nanofluids is their ability to transfer heat; this in turn depends upon their thermophysical properties. Indeed, the unique and often times highly anomalous thermal transport properties of nanofluids is the primary reason for the interest

expressed in them. While there are numerous methods and modes of thermal transport, only a select few (namely conduction, convection, boiling, and general thermal transport) will be addressed along with a brief review of how nanofluids are made and tested. The science of nanofluids is composed of a wide variety of sub-topics. Each of these examines a specific aspect of said science, and try's to determine its effect on the whole. These include the variations in thermal transport properties of nanofluids based upon: host fluid type, nanoparticle type, nanoparticle size/shape/morphology, nanoparticle loading, nanofluid temperature, the addition of surfactants/stabilizers/additives, production methods, etc. While each of these are well worth studying in their own right, it should also be noted that due to the rather large and unstructured nature of nanofluid science, this author focused on a more general overview of a variety of research topics pertaining to each of the above subjects, the ultimate goal of which was to gain a better understanding of nanofluids as a whole, and to determine whether the data gathered for this research was reasonable with respect to the best knowledge of current nanofluid science [1].

The following literature will cover a variety of topics in terms of nanofluid science, and have been reviewed with four specific goals in mind. The first is to present the author's research objectives. The second is to investigate the theoretical, numerical, or experimental details of how these objectives were satisfied. The third determines the final results and discussions of the work. The final goal describes how each of these studies impacts the current research.

2.4.2. Nanofluid History

Nanofluids are an invention of modern science, or at least their study and use by mankind is. In the early 1990's, Dr. Steven Choi of Argonne National Labs coined the term nanofluids to encompass the newly formed field of nanometer sized suspensions of nanoparticles in traditional coolant fluids for use as thermal management systems. Since that time, the field has blossomed to encompass a truly wide variety of research, topics, and disciplines with potential that varies from

the pedestrian to the world changing. The current state of the field is still in its early stages and only time will tell the true story [1].

2.4.3. Nanofluid Thermal Conductivity:

The thermal conductivity of nanofluids was one of the first thermophysical properties measured and the results of this early research demonstrated the anomalous behavior that would come to describe nanofluids. The following condensed literature works are presented in their entirety with a variety of research topics being explored for each [1].

Xinwei Wang et al. [81] tested two distinct types of nanoparticles: Al_2O_3 and CuO dispersed in water, vacuum pump fluid, engine oil, and ethylene glycol. Their experimental results show that the effective thermal conductivities are enhanced from a few percent to greater than 40% for the variety of nanofluids tested. They also compare these enhancements to several theoretical models and demonstrate that they do not match. This particular paper was of interest due to the fact that it simply and concisely expressed some of the key concepts of measuring the effective thermal conductivity of a variety of nanofluids. In addition, it presented some of the more current models for the thermal conductivity of a nanofluid and where these prediction models are lacking.

Rashmi Walvekar et al. [82] experimentally and theoretically studied the thermal conductivity of carbon nanotube based nanofluids. These carbon nanotube based nanofluids were stabilized using gum Arabic, with particle concentration values ranging from 1-2.5 wt%. The authors studied the effects of particle volume fraction and temperature on the thermal conductivity enhancements for each nanofluid. They then created a simple thermal conductivity model which demonstrates the effects of diameter and aspect ratio of the CNT’s on the nanofluids. The authors reported good agreement between their measured thermal conductivities, and those calculated by their models. This paper provided a unique and valuable insight into how

existing models and theories can be utilized to create predictive equations for specific nanofluids and research.

S. U. S. Choi et al. [83] produced carbon nanotubes suspended in oil and measured their effective thermal conductivities. The authors report that their measured thermal conductivities were anomalous, and far greater than current theoretical predictions. They also reported nonlinear increases with nanotube particle loading. These anomalous thermal conductivities show the inherent limits of traditional heat conduction models for two-phase solid to liquid suspensions. This paper is of great use to the current research, because it clearly and concisely demonstrates the use of carbon nanotubes to enhance the effective thermal conductivity of a fluid. In addition, they report a nonlinear correlation between particle loading and thermal conductivity, as well as demonstrating the anomalous nature of their nanofluids by comparison with several of the current modeling equations. Indeed, this early work by Choi et al. provided a great deal of the excitement and impetus for the last few decades' worth of study on the thermo-physical properties of nanofluids.

Sadollah Ebrahimi et al. [84] presented a theoretical model for the explanation of the enhancement found in the effective thermal conductivities of cylindrically shaped nanotube colloidal suspensions. The authors determined, based upon their model, that a decrease in nanotube diameter along with an increase in the thickness of the nanolayer (the wall that forms the nanotube) results in an increase in the effective thermal conductivities of the overall nanofluids. In addition, they showed that as the cylindrical nanotube diameters decrease and the wall thickness remains constant, the overall nanofluid effective thermal conductivity decreases. This paper was of particular importance because it sheds some light on why certain cryogenic nanofluids showed a marked increase in the effective thermal conductivity over others.

Jessica Townsend's and others' [85] work primarily focused on the various methods used in the measurement of the effective thermal conductivity of nanofluids. However, Townsend also reported the results from her own experimental work and several by other authors. Townsend then compared these results to each other and to several common analytical models. These results clearly demonstrate large thermal conductivity increases in a variety of nanofluids as the host fluid type, particle type, particle concentration value and temperature are varied. This work is very important to the current research, because it provides a good overview of the current work, methods, data, and analytical models on the subject of nanofluids.

A large group of researchers led by Jacopo Buongiorno et al. [86] provided an excellent overview of the repeatability of nanofluid research. This paper focuses on the report of the International Nanofluid Property Benchmark Exercise, or INPBE where over 30 organizations measured the thermal conductivity of identical samples of colloidally stable dispersions of nanoparticle-containing nanofluids. The various organizations used a variety of experimental measurement methods. The nanofluids consisted of aqueous and nonaqueous base fluids with metal and metal-oxide particles of spherical, near spherical and elongated shapes. The particle concentrations were allowed to vary from very low to relatively high. The data revealed that for most of the organizations, the reported results fell within a fairly narrow band (roughly ±10% or less), with the occasional outliers. The reported conductivity values tended to increase with particle concentration and aspect ratio. This benchmark study also found that although there were small anomalies and variations in the data, they tended to align quite nicely once normalized. In addition, the effective medium theory presented by Maxwell [86, 87] and generalized by Nan et al. [86, 88] provided a good predictive equation for the collected data. This report was of great importance to the current research, because it details one of the many attempts to collect,

correlate, and present a unified set of data, experimental methodologies, and theories for the effective thermal conductivity of nanofluids.

J. A. Eastman et al. [89] created a nanofluid by combining nanoparticle sized copper inclusions in ethylene glycol. Eastman reports that the measured effective thermal conductivity values were far greater than either pure ethylene glycol or ethylene glycol containing the same volume fractions of oxide nanoparticles. They demonstrated increases in the measured thermal conductivity of up to 40% with particle concentration values as low as 0.3%. The copper nanoparticles had a mean diameter of less than 10 nm. The authors report that they did not observe a strong correlation between the effective thermal conductivity of the nanofluid and the shape of the inclusion nanoparticle, which was predicted by several models. Instead, they observed that the thermal conductivity of the nanofluid varies with particle size, particle concentration, and thermal conductivity of the nanoparticles. This has helped to guide the current research by providing insight into the reactions of nanofluids as the properties of the constituent materials vary.

S. M. S. Murshed et al. [90] created nanofluids by dispersing TiO_2 nanoparticles of both rod-shaped (diameters ~10 nm and lengths ~40 nm) and spherical particles (with diameters ~15 nm) dispersed in water. They utilized a custom made, transient hot-wire apparatus with an integrated correlation model to solve for the effective thermal conductivities of the nanofluids. They also studied and determined the pH values and viscosities of their nanofluids. They showed that the effective thermal conductivity increased with inclusion particle volume fraction, and that the particle size and shape played an important and noticeable role at well. For both the rod-shaped and spherical particles with loading values of up to 5%, increases in effective thermal conductivity on the order of greater than 30% were measured. This was reported to be greater

than 10% above the standard Hamilton-Crosser model and 16% greater than the Bruggeman model. The current research uses a similar transient hot-wire method.

S. M. S. Murshed et al. [91] studied the combined properties of nanofluid thermal conductivity and viscosity. Murshed determined that both the effective thermal conductivity and the viscosity of the created nanofluids were substantially higher than that of the base host fluid. They also reported that both viscosity and thermal conductivity increased with TiO_2 nanoparticle volume fraction. Also of note was that the thermal conductivity seemed to have strong temperature dependence over the range of 20-60 °C with conductivity values of greater than 10% measured with particle concentration values of up to 0.05%. The authors compared their measured results to two static-based models for the prediction of the effective thermal conductivity of nanofluids containing spherical or cylindrical nanoparticles. The models showed reasonable good agreement with the experimental results.

Tae-Keun Hong et al. [92] created nanofluids based upon Fe nanoparticles suspended in ethylene glycol. The Fe nanoparticles were synthesized from nanocrystalline powder and chemical vapor condensation. Sonication with high powered pulses was used to improve the dispersion of the Fe-based nanofluids. The authors report the measured effective thermal conductivity increased by up to 18% with particle volume fractions of up to 0.55%. The researchers found, from comparisons with Cu-based nanofluids, that the suspension of highly conductivity nanoparticles does not always produce a great increase in nanofluids. This work is a good example of the role that nanoparticle type and thermal conductivity play in the effective thermal conductivity of a nanofluid, as well as presenting the use of a sonicator to improve dispersion of the nanoparticles in the fluid. Hong et al. [93] studied the effect of iron based nanoparticles and their cluster size on the effective thermal conductivity of nanofluids. They found that as the cluster sizes of nanoparticles decreases, thus causing an increase in the

nanoparticle volume fraction (as total mixing increases), the conductivity of the nanofluids increases nonlinearly. They attribute this nonlinearity to the rapid clustering and subsequent agglomeration of nanofluids.

S. Shaikh et al. [94] studied the thermal conductivity of three distinct nanofluids. These were based upon carbon nanotubes (CNT), exfoliated graphite (EXG) and heat treated nanofibers (HTT) with PAO oil as the host fluid. The authors utilized a modern version of the light flash technique and measured the effective thermal conductivity vs. particle volume fraction. The results demonstrated a maximum enhancement of roughly 161% with particle volume fractions up to 1.0% obtained with the CNT-based nanofluid. The EXH showed the next greatest increase, followed by the HTT based nanofluid. It should be noted that the authors determined that enhancements well above 100% were found for each type of nanofluid. The high thermal conductivity values make this work remarkable and demonstrate how effective nanofluids can be based addition of a small particle volume compared to the large of the base fluid.

Clement Kleinstreuer et al. [95] presented a study on the theoretical and experimental aspects of nanofluid thermal conductivity. In this work the authors explore the possibility of nanofluids in the cooling of microsystems as well as other industrial, commercial, and scientific applications. They focus primarily on dilute suspensions of well-dispersed, spherical nanoparticles in water or ethylene glycol. The authors explain how current models and experimental data lack consistency. To this end, the authors present a collection of some of the current work being done in nanofluid heat transport. They describe separately convection, conduction, experimental methodologies, and some of the current models and theories. Once again, this paper provides an overall review of the current state of nanofluids as a science when the review was written.

Huaqing Xie et al. [96] presented their work on the thermal conductivity enhancement caused by suspensions containing nanosized alumina particles. The authors have prepared various

nanofluids with Al_2O_3 nanoparticles with specific surface areas of roughly 5-124 m^2g^{-1}. The authors utilize a transient hot wire setup to measure the effective thermal conductivity of these aluminum oxide based nanofluids. They report great increases in the thermal conductivity with relatively small amounts of nanoparticles, as well as a trend of increasing thermal conductivity with respect to inclusion particle volume fraction. The enhanced thermal conductivity also increases with the difference between the pH value of the aqueous solution and the isoelectric point of the Al_2O_3 particles. The authors determined that the thermal conductivity enhancements are highly dependent upon the specific surface area of the nanoparticles and decreases inversely with respect to the base fluid's thermal conductivity. They compared their experimental results to modern predictive models and determined that an anomalous enhancement occurred. This work is valuable, because it explores how the nature of not only the nanoparticle but how the host fluid affects the overall behavior of the nanofluid.

Hrishikesh E. Patel et al. [97] measured the thermal conductivities of two distinct kinds of Au nanoparticle based nanofluids, with water and toluene acting as the base fluids. The nanoparticles had rough diameters of 10-20 nm and were made with citrate stabilization. They measured effective thermal conductivity enhancements of 5-21% with temperature variations of 30-60 °C at particle loading of up to 0.00026% by volume. For Au nanoparticles stabilized with a monolayer of oxtadecanethiol, enhancement values of 7-14% were measured with concentration values up to 0.011% wt. They determined that the effective thermal conductivity of the nanofluids tended to decrease inversely with Au nanoparticle diameter. They also determined that due to enhancements of roughly 9% even at vanishing nanoparticle concentration values, chemical factors such as direct metal to solvent contact are important to the enhancement of nanofluids. This paper is unique and important because it describes the use and results of a stabilizing agent

for nanoparticle inclusions with the addition of the oxtadecanethiol. This allows for smaller inclusion weight percentages to be used.

M. J. Assael et al. [98] added both MWCNT and Double-Walled Carbon Nanotubes (DWCNT) to water to create nanofluids. They also utilized Hexadecyltrimethl Ammonium Bromide and Nano-Sperse AQ as dispersants. They measured the effective thermal conductivity of these nanofluids with a custom-made transient hot wire apparatus. The authors measured thermal conductivity enhancements of better than 34% for particle volume fractions of up to 0.6%, at room temperature. This is of interest because it describes the use of surfactants in the stabilization of nanofluids and how this effects enhancement of their properties.

In Sarit K. Das et al. [1] an entire chapter is dedicated to the phenomena of conduction within two phase mixtures and nanofluids. This work reviews the fundamental laws and theories of conduction heat transfer along with the fundamentals of experimentally measuring said conduction. However by far the most valuable aspect of this work is the wonderfully detailed, diverse, and expansive literature review of the current experimental research being done in terms of metallic, non-metallic, oxide, and carbon based nanofluids. This book also presents a chapter on the current theories and models of thermal conductivity for nanofluids. In essence, this book is a plethora of knowledge on the subject of conduction within nanofluids, and has been of invaluable service to the current work.

2.4.4. Nanofluid Convection

Convection is another of the fundamental aspects of heat transfer and is an important and often times present mode of thermal transport within a nanofluid. However, because this particular research does not focus on convection, only a brief review was conducted. This was done mostly for the purposes of presenting a complete and well-rounded study of nanofluid thermal transport properties. If the reader so wishes, the following are excellent general

overviews of some of the current work being done in the field of nanofluid convection, and can easily be expanded upon.

J. Boungiorno [99] studied how many of the current nanofluid convective models are inadequate. Of particular is how nanoparticles increase the thermal dispersion and intensified turbulence of a nanofluid. This paper reviews seven distinct slip mechanisms that produce a relative velocity between the host fluid, and the inclusion nanoparticles. They concluded that only Brownian motion, and thermophoresis were significant enough to cause slip in nanofluids. Based on this, they created a two-component four equation non-homogeneous equilibrium model for mass, momentum, and heat transport in nanofluids. By using these results, they propose a new explanation for why nanofluids exhibit such large convective heat transfers. This review was impressive in terms of its depth, and the explanations they provided in terms of the convective heat transfer mechanisms. It is an excellent review of some of the current work being done in the field.

Khalil Khanafer et al. [100] investigated the heat transfer in a two-dimensional enclosure with nanofluids as the working medium. The authors investigate a series of parameters, and develop a model to analyze the heat transfer performances of various nanofluids with respect to nanoparticle dispersion. The authors compare their work with previous literature, and a series of effective thermal conductivity maps for the nanofluids, within the enclosure, are developed. In addition, the authors show that the variances within many of the current nanofluid models play an important role in the results. Finally, the authors present a heat transfer correlation between the average Nusselt number, various Grashof numbers and volume fractions. This research provided a good review of how various parameters within conventional models affect the end results, especially for convective heat transfer within nanofluids.

In Sarit K. Das et al. [1] an entire chapter is dedicated to the phenomena of convection within two phase mixtures and nanofluids. This work is fascinating to say the least, and includes reviews of the fundamental laws and theories of convection, boundary layer flow, turbulent flow, geometry concerns, forced and natural convection, current nanofluid convective models and theories, as well as physical property changes of nanofluids and particle based slurries. Essentially, many of the fundamental approaches of fluid mechanics coupled with heat transfer are addressed in terms of nanofluid or slurries acting as the working fluid. In addition, Das presents numerous examples of the current experimental work being conducted in the field of nanofluid convection [1].

2.4.5. Nanofluid Boiling

Boiling can be one of the most prominent forms of heat transfer within a fluid. Indeed, boiling is so effective in terms of heat transport that many thermal designs are based upon its effect. Therefore, understanding and quantifying the potential nanofluids have for boiling heat transfer is of extreme importance. Once again, this particular topic is not directly applicable to the current research. However, a general understanding of boiling, and the role it plays for nanofluids is essential for a well-rounded review.

Sarit K. Das et al. [1] reviews the boiling of nanofluids in a dedicated chapter of his book. It begins with a review of the fundamentals of boiling; these include pool boiling, nucleate boiling, bubble growth and departure, flowing or convective boiling, and the heat transfer mechanisms present in boiling. At this point, the role nanofluids play in boiling is discussed, along with numerous examples of the current work being done on this topic. This primarily consists of detailing much of the experimental methodologies and data collected by other authors and presenting them in a coherent fashion. This is a good starting point for the study of nanofluid boiling.

2.4.6. Nanofluid General Thermal Transport

When considering nanofluids, it is important to look at heat transfer in general. This is due to the fact that any real world application will often involve all the various thermal transport categories, and will at the very least be extremely complicated. Therefore, the next few reviewed works will focus on either the general heat transfer found within nanofluids, or on a broad overview of the various types present.

Sarit K. Das et al. [2] created a very broad overview of the various types of heat transfer possible within nanofluids. This work included discussions on the definitions of nanofluids, and their various unique characteristics, and what applications they might have in the future. The review also included discussions, experimental data, and current models and theories on nanofluid thermal conductivity, thermal convection, and boiling. Once again, this particular piece of literature provides a wonderful overview of some of the best and current thoughts on nanofluid science, and how they contribute to an understanding of general heat transfer.

J. A. Eastman et al. [7] provided a review of nanofluids including their synthesis, their characteristics, and their use. In addition, experimental data and some of the current work for the various thermal transport mechanisms' present in nanofluids for oxide, metallic, and carbon based nanoparticles are considered. The authors present their thoughts on the various aspects of thermal transport in nanofluids, and how each affects the overall outcome. Current theories and models for the various modes and combinations of heat transport are also discussed. Once again, this work provides a valuable overview of nanofluids for the current research.

Yulong Ding et al. [8] summarized a sampling of the recent work in nanofluid heat transfer. This summary includes heat conduction, convection, and boiling. The authors concluded that a substantial increase in the effective thermal conductivity of nanofluids is caused by nanoparticles, specifically nanoparticle structuring. The researchers measured a general decrease in the

convective heat transfer of nanofluids with respect to nanoparticle loading, and attribute this to the increase in nanofluid viscosities. Finally, the nucleate regime of boiling is observed to be enhanced within nanofluids. The authors conclude that a great deal of data scatter occurred, and that future work is required to fully characterize nanofluids. However, the variety of research presented in this work is truly useful. This, combined with the authors thoughts on the variances that occur within nanofluid research, make this a helpful review.

Pawel Keblinski et al. [3] created a collated review of the then current work on nanofluid production, experimental effective thermal conductivity, and conduction theories. The authors also worked on providing a simple review of the current works on nanofluid science. Keblinski et al. [4] also provided concise review of some the current controversies in terms of nanofluids thermal conductance in a later publication. The authors gave a critical analysis of some of the current experimental data in terms of thermal transport mechanisms. In addition, they prove that by taking into account linear particle aggregation many of the well-established effective medium theories adequately predict the behavior of a majority of the current experimental data. This work is important because it provides a critical review of whether or not nanofluids are anomalous at all.

Kun-Quan Ma and J. Lin [101] proposed the concept of using nanoparticles combined with liquid metals to create the ultimate coolant. Their goal was to create an engineering coolant with exceptional thermal conductivity that could be electromagnetically driven. The authors used a variety of current predictive models to forecast the behavior of their nanometal fluids. They examined the effects of particle size, cluster size and morphology, solid layer adsorption, and volume fraction etc. on their nanometals. This review is unique, because it approaches the concept of an ideal engineering fluid from a theoretical perspective and explores the use of

customized nanofluids in terms of applications which necessitates a full and general comprehension of nanofluid heat transfer.

A. Miner and U. Ghoshal. [102] offered a possible solution for the worlds future high performance cooling needs along with the applications and potential advantages of such a nanofluid. The researchers present analytical and experimental work that indicate heat transfer coefficients on the order of 10 $W/cm^2/K$ along with small pumps that operate at pressure greater than 8 kPa and 1% maximum efficiency are possible. This work is similar to the previous in that it provides unique and exciting ideas for the world's next generation coolants.

2.4.7. Nanofluid Production

The production of a nanofluid is not a simple process. Indeed, the final behavior of any nanofluid is greatly influenced by the synthesis steps taken in its creation. Nanofluid production can be broken up into two broad categories, One-step and two-step methods. The first is that of creating the nanofluid and its inclusion particles in one step. This often involves some kind of chemical, electrical, or explosive dispersion/condensation/reduction process. The second is the far more common method of creating the host fluid and the nanoparticles in two separate processes and then combining them. This style of nanofluid production includes a wide variety of techniques. The field of nanofluid production and the ultimate goal of creating well dispersed stable nanofluids is as complex and widely studied as nanofluids themselves. An excellent overview of the basics of nanofluid production is provided in [1].

2.4.8. Nanofluid Effective Thermal Conductivity Experimental Measurement

Because nanofluids have thermal transport and physical properties that vary greatly from those of their host fluids, great care must be taken with what experimental methodologies are used to measure their various features. As effective thermal conductivity is the primary concern

of the current research, it will also be the focus of this review. The effective thermal conductivity of a nanofluid can be orders of magnitudes greater than its base fluid, not to mention that when measuring nanofluids the least invasive process is often best, so that the fluid is as undisturbed as possible. These aspects among many others must be taken into account when choosing an appropriate thermal conductivity measurement system.

Jessica Townsend et al. [85] provides a review of some of the more popular thermal conductivity measurement techniques. These are sectioned in terms of transient, steady state, and optical methods. They include the transient hot wire, the thermal probe, the transient plane, hot disk, temperature oscillation, cut bar, coaxial cylinders, thermal comparator, optical transient grating, optical beam deflection, and laser flash, among others. Townsend compares each of the methods in terms of what types of nanofluids they have typically been used for, their useful ranges of temperature and thermal conductivity, reported accuracies, and their possible sources of errors. Townsend also reviews her own custom made transient wire and the experimental features and procedures that were developed for it, to test several different types of nanofluids for effective thermal conductivity.

Joseph G. Bleazard and A. S. Teja [103] discuss a custom made transient hot-wire measurement apparatus for the measurement of the effective thermal conductivity of electrically conductive liquids. The instrument is based upon a glass capillary tube filled with Mercury which acts as an insulated hot wire. This is used in conjunction with current conduction laws to calculate the effective thermal conductivity of nanofluids to within 2% accuracy. This particular work is unique in that the experimental technique and methodology described by the author can be used with extremely high temperatures, up to 493 K and prevents current leakage to the nanofluid.

2.4.9. Nanofluid Review Conclusions

The current and ongoing work in the field of nanofluid science is extensive and growing every day. It will need to be even more so to fully reach its potential as the world's next generation coolants. As of now, the field of nanofluids is still in its infant stages. Many of the current works and researchers differ greatly in terms of their experimental results ideas. Indeed, a consensus has not been reached on many of the key subjects within nanofluid science. A great deal of work is required to bring each aspect of the field of nanofluids into alignment, and to create a truly comprehensive and general agreement on the properties, behavior, and governing theories of nanofluid science. This entire section on the current literature of nanofluids has provided valuable insight into the expected behavior of the cryogenic nanofluids being studied in this research. In addition, this review has provided a good background in terms of the author's general understanding of nanofluid science.

2.5. Cryogenics Literature Review

2.5.1. Introduction

The term Cryogenics is based upon the ancient words for "freezing mixture," and "to produce," and in our modern technical world refers to a state of very low temperature, and the study of the physical phenomena and material characteristics that occur at those temperatures. For this research cryogenics will refer to the physical and thermal properties of cryogenic liquids, which are room temperature gases that have liquefied at extremely low temperatures. Specifically, cryogens will be referenced as any liquid or gas that exists in a non-solid state below 123 K [104].

Due to the fact that this research is based upon the concept of changing the inherent effective thermal conductivity of liquid oxygen, a complete understanding of the fundamental properties of pure LOX was absolutely required. This was accomplished through several means, the primary

being the use of the National Institute of Standards and Testing (NIST) online Chemistry Web-book. This online resource has an interactive table/graph representation of the pure properties of both LOX, and LN2. These web published results are based upon a series of papers presented in the Web-book's reference section. These literature works, among others, were used to provide the individual data sets, and validation for the all-encompassing picture presented on the website [105].

For this research some of NIST web-books contributing authors and their papers were reviewed, and used to obtain a more complete picture of the salient thermal and physical properties of both LOX, and LN2. A thorough sampling of these NIST references along with several other literature sources will be presented below. The thermo-physical properties of both LOX and LN2 will be explored, along with a review of their corresponding boiling curves, which were used in the analytical theory and design portion of this research. A brief review of the methods used by the respective authors in the determination of these properties is also presented. The thermal and physical properties of both LOX and LN2 were investigated for this work. However, due to the fact that LOX was used as the primary base fluid, a great deal more attention was focused on it. LN2 on the other hand was explored for its cooling and insulating properties, and for the future possibility of using it as the primary base fluid. A selection of the thermophysical properties which are required for the study of this research are presented below.

- LOX/LN2 boiling point, freezing point, liquid range
- LOX/LN2 boiling curves and the subsequent onset of convection, nucleate boiling, curvature inflection, and critical heat flux.
- LOX/LN2 effective thermal conductivity vs. temperature
- LOX/LN2 density vs. temperature
- LOX/LN2 viscosity vs. temperature

- LOX/LN2 heat capacity vs. temperature
- LOX/LN2 thermal diffusivity vs. temperature
- LOX/LN2 Density vs. temperature
- Etc.

2.5.2. History of Cryogenics

The history of cryogens is an interesting one. In fact, the vast majority of the universe is in a cryogenic temperature state. It is only near the more temperate and therefore forgiving regions of our celestial kingdom that the universe exceeds the cryogenic temperature barrier. To obtain a cryogenic liquid the first pioneers of cryogenic science had to discover and quantify the lighter elements of the periodic table. Once this not insignificant task was completed, they had to find a way to cool each gas down to its natural saturation point, and then beyond.

The history of mankind and that of cryogenic liquids dates back to before the time of Lord Kelvin, who demonstrated the existence of absolute zero. Scientists of the time such as Faraday had been able to liquefy most of the readily available gases, save those which required truly cold temperatures. These included oxygen, nitrogen, hydrogen, helium, and the noble gases, among others. It wouldn't be until work of Cailletet and Pictet who successfully liquefied oxygen that our modern era of cryogenics began. This level of discovery would continue through 1908 with Kamerlingh Onnes liquefying helium, and beyond into our current level of science [106].

Such is the importance of cryogenics that our present level of science, technology, and understanding could not exist without it. Cryogens, along with cryogenic temperatures are used in numerous industrial and technological applications, and indeed, many aspects of science cannot be studied outside of the cryogenic temperature range. Therefore, a more complete understanding of the world of the very cold is inherent to our own growth.

2.5.3. Cryogenic Thermo-Physical Properties Review

The thermal transport and physical properties of both LOX, and LN2 have long been explored, and current research into cryogenics focuses primarily on more complex features. Therefore, many of the papers presented in this review will be relatively dated. It should also be noted that for this research the only properties of interest were those of thermal conductivity, vaporization temperature and pressure, fluid density, fluid specific heat capacity, viscosity, and phase. There exists a delicate balance between the fluid temperature ranges of LN2 and LOX which dictates that LN2 can be used as a coolant for LOX. Therefore, LOX was chosen as the actual working base host fluid for the cryogenic nanofluids created in this research. Therefore, LOX is of primary importance in terms of quantifying its physical and thermal properties. It should be noted however that the following research papers on the thermo-physical properties of LN2 do not cover the measurement or quantification of thermal conductivity. As was stated before, this information is not critical, and can in fact be determined from NIST data. It should be noted that LN2 is one of the most widely used low temperature coolants. Therefore, a great deal of interest exists in terms of its potential for thermal transport and physical enhancement. The use of LN2 as the base fluid within a cryogenic nanofluid will eventually necessitate its quantification.

2.5.3.1. Liquid Oxygen & Liquid Nitrogen Thermo-Physical Properties

L. A. Hall [107] from the National bureau of standards presented a government report/bibliography to the department of commerce on the thermal conductivity of ten selected cryogenic liquids. The reviewed liquids included several types of Helium, noble gases, common mixture gases, and Oxygen. This paper consisted of a literature review and did not in general give specific data. Instead it simply referenced where that data could be found. For the purposes of this

thesis, the work by Hall provided a good starting point for the determination of what resources exist in terms of thermal transport properties for various cryogenic liquids.

A. Laesecke et al. [108] presented a rather complete listing of the then current research into the thermal properties of pure LOX. This paper focused on the data evaluation and a comprehensive literature review of both the thermal conductivity, and viscosity of pure LOX. Data was collected, correlated, and collated to form property tables for both viscosity and thermal conductivity for pressure ranges of 0.1 MPa to 100 MPa, and temperatures from 70 K to 1400 K. The research also presented transport equations and residual comparisons between data sets among other things. This paper was used for its thermal conductivity data tables from 70 K to 90 K for local ambient pressure values. This paper was not singular with this information, however, it provided a good review and confirmation of the relevant thermo-physical properties needed in the study of cryogenic nanofluids.

A joint research paper written by B. A. Younglove [109] from the NBS, and the Center for Applied Thermodynamics (CATS) from University of Idaho presented the thermo-physical properties of several cryogenic fluids including LOX. This work presented a fairly complete review of the more important thermal properties such as density, thermal conductivity, internal energy, enthalpy, entropy, heat capacity etc. as they vary with pressure and temperature. This paper also presents a standard set of predictive equations for the determination of thermo physical properties of the selected cryogenic fluids. For the purposes of this research, this paper was utilized as an exceptional overall review of the behavior, and properties of the reported fluids. This included triple points for numerous elements, and mixtures, comprehensive data tables, theories, and predictive equations etc.

R. J. Richards et al. [110] from the National Bureau of Standards presented a work encapsulating the literature of the time on the heat transfer from solid surfaces to cryogenic fluids.

These fluids encompassed Helium, Hydrogen, Oxygen, and Nitrogen. This work included around 156 distinct papers in its literature review and presented graphical representations of the heat transfer rates from a solid surface to a cryogenic fluid. These rates were found from both theoretically calculated and experimentally determined results along with the natural and forced convection rates ranging from non-boiling to maximum a heat flux. This paper provided a good review of how heat moves within and is transferred to a cryogenic fluid and provided valuable insight into the behavior of the selected thermal conductivity testing method for this research in terms of heat transfer flux, convection, and boiling.

A study on the heat capacity of Liquid oxygen from 12 K to its natural boiling point was presented by W. F. Giauque and H. Johnston [111] from the Chemical Laboratory of the University of California. Giauque studies the paramagnetic properties of Oxygen from its crystalline state to its gaseous state and how this effects its entropy. This research was conducted with the use of a high accuracy calorimetric measurement of Entropy, from roughly 12 K to the boiling point of LOX. This work provided a good, and much needed review and validation of the online chemistry's web book data on specific heat.

D. Celik and S. Van Sciver [112] studied the thermal conductivity of liquid oxygen below 80 K with pressures up to 1 MPa. Their experimental research was based upon the use of a highly accurate horizontal guarded flat-plate calorimeter. They tabulated their answers and compared them to the best literature of the time. This particular review was of great importance to the current work due to the fact that their reported effective thermal conductivity values for LOX where near the cryogenic temperature ranges utilized in the current work.

H. Ziebland and J. Burton [113] presented the thermal conductivity of both liquid and gaseous oxygen as it varies with both temperature (80-200 K) and pressure (1-130 atm). This review was useful, because like the others it provided validation of the NIST results used in this

research. It also provided a table of data values, along with a plot depicting the changes in LOX thermal conductivity with respect to both temperature and pressure.

R. T. Jacobsen et al. [114] completed a comprehensive study of the thermodynamic properties of Nitrogen from the freezing line to 2000 K from pressures up to 1000 MPa. The author provides a new and fundamental equation of the Helmholtz energy for thermodynamic properties of Nitrogen, along with several new independent equations for the vapor pressure, saturated vapor pressure, and liquid densities of LN2. Thermodynamic property tables were included within the defined temperature and pressure ranges. These tables included both isochoric and isobaric heat capacity, along with entropy, enthalpy, density etc. This paper served as a convenient reference for some of the more fundamental properties of LN2, and indeed proved to be quite helpful in validating the NIST data sets.

Roland Span et al. [115] set forth a new formulation for the thermodynamic properties of LN2. The work presents high accuracy recorded interface data for the P, ρ, T, for gaseous, liquid, and supercritical LN2. New instrumentation in the form of sphere resonators allowed superb measurements of the speed of sound, and caloric properties within LN2. In addition, procedures were developed to optimize the structure of the predictive equations of state along with special functional forms for the overall improved thermodynamic data representation near the critical region of LN2. Once again, this literature served as a suitable reference for the basic thermodynamic properties of LN2.

2.5.3.2. Cryogenic Boiling Curves

One of the most difficult aspects of working with cryogenic fluids is their relative phase instability. This is not surprising considering that several hundred degrees separate the temperature of the fluid compared to its environment. Therefore, the onset of natural convection and eventual boiling is of great concern. Especially, when considering that for this research, a

purely stationary fluid is desirable for an accurate and repeatable experimental thermal conductivity test. Therefore, the behavior of both LOX and LN2 near and at their inherent boiling points must be well understood, before any type of experimental design can be considered. For this particular research, the primary boiling information required was exactly how much heat flux, temperature gradient, and time could exist between a heated wire or surface and the subsequent cryogenic liquid. Therefore, detailed boiling curves are required.

V. Polupan [116] worked on the boiling crisis of Oxygen and Nitrogen mixtures. This research focuses primarily on the effect of Oxygen content within Nitrogen based cryogenic devices. Because periodic heating is inherent to cryogenic equipment, thermal fatigue plays an important role. Polupan's research focuses on how to predict the brittle fracture of metalwork based upon the heat transfer from an Oxygen-Nitrogen fluid. This research is valuable, because it presents quite a bit of data on how a liquid nitrogen bath with inherent Oxygen content behaves and boils.

E. G. Brentari et al. [117] from the National Bureau of Standards examined the salient works in the boiling heat transfer for four distinct cryogenic fluids i.e. Oxygen, Hydrogen, Nitrogen and Helium. Brentari presented experimental data collected from other sources on the nucleate film pool boiling of all mentioned cryogenics along with the boiling regimes of each. This work went a great deal of detail on each subject and explored several others. For use in this research the discussion on the behavior of Oxygen and Nitrogen in terms of nucleate pool boiling, boiling regimes, along with the presented data and predictive equations were extremely helpful.

Ping Wang [118] from the University of Southampton in his PhD dissertation presented the thermal bubble behavior of LN2 under electric fields. This work, although slightly off topic, provided one of the first truly viable reviews on the nature of LN2 boiling, and its subsequent boiling curve. It provided the allowable change in temperature i.e. temperature gradient to phase

change, for LN2 as either a host fluid, or the coolant fluid, and allowed the first set of predictive theoretical calculations to be completed for the current research. In addition, this paper provided a great deal of insight into the behavior of cryogenic fluids, and the proper methods of working with them.

Kun Yuan [119] from the University of Florida in his PhD dissertation on the two-phase chill down process and cryogenic boiling when subjected to terrestrial and microgravity gave an invaluable review of boiling heat transfer. This included typical boiling curves and discussions on their component parts, two flow phase regimes, gravity effects, and conduction models, etc. This work was very useful as a general resource on cryogenic boiling behavior.

P. G. Kosky and D. Lyon [120] conducted research into the pool nucleate boiling heat transfer curves for pure Oxygen, Nitrogen, Argon, Methane, and Carbon Tetrafluoride. They used a horizontal, flat, circular disk made of platinum as their sensor system. They varied their measurements from saturation pressures of 1 atm to roughly the critical pressure point for each cryogenic fluid being studied. The authors then compared their results to a variety of existing nucleate boiling correlations. This research was valuable to the current study, due to the fact that it provided insight into the boiling nature of a variety of cryogens.

2.5.3.3. Experimental Measurement of Cryogenic Liquids

Because cryogenic liquids exist at sub-cooled temperatures, the experimental determination of their nature can be quite difficult. This particular research studies the effective thermal conductivity of cryogenic nanofluids, and therefore in essence is based upon a cryogenic liquid measurement. Thus, a review of the more common methods of measurement for the thermal conductivity of a variety of cryogenic liquids is needed.

J. W. Ekin [121] gives an excellent review of some of the most useful, accurate, and common low temperature experimental testing techniques. This work is a complete text on the processes

and techniques for the experimental determination of low temperature properties and serves as an excellent reference for choosing and designing an appropriate measurement technique. For particular case of this research, this work by Ekin was used to learn more about the various techniques and systems that can be utilized in the measurement of a cryogenic nanofluid.

D. Celik [112] presented the design, theory, and use of horizontal, guarded, flat-plate calorimeter for the measurements of the thermo physical properties of LOX. He reported a great deal of stability in terms of temperature and pressure variations. In addition, the accuracy of Celik's experimental system was reported to be better 0.3%. This particular experimental setup was used to determine the thermal conductivity of LOX at and near the desired temperature range for the current study on cryogenic nanofluids. Therefore, it was of interest as a possible design.

David G. Cahill [122] worked on the measurement of thermal properties within a temperature range of 30 to 750 K with the use of a 3ω method. This particular work focused on the measurement of dielectric solids and, bulk amorphous solids, and crystalline structures etc. This research was a useful review in terms of the technique and application of the 3ω method at cryogenic temperatures.

H. Ziebland and J. Burton [123] presented the design and use of a coaxial cylinder method for the measurement of liquid and gaseous oxygen from 80-200 K. The coaxial cylinder method allows the measurement of fluids at high pressures and low temperatures, and is of particular use at cryogenic temperatures because it measure the fluid with an extremely thin fluid film, and in the vertical position, both of which reduces the risk of fluid movement, convection, and boiling. The method relies on the use of a heat emitting inner cylinder surrounded by the test fluid, and a final outer heat absorbing cylinder. Temperature sensors on both the inner and outer cylinders along with the fundamental equation of heat conduction allow for the solution of the thermal

conductivity of LOX. This work once again demonstrates the great care that must be taken when measuring the properties of cryogenic liquids.

2.5.3.4. Cryogenic Fluid Conclusions

This review provided the needed insights into the varied properties of both LOX and LN2 required for this research. These included the temperature depended thermal conductivity, heat capacity, viscosity, phase, etc. each of which were of great enough importance to the current research to require verification by independent sources. In addition, the behavior of LOX and LN2 near their boiling points was quantified, and will be used later in the analytical modeling for the THW experimental setup used in this work. Finally, a great deal of information was gleaned from the historical review of the various experimental methods utilized in the study of cryogenic liquids. Combined, this review provided a working knowledge of cryogenics. The actual thermophysical properties of LOX used in this research are presented below. These values represent the critical information required in the theoretical modeling, experimental prediction, and numerical solution process of the current research. It should also be noted that a great deal of other parameters were studied, and required for the successful completion of this research.

Table 2-1. LOX assorted required thermophysical properties vs. temperature

Temperature (K)	**Thermal Conductivity (W/mK)**	**Density (kg/m^3)**	**Heat Capacity (J/kgK)**	**Viscosity (μPas)**
77	0.17066	1204.7	1679.3	299.12
78	0.16924	1200.0	1679.9	288.40
79	0.16781	1195.3	1680.5	278.29
80	0.16637	1190.6	1681.3	268.74
81	0.16494	1185.8	1682.3	259.72
82	0.16350	1181.1	1683.4	251.19
83	0.16206	1176.3	1684.7	243.11
84	0.16061	1171.5	1686.1	235.44

85	0.15917	1166.7	1687.8	228.18
86	0.15772	1161.8	1689.6	221.27
87	0.15626	1156.9	1693.8	214.71
88	0.15481	1152.0	1696.2	208.46
89	0.15335	1147.1	1698.8	202.52
90	0.15189	1142.1	1699.4	196.85

2.6. Cryogenic Nanofluids

Cryogenic nanofluids are a new subsection of nanofluids and represent a before now unexplored class of enhanced high performance coolants. They consist of a cryogenic host liquid containing nanometer sized solid phase particle inclusions. These nanoparticles alter the base thermal transport and physical properties of their cryogens in a similar fashion as to traditional nanofluids, and thus allow an exciting new type of super coolant to be created. The discoveries that led up to the creation and testing of cryogenic nanofluids consists of the joint research into nanoparticles, cryogenics, and nanofluids. Therefore, their history is that of the combined research and discovery that went into the creation of their parent sciences. Because cryogenic nanofluids are a completely new type of nanofluid, there is no previous work, or literature pertaining to them. Indeed this will be the first of such. Therefore, any review would be impossible. The best that can be done are the extensive reviews into each of the parts that went into the creation of these CN's.

2.7. Summary

The field of nanofluid science is ever growing and exceedingly complex. This is primarily a result of the fact that the general field of nanofluids covers so many different topics, which include, but are certainly not limited to, the measurement of their thermo-physical and thermal transport properties, as well as, their production, stability, lifetime and ultimate usefulness. In addition, a great deal of research is focused on the basic nature, theory and predictive modeling of

various nanofluids and how nanoparticles shape, size, and other physical characteristics etc. combine with the nature of the host fluid to affect the thermal conductivity of a nanofluid. This review established the foundations for each of the salient aspects of nanofluids as they relate to the current research and identified the most common and useful methods of thermal conductivity measurement, specifically those techniques which apply to the quantification of the effective thermal conductivity of cryogenic nanofluids

CHAPTER 3

TRANSIENT HOT WIRE THEORY

3.1. Significance

To fully understand the nature of any physical phenomena we must first be able to describe and predict its behavior. To accomplish this we must determine what its governing equations are and what constraints apply to it. The information presented in this chapter is fundamentally that of a basic understanding of thermal conductivity and general thermal transport. Therefore, a great deal of the following work is based upon the information in fundamental heat transfer texts [1, 124-126].

3.2. Introduction

In this chapter we will be discussing the nature, general theory, and derivations of the Transient Hot Wire, the predictive temperature vs. time equations based upon this derivation, and the analytical design process that went into the creation of the experimental setup and numerical code used for this research.

3.3. Transient Hot Wire Theory and Models

3.3.1. Background

The transient hot wire thermal conductivity measurement technique is widely used to measure the thermal conductivity of solids and liquids. It works on the principle that a material's electrical resistivity is directly related to its temperature. This relationship is exploited by modern advanced data acquisition systems to back equate a thermal conductivity value.

A long thin metallic wire (which negates the wires own thermal effects), with a well-known relationship between electrical resistivity and temperature, is suspended either vertically or horizontally in the material whose thermal conductivity is to be measured. The wire is than heated

by sending a constant power through the wire thus energizing it. At this point the wire is acting as both a line heat source for the outer surrounding medium, and as a highly accurate temperature sensor for the wire itself and the localized material around the wire. During the constant power heating process the change in either the resistance of the suspended wire or the voltage drop across the wire is measured and this value along with the full knowledge of the total power used to energize the system allows the thermal conductivity of the surrounding medium to be calculated. Further information on the exact theory and working mechanisms of the THW system can be reviewed within the literature review chapter of this thesis.

To make full use of the Transient Hot Wire method we need to derive its general theory as well as the equations that predict its behavior. To this end the next two sections will focus on the THW governing and predictor equations. It should be noted that the transient hot wire technique assumes that pure conduction is the only mode of heat transfer present throughout the test. Convection is neglected due to the speed of the test, and the small heat fluxes present. While radiation is neglected because of the relatively low temperature differences present between the wire and the surrounding medium. Therefore, if the test is setup properly, it can be assumed that conduction is the only form of heat transfer present.

3.3.2. General Governing Equation

The general equation governing the THW method is that of the fundamental heat equation in cylindrical coordinates, which can be seen below in eq. (3.1). This equation describes the total possible heat transfer from a stationary, isotropic cylindrical body. Once again, the information below is derived from basic thermal transport texts [124-126].

$$\frac{1}{r}\frac{\partial}{\partial r}\left(kr\frac{\partial T}{\partial r}\right)+\frac{1}{r^2}\frac{\partial}{\partial \phi}\left(k\frac{\partial T}{\partial \phi}\right)+\frac{\partial}{\partial z}\left(k\frac{\partial T}{\partial z}\right)+\dot{q}=\rho c_p\frac{\partial T}{\partial t} \tag{3.1}$$

Above, (r,φ,z) denote cylindrical coordinates, T(t,r,φ,z) is the temperature, based upon location and time. The isotropic medium's constant material properties include the thermal conductivity k, the heat capacity c_p, and the density ρ. The expression also includes the possibility that the body generates its own heat in the form of cylindrical body volumetric heat generation $\dot{q}$. The left hand side of the equation describes the radial, azimuthal, and vertical heat flux components as well as the full body generation term, whereas the right hand side governs the hot wires temperature transience, which allows the total heat transfer of the cylindrical body to be time dependent.

A simplified form of this general equation will be used to describe the THW technique. The hot wire and its surrounding medium will be modeled as concentric cylinders with the wire being the inner cylinder, and the material of interest the outer. To create a solvable analytic model for the material of interest, we will focus on the outer cylinder only and let the inner hot wire cylinder act as a boundary condition, as shown below in figure 3-1.

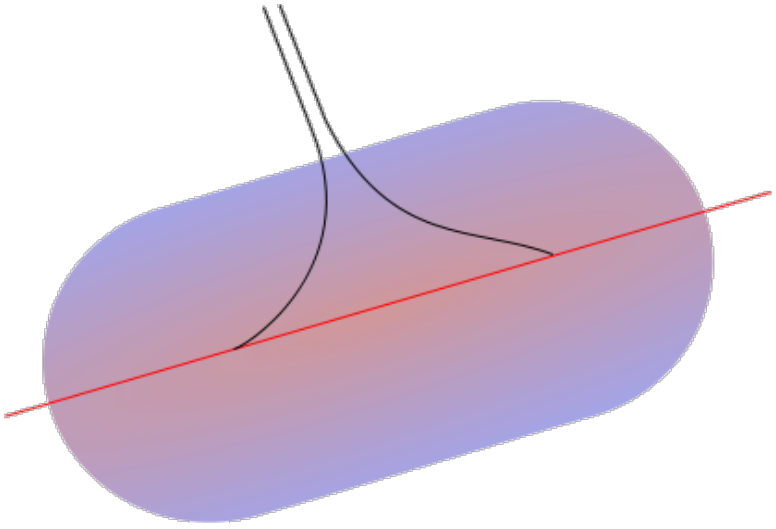

Figure 3-1. Thermal gradients within a simulated cylindrical body of fluid with energizing hot wire (hypothetical sensor leads attached).

The THW model assumes that the heat generation of the infinitely long and thin wire is solely produced by the wire, and only in the radial direction. Therefore, both the φ and z heat flux terms may be neglected along with the body generation term. Therefore, a reduced form of the equation eq. (3.3) can be derived by retaining and rearranging only the radial heat flux and transient terms and noting that the thermal diffusivity of a material is related to the conductivity as shown in eq. (3.2).

$$\alpha = \frac{k}{\rho c_p} \tag{3.2}$$

This yields the reduced general heat equation

$$\frac{1}{\alpha}\frac{\partial T}{\partial t} = \frac{1}{r}\frac{\partial}{\partial r}\left(r\frac{\partial T}{\partial r}\right) \tag{3.3}$$

This is an example of the general Fourier's equation with boundary conditions of constant heat generation at the center of the cylindrical medium and constant temperature at the infinite boundaries of the medium. Explicitly, the boundary conditions (BC's) for this case can be seen in eq. (3.4) and (3.5) below.

For t=0 and r=0

$$\lim_{r\to 0}\left(r\left(\frac{\partial T}{\partial r}\right)\right) = -\frac{q_w}{2\pi k_f} \tag{3.4}$$

where q is the heat liberated per unit time per unit length of the line source in W/m and k_f is the thermal conductivity of the fluid in W/mK.

For $t \geq 0 \; and \; r = \infty$

$$\lim_{r\to\infty}(T(r,t)) = 0 \tag{3.5}$$

An initial time condition (IC) dictating the behavior for the system with respect to time is also required. This IC will take the form provided in equation 3.6.

$$System\ Temperature = constant = 0 \; at \; t = 0 \tag{3.6}$$

The actual hot wire setup can quite easily meet these boundary conditions by making the diameter of the wire much smaller than either the length of the wire or the diameter of the surrounding medium. In addition, by supplying either a constant power or a constant current the heat generation can be made continuous. It should be noted that for the ideal case, of the THW method, the line source (in practice, a platinum hot wire for example) is considered to have an infinite thermal conductivity as well as zero heat capacity. These are reasonable assumptions due to the fact that the thermal conductivity of the platinum should be much higher than that of the surrounding medium and the small volume of the wire ensures that its heat capacity is also negligible. The general Fourier's equation can be solved by using the solution presented by Carslaw and Jaeger [124]. This particular solution will be studied in greater detail in the next section. For now we note that their solution provides the change in temperature vs. time of the medium at any radial distance r and is given in eq. (3.7). This equation is an analytical model of the temperature response of a material to a centralized continuous line heat source. It will be derived in the next section.

$$\Delta T(r,t) = T(r,t) - T_0 = \left(\frac{q_w}{4\pi k_f}\right) Ei\left(\frac{r^2}{4\alpha_f t}\right) \tag{3.7}$$

where from the equation above, α_f is the fluid's thermal diffusivity, and T_0 is the environmental temperature at the initial time. This can be rewritten in a series expansion as shown below in eq. (3.8).

$$\Delta T = \frac{q_w}{4\pi k_f}\left\{-\gamma + ln\left(\frac{4\alpha_f t}{r^2}\right) + \left[\frac{\frac{r^2}{4\alpha_f t}}{1\cdot 1!} - \frac{\left(\frac{r^2}{4\alpha_f t}\right)^2}{2\cdot 2!} + - \cdots + \cdots\right]\right\} \tag{3.8}$$

with γ=0.5772 being Euler's constant. The series expansion shown above can be simplified, by neglecting any higher order terms, to eq. (3.9) below. These simplifications will cause the analytical solution to become an approximation. However, much of the accuracy will be retained, certainly enough for the experimental procedure.

$$\Delta T = \frac{q_w}{4\pi k_f} ln\left(\frac{4k_f t}{r^2 \rho_f c_{pf}}\right) - \frac{\gamma q_w}{4\pi k_f} \tag{3.9}$$

The temperature change at any fixed radial point in the surrounding cylindrical medium for two time samples is shown in eq. (3.10) below.

$$\Delta T_2 - \Delta T_1 = \frac{q_w}{4\pi k_f} ln(\frac{t_2}{t_1}) \tag{3.10}$$

This equation can then be simplified to form the transient hot wire governing equation which is shown below in eq. (3.11).

$$k_f = \frac{q_w}{4\pi(T_2 - T_1)} ln(\frac{t_2}{t_1}) \tag{3.11}$$

Equation (3.11) creates a linear relationship between the changes in temperature of the surrounding material at some point close to the surface of the wire, with respect to the natural logarithm of time. Basically, by energizing the hot wire and measuring the slope of the resistance vs. time of the hot wire, the thermal conductivity of the surrounding medium can be found.

3.4. THW Temperature vs. Time Models

3.4.1. Introduction

In the previous section we provided the general governing equation for the THW experimental system. This was done by utilizing the solution to the general conduction equation by Carslaw and Jaeger and P. Vadasz [124, 127]. In this next section we will explore in detail the derivation of their solution along with the temperature vs. time models born from it.

3.4.2. Background

The model originally presented by Carslaw and Jaeger and P. Vadasz [124, 127] assumes through the use of the far field boundary condition, Eq. (3.12), that the temperature at an infinite radial location eventually reaches a state of thermal equilibrium. However, in all real world situations a small constant heat flux exists through said far field boundary. In fact each assumption made by the general governing equation can and should be questioned. Therefore, it must be determined whether the Carslaw and Jaeger assumptions are valid for the experimental setup of this work. To this end a number of additional models, which do not employ the same assumptions, are introduced and compared in this chapter. It will be concluded that the Carslaw and Jaeger model is in fact perfectly valid over the time, temperature, and energy scales being studied in this research.

$$\lim_{r\to\infty}(T(r,t)) = Constant \tag{3.12}$$

In addition to these theoretical concerns, the change in temperature of the fluid is one of the most important factors in the design of a cryogenic hot wire setup. If a room temperature fluid was used temperature gradients would not be of great importance due to the fact that a wide and stable range of liquid values exist before any great fluid instabilities/phase changes occur due to convection, density based buoyancy, or boiling. However, because a cryogenic liquid is already in an environment several hundred Kelvin hotter than its saturation point, a cryogenic fluid can become extremely unstable. Large fluid currents develop as heat fluxes enter the experimental containment area and large scale convection and fluid turbulence can occur. Basically, a cryogenic fluid surrounded by a room temperature environment will be in a constant state of boiling and motion. Therefore, the behavior of the selected cryogens (LN2 and LOX) around there saturation points and the temperature ranges used in this research need to be analyzed. To accomplish this, a temperature vs. time model for a THW must be developed. The following

discussions will present three of the more common methods for infinitely long and thin hot wire temperature analysis. Each has aspects which make it appealing for use in this work, and each will be compared to the others to determine which model is the most useful for the temperature analysis of this research.

3.4.3. Instantaneous Line Heat Source

We return now to the system introduced in Section 3.2.2. One of the first truly widespread and usable models of transient 1D cylindrical line source heating was created by Carslaw and Jaeger [124]. This model will predict the temperature change vs. time at any radial distance r of a cylindrical medium with an infinite line heat source at its center. The majority of this particular derivation was based upon the work of P. Vadasz [127].

When a long wire having a thin finite diameter, is energized by a set current, *I*, the flow of electrons is resisted (measured by the resistance, R_w in Ω) by the materials inherent electrical resistivity, ρ_{ew} (in Ω·m), and the wire dimensions of length L (in m), and area A (in m^2) as shown below.

$$R_w = \rho_{ew}\left(\frac{L_w}{A_w}\right) \tag{3.13}$$

This resistance generates a power per unit length via Ohm's law

$$q'_w = \rho_{ew}\left(\frac{I_w^2}{A_w}\right) \tag{3.14}$$

A THW system operates by converting the electrical power generated within the hot wire to a liberated heat flux density, q_f, in the fluid near the hot wire. This is accomplished by noting that the generated power of the wire per unit length is equal to the thermal power of the fluid as the radius in question approaches that of the wire. This is proven through the use of the general Fourier equation [124-126].

$$q_f = k_f A\left(\frac{\Delta T}{\Delta r}\right) \tag{3.15}$$

Where ΔT measures the temperature difference over the distance from the wire $\Delta r = r - r_w$, and A represents the surface area over which the thermal gradient acts. This can be compared to the THW electrical power by noting that the two powers become equal as the separating distance from the wire becomes small.

$$q'_w = \rho_{ew}\left(\frac{I_w^2}{A_w}\right) = \frac{q_f}{L_w} = \frac{2\pi k_f r_w L_w\left(\frac{\Delta T}{\Delta r}\right)}{L_w} \tag{3.16}$$

This heat flux can be converted from per unit length (W/m) into the corresponding amount of radial heat flux from the energized wire to the surrounding medium by multiplying the heat flux of the wire by the per unit length surface area of the wire. The differential temperature with respect to radial position is directly derived from the definition of heat flux and is referenced to a specific starting temperature as shown below.

$$\begin{aligned} q'_w = \left(q_f\right)_{r=r_w} \cdot \frac{(2\pi r_w L_w)}{L_w} = 2\pi r_w \cdot \left(q_f\right)_{r=r_w} = -2\pi r_w k_f \left(\frac{\partial T}{\partial r}\right)_{r=r_w} \\ = -2\pi k_f \left(r\frac{\partial T}{\partial r}\right)_{r=r_w} \end{aligned} \tag{3.17}$$

At this point, we will study the temperature of the surrounding fluid by returning to the general simplified 1D heat equation for a cylindrical body.

$$r\frac{\partial T}{\partial t} = \alpha\frac{\partial}{\partial r}\left(r\frac{\partial T}{\partial r}\right) \tag{3.18}$$

We will employ the source term shown in eq. (3.16) as an inner heat flux boundary condition in the limit as r approaches r_w, which is taken to be effectively zero. In addition to this center flux boundary condition, the cylindrical body is subjected to an outer constant temperature boundary condition, and an initial condition of zero temperature. Therefore, the boundary and initial conditions that govern this model are:

Boundary Conditions:

Inner

$$-\frac{q'_w}{2\pi k_f} = \lim_{r_w \to 0}\left(r\frac{\partial T}{\partial r}\right)_{r=r_w} \tag{3.19}$$

Outer

$$T = constant = 0 \; at \; r = \infty$$

Initial Condition:

$$T = constant = 0 \; at \; t = 0 \tag{3.20}$$

The solution to the Carslaw and Jaeger model is obtained by introducing a Boltzmann transformation. This is done by creating a dimensionless similarity variable η.

$$\eta = \frac{r^2}{4\alpha t} \tag{3.21}$$

where α is the thermal diffusivity as defined in Eq. (3.2). By taking the first and second derivatives of η and replacing the terms in eq. (3.18) with the corresponding derivatives of η, a new dimensionless governing ODE is created.

$$\frac{\partial}{\partial \eta}\left(\eta\frac{\partial T}{\partial \eta}\right) + \left(\eta\frac{\partial T}{\partial \eta}\right) = 0 \tag{3.22}$$

The boundary and initial conditions are transformed into dimensionless parameters as well, by substitution of η. The outer cylindrical wall boundary condition along with the systems initial condition are combined in terms of η, and the inner boundary flux condition is modified similarly.

$$\eta = \infty \; at \; T = 0 \tag{3.23}$$

$$-\frac{q'_w}{2\pi k_f} = \lim_{\eta \to 0}\left(2\eta\frac{\partial T}{\partial \eta}\right)_{\eta} \tag{3.24}$$

The new general governing eq. (3.22) combined with the modified boundary conditions and initial condition form the components of a second order ODE. This equation can be solved by first creating a variable Φ that encompasses the first order terms. This is shown below.

$$\Phi = \left(\eta \frac{\partial T}{\partial \eta}\right) \tag{3.25}$$

At this point, the ODE has been transformed from a second order to first order equation.

$$\Phi + \left(\frac{\partial \Phi}{\partial \eta}\right) = 0 \tag{3.26}$$

This simplified ODE has a solution of the general form.

$$\Phi = \left(\eta \frac{\partial T}{\partial \eta}\right) = A_0 e^{-\eta} \tag{3.27}$$

where A_0 is simply a constant. By integrating this general solution we obtain.

$$T = A_0 \int \frac{e^{-\eta}}{\eta} + B_0 \tag{3.28}$$

where B_0 is an integration constant. Finally, by introducing the transformed boundary conditions in eq. (3.23) and (3.24) and substituting them into the general solution presented in eq. (3.28) we can derive the general equation for the temperature at any radial point in a cylindrical body with constant center line heating.

$$T = \frac{q'_w}{4\pi k_f} \int_\eta^\infty \frac{e^{-\eta}}{\eta} d\eta = \frac{q'_w}{4\pi k_f} Ei(\eta) = \frac{q'_w}{4\pi k_f} Ei\left(\frac{r^2}{4\alpha t}\right) \tag{3.29}$$

where the exponential integral function $\mathrm{Ei}(\eta)$ is defined as

$$Ei(\eta) = \int_\eta^\infty \frac{e^{-\eta}}{\eta} d\eta \tag{3.30}$$

This equation will be used later as an analytical model to numerically curve fit the experimentally determined hot wire temperature vs. time data sets. Below (figure 3-2) is a graphical representation of the analytical temperature vs. time curves of the Carslaw and Jaeger model for a variety of potential THW current (I_w) values used in this research.

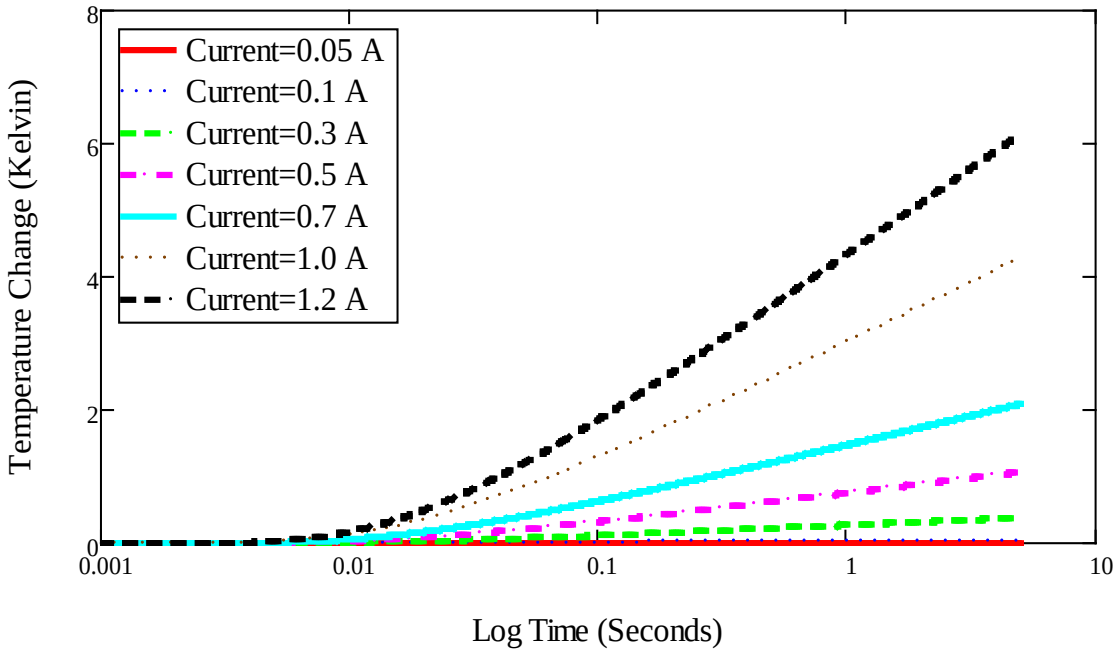

Figure 3-2. Temperature vs. time model (based upon eq. (3.29)) of an infinite line heat source undergoing instantaneous constant heating by a variety of energizing currents.

3.4.4. Pulsed Finite Line Heat Source

Another model for the transient change of temperature within a cylindrical body with center line heating is presented by Kluitenberg et al. [128]. This model will take into account the temperature reaching a period of steady state vs. time. In addition, it will allow for the real world situation of a finite length heat source. The same general assumptions that were assumed with the previous models apply to this one, and the general derivation begins with the Carslaw and Jaeger model [124].

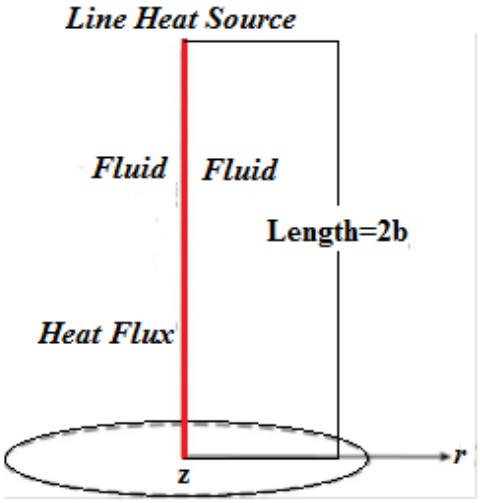

Figure 3-3. Simplified Infinite line heat source, used for the visualization of the various line heat source temperature vs. time models. Adapted from Peter Vadasz [127].

Kluitenberg presents a modification of the general Carlsow and Jaeger model which will not be re-derived here.

$$\Delta T = -\frac{q'_w}{4\pi k_f} Ei\left(-\frac{r^2}{4\alpha_f t}\right) \; for \; 0 < t < t_1 \tag{3.31}$$

The analytical solution for an instantaneous release of heat from an infinitesimally small center line heat source of length 2b (figure 3-3) into a surrounding medium with constant properties is determined by starting from the solution presented by Carslaw and Jaeger in eq. (3.31). It should be noted that this solution is valid for any radial point r, or axial point z at any time t. The instantaneous release of heat at a given point within the medium is described by

$$T(r,z,t) = \frac{Q}{8\left(\pi\alpha_f t\right)^{\frac{3}{2}}} \cdot e^{\left(-\frac{(r-r')^2+(z-z')^2}{4\alpha_f t}\right)} \tag{3.32}$$

where r', z' are arbitrary radial and axial locations of instantaneous heat release from the thermal source in (m). Q is the source strength per unit length in ($m^2 \cdot K$) and is defined as

$$Q = \frac{q'_w}{VHC_f} \tag{3.33}$$

where q'_w is the heat input of the wire to the medium per unit length in (J/m), and VHC is the volumetric heat capacity of the medium in (J/m^3·K). By integrating a series of point heat fluxes of strength Qdz' along the axial line heat source, from axial z location -b to b and setting the radial point to zero $r' = 0,\ z'$, we can obtain the following.

$$T(r,z,t) = \frac{Q}{8(\pi\alpha_f t)^{\frac{3}{2}}} \cdot e^{\left(-\frac{r^2}{4\alpha_f t}\right)} \cdot \int_{-b}^{b} e^{-\left[\frac{(z-z')}{\sqrt{4\alpha_f t}}\right]^2} dz' \tag{3.34}$$

At this point the following substitution can be made to simplify the analysis.

$$X = \frac{(z-z')}{\sqrt{4\alpha_f t}} \tag{3.35}$$

in which X is simply a variable. This allows a rewrite of the previous eq. (3.34).

$$T(r,z,t) = \frac{Q}{4\alpha_f t(\pi)^{\frac{3}{2}}} \cdot e^{\left(-\frac{r^2}{4\alpha_f t}\right)} \cdot \int_{z-b/\sqrt{4\alpha_f t}}^{z+b/\sqrt{4\alpha_f t}} e^{-X^2} dX \tag{3.36}$$

which can then be presented as

$$T(r,z,t) = \frac{Q'}{8\pi\alpha_f t} \cdot e^{\left(-\frac{r^2}{4\alpha_f t}\right)} \cdot \left\{ erf\left[\frac{(b+z)}{\sqrt{4\alpha_f t}}\right] + erf\left[\frac{(b-z)}{\sqrt{4\alpha_f t}}\right]\right\} \tag{3.37}$$

If the transient heating line is placed at the center of the surrounding medium at $(z = 0)$ the following simplification can be applied.

$$T(r,t) = \frac{Q'}{4\pi\alpha_f t} e^{\left(-\frac{r^2}{4\alpha_f t}\right)} \left\{ erf\left[\frac{(b)}{\sqrt{4\alpha_f t}}\right]\right\} \tag{3.38}$$

This solution can now be modified for the case of pulsating heating fluxes. This approach is outlined by Kluitenberg and Carslaw and Jaeger [124, 128].

$$T(r,t) = \frac{1}{4\pi\alpha_f} \cdot \int_0^t \phi(t') \cdot \frac{\left[e^{\left(-\frac{r^2}{4\alpha_f (t-t')}\right)} \cdot \left\{ erf\left[\frac{(b)}{\sqrt{4\alpha_f (t-t')}}\right]\right\}\right]}{(t-t')} dt' \tag{3.39}$$

where t' is an arbitrary point in time in (s). Due to the fact that the line heat source is pulsating, two separate heating regimes will exist, one for heating, and one for cooling.

Therefore, for pulsed heat input

$$\phi(t) = \begin{cases} Q'; & 0 < t \leq t_0 \\ 0; & t > t_0 \end{cases} \tag{3.40}$$

$$T(r,t) = \begin{cases} T_{heating}(r,t) & 0 < t \leq t_0 \\ T_{Cooling}(r,t) & t > t_0 \end{cases} \tag{3.41}$$

which introduces $Q^{'}$, a source strength term ($m^2 \cdot K/s$).

$$Q' = \frac{q'}{VHC} \tag{3.42}$$

This corresponds to the heating and cooling equations.

$$T_{Heating}(r,t) = \frac{Q'}{4\pi\alpha_f} \cdot \int_0^t \frac{\left[e^{\left(-\frac{r^2}{4\alpha_f(t-t')}\right)} \cdot \left\{ erf\left[\frac{(b)}{\sqrt{4\alpha_f(t-t')}} \right] \right\} \right]}{(t-t')} dt' \tag{3.43}$$

$$T_{Cooling}(r,t) = \frac{Q'}{4\pi\alpha_f} \cdot \int_0^{t_0} \frac{\left[e^{\left(-\frac{r^2}{4\alpha_f(t-t')}\right)} \cdot \left\{ erf\left[\frac{(b)}{\sqrt{4\alpha_f(t-t')}} \right] \right\} \right]}{(t-t')} dt' + \frac{1}{4\pi\alpha_f} \cdot \int_{t_0}^{t} 0 \, dt' \tag{3.44}$$

Finally, the following simplification and substitution can be made.

$$u = \frac{r^2}{4\alpha_f(t-t')} \tag{3.45}$$

Therefore, the final temperature vs. time modeling equations for a pulsed finite length heat source are

$$T_{Heating} = \frac{Q'}{4\pi\alpha_f} \int_{\frac{r^2}{4\alpha_f t}}^{\infty} u^{-1} e^{-u} \cdot erf\left(\frac{b}{r}\sqrt{u}\right) du \tag{3.46}$$

$$T_{Cooling} = \frac{Q'}{4\pi\alpha_f} \int_{\frac{r^2}{4\alpha_f t}}^{\frac{r^2}{4\alpha_f(t-t_0)}} u^{-1} e^{-u} \cdot erf\left(\frac{b}{r}\sqrt{u}\right) du \tag{3.47}$$

where the error function is defined by

$$erf(x) = \frac{2}{\sqrt{\pi}} \int_0^x e^{-t^2}\, dt \tag{3.48}$$

A graphical representation of pulsed line heatinf for the current work is shown in figure 3-4.

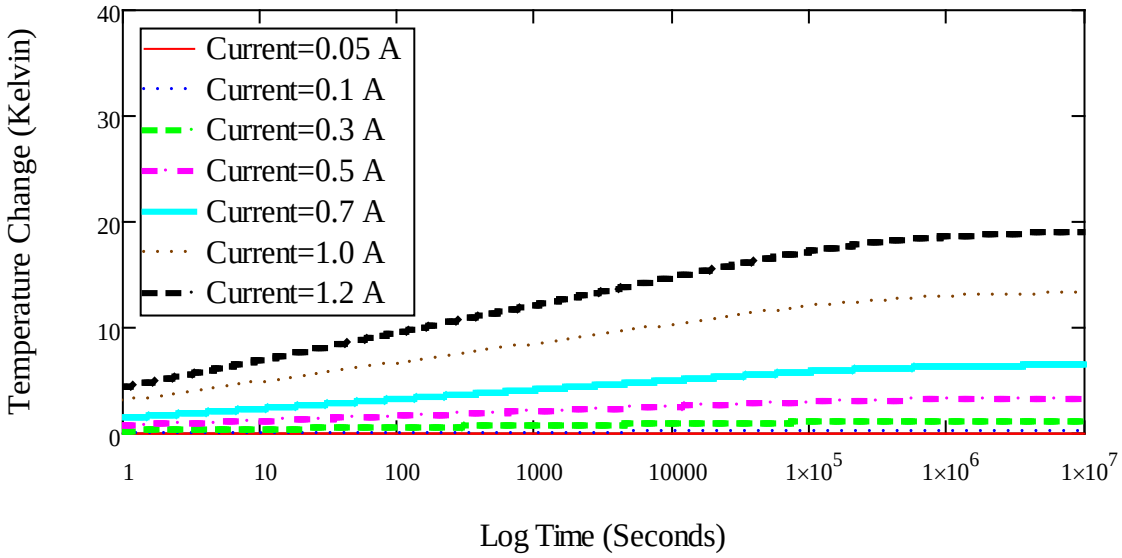

Figure 3-4. Temperature vs. time model (based upon eq. (3.46)) for an finite line heat source undergoing instantaneous heating by a variety of energizing currents.

3.4.5. Semi-Infinite Medium with Embedded Finite Length Heat Source

H. Y. Zeng et al. [129] presents an analytical solution to the transient temperature response of a finite length instantaneously energized line heat source embedded within a semi-infinite medium. This model allows for not only the real world situation of a non-infinite length heat source, but models the behavior of a medium with distinct boundaries as well. This model is used primarily in the analysis of systems for which the traditional simplified equations and their assumptions are not valid. Examples of when such an equation is not only appropriate, but mandatory, are the study of the thermal transience within boreholes, and geothermal heat

exchangers. A similar study done by T. V. Bandos et al. [130] gives additional information on the study of more advanced temperature response equations.

The general assumptions of H. Y. Zeng's derivation are:

- The surrounding medium can be approximated as homogeneous.
- The surrounding medium is at a uniform initial temperature.
- The boundaries of the surrounding medium maintain a constant temperature.
- The radial dimensions of the line heat source are sufficiently small to be neglected, and the line source can be approximated as infinitely small.
- The line heating source produces a constant heat flux.
- The initial temperature of the heating source along with the surrounding medium is a constant until the start time t (s).

The full details of this derivation can be found within the listed references, along with further considerations of the author. By selecting a differential element dh from the line source, which can be modeled as a point source, the temperature change at some given point at time t is represented by

$$dT = \frac{q'_w}{4\pi k_f} dh \cdot \frac{erfc\left(\frac{\sqrt{r^2 + (z-h)^2}}{2\sqrt{\alpha_f t}}\right)}{\sqrt{r^2 + (z-h)^2}} \tag{3.47}$$

where once again k_f and α_f denote the thermal conductivity and diffusivity of the surrounding medium. The total solution for the temperature change of a given point, within the cylindrical body with constant center line heating, can be derived by integrating over the length of the line source and is shown below (figure 3-5).

$$T = \frac{q'_w}{4\pi k_f}\int_0^H \left(\frac{erfc\left(\frac{\sqrt{r^2+(z-h)^2}}{2\sqrt{\alpha_f t}}\right)}{\sqrt{r^2+(z-h)^2}} - \frac{erfc\left(\frac{\sqrt{r^2+(z+h)^2}}{2\sqrt{\alpha_f t}}\right)}{\sqrt{r^2+(z+h)^2}} \right) dh \qquad (3.48)$$

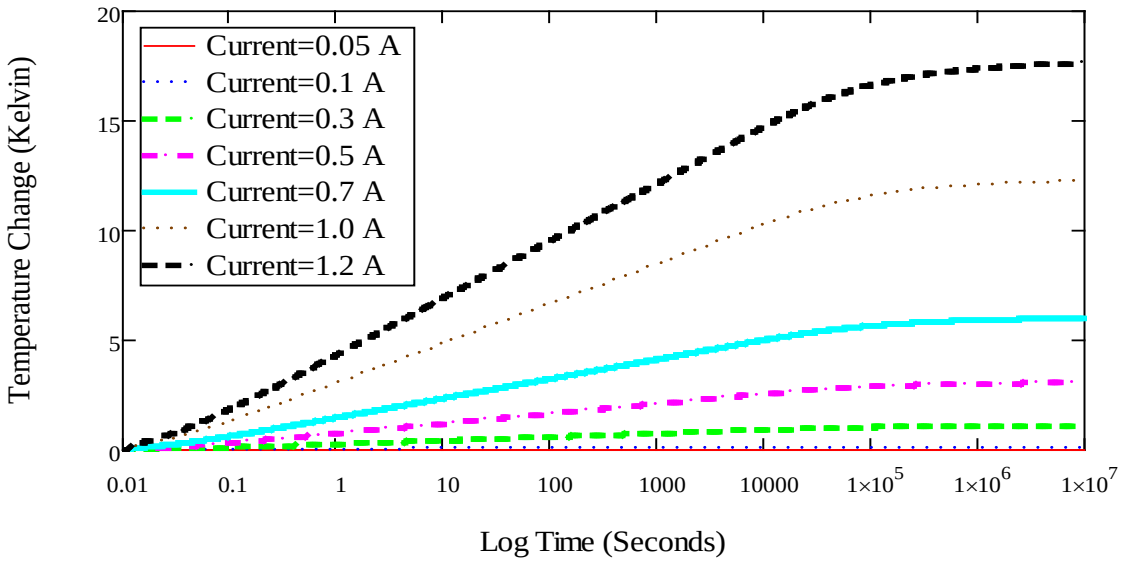

Figure 3-5. Temperature vs. time model (based upon eq. (3.48)) for a semi-infinite medium with a finite constant line heat source with a variety of energizing currents.

3.4.6. Conclusions

These models predict the same transient hot wire behavior all in slightly different ways. The model presented by P. Vadasz will be the most useful for modeling the initial transient heating, due to the fact that it only accounts for the initial and therefore linear heating of the hot wire. However, for designing the analytical model for the experimental setup the other two models will prove to be extremely useful. Therefore, each model will be utilized for this research. A comparison of each can be seen below in figure 3-6. The specific details of the THW modeling is provided in Appendix D of this thesis.

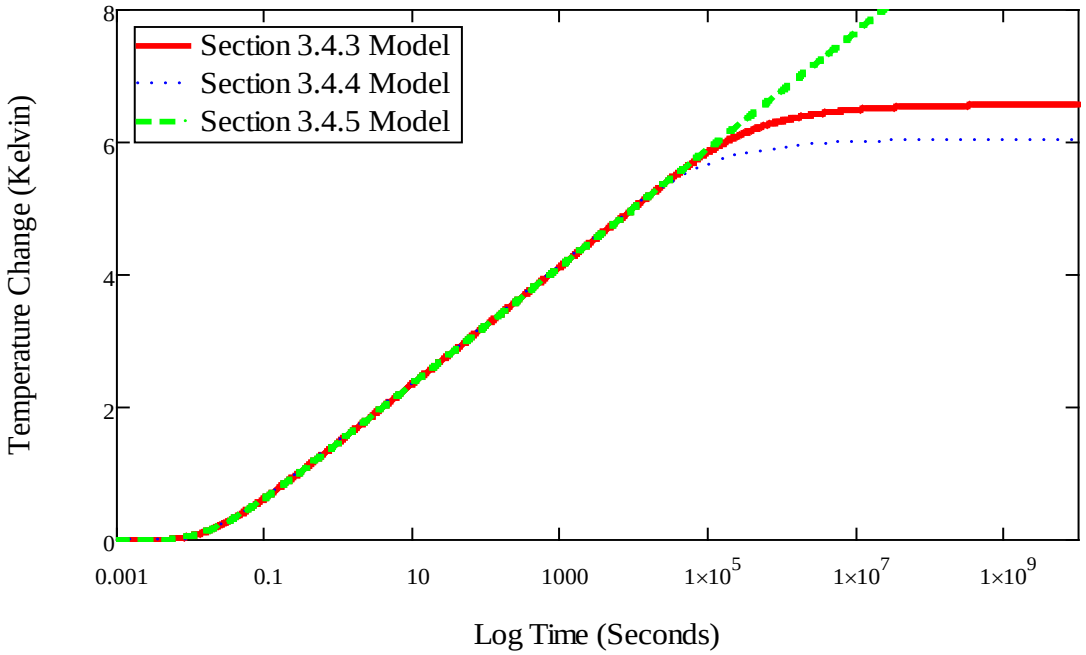

Figure 3-6. Analytical temperature vs. time Model Comparison at 0.7 A.

3.5. Analytical Design/Model

3.5.1. Significance

An analytical model serves as a testing and proving ground for ideas, theories, and experimental designs. This will help to ensure that design flaws, erroneous theories, and costly design mistakes are kept at a minimum. By first running extensive analytical and numerical modeling of any proposed experimental designs a rough estimate of how the system will behave can be created.

3.5.2. Introduction

The purpose of this analytical hot wire design is to create a well thought out transient hot wire experimental setup, that will accurately and repeatable be able to measure the thermal conductivity changes in cryogenic nanofluids.

Several design parameters need to be considered:

- Testing/host fluid type
- Coolant method
- Experimental system limitations
- THW material
- THW physical characteristics.
- THW energizing power
- Method of resistance vs. temperature calculation

3.5.3. Cryogenic Fluids: Host/Coolant

The first design parameter that needs to be determined is that of the testing fluid. The behavior of the transient hot wire will depend greatly on the surrounding medium. Because this research is focused on cryogenic nanofluids, a suitable cryogenic fluid must be chosen. A cryogenic fluid is defined, for the case of this work, as a pure gas that exists as a fluid below 183.25 K at a pressure of 101.3 kPa. A list of some of the more common cryogenic liquids is shown below (table 3-1 and figure 3-7) along with their freezing and boiling temperature points [131].

Ideally, a transient hot wire experimental setup would be enclosed within a cryogenic variable pressure and temperature chamber. This would allow the user to define and set initial temperature and pressure, and vary both of these parameters as desired. This chamber would give a great deal of experimental flexibility to the hot wire setup, and allow work within the entirety of the given cryogenic fluids stable temperature range. In addition, this chamber would allow for the safe handling of toxic, flammable, or otherwise hazardous gases. However, due to expense such a system was not available for this work. Therefore, three separate parameters will go into the

decision process for which cryogenic liquids will act as the base and coolant fluids for the cryogenic nanofluids.

Table 3-1. Assorted cryogenic fluid boiling and freezing points.

Fluid #	Cryogenic Fluid	Boiling Point (Kelvin)	Freezing Point (Kelvin)
1	Helium	4.22	1.0-1.5
2	Hydrogen	20.28	14.01
3	Neon	27.07	24.56
4	Oxygen	90.2	54.36
5	Nitrogen	63.15	77.36
6	CO	82	68
7	Fluorine	85.03	53.53
8	Argon	87.3	83.8
9	Methane	109-113	90.7
10	Krypton	119.93	115.79
11	Nitric Oxide	121	109
12	NF3	144	66
13	Xenon	165.03	161.4

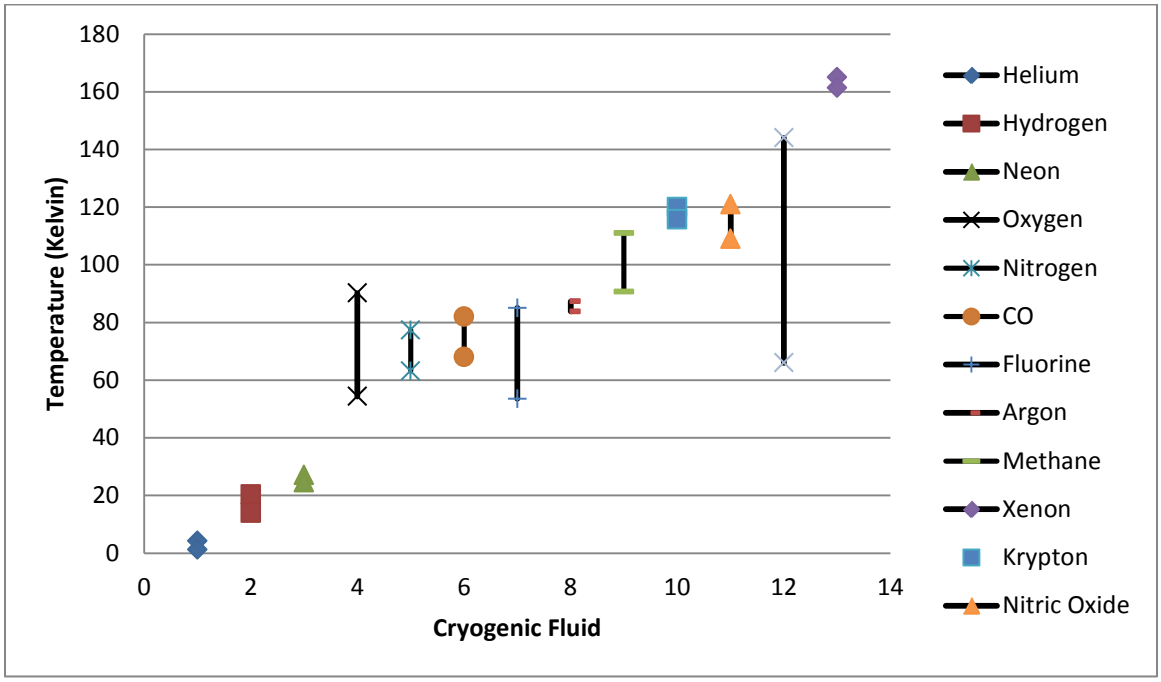

Figure 3-7. Assorted cryogenic fluid boiling and freezing points

The first will be common thermal uses. Many of these fluids do not serve the general purposes of thermal transfer. Therefore, while creating cryogenic nanofluids with them, would be a useful intellectual and scientific process. It would not prove to be useful in terms of commercial or industrial applications. The two most common coolants in the cryogenic list are liquid nitrogen, and liquid helium. Therefore, they will both be considered for use.

Another concern is that of danger. Many of the cryogenic fluids listed above create extremely hazardous gases. Some like liquid hydrogen are very flammable/explosive, and must be handles with care. Others like fluorine are extremely toxic. Therefore, due to the lack of containment available, the only gases that may be considered are ones that exist in a normal atmosphere, and are relatively non-hazardous.

Finally, because a cryogenic chamber is not available, a duel cryo-fluid system must be used, where one fluid acts as the nanofluid host liquid, while the other acts as a coolant in a

surrounding jacket. For this method to work, the two fluids must have very similar liquid ranges, with the host fluid being approximately 5-10 K cooler than the coolant. This allows for a wide range of available thermal gradients, while hopefully mitigating the possibility of one of the fluids freezing or boiling.

Based on these requirements, the only fluids which meet all the specified criteria are liquid oxygen as the test fluid, and liquid Nitrogen as the coolant. Therefore, the analytical design will use these two cryogenic fluids as the working mediums. Another aspect of these two cryogens that is appealing is there great availability, and low cost, along with the fact that when used in the proper concentrations, they produce non-toxic standard air. Therefore, from this point on the working test fluid for the thermal conductance measurement of cryogenic nanofluids is liquid oxygen (LOX), with a coolant fluid of liquid nitrogen (LN2), and the cryogenic temperature range of interest will be between 70 and 90K.

3.5.4. Experimental Limitations

The experimental limitations of this particular THW setup are primarily based upon the digital voltage meters available. While a variety of Data Acquisition Systems (DAQ's) were reviewed for their viability, the initial design process, along with peer recommendations led to the purchase of the Measurement Computing USB 1608FS voltage DAQ. It should be noted that in many ways this particular DAQ is not well suited to the current needs of this research. However, it was available, and it did provide an acceptable experimental foundation. The primary limitations of the USB 1608FS will be discussed at greater length along with the author's recommendations for more appropriate systems within the experimental design chapter of this work. The USB 1608FS is an 8 channel single input DAQ with 16 bit resolution, and accuracies that correspond to the available voltage ranges of ±1 to ±10 V. It also has a 32 bit internal counter capable of scan rates up to 200kS/s. A full review of the specifications can be found on

Measurement Computing's website [132]. These hardware limitations dictate certain inherent restrictions in terms of what voltage/power ranges can accurately be measured and how fast said values can be recorded. For the greatest accuracy, the THW voltage signal should be within the ±1 V range. This will ensure that the USB 1608FS is operating within the highest level of bit resolution and hardware accuracy. In addition, because this particular system is single input only, a forced differential must be imposed. This will lead to a scanning rate limitation of roughly 16kS/s. Therefore, for the purposes of an initial analytical design and model, the experimental DAQ will impose that the THW voltage level must be significantly less than ±1V, with a transient change on the order of several factors larger than the ±1 V accuracy range of (0.68 mV). In addition, the time scale of the system must be such that a great deal of the linear signal, within the transient voltage measurement, can be captured with the available channels and USB 1608FS scanning rate. The measurement limitations of the DAQ systems used in this research will primarily effect the THW material, morphology, testing time, and energizing current values used.

3.5.5. THW Material/Morphology

3.5.5.1. Background

The material from which the THW is made is an important design parameter albeit a very straight forward one. The vast majority of hot wire techniques rely on the highly desirable properties of platinum. These include good chemical resistance, reasonable thermal resistance, relative low cost, availability, and most importantly, a highly linear resistance to temperature response over a large temperature range. Therefore, for this research, the material of choice for the transient hot wire is platinum.

3.5.5.2. THW Diameter

The wire diameter needs to be small enough to approximate an infinitely thin line heat source. This is not difficult to obtain, due to the fact that the surrounding medium of interest is on the order of many radial magnitudes greater. Most small wire diameters will suffice, and have the added benefit of costing less. Common wire diameters used in THW systems range from 100 μm to 10 μm. The primary considerations involved when choosing a THW diameter is that of cost and available power. Because platinum is a very rare and valuable metal, even small wires can cost well up into the hundreds of dollars. Therefore, the size should be maintained as small as possible. In addition, the power requirements needed to produce the desired heat flux within a large diameter wire is often prohibitive and depends greatly upon the wire diameter. Thus it is important to size the wire diameter so that the desired current is well within the available power range of the experimental system, and the wire itself is within the available research budget. For the purposes of this work, the platinum wire chosen for the THW system was high purity five thousandths of an inch TC wire. This allowed for a relatively cheap, physically manageable wire, which, when combined with the available power supply generated electrical signals within the desirable ranges as set by the DAQ limitations mentioned earlier.

3.5.5.3. THW Length

The wire length is another important parameter to the hot wire test. The wire must be long enough to approximate and infinite length with respect to the wire diameter and cell dimensions. However, it cannot be so long as to cause voltage/resistance values outside the desirable range or become physically cumbersome. The current literature recommends wire lengths on the order of several thousand times the nominal diameter, which for practical purposes amounts to roughly a length of at least 5 inches, with most recommendations around 6-7 inches. Many current THW techniques rely on either a short duel wire setup or a long single wire. If the two wire method is

used, the wires are suspended parallel to each other with one being longer than the other. The difference in voltage drop between these two wires can be used to account for the end effects of the hot wire. If a single wire is used, then it is assumed that the greater length will diminish any inaccuracies caused by end effects. For the purposes of this research, a single wire with a length within the recommended values was used.

3.5.6. THW Resistivity vs. Temperature

3.5.6.1. Significance

The transient hot wire technique is based entirely upon the relationship between the natural resistivity of platinum, and its temperature. Without this, the hot wire temperature, and relative change in temperature could not be calculated, and the overall test would be ineffective. Platinum is used because of its thermal stability, chemical resistivity, and highly linear resistivity to temperature relationship.

3.5.6.2. Background

The uses for platinum in temperature sensing are quite varied, and span from powered RTD's and PRT's too passive thermocouple setups. Platinum is also used in a variety of other capacities, including pressure sensing, and fluid dynamic motion among many others.

The challenge for this research was to find a platinum resistivity model which would accurately predict the changes in temperature of the THW within the desired cryogenic temperature ranges. In addition, the model needed to be precise, accurate, and sensitive enough to detect slight changes in temperature over very brief periods of time within a severely noisy environment with only a minimal amount of power and therefore a small change in hot wire resistivity and temperature. Many different resistivity vs. temperature models can be used to convert a THW’s electrical resistance to temperature. Several of the more common methods will

be described below. The relative pros and cons of each will be discussed, along with a final review of the chosen method, and the reasoning behind it.

3.5.6.3. Callendar-Van Dusen Model

By far the most common method of platinum resistivity to temperature calculation is that of the Callendar-Van Dusen equation. The full version of the equation was established by M.S Van Dusen in 1925 [133-135] and is essentially a second order polynomial curve fit of experimentally determined platinum resistivity vs. temperature data. The following equation is a fairly good fit over the range of 0^oC to 661^oC.

$$R(T) = R_0(T) \cdot (1 + A \cdot T + B \cdot T^2) \tag{3.49}$$

where R(T) in Ω's is the resistance of the platinum wire based upon temperature T in K, and $R_0(T)$ is a base resistance value taken at some predefined temperature. A and B are simply experimentally determined constants. A more accurate third order equation can be used over a wider range of temperatures (-200^oC to 661^oC.).

$$R(T) = R_0(T) \cdot [1 + A \cdot T + B \cdot T^2 + (T - 100) \cdot C \cdot T^3] \tag{3.50}$$

The third order constant C is introduced along with the more accurate third order term. The constants A, B, and C can be experimentally determined by calibration of the platinum sensor at specific preset temperatures. The Callendar-Van Dusen equation is a well-established and respected method of resistivity vs. temperature calculation. However, it requires direct calibration of the system, especially for non-standard or custom made platinum sensor setups. This calibration can prove to be quite difficult without the proper equipment, and for the case of this research proved to be ineffective. In addition, because platinum tends to lose its linearity at low or cryogenic temperatures, it can become increasingly inaccurate at the sub-cooled temperatures utilized in this research. It should be noted that the Callendar-Van Dusen equation is highly

accurate and useful at less extreme temperatures, and in fact was utilized by this research for room temperature testing and experimental validation.

3.5.6.4. NPL Model

The United Kingdom's National Physics Laboratory (NPL) of London [136] is one of the premier scientific institutes in the world and has long been a leader in the field of measurements and standards. NPL published a review of the concepts behind platinum resistance thermometers and included a plot of resistivity vs. temperature (figure 388) of a series of common temperature sensing thermometer metals. This particular plot is extremely useful because it depicts the behavior of pure platinum below 100^{o}C. Based upon this information the NPL plot can be digitized and than converted into distinct data points. These points can then be curve fitted to an analytical equation or model, or can be used in conjunction with an interpolation scheme to calculate the relative temperature of the platinum hot wire.

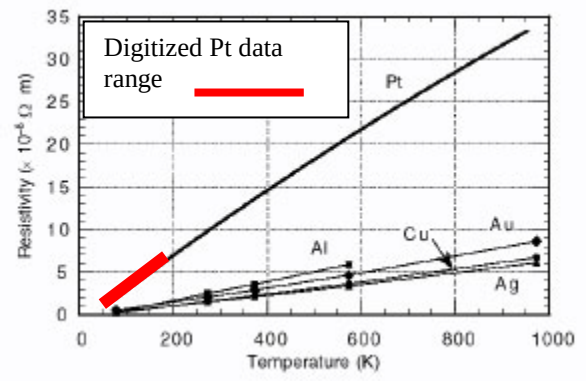

Figure 3-8. NPL thermometer data. Adapted from NPL website [136].

This particular model proved to be fairly accurate over more conventional temperature ranges, and did provide semi-accurate results at cryogenic temperatures. However, a great deal of

uncertainty and error is introduced by digitizing the plotted curves of platinum. In fact, it proved to be very nearly impossible to digitize the data with enough data points to take into account the relatively small changes in platinum resistivity and temperature experienced by the hot wire for this work. In addition, as can be seen from the plot above, not a great deal of data exists for the temperature range of interest (around 70-90 K). Therefore, this method was ultimately rejected due to its large sources of potential uncertainty and its relative lack of useful cryogenic temperature information.

3.5.6.5. PGM Model

The PGM database is an inclusive review of the physical, thermal, and electrical properties of the platinum metals group [137]. The PGM website gives a review of the electrical resistivity of platinum in table format. The values vary from roughly 20 K up to very high temperatures. Once again, these values can be tabulated and used to create a rough curve fit (figure 3-9) and therefore an analytical equation. However, there are only two or three data points within the actual cryogenic temperature range of interest for this research. Therefore, any deviation from the approximate curve fit would result in rather large errors in the calculation of temperature for the hot wire. Therefore, it was decided that the PGM database was not inclusive enough for use in this research. However, it was extensively used in the calculation of room temperature thermal conductivities, along with the initial prototype cryogenic hot wire testing.

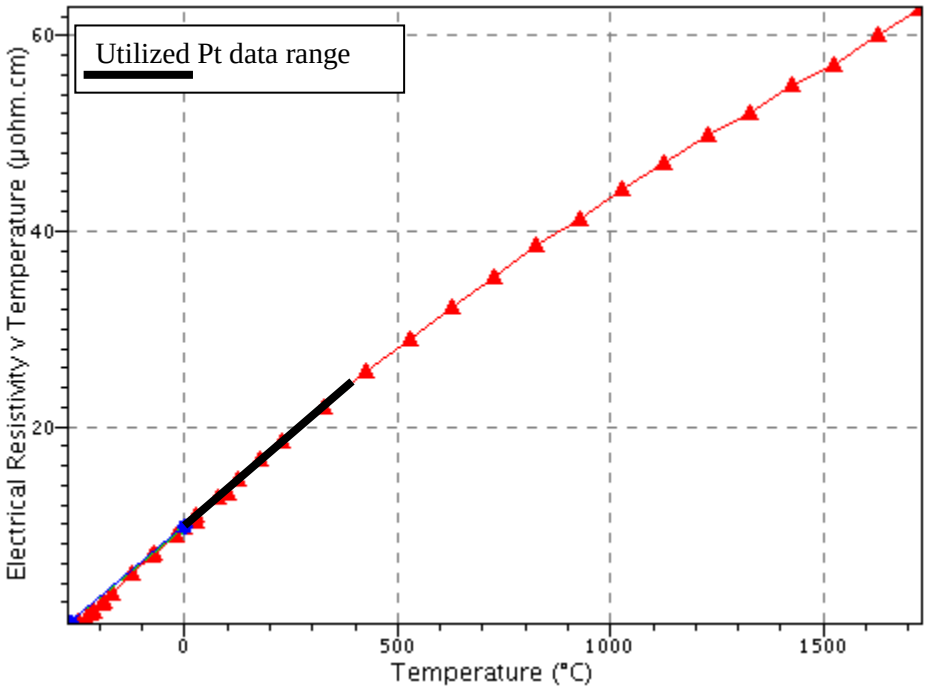

Figure 3-9. Tabulated platinum vs. resistivity data from the PGM database, adapted from PGM website [137].

3.5.6.6. Berry's Model

Dr. R. J. Berry published a paper on the relationship between the real and ideal resistivities of platinum [138]. The focus of this work was on the various parameters that have cause and effect on the resistivity of a given material (in this case platinum) and how these different values influence the analytical and experimental determination of the materials resistivity. Resistivity is dependent upon two primary factors. These are the inherent and variable material resistances to energy flow, and the more constant larger scale effects of defects and variations of the structure of the material. The natural resistance to the flow of energy by a material can be easily determined both theoretically and analytically, and can therefore be readily used in research applications. However, the physical defaults and specifics of a given materials structure which inhibits the flow of energy is dependent upon the individual material sample, and needs to be

determined for each case and sample being studied, and must in general be experimentally determined and certainly cannot be generalized to all materials or samples. Therefore, the exact resistance of a material depends upon both of these phenomena. However, because the physical defaults provide a constant and fairly unchanging resistance, they can be neglected when calculating the relative change in resistance and therefore temperature. Therefore, for this research the specific physical defects and characteristics of each sample were ignored, and instead the ideal resistivity of platinum was used to calculate the temperature change of the transient hot wire. In Berry's review of the thermal resistance behavior of platinum, he included a table of calculated ideal platinum resistivity values. This table included the entirety of the working experimental cryogenic range used in this research, and provided resistivity values at one Kelvin increments. This is by far the most useful and inclusive listing of platinum resistivity found by the authors. A graphical representation of Berry's data is shown below in figure 3-10.

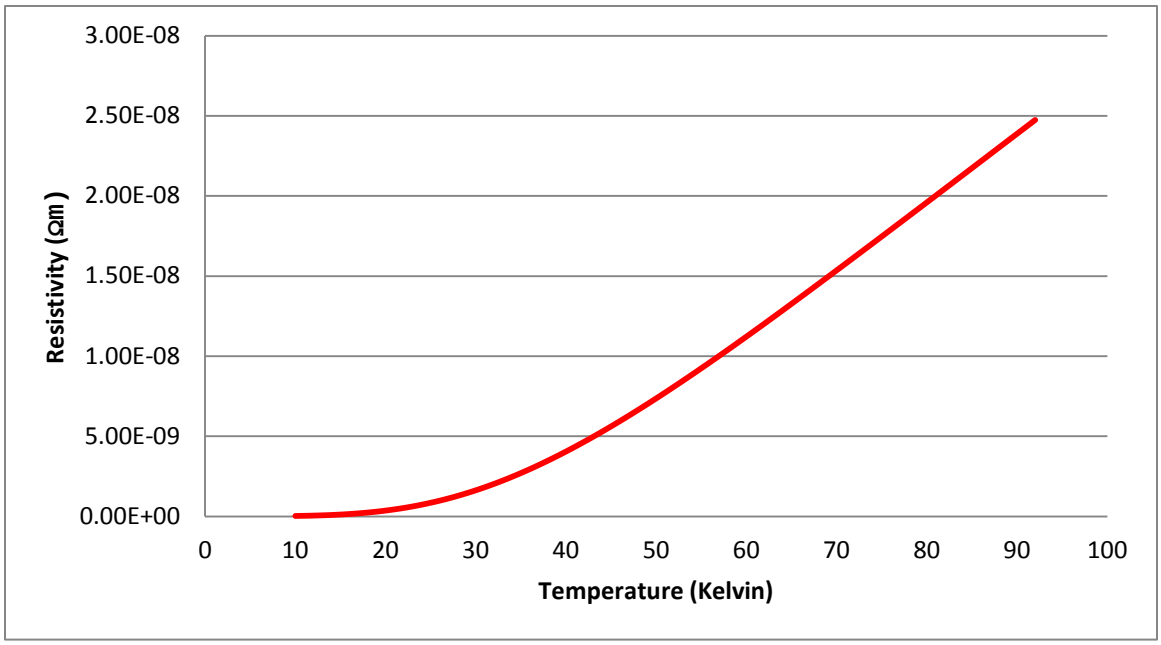

Figure 3-10. Platinum resistivity vs. temperature. Based upon Berry's work [138].

3.5.6.7. Conclusions

For this research Berry's method was chosen, because it provided the most detailed and inclusive review of the electrical resistivity of platinum within the reacquired cryogenic temperature range. This allowed the detailed extrapolation of the relative hot wire temperature change to be calculated with maximal accuracy, and sensitivity. The actual use of the data presented by Berry can be seen in the formulation and use of the numerical analysis code in the numerical modeling chapter. It should be noted that a direct calibration method would have been ideal for this research. This would have entailed using a four wire resistance measurement method to accurately calculate the exact electrical resistances of the hot wire, while using a variable temperature pressure chamber to slowly and exactly vary the temperature. From this direct calibration the exact behavior of the specific platinum hot wire used in this research could have been calculated. However, due to a lack of equipment, this ideal method was not possible.

3.5.7. Coupled Design Considerations

3.5.7.1. Background

One of the primary problems encountered in the analytical design of this experimental system was that of the intricate correlations between the THW energizing power, testing time, and allowable THW temperature change. Each of these factors depend upon the others and all need to be balanced along with the allowable parameters of the cryogenic host fluid and the available experimental systems to create a stable and friendly testing environment for the cryogenic nanofluids used in this research. The motivation for this analysis is to fully encapsulate the many factors which contribute to the experimental stability of this research. One of the more important of which is balancing the inputted heat flux, temperature gradient, and testing time to minimize fluid movement due to physical/thermal causes etc. The following discussion will review how each component of the governing theory equation are interrelated, and how each was calculated

and balanced to create a theoretical bases for the design and eventual behavior of the experimental THW setup and the cryogenic nanofluids. The interrelated nature of these parameters can be viewed below (figure 3-11).

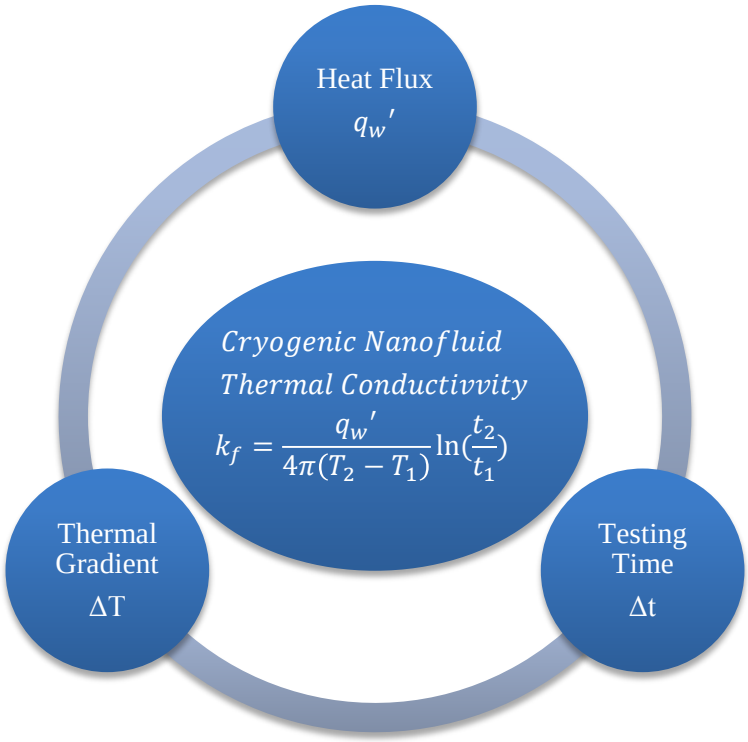

Figure 3-11. Interrelations between the components of the governing equation.

3.5.7.2. THW Energizing Power

The first variable parameter of the governing equation, that of energizing power and therefore heat flux, is entirely based upon the inputted current value and the wire physical parameters. It was already determined that the single wire setup would be made of platinum and that the length and diameter would be such as to ensure that the theoretical assumptions of an infinitely long and thin line source are appropriate, while limiting setup costs. The calculations of overall and

transient changes in voltage levels are based upon Ohm's laws which dictate the relationship of constant current to energizing power and thus THW heat flux. These laws, as shown in eq. (3.51), describe the measureable voltage differences used in the calculation of thermal conductivity. The measured power levels given by Ohm's laws are not the time dependent transience's of the wire, that are present due to the lack of a power/current feedback system, but are instead the overall power trends. However, the constant current nature of this system dictates the behavior of the THW voltage drop, wire heat flux, temperature, and therefore time. It is, in all reality, the governing force behind each of the other parameters. The equations used for the calculation of power are shown below, and are simply Ohm's laws.

$$P = I^2R \; or \; P = VI \tag{3.51}$$

where R is the total resistance of the platinum THW in Ω's, I is the energizing current in A's, and V is the voltage potential that exists differentially along the THW in V's. It should be noted that this value is divided by the total length of the wire to calculate the wire heat flux, and establish the proper units. Because the particular power supply available for this research is based upon a constant current system without feedback, the primary value that can be set is that of current I in amps.

The total current value has several constraints. On the low end, the value must be high enough to create a transient change in voltage and resistance across the THW that can easily, accurately, and repeatable be measured by the available DAQ. On the other hand, the inputted current value must be small enough to prevent fluid movement due to convection, buoyancy, or boiling within the defined testing time. Additionally, the upper limit of the current must be such that the overall voltage drop across the wire is less than 1 V.

3.5.7.3. THW Temperature Change

The heat flux generated by the wire is translated into a constant thermal gradient between the wire and the surrounding near field fluid, which generates a transient temperature change within said fluid. Because this difference in temperature is the thermal imbalance which drives the thermal conductivity measurement, great care must be taken so that the proper ΔT is selected. Based upon the best knowledge of the authors and peer reviewed research, a ΔT of less than a few Kelvin (1~5 K) is desirable when working with liquids [1]. This ensures that large thermal imbalances do not occur, which would force fluid motion. Therefore, based upon the LOX and LN2 fluid boiling curves shown below (figure 3-13) and by utilizing the temperature vs. time models derived in the previous sections (also shown), we can predict the heating fluxes and transient changes in temperatures for the given wires for several different energizing currents.

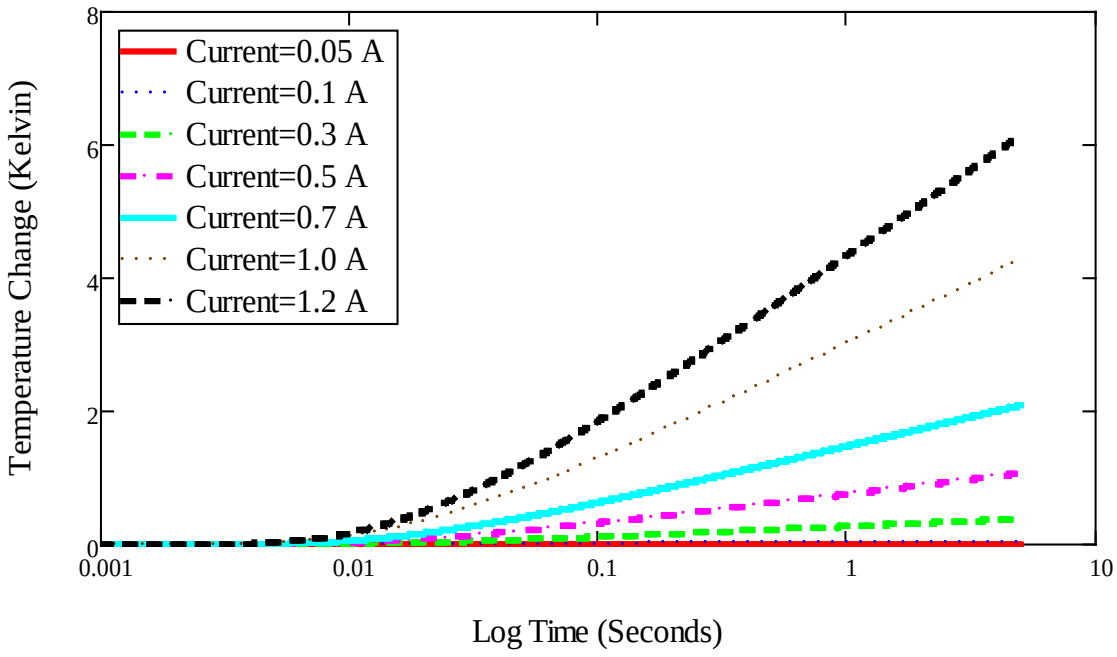

Figure 3-12. Temperature vs. time model depicting the potential change in temperature of an infinite line heat source undergoing instantaneous heating.

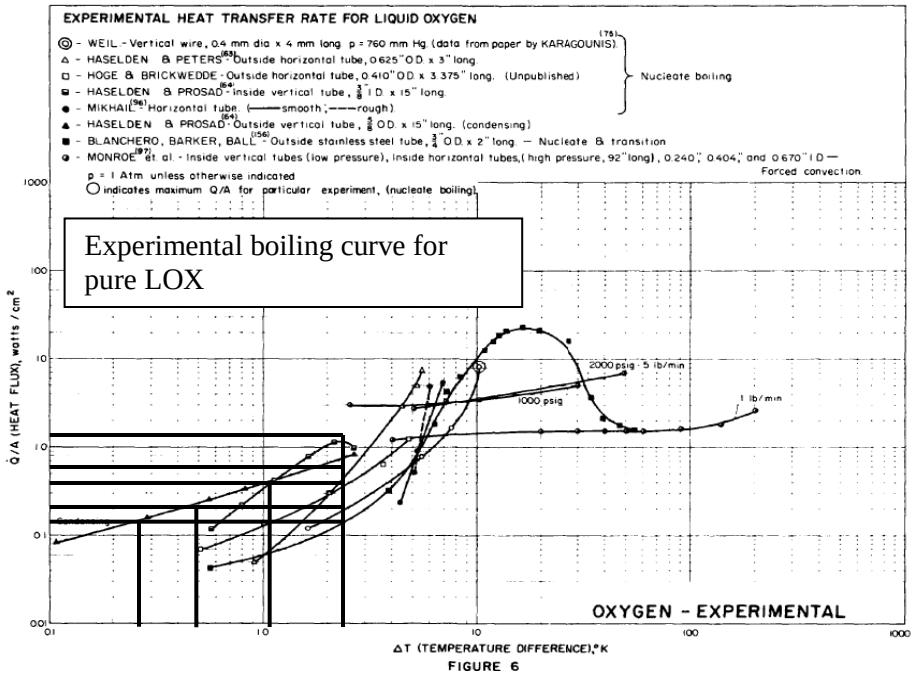

FIGURE 6

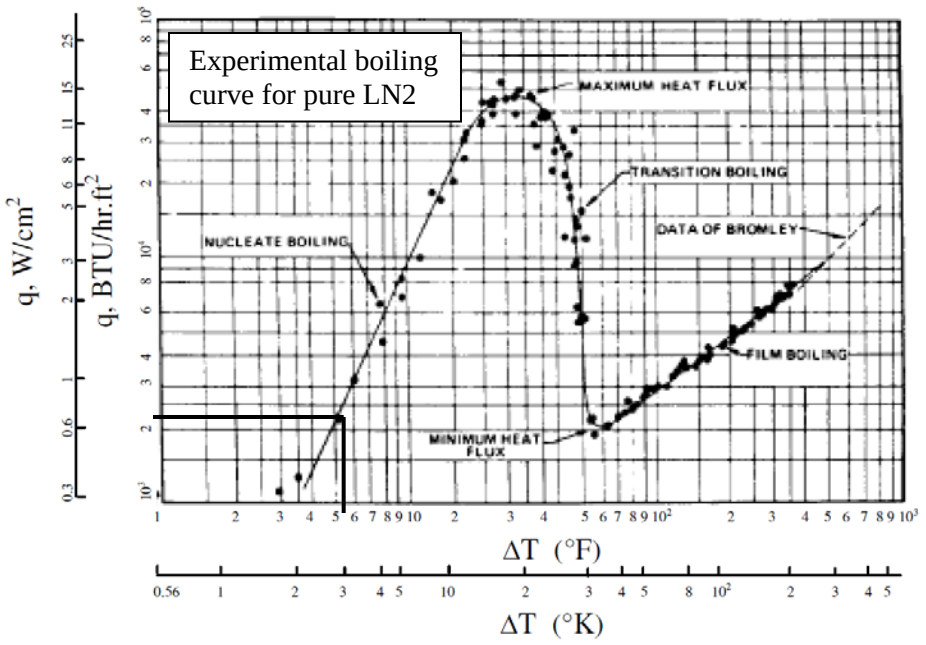

Figure 3-13. LOX & LN2 Boiling Curves, adapted from [139, 140].

As can be seen from the boiling curves above, a temperature gradient of less than 5 K will not cause either LOX or LN2 to produce nucleation point boiling. In addition, these low thermal gradient values produce equally small heat fluxes. Therefore, (from Fig. 3-12.) any current value below roughly 0.7-0.8 amps will not produce a temperature change above the 5 K allowed. This will ensure that boiling does not occur even if the liquid oxygen is near its saturation point. In fact, with the liquid nitrogen acting as a coolant, and no more than a 5 K change in temperature, the fluid should maintain a fairly stable state.

Theoretically large scale fluid motion and boiling will not be occurring in the LOX based cryogenic nanofluids because of the liquid nitrogen coolant, a small energizing current value, and a heat flux generated by a total change in temperature of less than 5 K. In fact, with the THW temperature parameters given as above, the fluid should only experience convection. However, convection is not taken into account by our governing equation. If any significant convection is occurring it would represent a serious error in our analytical models and experimental work. Therefore, to prevent natural convection the hot wire energized testing time must be kept short enough that the fluid does not have a chance to overcome its initial resistance to micro/macro motion via momentum changes and cannot, therefore, begin convection. This will be discussed further in the next section.

3.5.7.4. THW Total Testing Time

One of the primary concerns of the transient hot wire technique, when used for measuring liquids, is relative fluid motion. This can be caused by a variety of factors including thermally induced variable density driven flow and physical environmental factors such as force induced fluid currents etc. Because this test measures thermal conduction only, which assumes no relative fluid motion with respect to the transient hot wire, any instability within the host fluid can lead to large errors in the calculated thermal conductivity values. One of the primary methods for

negating the effects of fluid movement, within a transient thermal conductivity measurement system, is testing speed. By measuring the transient changes in temperature fast enough, the researcher can capture the entirety of the valuable experimental data before fluid momentum can create relative velocity gradients of any great size.

Therefore, before any experimental apparatus could be designed or built, a suitable testing time length must be determined. This time duration will measure the time between the initiation of energizing power, and therefore heating of the transient wire, and will end when a full transient curve, including the relevant linear section, has been measured. At this point the data acquisition will cease and a full THW heat curve will have been observed.

The allowable experimental testing time is governed by the cryogenic host fluid, the cooling jacket fluid, and the overall desired change in THW temperature. When fluids/gases are involved in a static (physical environmental factors are negated) fluid measurement and testing time is being considered, it is almost always closely correlated to fluid temperature rise. This is not the case for solids where movement or phase changes are not considerations. In the case of both LOX and LN2, the relative boiling curves (Fig. 3-13.) needed to be reviewed in order to determine the exact amount of fluid temperature change allowable before the onset of bulk fluid movement and boiling. This in turn would provide the allowable input heat flux which would allow the determination of an appropriate current, and therefore a calculation of total testing time.

The best current knowledge on the use of hot wire method for fluids is to maintain a total testing time of less than 5 s [1]. Therefore, to be on the conservative side, a powered testing time of roughly 4 s will be measured, and only an approximate 2-3 seconds of that data will be analyzed.

3.5.7.5. Summary

Ultimately, each of the transient parameters of the governing thermal conductivity equation has been carefully selected to not only favorably interact, but create a well-balanced experimental testing environment. The theoretical ranges of these three transient parameters can be used to set a testing current value, which will maintain the desired temperature and overall testing time within the constraints of the available experimental apparatuses. These will be that the current should be as close to 0.7 A as possible, and that the overall change in temperature of the THW should be less than 5 K with an overall testing time of less than 3-5 s. These theoretical design parameters allow the design and implementation of a full experimental setup with confidence, although it should be noted that theoretical designs are just that, and every design must be modified once it is tested and validated in the real world.

3.5.8. Nanoparticle Type

The final design parameter that must be decided upon is what kind of nanoparticles should act as the inclusion phase of the cryogenic nanofluid. The factors which dictate what type of nanoparticles can and should be used in a cryogenic nanofluid are quite complex. These include oxidation resistance, density, size, material, agglomeration, among many others. The densities of any inclusion particles should match those of the host fluid as closely as possible. The density of LOX is such that it can theoretically suspend a variety of reasonably sized nanoparticles. However, because the viscosity of LOX is very small, the inclusion particles will experience little viscous shear resistance to motion and settling. Therefore, even particles with relatively low densities often settle quickly in LOX. Another important factor is to choose stable particles that will not change their chemical structure or behavior in a pure oxygen bath. Therefore, easily oxidizing metals and particles that are prone to corrosion should not be considered. Numerous researchers agree that particle size plays an important role in the thermal conductivity changes of

nanofluids. Most theorize that the thermal conductivity is inversely related to particle size. Therefore, the smallest possible particles of a given material should be selected. However, several current theories also state that it is the clumping of the particles that give the Nanofluid its thermal conductivity increase. In addition, small particles tend to agglomerate faster and thus settle out of suspension more rapidly. Therefore, particle size is a balancing act that must be handled with great care, and a great deal of further research is required. The nanoparticle loading concentration is another important preliminary design factor. Many current research works focus on particle volume loadings of less than 1%. However, several researchers have investigated much higher loadings; see the nanofluid literature review of this thesis. Due to the fact that the fluid properties can change greatly with large amounts of particles, combined with the fact that high particle concentrations can, in fact, increase the settling rate of nanofluids not to mention greatly increase their cost. Small particle concentrations are the most desirable for the current work. Based upon the considerations mentioned above, it was decided that the unique thermal and physical properties of MWCNT's combined with their relatively low densities, average sizes, and environmentally inert nature provided an ideal starting point for the study of cryogenic nanofluids.

3.5.9. Cryogenic Nanofluid Mixing Method

The science of the creation process of nanofluid mixtures and suspensions is a growing field. Many researchers have succeeded in testing the various thermal and mechanical properties of nanofluids. However, making a truly useful, cost effective, and stable nanofluid is proving to be quite elusive. Therefore, a great deal of research is being done in the field of particle mixing and stabilization. The mixing methods available for this work would specifically fall under the category of creating two stage nanofluids, as discussed in the section on nanoparticle and nanofluid synthesis and fabrication. Many such methods exist, but arguably the most common is

that of sonication. A sonicator is a device that uses a modulated electrical signal to charge a pizo electric crystal attached to a tuned probe or flat plate. This signal is transformed from an EM signal to a mechanical vibration with extraordinarily high frequencies. These frequencies when introduced to a liquid will cause instantaneous cavitation. When these generated cavitation bubbles collapse they send shock waves throughout the surrounding fluid, which not only mix the inclusion particles, but break the ever present agglomerated clumps into much smaller clusters [142]. Because of the relative ease of use along with the versatility, this is one of the most common techniques available for mixing any kind of nanofluid. Other common types are vortex mixers, magnetic mixers, stirrers, etc. However, because of the availability of a sonicator, its prevalence in current nanofluid research, and the various advantages mentioned above, along with the unstable and delicate nature of cryogenic nanofluids, it was decided that sonication was probably the easiest and most effective method available for mixing the cryogenic nanofluids of this research.

3.5.10. Mixing Time

Conventional wisdom states that nanofluids should be mixed for as long as possible to create a well dispersed and stable mixture. However, researchers have investigated the correlation between sonication times and thermal conductivity increases, see nanofluid literature review. They have noted that the effective thermal conductivity of the nanofluids increase up to a certain point and then proceed to level off. Past this point any further sonication time will prove to be wasted. Thus, it is important to determine the optimal sonication time for any given nanofluid. In addition sonicators generate a tremendous amount of thermal energy and can easily boil most types of host fluid, not to mention possibly inflicting damage the inclusion nanoparticles. Therefore, mixing times can and should vary greatly and in general should also be performed with burst sonication.

Due to the low temperatures of cryogens, their stability cannot tolerate large heat fluxes, even with LN2 as a coolant. Thus, sonication times for cryogenic nanofluids need to be kept short, on the order of a handful of seconds or minutes spread out among several bursts. Another consideration is that the cold induced, by the cryogenic liquid, on the sonicator can easily reduce the effectiveness of the sonicator, or if taken to extremes, damage the pizo crystal or electronics. Therefore, for a cryogenic nanofluid a relatively short mixing time is required with sonication bursts, and several substantial cool down sessions. A mixing time of roughly 1-2 minutes with alternating burst sonication seems prudent for the current work.

3.5.11. Nanofluid Surfactants/Additives

The ultimate goal of creating stable well dispersed nanofluids has led to a great deal of research focused on the role of surfactants/additives in the behavior of nanofluids. This can be reviewed further in the provided literature review.

The most common type of added nanoparticle dispersant is the surfactant. Surfactants rely on the inherent polarity of fluids and the effects that can have on particle clustering and distribution. However, because the current work focuses on cryogenic nanofluids, specifically those with LOX as the host material, which is a non-polar fluid a more complicated situation, exists. There has been work done in the field of non-polar surfactants [143]. However, none of this work was readily applicable to the current situation. This leads naturally to the question of non-surfactant additives which could aid in the stabilization of cryogenic nanofluids. While several methods were considered and tried, namely changing and matching the surface charges of the MWCNT's, they were deemed either too complex or untenable for the current work and will not be repeated here. Therefore, it was decided that the cryogenic nanofluids used for this research would be synthesized and mixed without the use of surfactants/additives.

3.6. Conclusions

When creating any experimental system, a thorough and well thought out model of how it will behave is essential for both the basic understanding and ultimate viability of the system. The first step to this theoretical understanding was to fully derive and comprehend each of the governing heat transport equations that dictate the behavior of an energized THW. This included an in depth literature review of the primary governing equations for heat conduction in a two dimensional radial heat problem. Several such THW models were proposed, many of which can be reviewed in the theory chapter of this work. Ultimately, a simple energized infinite long/thin radial thermal transport model was chosen and utilized to predict the powered heating curves of the experimental hot wire. Finally, these general equations along with the total derived testing time, permitted heat flux and allowable change in temperature were employed to create a working theoretical model of how the experimental setup would behave when used to measure the effective thermal conductivity of a MWCNT based CN. These models were used, successfully, as a theoretical framework for the design and creation of the experimental setup.

In addition to a theoretical understanding of the THW system, a selection of the leading models and theories on the effective thermal conductivity of nanofluids were presented in this work. These models and theories included analyses of both static and dynamic mixture laws and are some of the best and most current ideas in the field of nanofluid science as to the behavior, nature and causality of nanofluids. A selection of the presented static mixture laws were used to model the potential effective thermal conductivities of the CN's created for this work and the ultimate results were informally compared to similar traditional nanofluid values. It should be noted, however, that although these theories, can in general, be compared to the current work, the authors have not officially drawn any conclusions as to the physics behind the anomalous effective thermal conductivity increases reported in this work. They do however, give an

excellent review as to the leading opinions of how the nature and behavior of nanofluids, and subsequently cryogenic nanofluids, can be predicted and understood.

CHAPTER 4

NANOFLUID THEORY

4.1. Significance

The need for isotropic, homogeneous, mixture models arise from the fact that in the real world many materials are mixtures, and exhibit the complex behaviors associated with them. Therefore, it is of great scientific importance to be able to accurately and reliably predict the behavior of multi-phase materials both for future design purposes and to further the theoretical understanding of the complex nature of mixtures.

4.2. Background

Nanofluids are a prime example of two phase homogeneous mixtures and therefore, to be completely understood, must be modeled for similar reasons. The theoretical modeling of nanofluids can be roughly broken into two separate categories; these are static and dynamic theories/models. A static model will assume that the host liquid and the inclusion particles within it are stationary with respect to each other, whereas a Dynamic model will assume that the particles and host liquid are constantly moving and interacting. Both of these models are valid, and it is reasonable to assume that a true model would have aspects of each theory. These two separate models are discussed briefly in this review and in far greater detail in the provided references [1]. Many theoretical models have been created over the years to model homogeneous multi-phase materials, and a sampling of these will be explored below.

When modeling an isotropic homogeneous mixture, the base material is referred to as the matrix, while any inclusion materials are referred to by their morphology and material type. For the case of nanofluids, we will assume that a single phase host liquid exists, and that a single type

of nanoparticle is suspended within it. Therefore, the liquid medium will be the matrix, while the particles are the solid discontinuous components.

The complex behaviors of nanofluids depend primarily on the details of their microstructures and how these structures interact on a physical and thermal level. These nanofluid characteristics include the following:

- Particle material
- Particle geometry
- Particle dimensions
- Particle distributions
- Particle motion
- Particle thermal conductivity
- Particle volume concentration
- Particle to particle interfacial effects
- Component properties
- Matrix material
- Matrix to particle interfacial effects
- Matrix thermal conductivity

Considering the fact that these characteristics are highly varied, extremely complex and that full knowledge of them is required to create a well-defined, thorough and correct model, it becomes readily apparent why so many different models exist, and why they are only approximations and are certainly not all inclusive. In fact, while a great many models perform fairly well at categorizing and explaining the behavior of certain types of nanofluids, an all-inclusive theory that quantifies the diverse nature of nanofluids has not yet been created [1].

Fundamentally, nanofluid modeling is quite complex; however, several reasonable methods exist for simplifying the analytical models and providing reasonable approximations. The first is to create theoretical upper and lower bounds for the thermal conductivity of nanofluids. These bounds basically provide the maximum and minimum thermal conductivity values that a nanofluid can exhibit. These will be referred to as the series and parallel boundary limits for the effective thermal conductivity of nanofluids. The second is to simplify the theoretical modeling of nanofluids by making a series of reasonable assumptions about the microstructures of the nanofluids, and their effective properties. This approach can be further explored in the literature [1].

The following analytical models can be modified for many different thermal, electrical, and physical transport properties of a given isotropic homogeneous mixture, due to the fact that the governing equations are all similar. However, the effective thermal conductivity of the combined material will be singularly analyzed in this review. It should also be noted that the actual mathematical solutions and representations of the models discussed below are presented in detail in Appendix C of this work.

4.3. Static Nanofluid Models

4.3.1. Background

A static nanofluid model assumes that the host fluid, and the nanoparticles contained within it are completely stationary and do not interact aside from a stabilized contact point of view. Static modeling relies on a series of assumptions about the microstructures of both the host liquid and the inclusion particles. In most cases, these assumptions are reasonable and provide significant simplifications which, by extension, allow useable analytical and experimental models to be created. A sampling of some of the numerous current static models for nanofluids will be

explored below. Each equation below is based upon the static model of thermal transport in nanofluids and each model is based upon an ever increasing level of complexity [1].

Due to the fact that static nanofluid models fundamentally rely upon simplifying assumptions, all of which are important and play major roles in the thermal and physical behavior of nanofluids, each will need to be discussed and analyzed [1].

The following will be discussed within the static modeling of nanofluids:

- Parallel and Series mixture laws
- Theoretical nanofluid modeling
- Simple mixture models
- Complex particle distribution models
- Particle geometry based models
- Additional models

4.3.2. Parallel vs. Series Mixture Laws

The thermal conductivity of a mixture must lie between the upper bounds of the inclusion particles and the lower bound of the host fluid itself. This is, of course, assuming that the solid particles exhibit a base thermal conductivity larger than that of the host fluid. These upper and lower bounds correspond to the parallel and series mixture distribution laws. Only a brief review of mixture theories will be presented here. For a more in depth discussion of the subject the readers should review the literature S. K. Das et al. [1].

A simple mixture model does not take into account any of the complex behaviors of nanofluids. It simply depends upon the base matrix and particle thermal conductivities, and the particle volume concentration.

$$k_e = f(k_m, k_p, v_p) \tag{4.1}$$

where k_e is the effective thermal conductivity of the mixture and $f(k_m, k_p, \nu_p)$ denotes a given function of the material conductivity, the inclusion nanoparticle thermal conductivity, and the particle volume concentration. The boundary conditions that exist for the simple model of effective thermal conductivity for a nanofluid are that the conductivity approaches that of the base fluid as the particle volume concentration goes to zero and approaches the thermal conductivity of the inclusion particle as the particle volume concentration approaches one.

$$f(k_m, k_p, 0) = k_m \; and \; f(k_m, k_p, 1) = k_p \tag{4.2}$$

These boundary conditions are the theoretical lower and upper bounds for the effective thermal conductivity increase of a nanofluid. An experimentally derived relationship that dictates these boundary behaviors was determined by Das et al., Nielson et al. and Nan et al. [1, 144, 145]. This equation is called the mixture rule

$$k_e^n = (1 - \nu_p)k_m^n + \nu_p k_p^n \qquad -1 \le n \le 1 \tag{4.3}$$

where n is a variable (-1 ≤ n ≤1). This can be rewritten in a more useful form as

$$k_e^n = \left\{1 + \nu_p \left[\left(\frac{k_p}{k_m}\right)^n - 1\right]\right\}^{\frac{1}{n}} k_m \quad -1 \le n \le 1 \tag{4.4}$$

For a particle volume concentration of n=1 this mixture law becomes the upper bound of the effective nanofluid thermal conductivity, this value than forms the parallel mixture rule.

$$k_e = (1 - \nu_p)k_m + \nu_p k_p = k_m + \nu_p(k_p - k_m) \tag{4.5}$$

The equation above states that the effective thermal conductivity of the nanofluid is simply a linear combination of the thermal conductivity of the base fluid and that of the solid particle.

For n=-1, the mixture rule becomes the following,

$$k_e = \frac{1}{(1 - \nu_p)k_m^{-1} + \nu_p k_p^{-1}} = k_m + \nu_p \frac{k_p - k_m}{k_p - \nu_p(k_p - k_m)} k_m \tag{4.6}$$

This forms the series mixture equation which is the lower bound of the possible thermal conductivity of a nanofluid.

The parallel and series boundaries for the cryogenic nanofluids presented in this work can be seen below. As shown below in figure 4-1, the regular length MWCNT's purchased from NanoAmor show the highest potential, while the short length nanotubes show the smallest possible increase. Dr. T. C. Shen's MWCNT's fall in between the commercial pair.

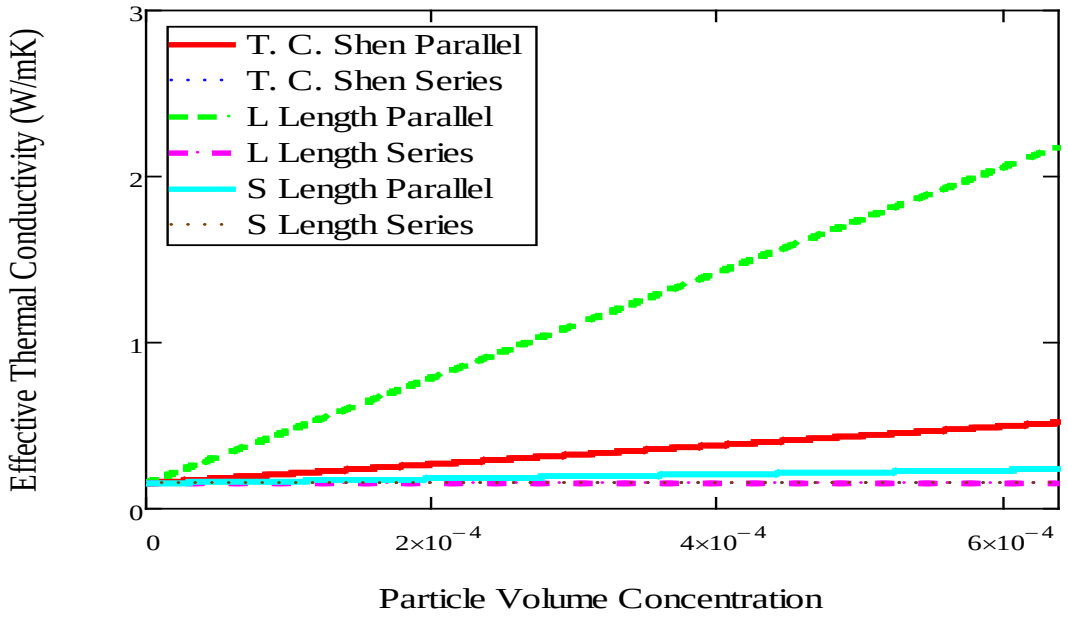

Figure 4-1. Series and parallel mixture laws applied to the CN's used in this research.

The wide range between the theoretical upper and lower bounds for the effective thermal conductivity demonstrate the need for predictive models. The specifics of the parallel and series mixture laws for the cryogenic nanofluids used in this research can be seen in Appendix C.

4.3.3. Simple Static Analytical Nanofluid Models

4.3.3.1. Introduction

Static models for Nanofluids are based upon several simplifying assumptions. The first is that the mixture is relatively dilute, with the fluid matrix being far more prevalent than any particles within them. Second the particles are all roughly the same size, shape, and material. And the particles remain stationary and do not interact with each other [1].

4.3.3.2. Maxwell's Model

The first of the truly simple isotropic homogeneous mixture equations was presented by Maxwell in 1873 [1, 122]. His model did not take into account particle interactions or shape, and only applied for conduction through a very dilute mixture and only predicts to a first order accuracy.

$$k_e = k_m + 3 \cdot \nu_p \cdot \frac{k_p - k_m}{2k_m + k_p} k_m \tag{4.7}$$

This model has proven to be quite useful over the years for a variety of applications, and while it has not proven overly accurate for nanofluid modeling, it has certainly demonstrated its worth and cemented itself as a brilliant early model for the effective thermal conductivity of simple two phase mixtures.

As can be seen in figure 4-2 and 4-3, the Maxwell model predicts a simple linear relationship between the effective thermal conductivity and the particle loading. In addition, it appears that the wide variation in particle thermal conductivity does not have any kind of effect on the predicted effective thermal conductivity. However, this is not exactly true. Instead the following graph shows that Maxwell's model dependence upon the thermal conductivity of the inclusion particles quickly reaches a steady state as the particle conductivity increases above that of the host fluid.

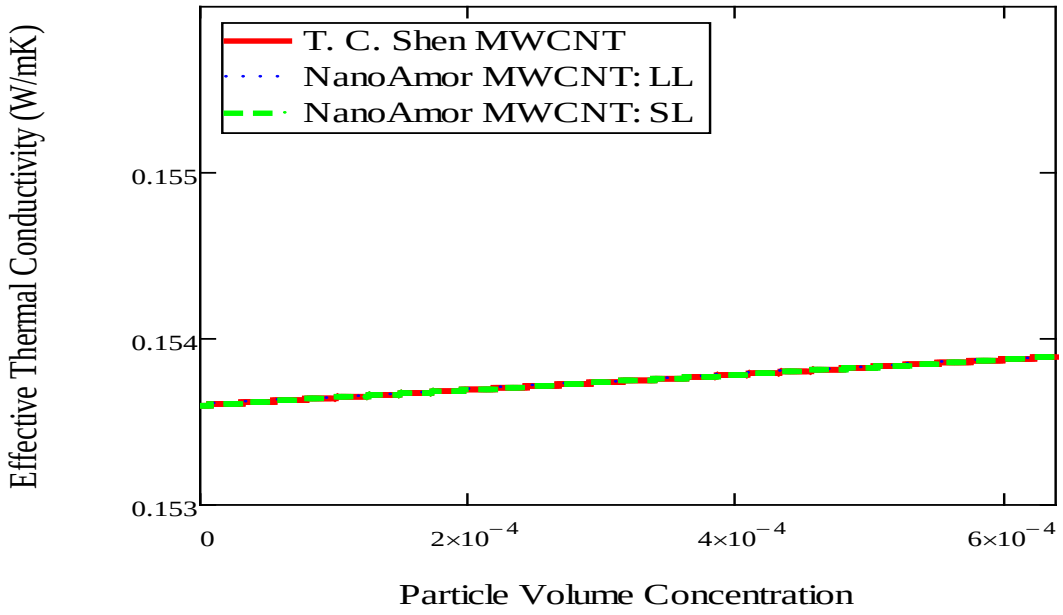

Figure 4-2. Maxwell's two phase effective thermal conductivity mixture model applied to the CN's used in this research.

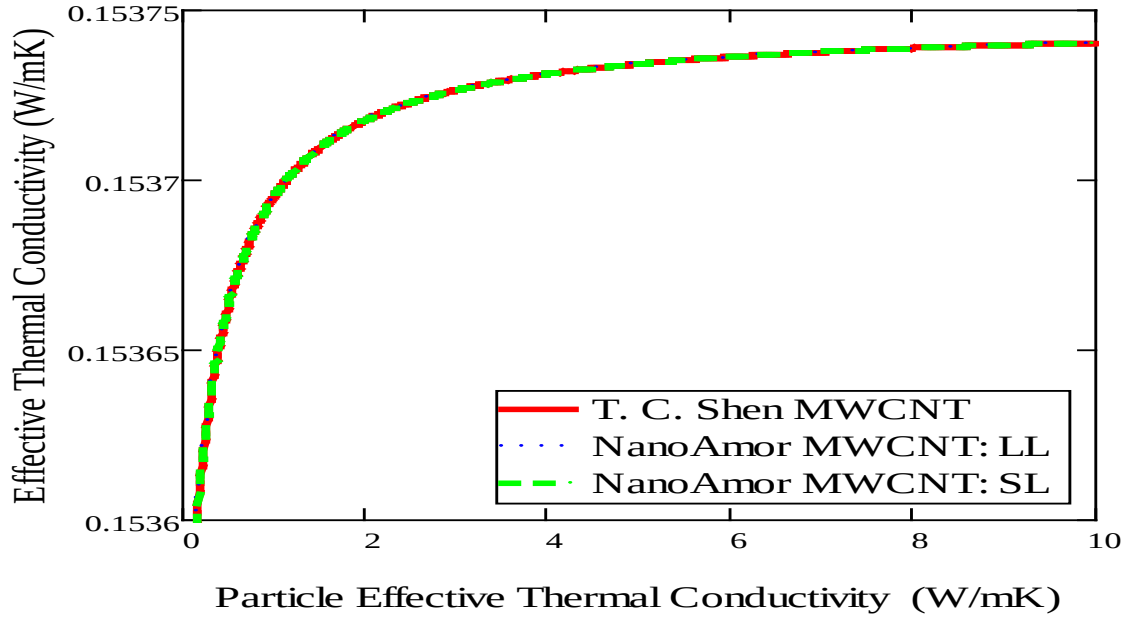

Figure 4-3. Maxwell's effective thermal conductivity mixture model taken to the theoretical thermal conductivity limit for the CN's used in this research.

Maxwell's model is suitable for the prediction of the effective thermal conductivity of dilute traditional millimeter and micrometer particle two phase mixtures, but proves wholly inadequate for nanofluids. Many researchers have extended Maxwell's theory, and this work can be reviewed in [1].

4.3.4. Complex Static Particle Distribution Models

4.3.4.1. Introduction

It seems obvious that the particle volume concentration alone cannot adequately describe the effective thermal conductivity of a nanofluid. The wide ranges possible between the parallel and series mixture rules states, that how the particles are distributed within the host fluid is of the utmost importance in the accurate modeling of a nanofluid. Therefore, models which take into account various possible particle distributions need to be analyzed.

4.3.4.2. Regular Static Nanoparticle Distribution Models

The first logical nanoparticle distribution to analyze is that of the particles being regularly distributed in a symmetric pattern throughout the base matrix fluid. Rayleigh was the first to create an analytical nanofluid model which took into account the regular distribution of particles within a fluid matrix. He assumed a simple cubic array of identical spherical particles His work can be seen in the literature Rayleigh et al. [1, 146]. An improvement on this simple model was first created by Meredith and Tobias [1, 147] which is given in equation 4.8, and represented graphically in figure 4-4. They extended Rayleigh's model and created a seemingly more accurate one with a greater allowable range of particle volume concentration

$$k_e = k_m + 3 \cdot \nu_p \cdot \left(1 - 1.227\nu_p^{\frac{7}{3}} \cdot \frac{k_p - k_m}{4k_m + 3k_p}\right) \cdot \frac{(k_p - k_m)}{2k_m + k_p - \nu_p\left[1 + 1.227\nu_p^{\frac{4}{3}} \cdot \frac{(2k_m + k_p) + 2.215\nu_p(k_p - k_m)}{(4k_m + 3k_p)}\right] \cdot (k_p - k_m)} k_m \quad (4.8)$$

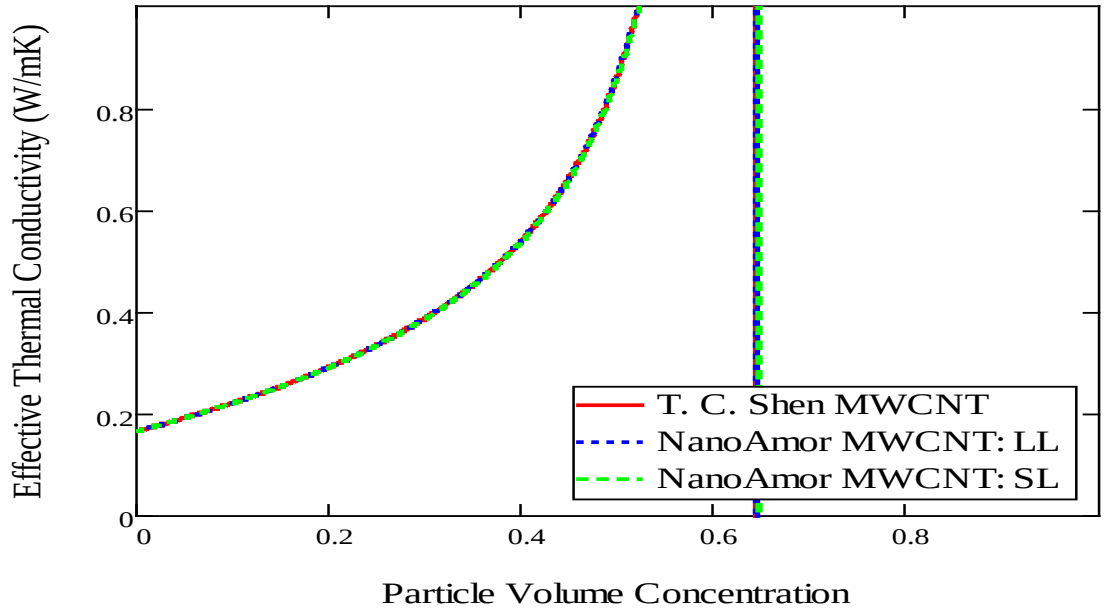

Figure 4-4. Regular ordered particle distribution effective thermal conductivity mixture model for the CN's used in this research.

It should be noted that assuming a regular cubic distribution of particles is not completely unreasonable in the calculation of the effective thermal conductivity of nanofluids. It will be shown that these models give results similar to those of other particle distributions. In fact, many additional models and techniques exist for the behavior of regular distribution of particles within a fluid and can be further review in the provided literature [1]. However, this particular assumption is certainly not inclusive when it comes to nanofluids as a whole, and in fact a great deal of further work can be reviewed and referenced from the provided literature.

4.3.4.3. Random Static Nanoparticle Distribution Models.

The concept behind the random model of particle distribution is that within the matrix, the particles can occupy all allowable positions with equal probability. This was first proposed by Jeffrey [1, 148] and can be reviewed in [1]. Davis [1, 149] created the following model which assumed perfectly spherical particles dispersed at random within the base fluid matrix.

$$k_e = k_m\left(1 + \frac{3(\alpha - 1)}{\alpha + 2 - (\alpha - 1)\nu_p}\right)\{\nu_p + f(\alpha)\nu_p{}^2 + 0(\nu_p{}^3)\} \tag{4.9}$$

Where α is a graphical based variable specific to this model. This equation has an additional level of complexity from the previous models and requires the use of the following plot adopted from Davis [149]. The complete derivation and explanation of this model can be further reviewed within Davis and S. K. Das et al. [1, 149].

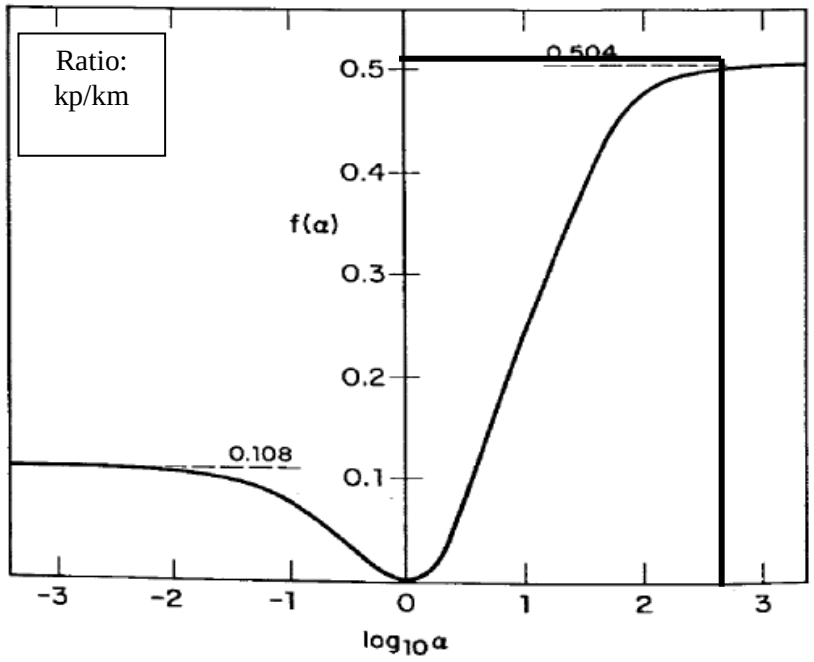

Figure 4-5. Variable function f(α) plotted as a function vs. the log of the same value, adopted from Davis [149].

The effective thermal conductivity increase for a random distribution for the cryogenic nanofluids studied in this research can be seen below in figure 4-6.

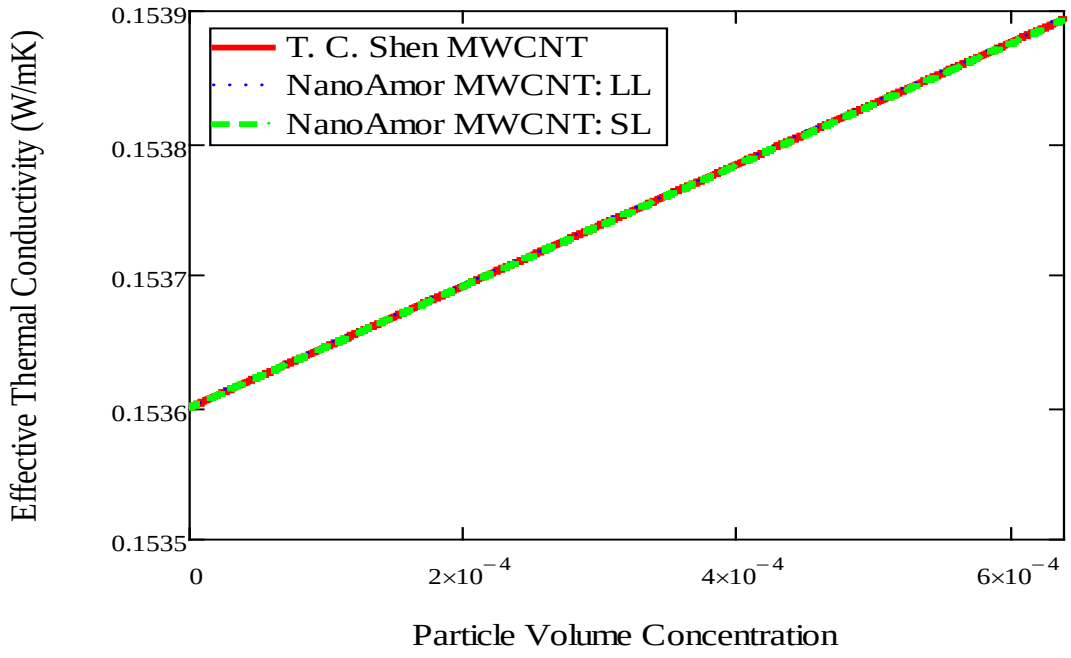

Figure 4-6. Random MWCNT particle distribution effective thermal conductivity mixture model for the CN's used in this research.

4.3.4.4. Combination Static Nanoparticle Distribution Models

A combination distribution does not rely on either a parallel or series mixture of particles. Instead, it is a combination of these two distributions. This method provides a better approximation due to the fact that it is highly likely that a real world nanofluid would exhibit both random and regular particle distributions.

Cheng and Vachon et al. modified an existing model by Tsao et al. and expanded upon the previous concepts. The details of their work and the work it is based upon can be seen in S. K.

Das et al. [1, 150, 151]. The combined MWCNT distribution for the cryogenics utilized in this research is shown below. Finally, by assuming a simple cubic lattice uniform distribution of nanoparticles with particles at the vertices, Yu and Choi et al. [1, 152] created the following equation which is represented graphically for the current research in figure 4-7.

$$k_e = \left\{ 1 - \sqrt[3]{\frac{3\nu_p}{4\pi}} \left[2 - \frac{\sqrt[3]{\frac{16}{(9\pi\nu_p)}}\, k_m}{\sqrt{k_p - k_m} \cdot \sqrt{\sqrt[3]{\frac{16}{(9\pi\nu_p)}}\, k_m + (k_p - k_m)}} \right] \cdot \ln \frac{\sqrt{\sqrt[3]{\frac{16}{(9\pi\nu_p)}}\, k_m + (k_p - k_m)} + \sqrt{k_p - k_m}}{\sqrt{\sqrt[3]{\frac{16}{(9\pi\nu_p)}}\, k_m + (k_p - k_m)} - \sqrt{k_p - k_m}} \right\}^{-1} k_m \tag{4.10}$$

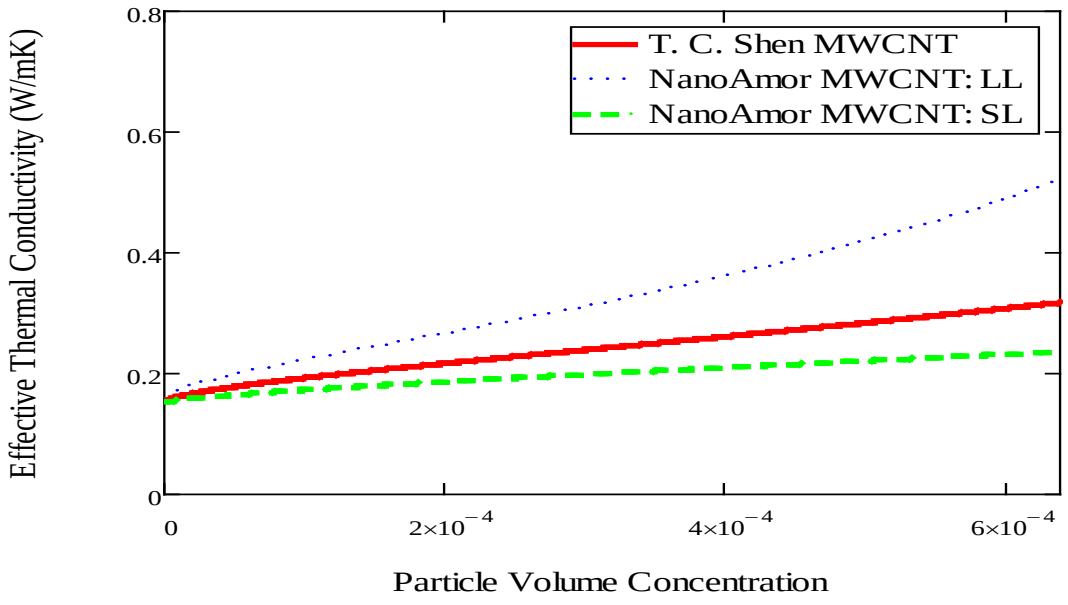

Figure 4-7. Combination MWCNT particle distribution effective thermal conductivity mixture model for the CN's used in this research.

This model has a unique feature, as the particle volume concentration increases, the curve switches concavity from down to up. This is unique and very promising and predicts that even at dilute particle concentrations significant effective thermal conductivity increases can be obtained.

4.3.5. Static Geometry Based Nanoparticle Models Introduction

For all of the preceding models the actual geometry and size of the nanoparticles have not been taken into account. It seems obvious that this would have a tremendous effect on the behavior of nanofluids, and indeed numerous experimental works [1] have proven that this is the case. The exact reasons behind how the shape and geometry of nanoparticles affect the thermal conductivity of their nanofluids is complicated and not well understood. However, it is well known that elongated particles contact each other more easily and therefore form chains and continuous clumps which allow more complex heat transfer modes to exist. On the other hand, spherical and ellipsoid particles have far more mobility and can create complex heat transfer regimes of their own.

Nanofluid analysis that accounts for the shape of the inclusion nanoparticles, often assume the nanoparticles to be ellipsoids. This is done for good reason. First, the very nature of ellipsoids allows simple geometry changes from long needles, to disks, to spheres. Additionally, despite numerous assumptions and simplifications, it is the only model with a closed solution for the effective thermal conductivity. The equation of an ellipse is shown below. The effective nanofluid thermal conductivity of this can be easily modified by simply inserting various particle geometries [1].

$$\frac{x^2}{a^2}+\frac{y^2}{b}+\frac{z^2}{c^2}=1 \tag{4.11}$$

where x, y, z, are simply elliptic geometry variables which describe the various parameters of shape, and a, b, c, are the variables representing the semi-axes. The methods used to solve for the

effective thermal conductivity of well dispersed ellipsoids is very similar to that of spheroids both of which are discussed in [1]. Without going into the specific details which can be reviewed in [1]. Nan et al. [1, 153] created a simple model for the effective thermal conductivity of carbon nanotubes based upon work done by Frick [1, 154, 155]. This can be seen below.

$$k_e = k_m + \frac{1}{3}\nu_p k_p \tag{4.12}$$

The theoretical effective thermal conductivity for the cryogenic nanofluids used in this research with rough estimates to the elliptic geometry of the MWCNT's is shown below in figure 4-8.

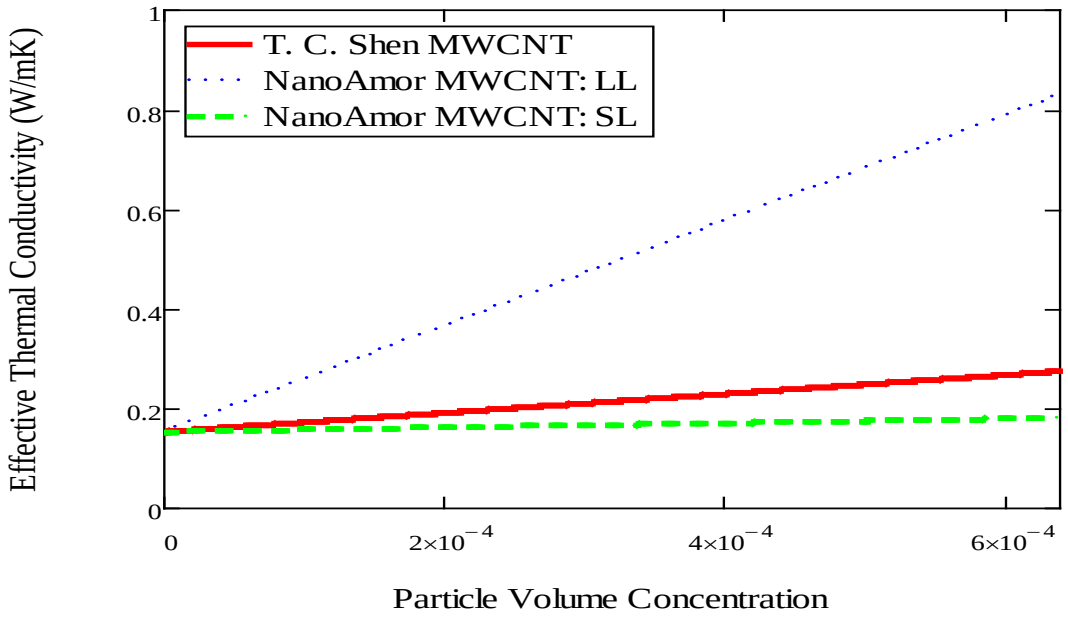

Figure 4-8. Geometry based MWCNT effective thermal conductivity mixture model for the CN's used in this research.

4.3.6. Conclusions

Many static models exist within the basic assumptions listed above, to completely review the entirety of this work would be a large task indeed, and will not be attempted here. In addition, many other models, governing theories, and assumptions have been used in an effort to increase the accuracy, repeatability, and universality of static nanofluid models. These include taking into account the equivalent medium theory, matrix to particle interfacial effects, and particle to particle interfacial effects etc.

However, the true behavior of Nanofluids is more complex and cannot be completely be described by a static model. It is not reasonable to assume that the host fluid and inclusive particles of a Nanofluid are perfectly still. Therefore, the exact behavior of a Nanofluid on a microscopic level must be determined and the mechanisms that exist and are driving all of the complex interactions need to be cataloged, explored, and fully understood before a comprehensive and useful model can be created. Therefore, a look at dynamic modeling is required [1].

4.4. Dynamic Nanofluid Models.

4.4.1. Introduction

The exact mechanisms or features of nanofluids that cause such unique thermal and physical transport behavior are still hotly debated. The very nature of nanofluids is one of great complexity. Therefore, it is probably safe to assume that to fully understand the nature of a nanofluid, and to be able to accurately and repeatedly predict its behavior, a much greater understanding of the fundamental characteristics of nanoparticles, fluid mechanics, and the interaction between a host material and the foreign materials included within it and how they combine to form an isotropic homogeneous mixture need to be analyzed. The following discussions will explore some of the more prevalent and classical theories of dynamic mixture

modeling, as well as several new cutting edge ideas. Due to the fact that these models and theories often rely on extremely complex, and little understood physical phenomena, actual analytical models do not often exist. Instead, this is more of a review of the current theories and explanations that exist for the thermal transport behavior of nanofluids. In the few cases where actual analytical or experimental models do exist, they are far too complex, and involve terms that are beyond the scope of the current research. Therefore, this will be a purely intellectual discussion on some of the more current ideas in the field of dynamic nanofluid modeling.

4.4.2. Background

Dynamic models work under the assumption that the host fluid and the nanoparticles within it are constantly moving and interacting physically, energetically and thermally on a microscopic level, and it is these interactions combined with the static nature of nanofluids that cause the unique and often anomalous behavior of nanofluids. It is readily apparent that a dynamic model combined with a comprehensive static model will provide the best analytical predictions for nanofluids. However, the sheer complexity of the dynamic nature of nanofluids is proving to be extremely difficult to encapsulate and fully explain. Therefore, a great deal of future work is required before any type of comprehensive dynamic/static analytical models exist for the prediction of the thermal and physical nature of nanofluids [1].

For this review, a simple discussion of some of the more prevalent theories on the dynamic thermal and physical behavior of nanofluids will be conducted, some of which can be seen below.

- Microscopic motion of host fluid and inclusion nanoparticles
- Microscopic forces acting on both fluid and particles—van der walls, electrostatic, electric double layer, stochastic forces, Brownian motion, and hydrodynamic force, etc.
- Increased surface area of nanoparticles
- Particle to particle interactions and collisions

- Brownian motion
- Molecular level layering of the host liquid at the liquid to particle boundary/interface
- Ballistic conduction within the Nanoparticle and diffusive conduction within the fluid
- Nanoparticle clustering
- Percolation theory
- Fractal theory
- Brownian motion based collisions of nanoparticles
- Nanoconvection
- Near field radiation
- Interaction between extremely small nanoparticles and liquid molecules
- Shape of nanoparticles
- Fluid temperature
- Particle drift velocity
- Drag of fluid pockets
- Kapitza resistance
- Thermal interactions between individual particles and fluid molecules.

The general methods for dynamic modeling of nanofluids falls into two primary categories: extension of existing models, and creation of entirely new ones. Both of these will be discussed in this review [1].

4.4.3. Dynamic Models

One of the first researchers to propose the dynamic nature of nanofluids was Wang et al. [1, 156]. They theorized that the enhanced effective thermal conductivity of nanofluid was based upon the microscopic motion of the nanoparticles within their host fluids. These small scale

motions were caused by forces acting on the matrix and particles due to the electric double layer at the particle interface, the stochastic force that causes Brownian motion, and the hydrodynamic force. No model was actually developed by Wang, because these forces cannot currently be calculated accurately. However, this work was the prelude to the hypothesis that particle size plays an important role in nanofluid conductivity increases, a theory that was later proven to be correct by numerous researchers [1]. In addition, they hypothesized that the chain linking of nanoparticles into clusters played an important role in the final effective thermal conductivity of nanofluids.

Xuan and Li [1, 157] proposed that several dynamic mechanisms could account for the enhanced effective thermal conductivity of nanofluids. These include increased particle surface area, particle to particle collisions, and the dynamic dispersion of the interacting particles. Later, Keblinski and Cahill [1, 158] proposed four distinct microscopic mechanisms to be the cause of enhanced thermal conductivity in nanofluids. These were: Brownian motion of the nanoparticles, ballistic conduction within the nanoparticles compared to diffusive conduction within the matrix, liquid layering at the molecular level at the particle fluid interface, and nanoparticle clustering. Research seems to indicate that dynamic mechanisms of heat transfer such as Brownian motion play a very important role in nanofluids containing spheroid particles, while more static mechanisms such as percolation dominate in nanotube based nanofluids. Many researchers such as Wang et al. and Keblinski et al. in the early phases of dynamic nanofluid model development have theorized that Brownian motion is one of the key aspects in the anomalous characteristics of nanofluids. Although in later scientific works, both researchers stated that Brownian motion did not in fact govern thermal transport within a nanofluid. Ultimately, Keblinski conclusively showed that nanofluid dynamic conduction was not driven by Brownian motion. It should be noted however, that many researchers such as Das et al. and Patel et al. [1, 159, 160] among

others still believe that Brownian motion plays an important role in modeling the strongly temperature dependent nature observed in nanofluids [1].

Xie et al. [1, 94] experimentally showed that nanofluids have a strong dependence on nanoparticle size and studied the roles of size and temperature on nanofluids with Brownian motion. This confirmation that matrix temperature plays an important role is consistent with the fact that Brownian motion is temperature dependent. In addition, numerous current dynamic nanofluid models are based on the fact that nanoconvection caused by nanoparticle motion is one of the most important characteristic of thermal transport within nanofluids.

Xuan et al. [1, 161] predicted that the effect of Brownian motion and the aggregation of nanoparticle structures and clustering, which are known as fractals, play a huge part in nanofluids. This theory was used to create a dynamic model which showed good agreement with experimental nanofluids. Xuan's work also demonstrated, perhaps the first to do so, that fluid temperature plays a critical role in the ultimate effective thermal conductivity of a nanofluid. Yu et al. [1, 162] theorized that drifting nanoparticles drag small volumes of the fluid matrix with them and can interact to create nanoconvection on a particle by particle bases. These floating nanoparticles drag liquid pockets with them and create randomly moving nanofluid/nanoparticle cells, which interacts thermally and physically with their neighbors thus creating micro-mixing and ultimately large scale heat transfers. They also reported that at least a small enhancement in the effective thermal conductivity of nanofluids is caused by particle collisions and thermal gradient based drift velocity/convection. These researchers created a model that showed that this micro-mixing effect was very important and prevalent with highly dense nanofluids >1% along with the importance of inter-particle potential. They were able to show good agreement with some experimental work as well.

Jang and Choi [1, 163] created, for the first time, a dynamic nanofluid model which takes into account the effect of a single Brownian motion driven nanoparticle and its induced nanoconvection on a nanofluid. Their model included four distinct modes of energy transport. These include collision between the matrix fluid molecules, also known as diffusive thermal conductivity, the diffusive thermal conductivity of the fluid matrix combined with the thermal conductivity of the inclusion particles (this refers to the interfacial response of the matrix and the particles or the Kapitza resistance), the dynamic collision of the nanoparticles (these collisions are caused by particle motion due to Brownian motion) and the heat transfer through the dynamic interaction of nanoparticles with the matrix fluid molecules. The final mode, which had previously been largely overlooked, has proven to be one of the more important features in the temperature and size dependency of thermal conductivity for nanofluids. These models showed good agreement with experimental data, and correctly predicted the temperature dependence of nanofluids along with the size dependency of nanofluids. The most important aspect of their work was to show that Brownian motion causes nanoconvection like effect on nanoparticles. They also showed that localized short time length micro-scale convection is induced by the Brownian motion of the nanoparticles and this mode of thermal transport plays an important role in the thermal conductivity enhancement of nanofluids. These nanoconvection models add to the already existing conduction models and might be the turning point in finally creating a true nanofluid model. In addition, Jang and Choi [1, 163] discovered that nano-scale convection increases with decreasing particle size due to increased Brownian motion of the nanoparticles and thus convective heat transfer. This was discovered by analyzing the fundamental differences between static composite models, and dynamic fluid models. And the fact that often the fluid and solid isotropic homogeneous mixtures show opposite trends when it comes to thermal conductivity and nanoparticle size.

A unique theory presented by Kumar et al. [1, 164] combined the dynamic and static models into parallel paths of thermal transport. The static model accounts for the dependency of nanofluids on nanoparticle size, while the dynamic model accounts for their temperature dependency. They theorized that the two parallel heat paths interacted with the liquid molecules and the nanoparticles separately. The authors coined these the “stationary particle model” and the “moving particle model.” Further details into Kumar’s work can be seen in the attached literature [1]. By extension Koo and Kleinstreuer [1, 165, 166] theorized that nanoparticle dynamically drag fluid cells with them, thus creating micro-mixing. They created one of the first nanofluid models that theorized the effects of Brownian motion on nanoparticle nanoconvection and micro-mixing. They also studied the effects of inter-nanoparticle potential. Their work showed good agreement with some experimental work. These authors also demonstrated that the effects of Brownian motion were far more important than those of thermophoretic and osmophoretic motions and that nanoparticle interactions can be neglected when particle volume concentrations are low <0.5%. Prasher et al. [1, 167, 168] developed a dynamic model which included the effects of Brownian motion on the inclusion particles and thus their nanoconvection with multiple nanoparticles in a fluid and thus to create a nanoconvection model for more than a single nanoparticle. Further work by Prasher in extending the theories of Jang and Choi [1, 163], were able to prove that localized micro-scale nanoconvection caused by Brownian motion of the nanoparticles was the primary mode of heat transfer within a nanofluid. They were able to do this through an order of magnitude analysis of the various possible heat transfer modes of thermal energy.

Ren et al. [1, 169] created a dynamic nanofluid model which takes into account the kinetic theory based micro-convection and liquid layering of fluid to particle interfacial contact. The authors also included the conduction through both the inclusion nanoparticles and the host liquid

matrix in their theories. They considered a nano-layer of thickness roughly a few nanometers around a given nanoparticle and were able to calculate the thermal conductivity of this nano-layer by combining and averaging the conductivities of the matrix fluid around it and that of the nanoparticle itself. This model predicted the dependency of nanoparticle concentration, size, and temperature. These predictions matched some experimental data. Patel et al. [1, 170] created a model based upon micro-convection created by Brownian motion and the specific surface area of the inclusive nanoparticles. They modeled this convection with empirically derived Nusselt numbers and definitions and obtained good experimental agreement. Additionally, Chon et al. [1, 171] created a model for the nanoconvection of dynamic nanoparticles within a nanofluid derived completely from experimental data and were able to calculate the Brownian velocity by using the mean free path as a characteristic length. Their model shows the relationships between nanoparticle size and temperature on the effective thermal conductivity of a nanofluid. Their work can be further reviewed in [1]. Xu et al. [1, 172] were possibly the first to develop a fractal convection model which took into account the fractal size distribution of the particles and the nanoconvection induced by Brownian particle driven motion. Their model accounts for nanofluid dependence on particle volume concentration, size, fractal dimension and temperature. Similar to this work, Wang et al. [173] created a model based upon the effective medium approximation and the fractal theory for the depiction of nanoparticle clusters and radial distributions. The authors use the suspension properties of nanoparticles, based upon percolation theory within fluids, along with nanoparticle size effects and surface adsorption to create their theoretical model. Ultimately, they found good agreement with experimental results of dilute suspensions of metallic based nanofluids.

Evans et al. [174] used a kinetic based theory to analyze the characteristics of heat flow within nanoparticle/fluid suspensions. They did this to show that the hydrodynamic effects often

found with Brownian motion do not greatly influence the effective thermal conductivities of nanofluids. The authors dynamic theory is supported by a molecular dynamics based simulation on well dispersed nanofluids, the effective medium theory, and recent experimental results on dispersed and stabilized metallic based nanofluids.

Prasher et al. [175] performed a detailed review of how the aggregation kinetics of nanoparticles combined with colloidal chemistry and the physics of thermal transport can have a profound effect on the ultimate conductivity of their nanofluids. The author's state that many of the anomalous behavior associated with nanofluids can be explained by taking into account aggregation kinetics.

Domingues et al. [176] created an effective thermal conductivity model based upon the fluctuation-dissipation theorem to analyze the thermal transport between two nanoparticles separated by sun-micron distances. The author's used both a molecular dynamics and a Coulomb interaction between fluctuating dipoles approach. Ultimately, both methods agree for certain nanoparticle separation distances.

4.4.4. Conclusions

The dynamic theories presented by the researchers above offer a great deal of insight into the potential reasoning behind the nature and behavior of nanofluids. It is extremely likely that a conclusive theory or model will not be discovered until a great deal more information is accumulated. Therefore, for now, these theories will remain just such and the field of nanofluids will remain primarily experimental. The study of nanofluids will have to continue without researchers truly yet knowing the physical phenomena that govern their behavior and nature.

Due to the fact that this is the first cryogenic nanofluid in existence and certainly the first one tested for enhancement in thermal conductivity, all presented results are singular in terms of comparison with other authors. A full verification and exploration of the physical and thermal

properties of cryogenic nanofluids, along with their potential abilities and applications will fall to future researchers. Truly, a great deal more work will be required before the field of cryogenic nanofluids is fully understood.

When comparing the effective thermal conductivity results of the above CN's to more traditional nanofluids, it should be kept in mind that the current models and theories of nanofluid behavior are still in their relative infancy. A true governing method, theory, or equation has not been found for traditional nanofluids, much less cryogenic ones. Some of the more common static models and dynamic theories along with data collected by other researchers on more traditional MWCNT based nanofluids were presented in the nanofluid theory and literature review chapters of this thesis. The results of the MWCNT based CN's studied in this research were informally compared to the adapted static models, traditional MWCNT nanofluid data and most relevant dynamic theories. In general, the static models did not match the measured data. This is undoubtedly due to the fact that nanofluids of any kind are complicated without parallel. When compared to a selection of traditional MWCNT nanofluids the measured results showed good agreement. At least, the order of magnitude increases of the effective thermal conductivity values were similar within comparable nanoparticle volume concentration ranges. The dynamic theories presented in this work are not at this time comparable to the measured results. This is due to the fact that creating a dynamic or mixed model of a cryogenic nanofluid is incredibly complex, difficult and well beyond the current scope of the field and is certainly outside the objectives of this research. However, based upon the unofficial comparisons made within this research, the authors feel confident that their results are within reason, when compared to traditional nanofluids.

The static models presented above for the effective thermal conductivity are compared to the measured cryogenic nanofluids effective thermal conductivity in Appendix C.

CHAPTER 5

EXPERIMENTAL SETUP

5.1. Background

The experimental setup used in this research to calculate the thermal conductivity of cryogenic nanofluids is a customized version of the transient hot wire technique. The design is loosely based upon the ASTM standards for the thermal conductivity measurement of fluids and refractory brick, as well as several designs of THW systems by other researchers, see the literature review of THW systems presented earlier in this thesis. The THW system used in this research was, by necessity, modified by including the best design characteristics of the ASTM standards and hot wire setups presented in the previously studied literature. The design was also highly depended upon the equipment that was already available or could be purchased. The reason for these modifications was that, unlike more traditional thermal conductivity measurements, this design would include all the difficulties associated with testing a nanofluid, combined with those of testing a cryogenic liquid. This chapter will focus primarily on the details of the experimental setup used in this research as well as some of the thought and reasoning that went into the design. Finally, a detailed step by step review of the testing procedure for obtaining the thermal conductivities of both the base liquid Oxygen and the various cryogenic nanofluids explored in this research is presented.

5.2. Introduction

The theoretical design and modeling that went into this experimental setup was extensive and can be reviewed in detail within the theory chapter of this thesis. However, theoretical designs and analytical behavior models can only go so far in predicting how an actual experimental setup will perform. Many parameters are unknown or turn out to be different than was expected.

Whereas in the theory section the discussion was on how this experimental transient hot wire setup should work, this section will discuss how it actually worked.

A transient hot wire test is, in all actuality, very simple: a long thin platinum wire is suspended either vertically or horizontally within the medium for which the thermal conductivity is to be measured. A power source is used to energize the wire for a brief period of time. This flow of power causes the hot wire to momentarily heat up due to resistive heating, which results in a change in the platinum hot wires resistivity. From this variation in resistivity the change in the hot wires temperature can be directly determined via calculation. Therefore, with this knowledge plus that of the exact dimensions of the hot wire and the total testing time, the thermal conductivity of the surrounding medium can be calculated from the cylindrical transient heating governing equation derived in the theory chapter of this thesis.

$$k_f = \frac{q'_w}{4\pi(T_2 - T_1)} ln(\frac{t_2}{t_1}) \tag{5.1}$$

Therefore, the basic operations of an experimental transient hot wire thermal conductivity measurement setup is that of measuring the change in resistivity of a platinum wire suspended within the material of interest, with precisely known dimensions, with a known amount of power. With such a simple operating theory it is not surprising that a veritable cornucopia of custom designs and experimental setups exist. These experimental designs can range from the simple to the extremely complex. Some of these custom designs focus on a particular aspect of the transient hot wire test and strive to improve that one parameter. Others try to improve the accuracy, precision, reliability, robustness, or ease of use of the THW method in general. Still others focus on modifying the transient hot wire method for new materials, situations, or operating parameters. In addition to the numerous custom designs, more traditional experimental setups such as the ASTM standards give exact step by step instructions for how to use the THW method to measure the thermal conductivity of fluids, and a assortment of other types of materials. The variety in

experimental transient hot wire designs proves that a given situation will necessitate an experimental setup which is designed specifically for it. The standard methods can be used as a baseline and the numerous other custom designs can be used for ideas and inspiration, however, in the final analysis each situation will require a specially designed custom made transient how wire experimental setup.

5.3. Cryogenic Nanofluid Experimental THW Design

The fact that this research calls for not only a nanofluid, but a cryogenic nanofluid means that it, too, will require a custom design. One of the unique aspects of this research is that the operating temperatures are extremely low. Traditionally, the thermal conductivity of cryogenic fluids are tested with the use of temperature and pressure controlled chambers and the use of the modified planer heat source thermal conductivity test among others. However, due to the fact that this method requires technology that was not available, plus a much more sophisticated experimental setup, coupled with a far more complex post analysis procedure, it was not deemed appropriate for use in the current research. In addition, a nanofluid would be difficult to test due to the fairly long periods of time required to reach steady state values. Therefore, it was decided to utilize a custom designed THW system. Further thoughts into the ultimate decision to utilize the THW method for this work can be seen in the literature review chapter of this thesis.

The materials used in the experimental setup of this research had to not only withstand the thermal shocks associated with a rapid temperature decline to temperatures as low as 77 K, but had to be able to act as a stable and coherent unit at those temperatures. This means that all materials chosen had to have similar and small coefficients of thermal expansion. Another aspect of this unique system was that of the highly oxidizing nature of LOX. Any and all materials that come into contact with liquid oxygen will experience a severe and much more rapid oxidation rate than would normally be encountered. Therefore, every material chosen for this research

needed to be as environmentally neutral as possible; this includes the materials for the experimental setup as well as those of the nanoparticles. A final aspect of this particular research that needed to be accounted for was that of the relatively high current values, coupled with small voltage signals. Because the platinum hot wire, as well as all the power and voltage signal wires, is submerged in cryogenic liquids the relative resistivity values of these materials are very small, in some cases approaching that of a superconductor. Therefore, to achieve a measureable change in voltage, and thus resistance, a substantial amount of current is required, far more than would normally be called for in a near room temperature, or elevated temperature thermal conductivity hot wire test.

Ultimately, a system was developed that could handle not only the cold temperatures of the cryogenic fluids, as well as the largely oxidizing environment of the liquid oxygen, but also the large current values coupled with the relatively small and noisy voltage levels. The equipment used in this research is listed below along with a brief description of what each component does, why it was chosen, and how it interacts with the system as a whole. The simplified diagram below shows the layout of the experimental setup. The entire system is built within a series circuit, with the voltage meter acting as a parallel measurement. Finally, it should be noted that a series of design iterations led to the final evolution of the existing experimental setup. These real world experience driven improvements included a variety of practical and necessary modifications to the total electrical systems (both inner and outer), the inner voltage measurement systems, the shielding, both inner and outer containment vessels, the cooling system, the mixing process, and the inner THW harness design. Voltage signal measurement enhancements were explored via the use of signal filters and amplifiers, along with Wheatstone bridge circuits, etc. Ultimately, these experience based improvements and upgrades led to the perfection of the existing experimental system.

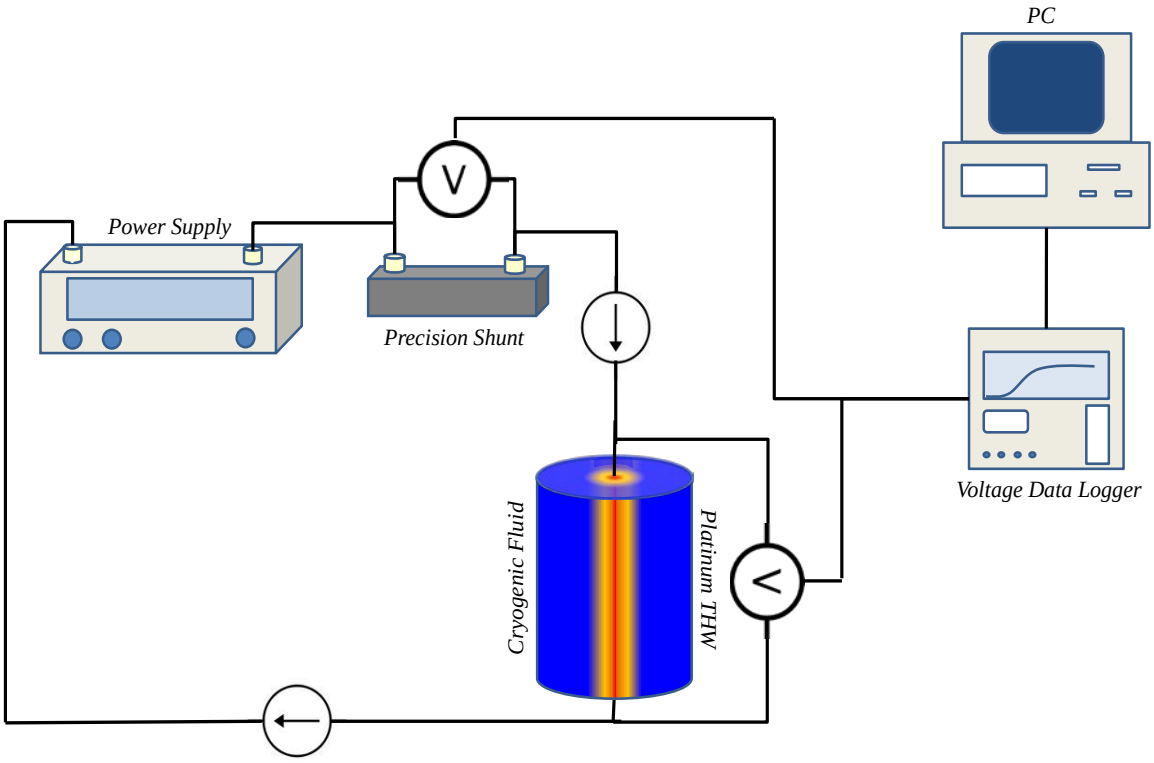

Figure 5-1. Simplified diagram of the custom design and made experimental THW setup utilized in this work.

Experimental Equipment List:

- TDK Lambda UP36-12 constant current power supply
- Power cord noise reducing induction collar
- Dual 22 gauge shielded (mesh/foil) power wire
- Power juncture terminal
- Hot wire experimental harness
- Current sensing shunt
- Shielded cabinet enclosure
- Dual 22 gauge shielded (mesh/foil) voltage sensing wires 4-wire
- USB 1608 FS voltage analog to digital DAQ

- Governing computer
- Inner cryogenic chamber
- Outer cryogenic cooling chamber
- Thermally insulated cryogenic chamber
- Styrofoam bottom insulation.
- Nanoparticle mass scale
- Probe sonicator mixer
- Inner mixing beaker
- Outer cooling beaker
- Nanoparticle beaker containers
- Stirring rods
- MWCNT nanoparticles
- Cryogenic storage tanks
- Cryogenic transport tanks
- Assorted tools
- Cryogenic safety gear

Hot wire experimental wire harness

- Brass power transfer bolts
- Nylon support washers
- Nylon support bolt and nut
- Steel support spacers
- Copper spring power transfer wires
- Platinum hot wire

5.4. THW Experimental Wire Harness

The experimental THW harness provided the support and structure for the suspended platinum wire along with the power leads and voltage measurement wires (see figure 5-2).

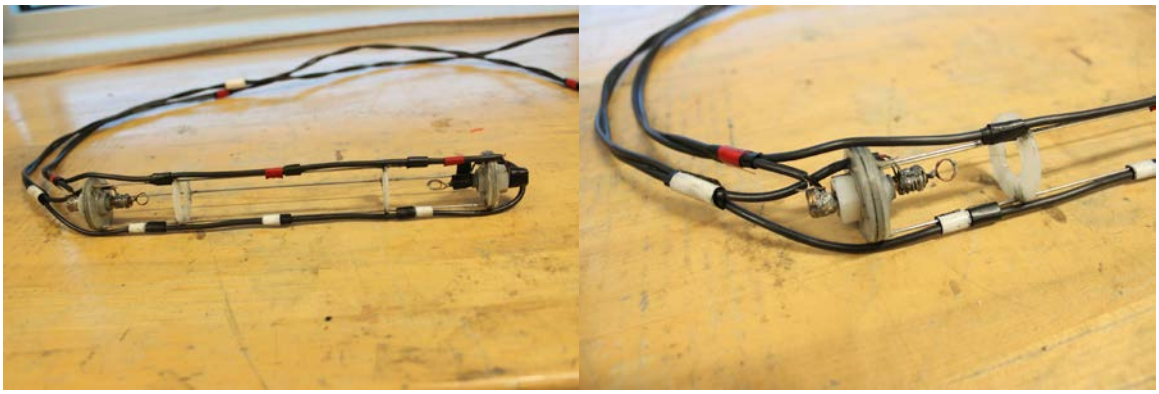

Figure 5-2. Experimental THW harness.

5.4.1. THW Experimental Wire Harness: Brass Bolts

The brass bolts for this experiment are 10 X 24 X 1.5 pure brass hardware bolts. They are used to transfer the constant current generated by the power supply to the hot wire and as electrical attachment points for the voltage sensing wires. It should be noted that said voltage wires are attached via solder and insulated with electrical tape.

5.4.2. THW Experimental Wire Harness: Nylon Washers, Nuts & Bolts

Nylon washers and bolts were used in this research because of their physical stability at cryogenic temperatures and their immunity to the highly oxidizing environment provided by LOX. Another key factor in choosing nylon is that it acts as a superb electrical insulator, thus guaranteeing that no stray currents escape from the system's current loop into the wire harness or experimental setup. The nylon bolts are used to stabilize the brass electrical bolt and to provide

insulation. The various nylon washers were used as electrically isolative spacers, and frame stabilizers for the hot wire harness.

5.4.3. THW Experimental Wire Harness: Steel Support Rods

Thin steel rods were used to provide the hot wire harness structure and spacing. These were originally, MIG stainless steel welding wires and were shortened to create the desired hot wire length. They ensure that a cylindrical medium of cryogenic nanofluids were created in the immediate vicinity of the THW.

5.4.4. THW Experimental Wire Harness: Platinum Wire

The platinum wire used for this research is a five thousandth of an inch platinum thermocouple wire purchased from omega.com. This was done because Omega offered 99.99% pure platinum wire in the size range required for this test and the cost was less than that of other precious metal distributors. The platinum wire acts as the energizing/sensing wire for this system and is suspended between the stabilized Brass bolts. It carries the electrical current generated by the power supply and is measured in a four wire voltage sensing loop by the DAQ.

5.4.5. THW Experimental Wire Harness: Copper Connection Wire

The wound copper spring loops used to attach the platinum hot wire to the test harness are made from stripped 22 gauge copper wire. The wire is laid bare and wrapped around the threads of the copper bolt. Six distinct wraps are made and then the end is coiled into a double closed helix and secured to the neck of the wire loop. The platinum wire is securely triple tied off to the Brass bolt and a dot of silver solder is used to cement the copper loop and guarantee the electrical contact between the two metals.

5.4.6. THW Experimental Wire Harness: Electrical Tape

The power and voltage electrical contact points were covered by standard black electrical tape. This ensured that no stray contact with conductive material existed between any of the power or sensing leads. In addition, red and white electrical tapes were used along with black to color code the various wires of the experimental harness. This allowed the rapid and accurate identification of the bundled wires and prevented the accidental energizing of the sensitive voltage sensing leads.

5.5. THW Experimental Setup

The experimental THW setup for this research consisted of three primary facets; these included the experimental wire harness, which acted as the measurement probe of the cryogenic nanofluid and was discussed above. The second is the overall setup which includes the power supply, the measurement DAQ, precision shunt, Etc. The final aspect was that of the laboratory space in general. This served the purpose of preparing and maintaining the actual experimental setup along with the space in which this research was conducted. Figures 5-3 through 5-5 provide an idea of the general experimental setup within the given laboratory space. Figure 5-3 shows the primary workstation for the research and provides the space needed for the preparation of the CN's as well as the computer interface and power supply. The shielded cabinet containing the inner THW setup is also shown. Figure 5-4 details the workspace utilized in the actual design and construction of the experimental setup. This includes the space required for the maintenance, and storage of the assorted THW experimental components, as well as the visual inspection and long term storage of the CN's. The interior of the experimental enclosure is shown in figure 5-5 and clearly shows the inner and outer chambers used to control the temperature and stability of the CN's. The entirety of the THW itself is also shown along with the wiring, voltage data acquisition system, and precision shunt.

Figure 5-3. Front facing photograph of experimental laboratory space.

Figure 5-4. Rear facing photograph of experimental laboratory space.

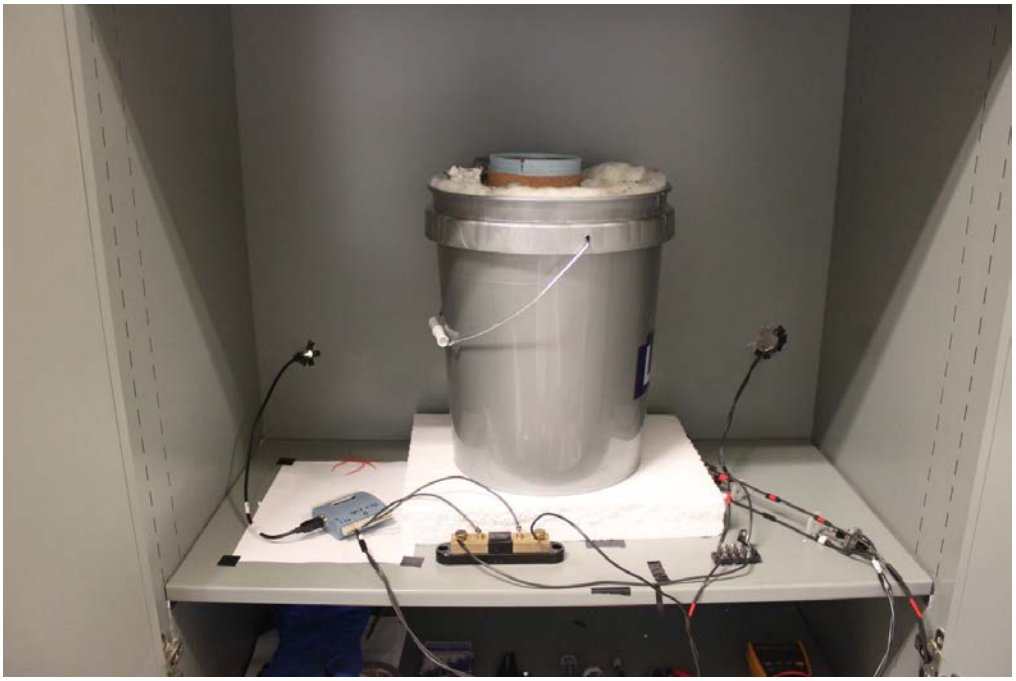

Figure 5-5. Enclosed and shielded THW experimental setup.

5.5.1. THW Experimental Setup: Power Supply

The entire experimental THW setup is driven by the power supply. The power supply provides a preset amount of current to the entire system, which generates the thermal and voltage gradients within the near field fluid and allows the back calculation of the effective thermal conductivity. The TDK lambda UP36-12 (figures 5-6 and 5-7) is a, 0-36 V 0-12 A, constant current and voltage power supply [177]. This power supply has the advantage of having very large voltage and current ranges. In addition, it allows for over and under voltage protection. It does not have a power/voltage/current feedback system. Therefore, as the platinum wire's electrical resistivity changes, so will at least one of the power supply parameters.

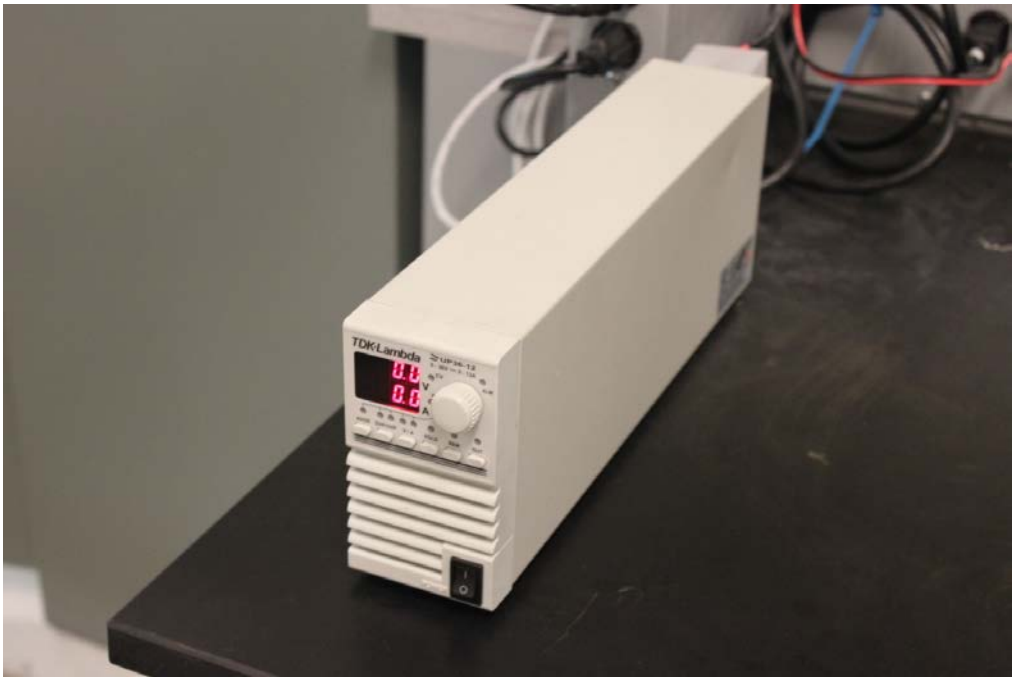

Figure 5-6. TDK Lambda constant current power supply.

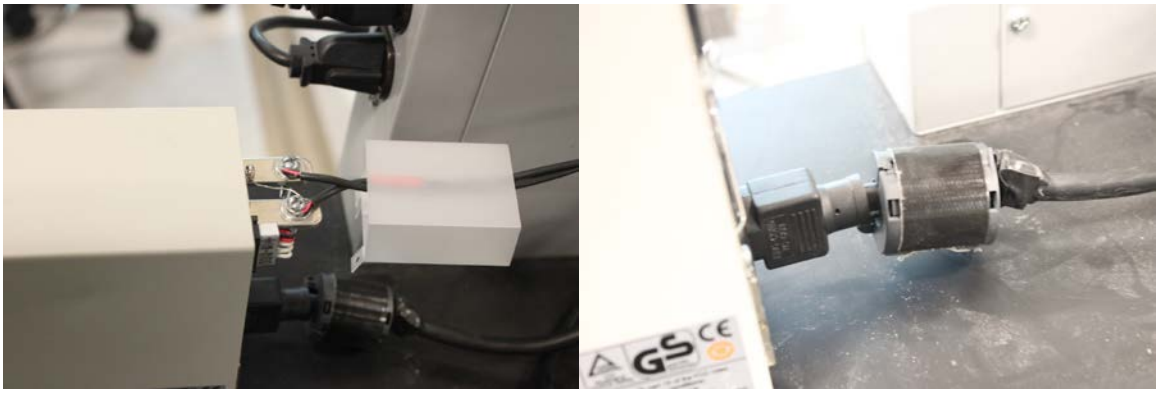

Figure 5-7. Constant current contact points for power supply, induction collar also featured.

A final aspect of why this power supply was used in this research is because several were available in the thermal fluids lab (MTL). As was mentioned previously, a constant power source would have been more desirable. In addition, many previous researchers have made due with a constant current source.

5.5.2. THW Experimental Setup: Power Supply Noise

This experiment was plagued by a fair bit of environmental noise. The exact source of the random noise detected in the voltage signal was never fully determined; however numerous sources could have been the culprits such as the fluorescent lights, noisy ground sources within the building's power system, and any number of electronic signals produced by the copious amounts of nearby electronics. However, the source could have also originated within the power supply itself. When power supplies convert the available 120 V AC voltage source from a standard wall socket into the desired constant DC current value, it does so by the use of a rectifier. During this process a high frequency hum can be generated by the conversion electronics [178]. This high level random noise is than projected onto your DC offset as a small scale noise level. This type of noise can be very hard to detect, and often must simply be assumed to exist and compensated for. One way of doing this is to add an induction coil surrounding the power supply line. This induction collar will act as a damper to the supplied power. It works by the fact that a flow of electrons generate an electromagnetic signal, which in a non-energized current capable material, will generate a magnetic field and hence a current of its own. By forcing the power supply current to induce this magnetic field in a large induction coil it acts as a damper to the signal itself. Thus, only powerful slow periodic noise values are allowed to exist undamped (the DC offset signal being the primary of these). Therefore, to combat the possibility of random high frequency noise generated by the power supply, an induction collar was added to the power lines. In addition, another collar was added to the power supplies own power cord. This would, in theory, dampen out any erroneous or undesirable signals from the building's own power source.

5.5.3. THW Experimental Setup: Power/Current Wires

The power carrying and signal carrying wires used in an experiment are very important. These wires will not only carry the current supply which will heat the THW in a steady and

constant manner, but then also carry the return signal to the data acquisition unit. Therefore, a great deal of care and thought must go into their selection. The first thing to decide upon is the material, size, and type of wire used. The most obvious material choice is that of copper. Being a good conductor, fairly oxidation and chemically resistant, and commonly available make it an ideal choice. However, in all reality because the hot wire is made from platinum, ideally, the wire connection points and wires themselves would also be made of platinum. This would ensure that no voltage sources were generated by TC interactions. However, this would be extremely expensive and in all reality not necessary except for special circumstances.

The wire size should be large enough to comfortable carry the required current/power, while being small enough to handle and manipulate easily. In addition, the wire diameter and length should be such as to not act as a noise catching antenna for the entire system. A wire gauge of 22 was chosen for this research. This diameter of wire is easy to handle and manipulate and can easily tolerate the current values required for this research. The types of wire available are often broken into solid strand or multi-strand. While the multi-strand wires are more flexible, durable, and can carry more power, making them ideal for transporting the power for the system, they are more difficult to work with and attach to the even thinner platinum wire. Because of these factors, the single strand 22 gauge wires were chosen to carry both the energizing power and the return sensing voltage.

Another important aspect of wire selection is that of whether to shield the wire. Unshielded wire is cheaper, smaller, and more readily available. However, a great deal of system noise can be picked up from the environment and then introduced to your system by unshielded wires. Therefore, for a small signal detection system such as this, a shielded wire setup is highly recommended. Shielded wires come in three primary categories foil shielded, mesh shielded, and dual. The foil shield provides protection against small amplitude high frequency signals, while

the mesh does the same for low frequencies. Because this system is exposed to a variety of noise signals, a double shielded wire system with an outer foil shield, and an inner mesh shield was chosen (figure 5-8).

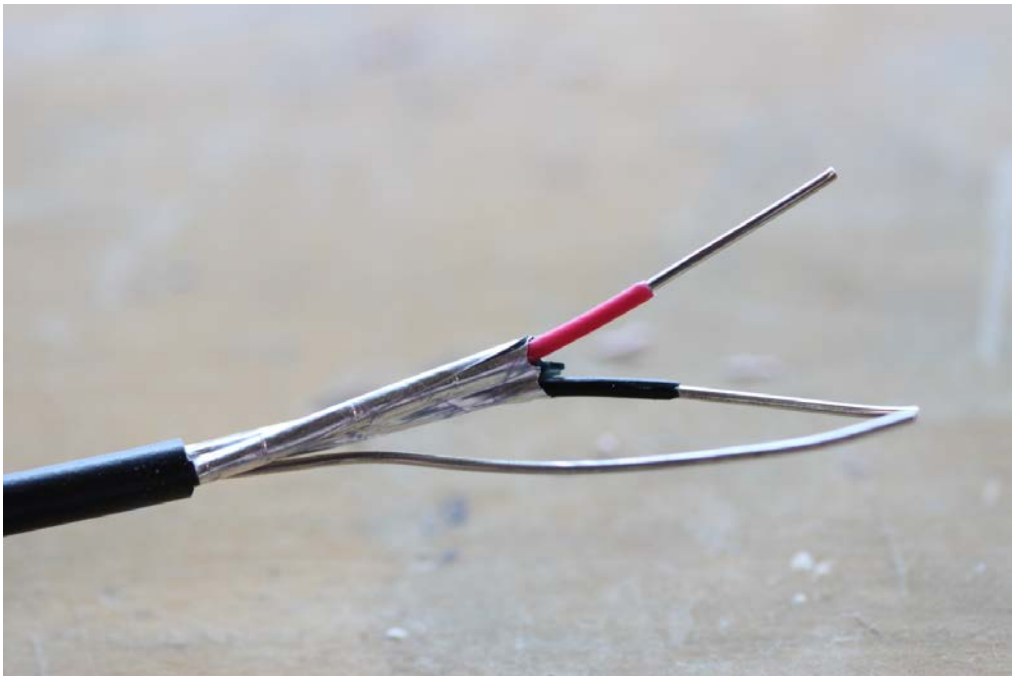

Figure 5-8. Shielded power and signal wires.

It should be noted that in previous versions of the experimental system, unshielded 22 gauge wire was used, with a single strand type used for the voltage signal wires, and a multi-stranded type used for the power carrying wires. However, this setup proved to be fairly noisy. A final note to be made is that because both the power and voltage signal carrying wires will by necessity be submerged in the base liquid, in this case LOX. An appropriately resistant outer wire cover material is needed. For this research wires with PVC outer coatings and PP inner coatings were chosen [178].

5.5.4. THW Experimental Setup: Voltage Wire Setup

The dual core wires used for the transference of the platinum hot wires voltage signals were set up in a four wire system. This was done for two reasons, the first being that by soldering the two dual wires one on top of the other a four wire resistance measurement setup was created. A four wire resistance test uses two wires to carry the trace currents, while the other two do the actual measuring. This allows the differences between the wires to be neglected, which removes any resistance due to connectors or test wires. This would allow for the very accurate measurement of the hot wire's resistance if needed, which would be required if it was decided to perform a full temperature range calibration test. The second reason was that if so desired, the two wires could be simultaneously measured for voltage. Therefore, any common voltages between the two wires could be subtracted from each other. This would ensure that the two wires do not act as noise antennas. However, this is already accomplished for the most part by the fact that this experimental setup uses a forced voltage differential to measure the change in the hot wire's resistance.

5.5.5. THW Experimental Setup: Power Junction

The power juncture terminal used in this experiment was simply a steel screw terminal power transfer point. This was needed so that the power supply wires could extend from the actual power supply into the shielded enclosure and attach to a specific solid point without having to have the entirety of the power wire series being connected. This allowed for the hot wire harness to be easily removed and or replaced without needing to completely deconstruct the entire experimental system. The particular power junction used for this research can be seen below in figure 5-9.

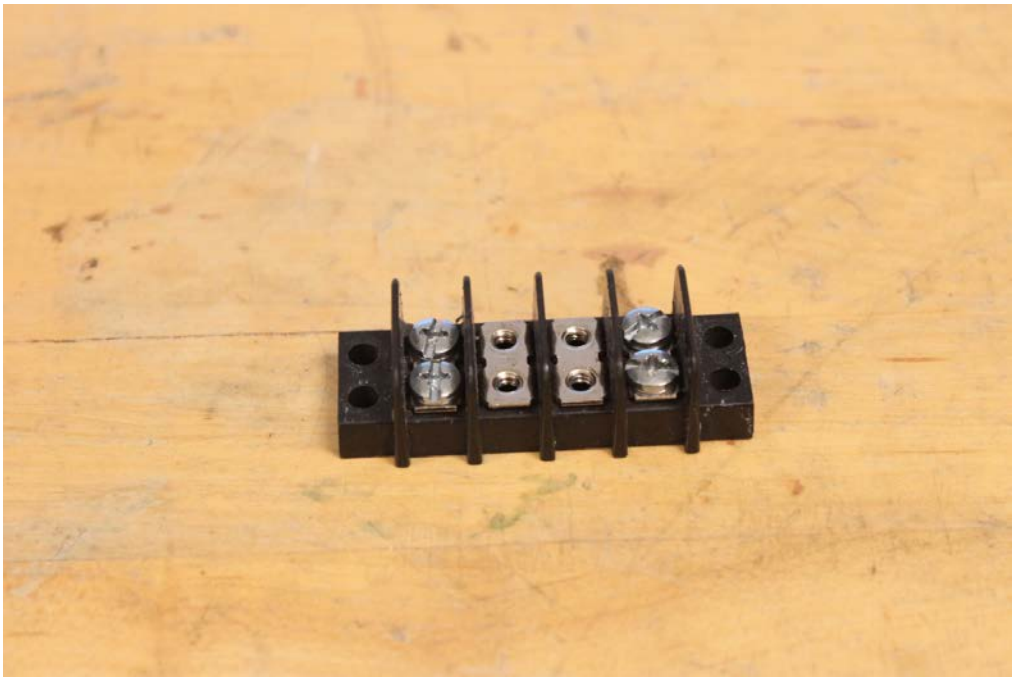

Figure 5-9. Experimental power transfer junction.

5.5.6. THW Experimental Setup: Current Sensing Shunt

This system was set up in an electrical series, so that the constant current value produced by the power supply is the same throughout the system. This is based upon Kirchhoff's voltage and current laws. The shunt in this system is used as precision current sensor. In essence, the shunt acts as a high power/current precision resistor which when placed in series with the hot wire allows the exact total system current value to be determined. For this research, a Galco 100 milli Volt shunt with a current rating of up to 10 A was used (figure 5-10). This particular brand was chosen due to its relatively high precision, large available current values, and low cost [179].

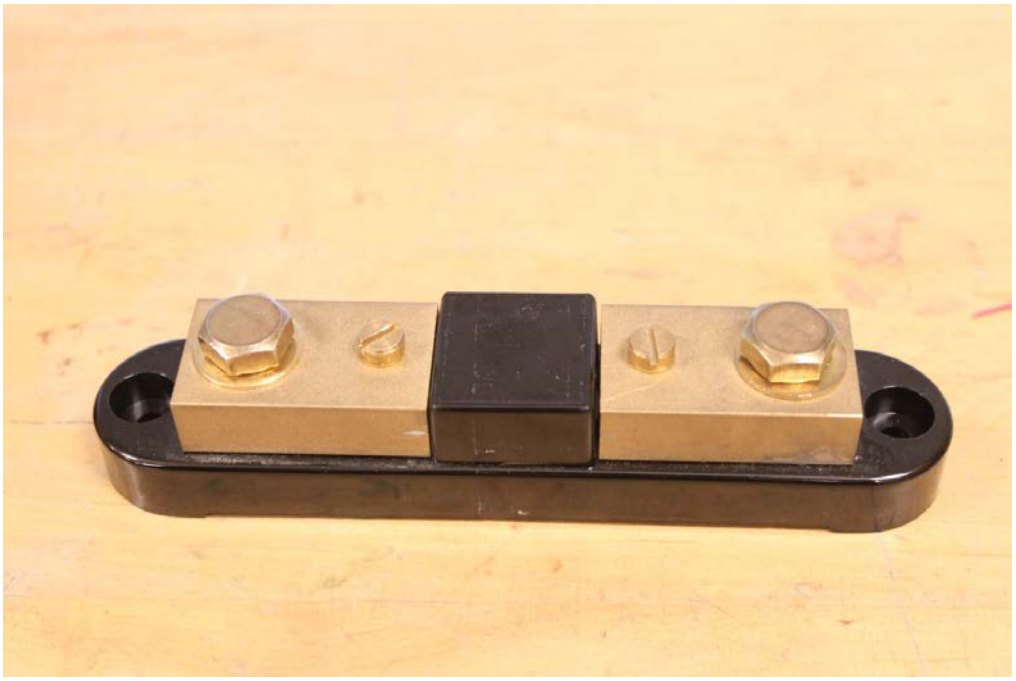

Figure 5-10. Precision current sensing shunt

5.5.7. THW Experimental Setup: Outer Shielding

The outer electromagnetic shielding cabinet was designed to act as a large, simple, Faraday's cage. The idea being that any unwanted environmental electromagnetic noise signals would be absorbed by the steel of the cabinet and directly shunted into the ground system (through a connected series of high capacity wires) for the MTL labs building However, this particular method of shielding did not appear to work, at least no noticeable EM shielding effects were detected.

5.5.8. THW Experimental Setup: DAQ

The system used to measure the hot wire voltage signals is quite possibly the most important piece of the entire experimental setup. The rest of the system could be perfect and if it could not be accurately measured, than the entirety of the experimental setup is irrelevant. The DAQ system

used for this research is made by Measurement Computing Systems, and is the USB 1608 FS model (figure 5-11). This is a mid-priced, analog to digital voltage DAQ.

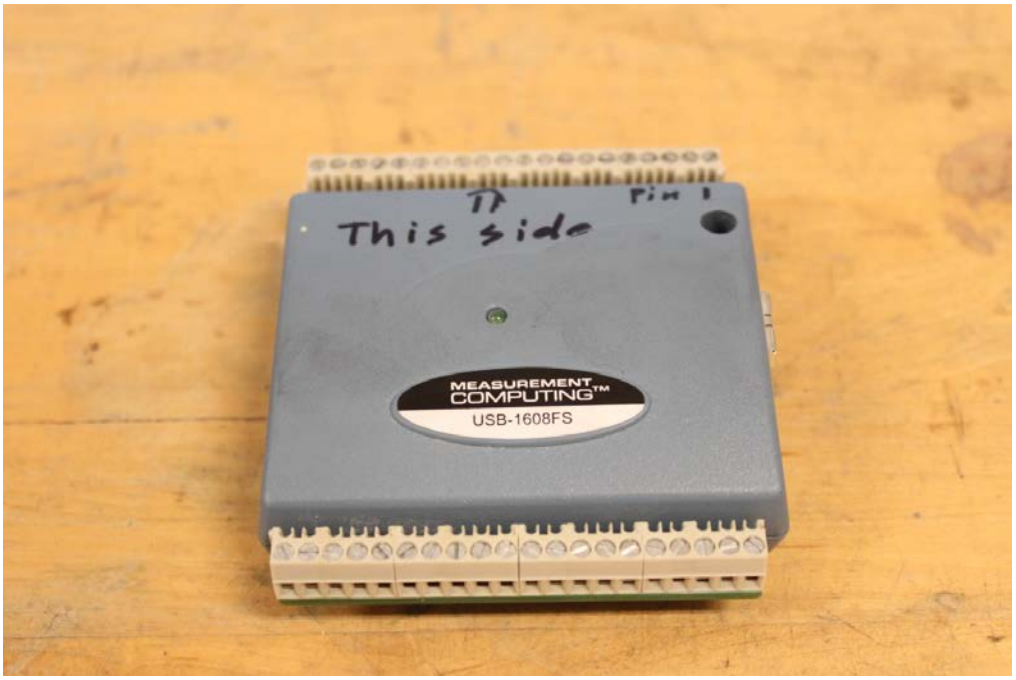

Figure 5-11. Experimental voltage DAQ measurement computing USB 1608FS.

5.5.9. THW Experimental Setup: Inner, Outer Experimental Cryogenic Enclosures

The inner cryogenic container used for this research was simply a 500 mL chemically inert plastic graduated cylinder. It was used to house the actual cryogenic nanofluid, in this case LOX. The volume of the graduated cylinder was determined from the size of the wire harness. In addition, the graduated cylinder needed to be tall enough to fully enclose the 6 inch plus hot wire harness, with at least an inch or two to spare and it had to be wide enough to allow the entire harness to slip in and out easily. The outer container is a 1/8 inch thick, 4 inch diameter, 14.5 inch long stainless steel pipe with a quarter inch butt plate welded onto the bottom of the pipe. This

outer container will support the cooling LN2 bath, and the inner chamber (graduated cylinder) filled with LOX.

Both the inner and outer cryogenic chambers are contained within the final outer container (figure 5-12). The LN2 outer steel bath is wrapped in a fine layer of flexible Styrofoam along with two distinct layers of insulating cork. Finally, this is surrounded by several inches of fiberglass housing insulation (R value of 34). The entireties of these enclosures are then placed within a 5 gallon plastic bucket. The three distinct layers of insulation provide, hopefully, a measure of protection from the large environmental temperature differences present in this research and presumably help to conserve both cryogenic baths from evaporation and environmental thermal/physical influences. Each of these types of insulation were chosen for their flexibility and high thermal resistance values. A large square of Styrofoam is placed beneath the total outer bucket to act as a thermal insulator between the bottom of the cryogenic chambers, and the ground. Finally, a small Styrofoam cutout is placed as cork in the inner cryogenic LOX chamber to prevent atmospheric and environmental influences on the cryogenic nanofluid.

Figure 5-12. Experimental outer and inner containers with insulation.

5.5.10. THW Experimental Setup: Mass Scale

In order to determine the desired volume percentage of nanoparticles for a specific test, the mass of the bulk particles was measured for each of the desired concentration values. This is done by using the bulk mass value, along with the nanoparticles true density to calculate the volume percentage of nanoparticles. The mass scale shown below in figure 5-13 is accurate to 1/1000 of a gram and, after careful calibration, was used to measure the mass of each of the assorted MWCNT concentration values.

Figure 5-13. Mass measurement scale.

Due to the fact that the true density of nanoparticles is often far larger than the bulk density, which is caused by large packing orders, the reported true density value, provided by the

manufacturers, was used in conjunction with the following equation to calculate the desired volume percentage concentration values.

$$Volume\ Percentage = \left[\frac{1}{\frac{\left(\frac{\rho_{Nanoparticle}}{m_{Nanoparticle}}\right)}{V_{Total}}}\right] \cdot 100 \tag{5.2}$$

where $\rho_{Nanoparticle}$, $m_{Nanoparticle}$, and V_{Total} are the true densities of the nanoparticles in (kg/m^3), the measured bulk mass of the nanoparticles in kg and the total volume of nanoparticles in m^3.

5.5.11. THW Experimental Setup: Mixing Sonicator

The sonication probe used during the mixing process is a Cole Parmer Ultrasonic Homogenizer (Model # CP501, figure 5-14). This particular system was used because it was already available within a neighboring lab. The probe is made from titanium with a tip length of 2.5 in and a diameter of 0.5 in. This exact tip geometry was not ideal for this research; however it would have been unduly costly to replace it. The sonicator is used to mix the nanoparticles into the liquid oxygen. This is done by a voltage signal generator attached to a pizo electric crystal which transforms the electrical signal into tuned oscillations with an extremely high frequency, and small variable amplitudes. This high frequency small amplitude vibration (in the micro-meter range) causes cavitation within the fluid. When these cavitation bubbles collapse, a shock wave is generated, this provides not only a thorough mixing force, but a significant amount of fluidic shear force which helps to break up nanoparticle agglomerations and clusters. Sonicators can generate a great deal of heat during operation, this can be difficult to manage at cryogenic temperatures, because the large thermal mass of the titanium probe tip and sonicator body combined with the heat generated during operation can easily cause gas bubbles to form around

the probe tip. If this occurs, than the mixing efficiency of the probe sonicator quickly drops off. In addition, the extreme cold of the cryogenic liquids can easily damage the electronics of the sonicator, and cause the efficiency of the probe to decline sharply. Therefore, it is important to use the sonicator as a mixing tool with small predefined bursts over a length of time.

Figure 5-14. Sonication mixing probe.

5.5.12. THW Experimental Setup: Mixing/Storage Beakers

The various mixing and storage beakers for this research are all borosilicate chemically inert glass beakers and containers. The 500 mL and 1500 mL beakers are used as the inner and outer coolant chambers for the mixing of the cryogenic nanofluids. Glass stir rods are used to provide bulk mixing during the sonication process. The smaller beakers are used as short term nanoparticle storage containers. In total, the glassware used for this research is shown below in figure 5-15.

Figure 5-15. Mixing and storage beakers.

5.5.13. THW Experimental Setup: Cryogenic Storage Tanks

Several different types of cryogenic storage tanks are used in this research. For long term storage, the FNL Lab 10 Cryogenic Dewar's are used (figure 5-16). This is because they have relatively large available volumes (10 L) and they are designed with duel wall vacuum seals and radiation shields. This allows them to store both liquid Oxygen and liquid Nitrogen for significant periods of time. The smaller Dewar's are thermoses and are used for short term storage and transportation. During an actual test these smaller containers are repeatedly filled and used to top of fluid volumes throughout the entirety of the test. Because the available storage Dewar's, for both LOX and LN2, had roughly 10 L's capacity, only a single day's worth of testing, encompassing one type of CN for the entirety of the required concentration values, was possible. This necessitated numerous refills which significantly lengthened the overall time required to fully study the assorted CN's

Figure 5-16. Cryogenic transport and storage containers.

5.5.14. THW Experimental Setup: Experimental Tools

Numerous assorted tools (figure 5-17) are used throughout this research from manipulators to basic hand tools for the construction and maintenance of the experimental setup. Also, multie-meters were used to check the electrical coherency of the experimental setup.

Figure 5-17. Experimental tools.

5.5.15. THW Experimental Setup: Cryogenic Safety Gear

Due to the inerrant dangers of close proximity and manipulation of cryogenic liquids, a basic set of safety equipment is required. These include: eye safety, ear protection, cryogenic cold temperature gloves and bib, and an oxygen level sensor. When used properly the safety gear described above can easily protect a researcher from the dangers of cryogenic fluids. To ensure that the continued boiling of the cryogenics did not endanger the laboratory as a whole, the exact procedure was checked with the university safety office, and the oxygen meter was kept on and calibrated to safe breathing levels. In addition, the theoretical displacement of the laboratory air, when faced with a catastrophic release of all of the available cryogenics, was calculated to ensure that at no point was there a sufficient quantity of LOX or LN2 to cause harm. Because of these precautions, and the use of the safety gear shown below in figure 5-18, the use of both LN2 and LOX was considered relatively safe.

Figure 5-18. Cryogenic safety gear.

5.5.16. THW Experimental Setup: Nanoparticles

The MWCNT's used for this research consist of three distinct types of multi walled carbon nanotubes. These MWCNT's were chosen because of their unique thermal and physical properties including extremely high individual thermal conductivities. In addition, numerous examples of MWCNT's having exciting and diverse effects on nanofluids have been recorded. Finally, carbon proved to be one of the only common nanoparticle materials that have a true density small enough to easily suspend and disperse within liquid Oxygen. Therefore, it was decided that they offered the best choice for a first attempt at not only the creation of a cryogenic nanofluid, but the testing of that cryogenic nanofluids effective thermal conductivity. Each of the MWCNT's utilized in this work was stored in bulk and are shown below in figure 5-19.

Figure 5-19. Assorted MWCNT's used throughout this research.

5.6. Experimental Procedure

5.6.1. Introduction

The experimental procedure created for this research was based upon a great deal of thought, theory and not a little bit of trial and error. The following will be a stepwise description of the testing procedure with any notable features discussed in greater detail. This procedural review will focus primarily on the testing of liquid oxygen with the various types of MWCNT's specified in the nanoparticle profile chapter of this work. An additional note on the experimental procedure would be to point out that several experimental THW harnesses were used throughout this research. In fact, often a single type of nanofluid was measured with a THW before that wire was retired and a new setup created. This ensured that potential contamination or degradation of the system or the wire was kept to a minimum.

5.6.1.1. Experimental Procedure: Preliminary Steps

The testing of the effective thermal conductivity of cryogenic nanofluids cannot begin without thorough preparation. This is of the utmost importance, because cryogenic nanofluids are a dynamic system and therefore are changing in a variety of ways with every passing moment. Therefore, once they have been mixed/created no time should be wasted in their testing. However, before the cryogens are mixed or inserted into the testing chamber, a few preparation steps must first be taken to ensure a smooth complication free test. These preliminary steps can be taken in any order, although, it is generally best to prepare the cryogens and perform the systems checks last.

5.6.1.1.1. *Preliminary Experimental Equipment Check*

The first preliminary step is to check the cryogenic fluid levels and purchase more if necessary. This includes both the host LOX fluid and the cooling jacket fluid LN2. The nanoparticles masses, which once separated, will give the pre-specified particle volume concentrations, can now be measured out based on total volume and bulk mass. Once each of the nanoparticle concentration levels (percentage by volume) are measured and separated, the beakers, graduated cylinders, and stirring rods used for the experiment should be cleaned and prepared for use. In addition, the hot wire experimental harness needs to be cleaned prior to each test. Specifically, the platinum wire should be checked visually for obvious contamination, debris or defects. Finally, all of the tools which will be used for the experiment must be laid out, the cryogenic storage tanks can then be filled, and ready amounts placed in the smaller vacuum Dewars. One of the last preparatory steps should be that of setting the probe sonicator to the desired settings. An amplitude, and burst time should be decided upon and set. For this research those were 60 micrometers and 20 seconds.

5.6.1.1.2. *Preliminary Experimental Systems Check*

The wiring for the entire experimental setup needs to be inspected prior to every experimental run. This entails using a multi-meter to check for circuit breaks, shorts, or any other electrical or connection problem with the wiring of the THW setup. The data acquisition system should be recalibrated prior to each day of testing. At this point, the governing computer used for the experiment can be turned on and a unique file name and appropriate subfolders made. The power supply can then be turned on and set to the pre-selected constant current value. This value was determined from the analytical design models in the theory chapter of this thesis. A constant current value of 0.7 A was chosen for these tests. Once this has been completed, the final DAQ settings can be set, these include voltage ranges, testing time, sample rate, and channels to be measured, as well as the file name and destination. A series of dry runs should be performed on the entire experimental THW setup prior to each cryogenic nanofluid test. These practice runs will ensure that the power supply, wiring system, electrical connectors, platinum THW, shunt, data acquisition system and computer are working properly and that all facets of the experimental setup and system are ready for the analysis of the effective thermal conductivity of cryogenic nanofluids.

5.6.1.2. Experimental Calibration and Validation

Before any actual cryogenic nanofluids can or should be tested the experimental system should be first calibrated and validated with pure LOX. This ensures that the system is measuring and calculating the correct effective thermal conductivity values for a given test and situation. It also allows for the detection and subsequent fixing/adjustment of any of a considerable number of experimental variables or factors which can change between experimental setups or even days. This calibration/validation was performed for every day of testing.

5.6.1.2.1. *Analysis of Pure LOX*

The procedure for the calibration and validation of the experimental setup via pure LOX testing begins by filling the outer storage tank with the cryogenic coolant, in this case LN2. This will take a substantial amount of liquid Nitrogen and some time (several minutes, to allow for cool down of the chamber and eventual calming of the LN2). Once the boiling of the LN2 inside the outer chamber has subsided and the temperature appears to have stabilized, the inner test chamber can be pre-cooled in a liquid nitrogen bath. Once it has reached a steady equilibrium temperature, the cooling LN2 can be poured out and a set amount of liquid oxygen (roughly 500 mL) can be poured into the inner testing chamber. This is a delicate point of the procedure; the inner chamber must be fully filled with LOX, which with the current setup will amount to roughly 500 mL. The outer coolant container, filled with LN2, should be full enough that the fluid level comes to roughly one inch below that of the liquid oxygen. However, due to the temperature differences between the two cryogenic fluids, robust boiling will occur within the LN2. If care is not taken, small trace amounts of LN2 can spill over into the LOX container. This, in and of itself, is not a cause for concern, because the two fluids have extremely different densities, with LN2 being substantially smaller than that of LOX. Therefore, the two fluids are immiscible with each other and the LN2 will form a layer on top of the LOX until it boils off. However, because the goal of this procedure is to test the base thermal conductivity of pure LOX and LOX mixed with nanoparticles, any impurities introduced by the LN2 should be avoided as much as possible. Therefore, it is important to lower the LOX chamber into the outer LN2 container slowly and to allow the temperatures to equalize slowly. If the LN2 bath is overfilled, and time is an issue, a hot object can be inserted into the LN2 bath and some of the excess fluid boiled off. Once the two containers are merged and the temperatures have equalized, the entire outer cryogenic chamber (inner LOX chamber, coolant chamber, insulation, and bucket) can be

lifted into the electrically shielded cabinet and placed on top of the bottom Styrofoam insulator. The hot wire harness can then be slowly lowered into the liquid Oxygen. This, once again, should be done slowly to prevent any damage to the hot wire setup due to thermal shock. Once the hot wire harness has been fully submerged, both cryogenic fluids levels should be checked. The entire setup, at this point, needs to be left to thermally/physically stabilize for several moments to allow any currents or turbulences caused by the introduction of the hot wire or the movements of the chamber to subside. This can be checked by placing a floating Styrofoam bob onto the top surface of the fluid and checking for relative motion. This is a fairly rough check and the primary method is to simply give the fluids a few seconds to become stable. Once they have, the actual testing of the pure LOX may begin.

The base liquid oxygen calibration values are tested twenty distinct times for effective thermal conductivity within a single experimental run. This allows for a substantial amount of post statistical processing. The data acquisition program is engaged and a period of roughly one second is allowed to pass. At this point the power supply is manually turned on, and the flow of constant current begins. This will introduce a variable power starting time, which will be taken into account and removed in the post processing work done by the numerical code. An entire thermal conductivity test lasts exactly five seconds (the total testing time specified here was decided upon based upon the analysis done in the theory chapter of this thesis), with approximately four of those seconds being powered. Once the program has reached the five second mark, determined by the number of samples to be taken per channel and the sample rate, the program will terminate and save the data to the specified file. A period of approximately 15 seconds is allowed to pass. This unpowered down time will theoretically allow any fluid motion caused by the convective heating of the hot wire to subside. At this point the governing program is restarted and the entire process begins again. This will be repeated twenty times.

5.6.1.3. Experimental Procedure for the Measurement of Cryogenic Nanofluids

At this point, the actual cryogenic nanofluids can be tested. This will begin by changing the name of the data destination folder (in which the measured thermal conductivity data will be stored) to one appropriate for a cryogenic nanofluid. The THW experimental harness can now be removed from the LOX calibration fluid and placed it carefully aside to dry and thermally equalize with the natural environment. The liquid oxygen used for the calibration test can be reused in for the first batch of cryogenic nanofluid. Two beakers one with a volume of 500 mL and the other large enough to fit the first one inside comfortable should be placed near the sonicator on an insulating pad of styrofoam. The outer beaker can be filled with liquid nitrogen and allowed to cool for several moments. Once the temperature of the outer beaker has reached a steady state value more LN2 can be added and the empty inner beaker can be placed within this LN2 bath. The inner 500 mL beaker can now be allowed to pre-cool until it appears to reach a steady chilled state. While this is happening, the levels of cryogens for the experimental test chambers, both inner and outer containers, should be checked and more added if necessary. Once the mixing beakers have reached their stable cold temperatures, liquid oxygen can be poured into the inner beaker. Once again the levels of LOX and LN2 should be monitored carefully within the beakers. The inner beaker should hold roughly 500 mL to match that of the inner test chamber and the outer beaker should hold a sufficient amount of LN2 to keep the oxygen at sub boiling temperatures. The inner beaker should once again be lowered slowly into the outer beaker bath and careful attention should be paid so that no LN2 contamination is introduced into the pure LOX. Once both fluids have reached a steady temperature and the LOX is no longer boiling or showing notable turbulence, the mixing apparatuses should begin their cool down process. This will consist of placing the entirety of the probe tip into the pure lox bath, and allowing it to cool. At the same time, the stirring rod can also be paced into the LOX bath. Once the fluid has stopped

boiling around the probe tip and glass stirring rod, the actual nanoparticle mixing can begin. The premeasured nanoparticle volume concentrations should be in individually labeled containers ranging from small concentrations up to large particle volume amounts. The first sample to be tested should be placed nearby to facilitate speed, the sonicator tip should be raised and an assistant researcher should hold the glass stir rod. The primary researcher will at this point gently tip the nanoparticles into the LOX. Great care should be taken at this point, while the cryogenic fluid is at an extremely low temperature, the nanoparticles are not. Therefore, if they are allowed to fall too quickly into the base LOX, they will experience micro-scale boiling and very energetically aerosol themselves into the atmosphere. Therefore, the nanoparticles should be poured slowly and with great care. Once the majority of the particles have been introduced into the host fluid the assistant should gently tap the bottom of the nanoparticle container to facilitate the inclusion of the rest. Once all of the particles have been introduced into the fluid, the beaker should be held with a small manipulator and briefly dipped into the base liquid Oxygen. This will remove any lingering nanoparticles. At this point in the mixing process time becomes an issue. Because these cryogenic nanofluids are not inherently stable, once mixing ceases agglomeration and settling will occur rapidly. Therefore, from this point on a certain amount of haste is required. The already pre-cooled sonicator tip should be lowered into the bath, and the assistant can begin bulk mixing with the glass stir rod. The sonicator variables have already been set at this point, and the sonicator will give burst mixing for a period of 20 seconds as the primary researcher, with the protection of cryogenic gloves, manipulates the two beakers in circular and up and down motions, while the assistant gently stirs the entirety of the cryogenic nanofluid bath. This entire process will occur three separate times, for a total of a full minute of sonication mixing. Between each of the three separate sonicator bursts, a break of five seconds will be observed. This will allow the turbulence within the various fluids to calm down and the sonicator tip to cool down. A

great deal of energy is released during sonication and if cool down breaks are not given, the sonicator tip can become heated, which will result in a gas bubble forming around the tip. If bubble formation occurs, then the sonicator will be vibrating in a gas and the mixing efficiency will drop significantly.

Once the mixing process has been completed, the newly mixed cryogenic nanofluid must be quickly poured into the inner testing chamber and placed back within the outer LN2 coolant bath. Then the entire testing chamber must be carefully placed back into the electromagnetically insulating metal cabinet. Once these steps have been completed, the hot wire harness is than once again slowly lowered into the cryogenic nanofluid and the fluid levels are checked and leveled if necessary. At this point the fluid motion should be visually checked by observing the motion of the macro-scale fluid bob and the actual particles within the fluid. Once it has been determined that most of the large scale fluid motion has ceased, the effective thermal conductivity measurement of the cryogenic nanofluid can begin. This process is once again based upon a series of five second conductivity tests, with fifteen second breaks in between. However, for a cryogenic nanofluid only ten distinct tests are completed for a given nanoparticle volume concentration. This is due to the fact that with the inclusion of nanoparticles, the thermal conductivity test has become extremely dynamic and therefore a longer testing time would only serve to allow the nanoparticles to agglomerate and settle even more. Once all ten tests have been completed the hot wire harness can be removed from the cryogenic nanofluid and that particular sample can be discarded into a Styrofoam waste receptacle where it will be allowed to evaporate in due time. This entire process will be repeated for each of the nanoparticle volume concentrations of interest.

5.6.1.4. Experimental System Shutdown

Once all the various samples have been thoroughly tested, the entire apparatus can be shut down. This will be done by first removing the hot wire harness and allowing it to fully warm to environmental levels. The excess cryogenic fluids can be discarded or saved and the power supply and sonicator can be turned off. The probe tip should be allowed to slowly warm back up. The collected test data can be transferred from the measurement computer to the computer on which it will be processed. Once the hot wire harness has reached a more suitable temperature level, it can be placed into a room temperature water bath. This will ensure that any lingering nanoparticles will remain within the fluid. This water bath allows the THW harness to be more easily cleaned. Finally, the entirety of the experimental test apparatus should be cleaned post test and prepared for the next round of testing.

5.7. Experimental Factors and Variables

5.7.1. Introduction

The following discussions will focus on a few notable aspects of this experimental setup and the subsequent mixing and stabilization process for the CN's. It is the hope of the author that the following thoughts will shed further light into the inner workings of this experimental setup and hopefully aid future researchers in reproducing, or continuing this work.

5.7.2. Inner Test Chamber Heating

An aspect of this research that should be mentioned is that of bottom and top heating of the inner test chamber. As is explained in the experimental chapter of this thesis, an inner test chamber contains the test fluid and is surrounded by a well insulated outer coolant chamber. However, the top of both chambers are left open to the environment. This is due to the intrinsic nature of the experimental setup and every effort was taken to ensure that this affected the test in

the smallest way possible. The level of cooling LN2 was always kept well above the lip of the inner test chamber and the actual THW harness was submerged several inches below the inner test chamber fluid level. Finally, an insulating cover of styrofoam was placed over the top of the entire apparatus during testing to help eliminate direct thermal transport to the environment. This, however, does not prevent the upper surface of the testing fluid to become agitated due to fluid boiling, evaporation and thermal induced movement. It was assumed, however, that this would not greatly affect the platinum hot wire, which was, suspended vertically, deeper in the colder and better thermally maintained levels of the inner test chamber. The bottom of the chamber while kept quite cold with the outer coolant and maintained above the bottom level of the surrounding chamber, by a block of insulative material, is in direct conductive contact with the surroundings. Therefore, it is entirely possible that a small amount of heating at the bottom of the test chamber caused natural convection induced fluid flow within the inner test chamber. It is also possible, although not directly observed, that bubble formation and small scale boiling were occurring as well. If either of these heating regimes were present then two distinct consequences exist, the first being that of fluid convection across the THW. A transient hot wire relies on an absolutely stationary fluid and, therefore, a purely conductive environment. However, if there was a temperature gradient present at the bottom of the test chamber, it is possible that a slow upward differential buoyancy based fluid movement was present. However, it was decided that within the limitations of this research this affect was in all probability small and therefore negligible. This assumption is valid due to the fact that the bottom of the test chamber is well insulated and surrounded by the coolant fluid. In addition, numerous calibration tests done at cryogenic temperatures did not produce a noticeable error, nor a repeatable bias that could be traced back to this particular experimental feature.

The second effect, that of bottom heating, is a downward drag caused by the upward fluid movement, or release of bottom surface bubbles. If bubbles form and subsequently flow upward, or, indeed, if fluid movement of any kind is forced upward, then a downward drag force is created due to this fluid displacement. This would cause the cryogenic host fluid containing discrete nanoparticles to potentially drag those particles towards the bottom of the inner test chamber. This would accelerate the already noticeable clumping, aggregation and subsequent settling of the suspended nanoparticles. However, once again this aspect of the test is unsubstantiated and is negligible in comparison to far more noticeable features.

5.7.3. Additional Notes On Mixing

The mixing method used in this research was that of probe sonication. This was done because it is by far the simplest and most prevalent method in use. However, an unexpected behavior was observed with the use of a sonicator in this particular research. Because the probe sonicator used in this work has a relatively large mass and thus a great deal of thermal mass in its tip, it needed to be pre-cooled before use in the mixing of cryogenic nanofluids. The reason for this is that if the tip was not pre-cooled before it was inserted into the cryogenic fluid, the large temperature gradient between the sonicator tip and the fluid would cause a localized evaporative bubble to form adjacent to the tip. This would, in effect, neutralize the purpose of the sonicator because the high frequency, low amplitude vibrations of the sonicator, which traditionally cause cavitation mixing, would now take place in small gas bubble. This would greatly decrease the relative effectiveness of the mixing. However, the sonicator is also extremely susceptible to temperature and only operates at peak efficiency within a small thermal window. Therefore, a great deal of care needed to be taken that the sonicator tip was cold enough that it did not immediately vaporize the surrounding fluid, but was not submerged so long in the cryogenic liquid, that the temperature dropped below safe levels within the piezoelectric crystal or controls. This balance

was extremely difficult to achieve and, in fact, was often not. Therefore, it is possible that some of the nanoparticle concentrations for the various tests and days were not as well mixed as others. In fact, this was directly observed by the researchers in terms of the vigor of the initial mixing and the audible vibrations caused by the sonicator. Both of which dropped of significantly as the tests progressed within a given testing time. This is an unfortunate occurrence, however, it is not a fixable one with the current level of technology in use by this research. Other methods exist in terms of mixing and specifically in keeping the sonicator within its limited temperature band. These can be further reviewed in the future work chapter of this thesis.

5.7.4. Stabilization of Nanofluids

Particle settling is a consistent problem with many types of nanofluids. In fact, for every paper published on the topic of the physical and thermal characteristics of nanoparticles another is seemingly published on the processes and science of making a stably suspended nanofluid. Several aspects that can affect the suspension characteristics of a given nanofluid or cryogenic nanofluid are:

- Time
- Fluid Density
- Particle density
- Particle surface interactions
- Particle size
- Particle volume/mass concentration, etc.

A stabilized nanofluid suspension is initially based upon closely matching the densities of the fluid and the nanoparticle. This is determined from basic buoyancy laws. However, one of the features of nanofluids that is of particular interest is the fact that when a particle is small enough,

in the nano range, buoyancy stops becoming a governing factor. This is because the inclusion nanoparticles are now on such a scale that large macro effects, such as bulk fluid movement and gravity, are no longer as much of a concern.

An additional characteristic of the suspension properties of nanoparticles are that they are small enough that roughly ninety percent of their mass is on the surface. This causes a great deal of surface forces to exist. These interactions can either be attractive or repulsive; either way it plays a large role in the stability of a nanofluid. It should be noted that the authors observed this effect almost immediately after mixing was complete, in the form of rapid nanoparticle clumping. Many current research works in the field of nanofluids propose that as the particle concentrations of nanofluids increase, the natural interactions between particles also increase. This causes a greater likelihood of surface force interaction and clumping. When this occurs, the particles are no longer nanometer sized and are subject to the natural forces which affect the macro world. Hence stability is lost and the nanofluid tends to settle. However, it should be noted that this particle clumping and surface interactions between particles is attributed by some researchers to be one of the primary features of nanofluids that cause their anomalous behavior. In conclusion, the proper stabilization of nanofluids is quite difficult and well worth study. The stabilization factors mentioned above were used, to the best ability of the authors, to choose the MWCNT inclusion particles for the CN created in this work.

5.8. Possible Future Experimental Improvements

5.8.1. Introduction

The future goals of this research are to continue exploring the thermal transport properties of cryogenic nanofluids. To accomplish this, some improvements to the existing experimental setup and procedure will need to be made, a selection of which is discussed briefly below.

5.8.2. Variable Temperature and Pressure Chamber

A very important addition to the current research, that that would greatly aid the study of CN's, is that of adding a variable pressure and temperature chamber. This chamber would be capable of maintaining stable temperatures between elevated room and low end cryogenic values. In addition, it would also be able to vary its internal pressure from many times that of atmospheric, down to a low vacuum. This chamber would allow the variations of temperature in cryogenic nanofluids to be studied and could help to confirm whether similar temperature vs. thermal conductivity trends exist in cryogenic nanofluids, as they do in traditional nanofluids. In addition, by being able to set the internal pressure of the chamber the various cryogenic fluids could be kept in their liquid form for larger temperature ranges. Also, the effects of pressure on the thermal transport properties cryogenic nanofluids could be studied.

If a fully regulatable enclosure is not available, than a custom made Styrofoam outer coolant container needs to be built. This would allow a far smaller amount of secondary coolant to be used in the process of keeping the primary cryogenic testing liquid cold. Due to the highly desirable thermal insulative properties of Styrofoam, a simple cylindrical hole could be cut within a block, to the proper shape and size of the inner test chamber, and this would ensure that proper cooling occurred, without wasting large quantities of outer coolant. This would ultimately reduce waste, cost and allow more tests to be done with the small supplies of cryogens available.

5.8.3. Variable Feedback Based Power Supply

The hot wire analytical governing equation and subsequent models (shown in the theory chapter of this work) all assume a constant power source is available to energize the THW. Therefore, a new constant power source with high accuracy and controlled feedback could increase the accuracy of the experimental setup and allow the ideal model to be more closely approximated. In addition, this new power supply should be programmable, which would allow

the governing experimental code to regulate not only the data acquisition, but the turning on and off of the power supply itself. This would allow a far more accurate and repeatable hot wire test, and would greatly simplify not only the subsequent numerical analysis, but would reduce the required input, which would increase the accuracy, reliability, and repeatability of the test.

In addition to a new power supply, the entire THW setup could be created within a parallel electrical circuit. In essence, the arm of one of the parallel lines would hold the entirety of the platinum hot wire system. The other would host a single resistor with a comparable value to that of the hot wire, shunt, power, and voltage lines. A make before break switch would separate the two arms of the parallel system and be controlled by the DAQ and governing experimental program. The power would initially be turned on and allowed to run for a set period of time within the blank resistor arm of the circuit. At a specified time, the switch would be thrown and the full power of the system would be shunted into the hot wire setup. This would prevent the transient startup behavior of the power supply from affecting the actual heating of the hot wire and, therefore, complicating the subsequent analysis. This would be possible, because the speed of most modern switches are far faster than that of the time required to fully energize a constant source power supply.

5.8.4. Experimental Setup

The future improvements to the overall experimental setup could include a higher performance differential voltage measurement DAQ, with improved range, accuracy, and precision. The experimental harness could be upgraded with pure platinum connector studs and tension springs, to ensure a measureable and established THW length. Imbedded temperature sensors could measure in real time the hot wire and near fluid temperature. The inner fluid test chamber could be shrunk in size (<200 mL) to ensure that only small samples are tested and to negate inner test chamber fluid movement. Finally, a new more powerful sonicator with a longer

and thinner probe could be used to increase the dispersion and stability characteristics of cryogenic nanofluids.

5.9. Summary

5.9.1. Experimental Design

The transient hot wire method was chosen due to its general flexibility, accuracy, and unparalleled adaptability. One of the primary goals of this work, was to adapt the already working theory and experimental setup of a THW to a before now unexplored field. Truly, hot wire systems are not, in general, used to test cryogenic fluids, and indeed until now, to the best knowledge of the authors, have never been used to measure the effective thermal conductivity of a cryogenic nanofluid. For this research, the basic design of a transient how wire had to be completely redone and adapted to allow for both cryogenic temperatures and the generally unforgiving nature of a CN and its environment. This is demonstrated by the fact that many of the experimental features that are taken for granted when working with a cryogenic fluid, such as a variable pressure and temperature chamber, signal isolation and amplification systems, bridge circuitry analysis, constant current, voltage, and power supplies with substantial accuracy and detailed control, along with high accuracy and speed differential DAQ measurement equipment, were not available. For each experimental aspect of this research, a great deal of thought was put into how to make the available technology work and how to create a highly accurate, repeatable, and stable environment for the testing of the effective thermal conductivity of a CN.

5.9.2. Cryogenic Nanofluid Creation

The production of nanofluids is complex and difficult at the best of times and, once again, takes a great deal of technology and thought. For the case of this research and to the best of the author’s knowledge, no cryogenic nanofluid has ever been purposefully made. Therefore, the

creation process of several well dispersed and semi-stable suspensions of MWCNT based CN's was a substantial task. Some amount of effort in the literature review was focused on the current and most common techniques of nanofluid production. However, once again, the lack of both technology and the cryogenic nature of CN's would make the adaptation of these techniques very difficult for the current research. Therefore, the most basic technique was, by default, the best available option. Probe sonication was used in burst mode to adequately mix the nanoparticles into the base host LOX. It was determined by visual inspection, that a dispersed and semi-stable suspension was achieved. Although the exact nature of the dispersion and the stability of the CN's is not well understood, the MWCNT distribution was certainly enough to not only test, but to cause significant increases in the effective thermal conductivity of each CN. Finally, it can be concluded that despite certain limitations, the overall goal of creating several unique CN's was absolutely achieved.

CHAPTER 6

NUMERICAL MODELING

6.1. Introduction

Numerical methods are used when a problem is too complex for a strictly analytical solution to exist or be productive, or when the shear repetitiveness of the calculations required is prohibitive. For the case of this research both of these were true. The following discussion will be an in depth review of the numerical methods used in the analysis of the cryogenic nanofluids created for this work. The actual numerical processing for this research is done in MATLAB. The reason for this is that MATLAB provides a simple, versatile, fast data analysis tool with a built in plotting package. The actual computer codes used in this research can be found in Appendix B.

6.2. Previous Numerical Work

Extensive numerical modeling was done near the beginning of this research to complement and extend the existing analytical design models and to predict the eventual behavior of the experimental setup. However, these models were completed at an early enough stage of the design process, that they proved to be out dated and ineffectual when it came to designing the final experimental setup and procedure. For this reason, they are not discussed or reproduced here. However, upon request of the author, they can be presented.

6.3. Numerical Analysis of Experimentally Determined Data

6.3.1. Initial Data Acquisition

The numerical aspects of this research begin with the acquisition of the data required to calculate the thermal conductivity of the cryogenic nanofluids. This procedure will be discussed in far greater detail in the following sections. However, as was mentioned in the theory chapter, under the analytical design process, the data required for this custom made hot wire setup are the

voltage drops across the hot wire and the current sensing shunt. Because this hot wire setup is built with a forced voltage sensing differential, three distinct voltage points must be measured to back calculate the desired voltage drops. This was done by interfacing the voltage measurement system, in this case an A/D data acquisition analog converter, with LabView and allowing this program to digitally sample the voltage change of the hot wire and shunt. The LabView code used was a modified version of an existing driver program for the USB 1608FS DAQ system used in this research. The block diagram and front panel interface for the LabView data acquisition program used in this research can be seen in Fig. 6-1.

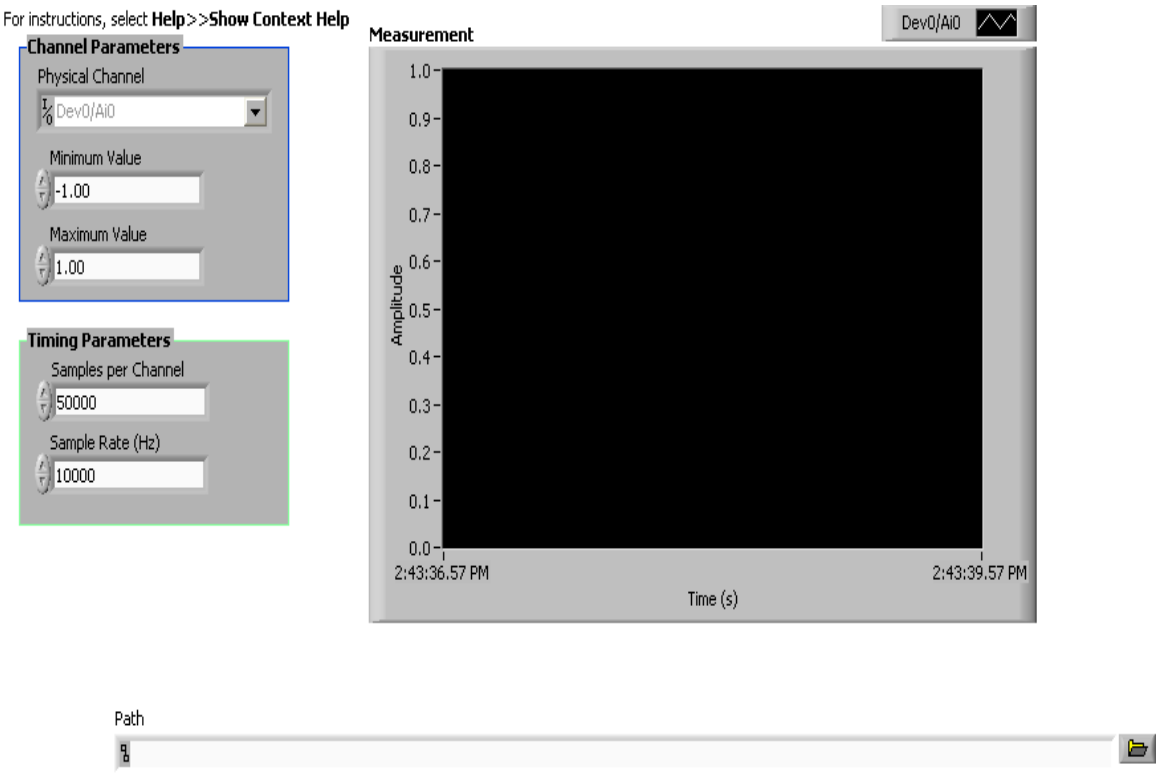

Figure 6-1. Numerical LabView front panel interface.

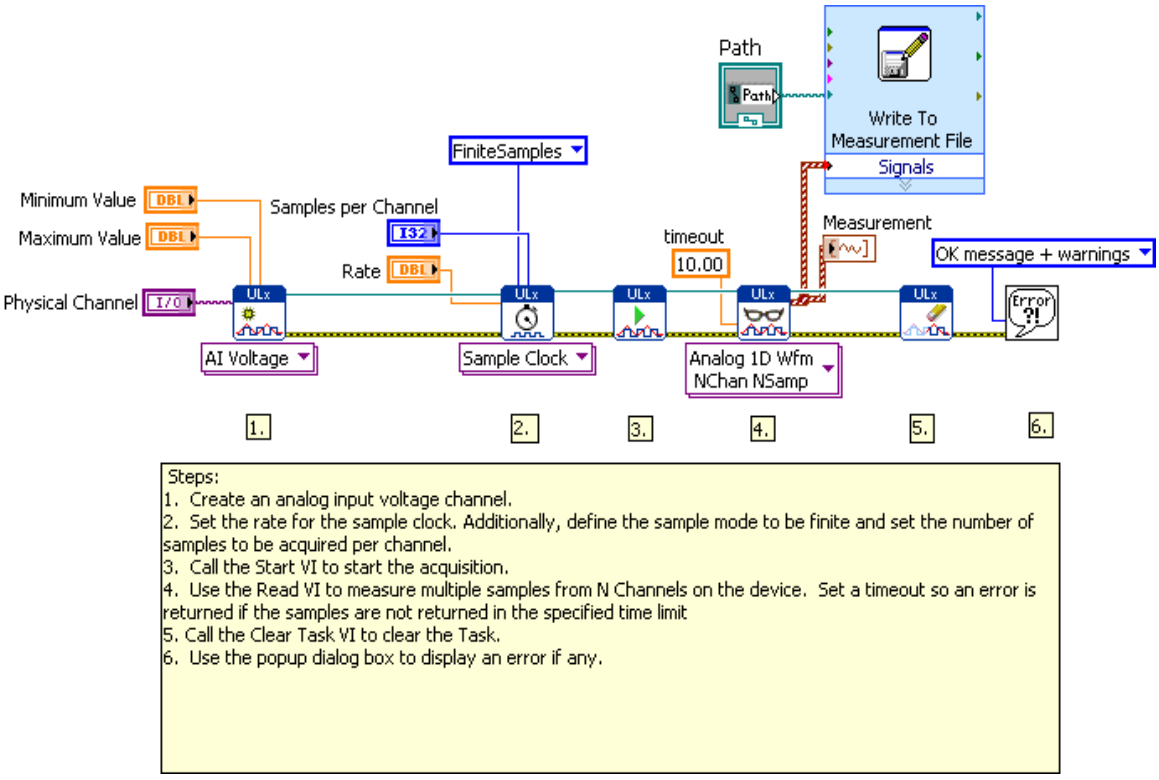

Figure 6-2. Numerical LabView block diagram code.

As can be seen in Fig. 6-2, the LabView VI connects with the physical voltage meter and the user is asked to input the voltage channels to be measured, the voltage range, the number of samples per channel, and the sampling rate. This information is then used to modify the VI's internal channels and timing clock, which, in turn, allows for the digital sampling of the analog voltage signals for the hot wire and shunt. The front panel diagram is also used to input the data path and file names to store the results. As was discussed previously and will be in greater detail later, this LabView VI is used to digitize the voltage levels at three distinct points within the custom made hot wire setup. These are the two ends of the platinum hot wire and the front end of the shunt. The ground of the DAQ is chosen to be the same as that of the hot wire common ground, and all voltage levels are referenced and grounded on the negative terminal of the

precision shunt. Finally, this LabView program saves the discrete sample times, and the overall test time, as well as the three distinct voltage values into specifically named text files. These text files can then be compiled and imported into a computer which will complete the final data analyses.

6.3.2. Numerical Analysis

6.3.2.1. Introduction

The following numerical codes will calculate the effective thermal conductivity of the cryogenic nanofluids created in this research and report their values and uncertainties as well as numerous intermediate values. The numerical analysis code created for this work consists of two primary programs and two task subroutines. Example results will be shown in the following discussions for both a pure base LOX test, as well as that of an example MWCNT cryogenic nanofluid test. These results will demonstrate some of trends and specifics of the analysis, as well as some of the challenges encountered when analyzing the thermal conductivity of cryogenic nanofluids. It should be noted, that these programs are extremely versatile and can, with a little modification, be used to test the thermal conductivity of any material.

A detail of this numerical code which should be mentioned is that due to the fact that the power supply is in all practically not programmable, it must be started and stopped by hand. Therefore, there will be a distinct variation in the starting times of the useable hot wire data. Therefore, several sections of this code specifically determine the starting and stopping time of the test and determine the range of data to be analyzed.

6.3.2.2. Numerical Governing Program

The first program used in this numerical code is one that creates a series of MATLAB file names to read in the raw data saved by LabView and send it to a governing program which will

actually perform all of the needed calculations. The fast data loader program begins by clearing all previously defined data, clearing the workspace and closing all open figures. The user than defines a path to the general files containing the hot wire raw voltage files. At this point, the code automatically specifies which hot wire current values are two be analyzed, and if the test is determining the thermal conductivity of pure liquid oxygen, or a cryogenic nanofluid. It then creates a loop to cycle through each current setting and particle volume concentration. If the data is for a cryogenic nanofluid, the program sets a specific testing current and automatically cycles through the various nanoparticle volume concentration data sets collected by the LabView experimental testing program. At this point, the specific data and file paths are set by a section of code, which will mimic the specific file name compilation created in LabView and allow the saved text files to be opened sequentially by MATLAB. These file names are than cycled, based upon any one or all of the following parameters: testing current, particle volume concentration, data set, or data analysis run.

6.3.2.3. Numerical Fast Data Analyzer Code

6.3.2.3.1. *Introduction*

The data which has now been compiled and properly named is imported into the fast data analyzer. This program is the primary governing program (although it is technically a subroutine of the code discussed above) and performs all of the necessary calculations in the determination of the effective thermal conductivity of a cryogenic nanofluid.

6.3.2.3.2. *Numerical Fast Data Analyzer Subroutine*

The fast data analyzer program is technically a subroutine of the fast data loader program, however, it is truly the general driving code for this numerical analysis and is only a subroutine to the fast data loader program so that the correct files are imported and in the correct sequence.

This code begins by reading in the raw hot wire data path and file name and using these too open the correct text files containing the THW raw voltage data. The program than reads in the stepwise testing time and the voltage values from all three channels and assigns them to named arrays. These raw data arrays are than renamed and set as Time and Ch0-Ch2. At this point, the program sets the details of the hot wire geometry, length, diameter, and area. These will be used later in the analysis of the governing thermal transport heat equation. The program than calculates the voltage drop across the hot wire and the current shunt.

$$\Delta V_{HW} = Cho - Ch1 \tag{6.1}$$

where ΔV_{HW} is the measured THW voltage in V's, and Ch0 and Ch1 are the raw voltage values. Because the DAQ used to measure the voltages of this custom hot wire system has singular input, it is necessary to create a forced differential within the system itself. This is done by simply measuring the voltage at either end of the hot wire with respect to the common ground and then subtracting these two values from each other. The THW experimental system created for this research is based upon a singular current loop, which means that the current within the hot wire is the same as that within the shunt. Therefore, the precision resistance shunt can be used as a high precision current sensor. The voltage drop across the shunt is directly referenced to the system's common ground and therefore does not need to be differenced with respect to anything else. This value can then be used to directly measure the total systems current value.

$$I_{HW} = \frac{Ch2}{0.01\,\Omega} \tag{6.2}$$

where I_{HW} is the constant current within the system in A's. The hot wire resistance and power can now be calculated from the corrected hot wire voltage drop and the system total current using Ohms laws.

$$R_{HW} = \frac{\Delta V_{HW}}{I_{HW}} \tag{6.3}$$

$$P_{HW} = I_{HW} \cdot \Delta V_{HW} \tag{6.4}$$

where R_{HW} and P_{HW} are the THW resistance, in Ω's and power, in W's.

A significant problem with the custom hot wire system used in this research was that of measurement EM interference. The measured voltage values proved to be extremely noisy, so much so, that it was affecting the ability of the early stage numerical codes to accurately predict the thermal conductivity of the nanofluids. A great deal of work went into trying to eliminate or subdue this noise and progress was made in the form of using shielded wires, shielded enclosures, power supply induction dampers, amplifiers, and electric filters etc. However, a persistent random noise level of approximately 3 mV was present no matter what steps were taken. This noise is most likely due to the fact that the voltages measured in this research are extremely small and are only slightly larger than the low voltage accuracy of the DAQ used. Therefore, it was decided that this low level random noise was in the system permanently and would be filtered out in post processing. Therefore, throughout this data analysis program, various data filtering and smoothing actions were performed on the data. The first such step was to smooth the hot wire resistance measurement. This is done by using MATLAB's intrinsic smooth function to reduce the noise present within the calculated hot wire resistance. The resistivity of the platinum wire is then calculated from the hot wire geometry and the now smoothed hot wire resistance.

$$\rho_{HW} = R_{HW} \cdot \frac{A_{HW}}{L_{HW}} \tag{6.5}$$

where ρ_{HW} is the measured resistivity of the THW in Ω·m and A_{HW}, L_{HW} are the surface area and length of the hot wire in m^2 and m's. The variations in resistivity for the platinum hot wire will be used to calculate the temperature of the hot wire later in the code with the use of the general governing equation derived in the theory chapter. In this numerical analysis the log of

time is primarily used for the calculation of thermal conductivities, therefore, from this point on log time will be used as the primary measurement of time. The following figures and plots are examples of the system currents encountered in liquid oxygen and MWCNT cryogenic nanofluids.

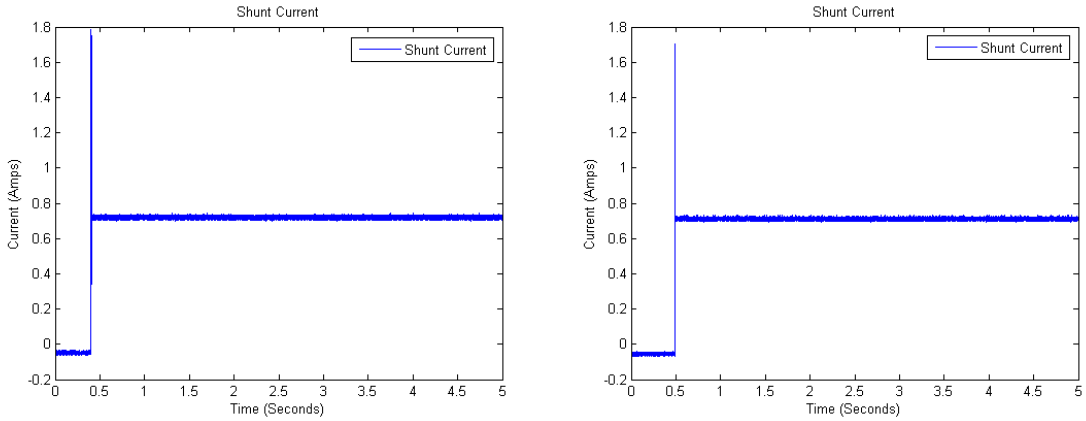

Figure 6-3. THW measured and analyzed constant current for base LOX and a sample cryogenic nanofluid.

As can be seen (figure 6-3) the system current is very stable and constant throughout the entire testing time.

Three distinct regions exist within the plots above, the first is the region before the system has been energized and the system current is zero. The second appears as a spike which is caused by the transience of the power supply ramping up. The third is the, quasi steady state, fully energized constant current region where the actual heating of the wire occurs. At this point, the program needs to decide on when it's going to start analyzing the data for the effective thermal conductivity. It is obvious that it needs to begin its analysis after the system is fully energized, while still soon enough to capture the initial transient heating of the wire. Therefore, the code will

find the point in time where the power supply is turned on and then begin analyzing the data at some period of time after that. The code begins by finding the average unpowered hot wire current value. The code does this by stepping through the hot wire current array and finding the point where the average changes by more than 50%. Basically, the code takes advantage of the initial transient nature of the power supply to determine the time value of when power was supplied to the system. This time value then becomes the figurative start time of the test. At this point an allowable variance in starting time is determined by the program. The power supply has a distinct initial transience along with a measureable ramp up time. Neither of these features is predicted by the governing general equation, which assumes an instantaneous constant current. Therefore, to allow for this, the program will create a range of allowable start times. This range will be one tenth of a second on either side of the calculated start time. This range of possible start times will be used by the code later to calculate the optimal start time. The extremes of this start time range are saved to array position variables.

The temperature of the hot wire now needs to be calculated. The platinum resistivity data and the corresponding temperature values are taken from the research conducted by Berry et al. [138] and are opened and read into temporary variables. The resistance of the wire, based upon Berry's data, is than calculated using the definition of resistivity as was done before in eq. (6.5). The temperature of the platinum hot wire is then calculated using MATLAB intrinsic cubic interpolation function, to match the large hot wire resistance array to the much smaller resistance vs. temperature array presented by Berry. This code basically uses a third order interpolation function to determine the nearest temperature value by interpolating between each of the calculated hot wire resistance values and those presented by Berry. The newly calculated hot wire temperature data is now smoothed by the same MATLAB function used previously. Figures

showing the smoothed and unsmoothed hot wire temperatures for base LOX and a cryogenic nanofluid can be seen below in figure 6-4.

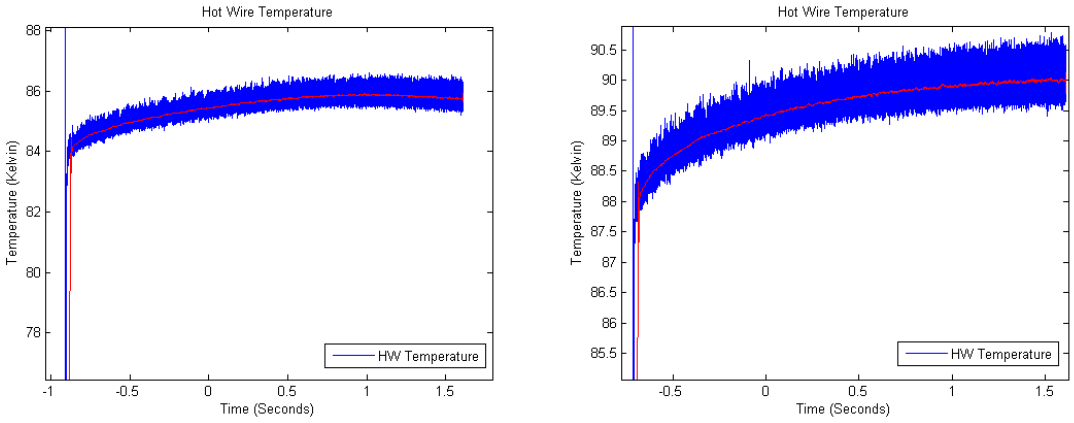

Figure 6-4. THW smoothed and un-smoothed temperature data for base LOX and a sample cryogenic nanofluid.

Because this is a fluidic system, any heat introduced by the hot wire will cause fluid convection. This convective heat transfer can be seen in certain data sets as a maximum temperature point, after which the temperature begins to decrease. This temperature decrease is due to natural convection around the hot wire. Therefore, the exact region of data that will be analyzed and used to calculate the effective thermal conductivity needs to be carefully chosen. This analyses region needs to be as close to the transient energizing start time as possible, because this region will provide the most information due to the fact that its rate of overall change is greater and therefore will be more easily modeled by the temperature vs. time method chosen in the theory chapter. However, the start point for data analysis cannot be too close to the transient start up time, due to the fact that the data could become corrupted by trying to model the initial ramp up current of the power supply, which cannot be modeled by the temperature analysis

equation. The end point for the range of data to be analyzed needs to be chosen with equal care. It is desirable to capture as much of the data as possible to fully define the linear heating region of the hot wire test. However, due to the fact that thermal convection can begin as early as 3-5 seconds, with the heat fluxes used in this experiment, it is important to take into account data that has yet reached a maximum temperature value, or begun to cool. Therefore, a time segment must be chosen in which the optimal range of data lays i.e. which provides the maximum amount of useable information, but does not allow any unmodelable data to be included in the analysis.

The code determines the analysis start point by once again finding the transient power up time and adding on five hundredths of a second. This time was carefully selected by numerous numerical runs done by hand, ultimately, a time of five hundredths of a second was determined as the optimal time to buffer the starting point for the useable data analysis range. This time allows for the power supply ramping stage and initial transience to quiet down while still providing an extremely early look into the transient response of the heating hot wire. The analysis end point is determined by calculating the maximum temperature value within the measured data. Once this point is found and its position within the array determined, only half of the total available data up to this point is analyzed. This is a safety measure to ensure that the hot wire data studied is only that which experiences linear or near linear heating. Once both the starting time and ending time have been determined for a specific data set, the array locations for both are determined and stored in position variables. At this point in the code, the user has the option to plot all of the intermediate thermal conductivity calculations. These include hot wire resistance, voltage drop, power, temperature and the resistivity/resistance values predicted by Berry. These figures (6-5, 6-6, 6-7, 6-8) include both base LOX and a typical MWCNT cryogenic nanofluid. It should be noted that in general these plots are nearly identical. This is due to the fact that all of the measurements/changes performed and observed in this research are subtle.

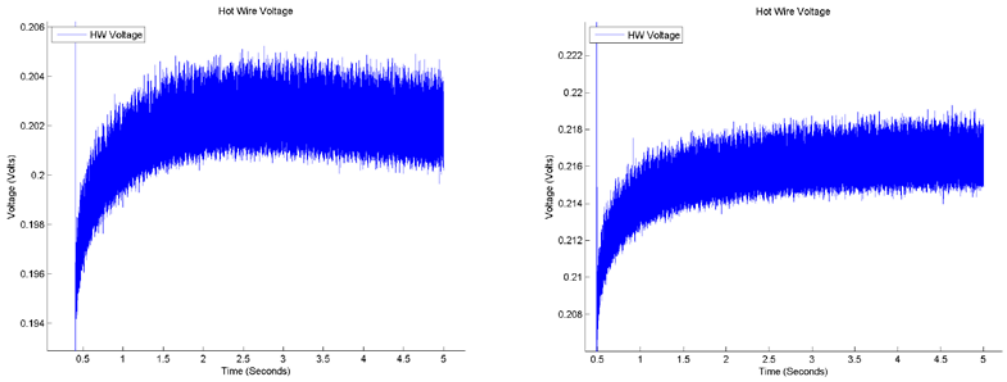

Figure 6-5. THW voltage data for base LOX and a sample cryogenic nanofluid.

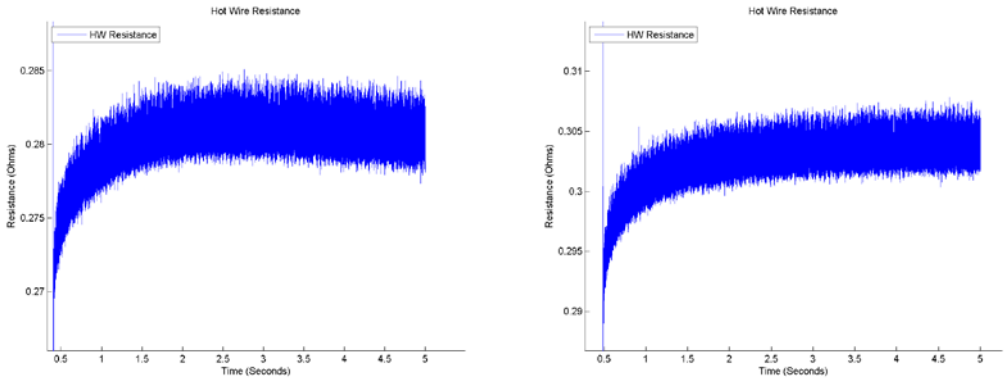

Figure 6-6. THW resistance data for base LOX and a sample cryogenic nanofluid.

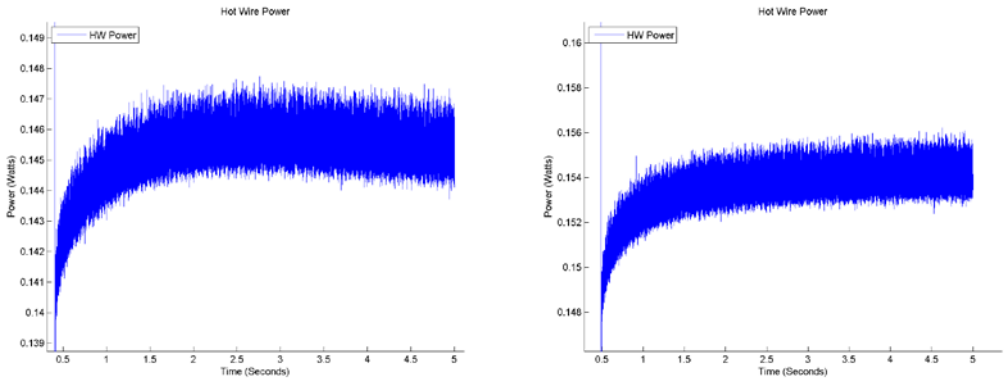

Figure 6-7. THW power data for base LOX and a sample cryogenic nanofluid.

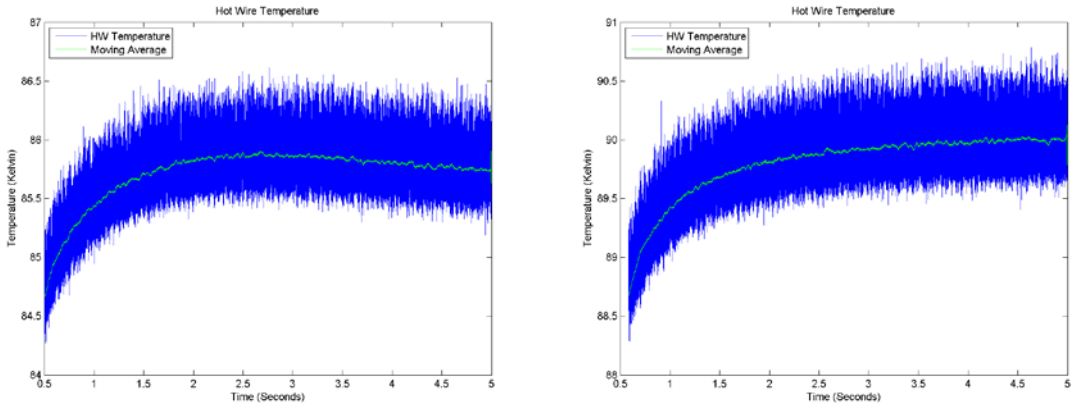

Figure 6-8. THW temperature data, with smoothed temperature curve, for base LOX and a sample cryogenic nanofluid.

The program will now calculate the total hot wire power (subsequent heat flux) that will be used in the analysis of the thermal conductivity. This value is once again smoothed before the average value is determined. Ideally, a constant power supply would be used for this research; however, the only system available is a constant current system. This is unfortunate because the general governing equation assumes that the power supplied to the hot wire is constant and therefore produces a constant radial heat flux to the surrounding medium. This will be approximated, by the current program, by finding the average power supply within the chosen data analysis range and using this value as an assumed constant power. This assumption is not strictly true and will introduce some error into the calculation of the effective thermal conductivity. However, by using the average power value and by assuming that the true value lies somewhere near the medium value and away from the extremes of power, this can be a reasonable assumption. In addition, the maximum error that can be introduced by this approximation was found by assuming that the true power was one of the extremes, either high or low and calculating the percent difference between those values and the medium. The result was less than two percent and therefore considered negligible when compared to the overall system

uncertainty, which will be discussed more fully in subsequent chapters. Considering the fact that the variable power will be somewhere well within the two extremes of the power limit, it should be noted that any uncertainty caused by assuming the power is constant will appear directly as a linear error in the calculation.

The numerical analysis code will, at this point, read in and calculate the various required thermo-physical properties of the medium of interest. The code will read in the cryogenic fluid properties corresponding to the calculated average temperature value. These are the material properties required by the temperature vs. time model. These required variables include the fluids specific heat capacity and density. Once again, by assuming that the fluid properties are constant (when in fact they are temperature variable) a small error will be introduced to the calculated effective thermal conductivity. However, for the cryogens used in this research the variations in density and specific heat caused by the ever changing fluid temperature created negligible effects on thermal conductivity. Plus by reviewing the temperature vs. time equation in the theory chapter, it can be seen that neither parameter has all that great of an effect on the overall calculated value.

Finally, the numerical code is ready to calculate the actual effective thermal conductivity of the cryogenic nanofluid. It will do this by performing a least squares non-linear curve fit on the provided temperature vs. time data. This curve fit utilizes the temperature vs. time model and modifies/fits it to the experimental temperature vs. time data. This is done by utilizing MATLAB's intrinsic least squares non-linear equation solver also known as lsqnonlin. The function lsqnonlin takes in a predefined equation; the coefficients of the equation can either be set by the user or be left as variables. MATLAB will then proceed to cycle the specified variables until the equation fits the provided data with the smallest residual of the norm possible. For the specific case of this non-linear curve fit three distinct parameters are allowed to vary, these are

the starting time of the data analyzed, the thermal conductivity, and the starting temperature. The initial temperature is allowed to vary because of the transient ramping up stage of the power supply. This temperature transience causes a deceptively large change in the curvature of the data. Without knowing exactly when the power was fully on and how much heating occurred during the ramp up time, it is very difficult to pinpoint an exact starting temperature. Therefore, the program is allowed to pick out the starting temperature that fits the data best. The more detailed reason for allowing the initial start time to vary is that because the power supply is turned on by hand, the power is not turned on at time equal to zero, which is what the temperature vs. time model assumes. Therefore, the code is allowed to vary the start time from a tenth of a second before the onset of power, to a tenth of a second afterward. By doing this, the program will automatically determine how much time there was before the power was turned on and reached full capacity and subtract this time off of the data analysis range time that was selected earlier. Therefore, the non-zero starting time of the power along with its transient ramping up stage are taken into account. The temperature vs. time model will be coded directly into MATLAB's lsqnonlin solver, which takes the form of a subroutine that can be modified for the specific equations to be solved and have constants imported into it. The constant fluid properties along with the variables of interest will be sent to the lsqnonlin subroutine and the best fit thermal conductivity and initial temperature will be returned.

The least squares non-linear curve fit subroutine returns the best fit values for the two variable coefficients of thermal conductivity and temperature. In addition, the code will return the residuals of the norm. All of these values are then stored in arrays, along with the newly shifted time arrays. The conductivity value is than compared to the expected NIST conductivity value and the total error is calculated. The thermal conductivity values at the minimum value of the residual of the norm along with its corresponding initial temperature are than reinserted into the

temperature vs. time model and a plot of the temperature curve fit compared to the smoothed and unsmoothed data is produced. This model also includes the percent difference between the smoothed temperature data and the solved for predictive temperature. These differences are generally less than one percent. In addition, the plot of the residual of the norms for the lsqnonlin curve fit and the thermal conductivity error are also shown. These two plots along with the calculated error and time shift are the primary ways of determining if the calculated thermal conductivity is correct.

To determine whether the curve fit was successful and if the calculated thermal conductivity is correct, it is necessary to examine the residual of the norms. A fit may be considered good if the residual of the norm is less than 5 for that particular test (this value is arbitrarily chosen by the researchers based upon experience) and in addition if that point can be used to calculate a conductivity value that is similar to those predicted by NIST. This is of particular importance in the testing of base LOX values, because the differences between the calculated values and the expected values will be used in determining the random uncertainty of the test along with its bias. When testing a nanofluid, these differences will be used along with the base LOX values to calculate the change in thermal conductivity of the cryogenic nanofluid. A second parameter to pay close attention to is how closely the new temperature vs. time model fits the experimentally determined smoothed data. For a good fit, the majority of the curve's points should fall within one percent of the calculated value. A final parameter than can be checked is that of time shift. The analysis time should be shifted back by the same amount of time as was measured from the start of the test to before the hot wire was energized, plus the additional shift produced by neglecting the transient ramp up time discussed earlier. If all of these parameters fall within reasonable limits, it can be assumed that the test along with the numerical analysis worked properly and that the calculated effective thermal conductivity value is correct within its given

uncertainty bounds. Ultimately, the fast data analysis program simply displays the calculated values and results while importing and saving the entirety of the variables and data used in that run to a properly named M file. Examples of the final curve fitted data, percent change in effective thermal conductivity, and residual of the norm are shown below. It should also be noted, that despite the great care taken in the numerical analysis of this work, not all data sets could be modeled with relative perfection. Therefore, it can be assumed that some of the variance and subsequent scatter in the calculated effective thermal conductivity of the various cryogenic nanofluids studied in this work can be traced back to errors in the numerical curve fitting and solution process. Specifically, figure 6-9 details the typical behavior of the experimentally curve fitted data with respect to the unfiltered measured/extrapolated temperature. The fit variation, in percent, is also represented. Figure 6-10 details the comparison of the residual of the norm to the calculated effective thermal conductivity value. The graphically represented minimum value represents the best fit. Thus, the matching calculated value for the change in the effective thermal conductivity is taken to be the materials true thermal conductivity.

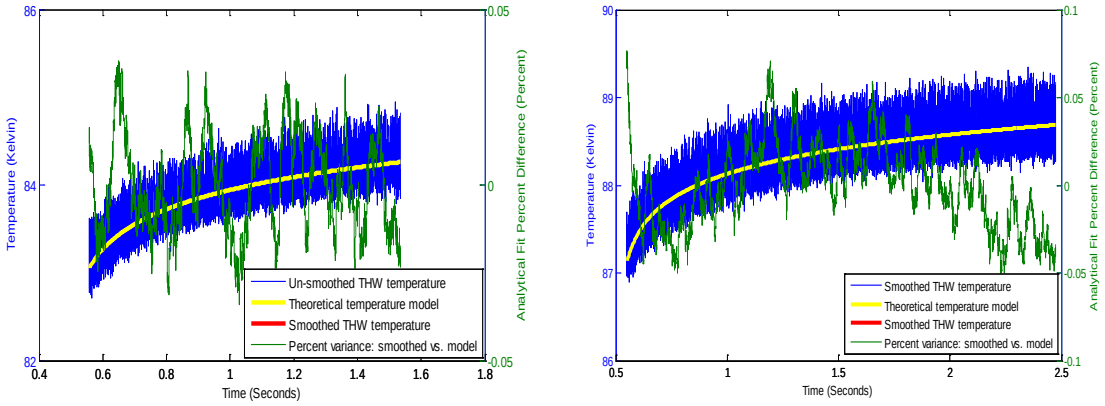

Figure 6-9. THW temperature vs. time data with modeled curve fit and point by point percentage variations for base LOX and a sample cryogenic nanofluid.

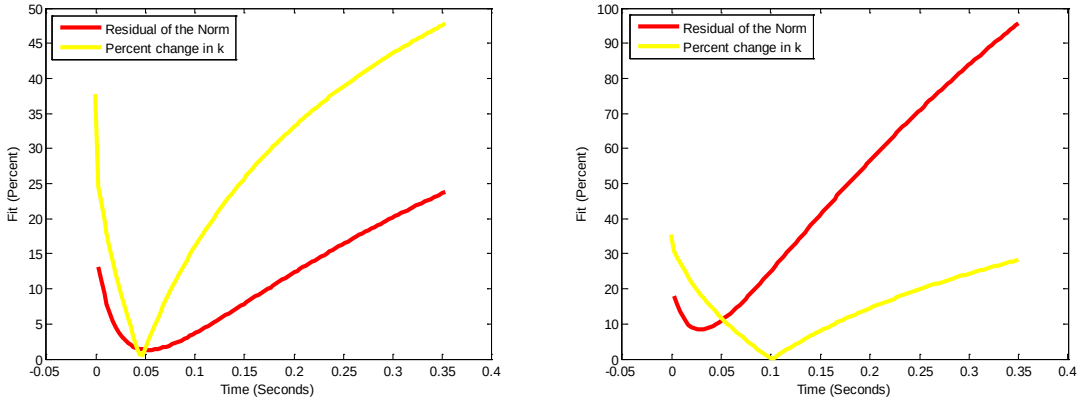

Figure 6-10. Residual of the norm vs. the percentage difference between the calculated and expected effective thermal conductivities values as they vary with time.

6.3.2.3.3. *Numerical Fast Data Processor Subroutine*

The next stage of the analysis begins with the use of a fast data processor subroutine. This subroutine will once again create a naming scheme that matches those produced by the fast data loader and utilized by the fast data analyzer. The data processor subroutine will cycle through the hot wire currents, nanoparticle volume concentrations, data sets, and individual runs collected during the entirety of the series of cryogenic nanofluids tests and reopen the saved M files containing the newly calculated thermal conductivity values along with the calculated error and or thermal conductivity increase. The fast data processor will begin by saving each of the thermal conductivity values and error values calculated throughout a given day of testing into arrays and then will proceed to simply average them. The data is averaged first by run, then by data set and finally by particle volume concentration or by system current, depending on whether the base LOX or a cryogenic nanofluid is being tested. The now fully averaged thermal conductivity values are than run through an outlier rejection test. The test used for this research is that of Chauvenet's criteria [180]. The number of data sets analyzed is used to correctly determine the test factor used and the standard deviation. The code than analyzes each of the thermal

conductivity values for an entire series of data sets and checks for outliers. If one is detected, it stores the value and its location so that it can be neglected in the future. The standard deviation of both the calculated error and thermal conductivity are calculated and the expected thermal conductivity values are also averaged together. For the case of testing base LOX the difference between these two averaged values gives the test bias, and the random uncertainty is calculated by using the methods of [2], which can be reviewed further in the uncertainty analysis chapter of this work. Finally, the calculated thermal conductivity, NIST expected thermal conductivity and average calculated thermal conductivity are plotted. The percent errors are also shown. Finally, the maximum, minimum, average, and data range/scattering are collected along with all of the salient effective thermal conductivity details and outputted to text files.

This process is repeated for each current level, if testing base LOX or particle volume concentration level if, testing a cryogenic nanofluid and the results can be combined to create a total thermal conductivity increase vs. particle loading plot.

6.4. Summary

The numerical analysis code developed for this research allowed the rather complicated and difficult calculations of effective thermal conductivity to be performed rapidly, consistently, and repeatedly for a variety of pure LOX samples and cryogenic nanofluids over several months of testing. This program and the numerical processing power it contained were truly essential to the experimental process of this research.

Due to the fairly complex nature of the post processing data analysis, inherent within the transient hot wire system, it became fairly obvious early on in this research that a custom programmed, robust post processing data analysis tool would be required. This program would account for the intrinsically noisy and subtle signals being detected by the experimental system and would automatically perform all the calculations required to go from a raw voltage signal

drop across the transient hot wire to a fully formulated effective thermal conductivity value for the surrounding CN. The authors of this research were able to create such a code, which aided greatly in the overall study of the CN's created for this work. The details of the code and the operation of this program can be reviewed in the numerical modeling chapter of this thesis, and in appendix B of this work.

CHAPTER 7

UNCERTAINTY ANALYSIS

7.1. Background

The uncertainty study for this research began with an initial predictive uncertainty analysis. The purpose of this preliminary review was to determine, roughly, what kind of accuracies, uncertainties, and errors were to be reasonably expected with the THW experimental setup. Therefore, a full system analysis was done for the experimental setup using the methods of Coleman and Steele [180]. This preliminary analysis of the uncertainty of the custom made THW system was validated with room temperature water and pure 99.9% Glycerol. The exact details of this initial predictive uncertainty model are not repeated here. However, they can be reviewed by request of the authors. This particular exclusion was due to the fact that once an actual experimental determination of the THW uncertainty was completed with pure LOX it was purely redundant. The following discussions will focus on the post processing uncertainty analysis done with the calibration data determined from each test day's measurement of pure LOX.

7.2. Introduction

Once the effective thermal conductivity of pure LOX and actual cryogenic nanofluids had been measured, a new uncertainty analysis was required. This updated uncertainty study would be used to calculate the actual experimental bias and random uncertainty for the cryogenic nanofluids studied in this research. The preliminary and current uncertainty analyses show good agreement, with the cryogenic testing being slightly more accurate. This is to be expected, due to the fact that the room temperature analysis utilized a linear curve fit, while the cryogenic tests utilized the temperature vs. time exponential integral fit. In addition, it is reasonable to assume that a predicted uncertainty would prove to be less accurate than an actual test.

The ultimate goal of this work is to determine the accuracy of the custom THW experimental system developed within this research, as well as determining the overall confidence intervals for the measured effective thermal conductivity. This updated uncertainty study compared the experimental thermal conductivity of base LOX and those of the MWCNT based cryogenic nanofluids to reference values found from NIST [105] etc. The average differences between the measured pure LOX and the theoretical values provided by NIST give the general experimental bias of this particular test. Similarly, the random uncertainty is calculated by the methods presented below. Together, these two uncertainty values can be used to fully quantify the overall uncertainty of the measured effective thermal conductivity. The actual experimental uncertainty values can be reviewed within the summary of this chapter, and are further represented in the results chapter of the thesis.

7.3. Uncertainty Analysis

7.3.1. Introduction

Because the base thermal conductivity values of liquid oxygen are already known, through direct experimental measurement and data collected by NIST as well as others (see cryogenic literature review), a direct comparison between the calculated and expected results is possible. When calculating the experimental bias and random uncertainties for the cryogenic nanofluids, the actual error analysis will be done on the base liquid oxygen tests only. These pre-calculated results will then be projected onto the cryogenic nanofluids. The reason for this is that by measuring the base liquid oxygen without any nanoparticles, a sense of the accuracy and repeatability of the experimental test can be obtained. Whereas, if the uncertainty analysis was done on the cryogenic nanofluids directly, misleading results would be obtained due to the fact that many additional parameters exist for these complex fluids. Basically, by performing a base LOX calibration test with every set of measured cryogenic nanofluid data, the experimental

system's bias error and random uncertainties can be calculated and then used for the cryogenic nanofluid data without having the unduly complex transient behavior of the nanofluids give erroneous uncertainty results.

7.3.2. Uncertainty Calculation

The uncertainty analysis for the cryogenic nanofluids began with the determination of the exact error of the calculated thermal conductivity of base liquid oxygen with respect to reported NIST values. By doing this a bias error for that particular test set can be determined. In this case the bias is indeed an error, because the calculated values are being compared directly to reported NIST values. The calculated thermal conductivity values of base LOX for a given data set are averaged together, and then subtracted from the average reported thermal conductivity of LOX as can be seen below.

$$Bias\ Error = Average\ reported\ k_f - Average\ calculated\ k_f \tag{7.1}$$

The calculated values from this equation can then be used as an approximation of the overall experimental bias. The random uncertainties are calculated by finding the error of each baseline thermal conductance measurement separately and using the small sample size Student T-distribution to calculate a 95% confidence interval for each data point. The first step, however, is to determine the error value for each individual data point. This is done by comparing the numerically calculated result to the corresponding NIST data point.

$$Error = \frac{X_i - X_{exp}}{X_{exp}} \tag{7.2}$$

where X_i and X_{exp} are the variables containing the specified data point value and its corresponding expected value. At this point, the average of all the baseline LOX thermal conductivity values is calculated.

$$\bar{X} = \frac{\sum_{i=1}^{n} X_i}{n} \tag{7.3}$$

where $\bar{X}$ and n are an average variable and a variable containing the numerical total number of averaged values. At this point, the standard deviation is computed.

$$s_x = [\frac{1}{N-1}\sum_{i=1}^{N}(X_i - \bar{X})^2]^{1/2} \tag{7.4}$$

where s_x is the calculated standard deviation of the data and N is is the number of individual measurements. At this point the random uncertainty can be determined by using the small sample size Student-T distribution, which is done by first calculating the degrees of freedom for the student-T model

$$Degrees\ of\ freedom\ v = n - 1 \tag{7.5}$$

This will give used to determine the Student-T coefficient, t_{95}, from Coleman and Steel [105], which for the base LOX values can be seen below.

$$t_{95} = 2.093 \tag{7.6}$$

This coefficient can then be used to determine the random uncertainty values and their percentages based upon the following equations.

$$\mu_+ = +t_{95}\frac{s_x}{\sqrt{n}}$$
$$\mu_- = -t_{95}\frac{s_x}{\sqrt{n}} \tag{7.7}$$

$$\mu_+ = \frac{\left(+t_{95}\frac{s_x}{\sqrt{n}}\right)}{k_{calc}} \cdot 100$$
$$\mu_- = \frac{\left(-t_{95}\frac{s_x}{\sqrt{n}}\right)}{k_{calc}} \cdot 100 \tag{7.8}$$

where k_{calc} is simply the calculated effective thermal conductivity value. Finally, the confidence range over which a single point along with the rest of the data can vary, with a 95% confidence interval, is calculated below.

$$prob\left(\bar{X} - t_{95}\frac{S_x}{\sqrt{n}} \leq \mu \leq \bar{X} + t_{95}\frac{S_x}{\sqrt{n}}\right) = .95 \tag{7.9}$$

where μ is the uncertainty range for a specific data point with the confidence interval listed above. The total uncertainty can be determined from adding the bias and random uncertainties in terms of their squares and analyzing with the student-T distribution.

$$\mu_{total} = t_{95} \cdot \frac{\left(\sqrt{(Bias)^2 + \left(t_{95}\frac{S_x}{\sqrt{n}}\right)^2}\right)}{Average(k_{calc})} \cdot 100 \tag{7.10}$$

where μ_{total} is simply the total confidence interval for a specific data point. These results will then be used to fully quantify the uncertainty and errors of the cryogenic nanofluids. The calculated bias error will be added or subtracted from each data point within the corresponding thermal conductivity values for the cryogenic nanofluids and the random uncertainties will be used as uncertainty/confidence bars for each data point. It should be noted that NIST reports an average random uncertainty of

$$NIST\ Uncertainty\ k_{lox} = 2\% \tag{7.11}$$

where k_{lox} is the literature based reported effective thermal conductivity values for LOX. Examples of how this uncertainty analysis is implemented for both a pure LOX test and a cryogenic nanofluid test are shown below.

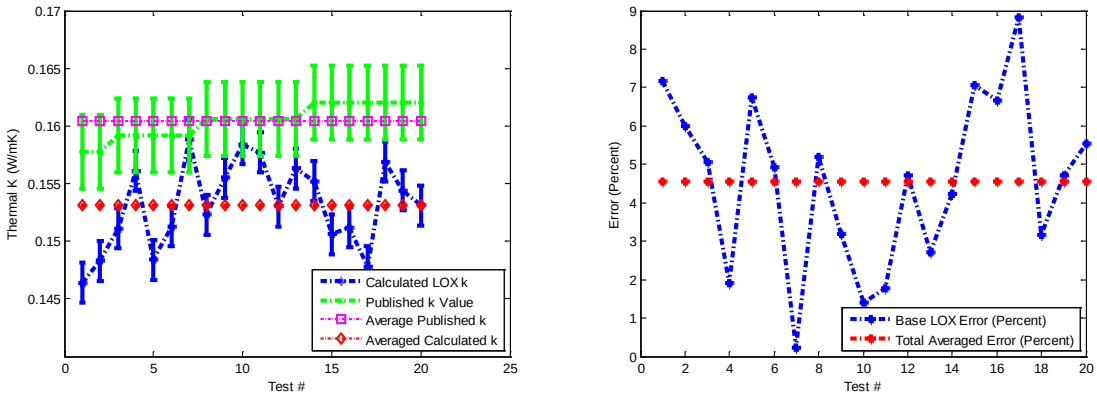

Figure 7-1. Measured effective thermal conductivity (values and total average) for pure LOX vs. expected pure LOX effective thermal conductivity (values and total average). Percentage change in effective thermal conductivity with calculated average variance also shown.

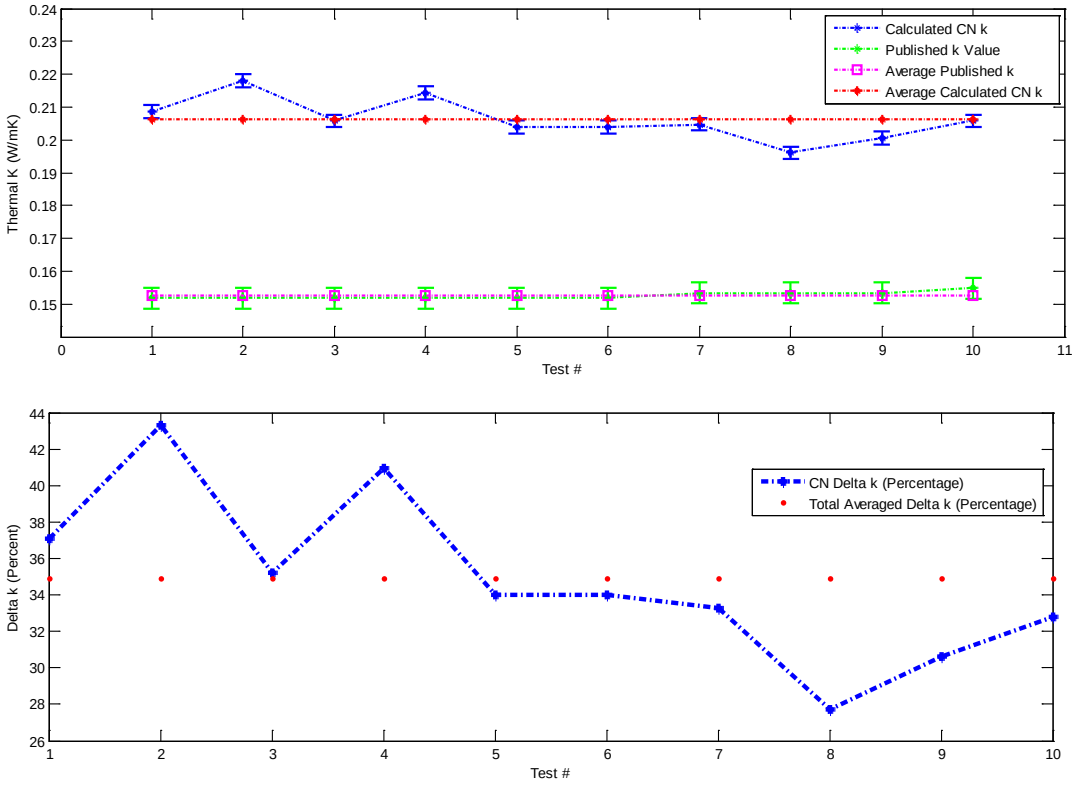

Figure 7-2. Measured effective thermal conductivity (values and total average) for a typical CN vs. expected pure LOX effective thermal conductivity (values and total average). Percentage change in effective thermal conductivity with calculated average increase also shown.

7.4. Summary

The actual calculated experimental random uncertainties and bias values can be seen below in table 7-1. These values are based upon the pure LOX calibration data collected on each day of testing.

Table 7-1. THW experimental random uncertainties and bias values.

Cryogenic Nanofluid Test	Experimental Random Uncertainty (W/mK)	Experimental Random Uncertainty Percent (%)	Experimental Bias (W/mK)	Experimental Bias Percent (%)
Test Day #1 Calibration	0.001742	1.13725	0.007321	4.561
Test Day #2 Calibration	0.001939	1.31136	0.0105	6.671
Test Day # 3 Calibration	0.001648	0.990606	-0.00315	-2.0953
Test Day # 4 Calibration	0.002248	1.51151	0.00771	5.023
Test Day # 5 Calibration	0.001913	1.16721	0.000899	2.136
Test Day # 6 Calibration	0.001963	1.30659	0.007196	4.5931
Test Day # 7 Calibration	0.004074	2.5526	0.002524	4.7585
Test Day # 8 Calibration	0.002238	1.39837	-0.00134	-2.4639

Each pair of testing days roughly corresponds to an inner THW wire harness setup. There existed multiple THW wire harnesses, and each was used for a singular type of cryogenic nanofluid and then discarded. In addition, test days 1-2, above correspond to the cryogenic nanofluids based upon Dr. T. C. Shen's MWCNT's and represent the two separate days of testing. Test days 3-6 characterize the NanoAmor stock # 1204YJ MWCNT based cryogenic nanofluids. Similarly, test days 7-8 signify the random uncertainties and biases recorded for the

wire harness utilized in the study of NanoAmor stock # 1235YJS MWCNT’s based cryogenic nanofluids.

CHAPTER 8

NANOPARTICLE PROFILES

8.1. Introduction

The specifics of the nanoparticles used within a nanofluid play a very important role in the overall behavior of said nanofluid. Therefore, a comprehensive review of the salient details of any and all nanoparticle features is not only prudent, but necessary. The following review will present a variety of the known information for each of the MWCNT's used in this research. In addition, any specific features of the MWCNT's that may have played a part in the final results will be discussed, along with the methods used to calculate the desired nanoparticle volume fractions and their actual values. The information on the MWCNT's utilized within this research is entirely based upon the NanoAmor website and personal conversations with Dr. T. C. Shen.

8.2. Background

To provide potential readers with a variety of effective thermal conductivity curves for analysis, several distinct MWCNT's were chosen for this research. MWCNT's are highly unique and have impressive thermal conductive properties. In addition, they are currently very popular in modern nanofluid and scientific research. The primary differences between the MWCNT particles tested in this work are their physical characteristics. Each of the MWCNT's has a distinct physical shape and varies from the others by at least one key feature. These differences are most notably shape, size, # of walls, diameters, lengths, density, etc. As was mentioned earlier, the only nanoparticles used in this research are carbon based. This is due to the intrinsic difficulties that arise when trying to create and stabilize a cryogenic nanofluid with the mixing techniques available. Finally, MWCNT's are relatively low cost and easy to obtain, as opposed to SWCNT's or DWCNT's.

The first MWCNT's used in this research were provided by Dr. T.C. Shen and provided the starting point and templates for the later MWCNT's. Dr. Shen performs research into the growth of large scale MWCNT forests. Therefore, in an attempt to create a constant comparison point two additional MWCNT types were chosen from the commercial options available from NanoAmorphous Materials Inc. These commercially produced MWCNT's have reportedly identical physical and material makeups, aside from the fact that one is significantly longer than the other. It should be noted that both of the commercial MWCNT's have significantly smaller dimensions than those created by Dr. Shen. This was done so that comparisons between the effective thermal conductivities based upon relative size and length could be made.

Five grams of each of the MWCNT's were purchased, or obtained from Dr. Shen, for use in this research. This particular mass was chosen because of the not insignificant cost of modern nanoparticles. In addition, it was concluded that without any knowledge or assurances of how these particles would behave, in terms of dispersion and stability within their host LOX and whether they would in fact produce a noticeable increase in the effective thermal conductivity of their cryogenic nanofluids, purchasing less of any given MWCNT was wise. However, five grams when utilized properly with the nanoparticle volume fractions described below is enough to complete two full measurement runs of the effective thermal conductivity of a given cryognenic nanofluid, from the smallest to the largest volume fractions, with a reasonable amount of MWCNT's left in reserve. It should be noted once again, that the ability to determine the exact nature of nanoparticle dispersals, time varying particle positioning, volume concentrations and settling patterns and times is extremely limited. However, a rough approximation of the particle volume dispersal and settling times can be determined from periodic visual inspections of the mixed cryogenic nanofluids color, particle motion, and transparency and from the effective thermal conductivity trends in the intermediate test values.

8.3. MWCNT: NanoAmor Stock# 1235YJS

The MWCNT's coined "short tailed" are simply mid-level short length easily dispersible NanoAmor multi-walled Carbon nanotubes. They were chosen for this research due to the fact that their relative diameters, number of walls, and densities complimented a matching longer MWCNT sold by the same company. This allowed for not only a variety of particles to be tested but for the effect of length and ease of dispensability on effective thermal conductivity to be studied. The specifics of this MWCNT are presented below in table 8-1. The small size, and shorter length allow these particles to be dispersed with a minimum amount of effort and to stay fairly well dispersed for at least a few minutes of testing time (on average less than 10 minutes) [181].

Table 8-1. NanoAmor stock # 1235YJ MWCNT profile.

NanoAmor MWCNT Stock# **1235YJS**	
Particle Type	MWCNT
Purity	>95% Carbon
OD	8-15 nm
ID	3-5 nm
Length	0.5-2 μm
SSA	180-240 m^2/gm
Bulk Density	0.05 gm/cm^3
True Density	2.1 gm/cm^3
Primary Color	Black

8.4. MWCNT: NanoAmor Stock# 1204YJ

The longer MWCNT's, "coined Long Tailed," (figure 8-1) were chosen to match the approximate inner and outer diameters, as well as the general morphology of their shorter NanoAmor MWCNT counterparts. The relative diameters of these particles is small enough to very decisively fall within the nano size realm and explore the effects of long thin MWCNT

nanoparticles within a cryogenic nanofluid [182]. The specific physical characteristics of the longer MWCNT's are given in table 8-2.

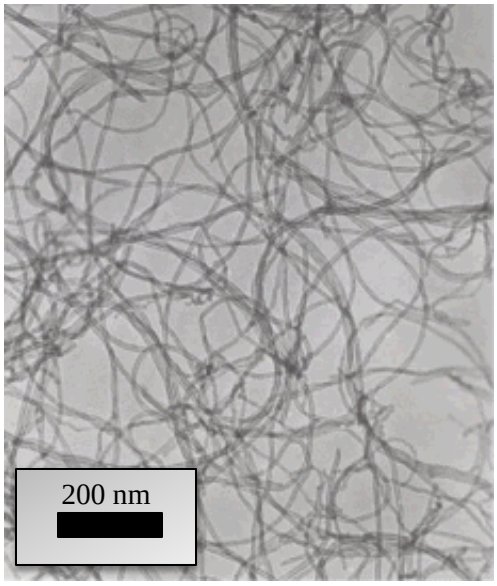

Figure 8-1. NanoAmor MWCNT's Stock #1204YJ. Adapted from [182]

Table 8-2. NanoAmor stock # 1204YJ MWCNT profile.

NanoAmor MWCNT Stock# **1204YJ**	
Particle Type	MWCNT
Purity	>95% Carbon
OD	8-15 nm
ID	3-5 nm
Length	10-50 μm
SSA	180-240 m^2/g
Bulk Density	0.05 gm/cm^3
True Density	2.1 gm/cm^3
Primary Color	Black

8.5. MWCNT: USU #1

Dr. T. C. Shen is a researcher at Utah State University (USU). Among his many research topics and interests are the growth and study of large MWCNT forests (figure 8-2). Due to Dr. Shen's generosity and the convenient nature of his work, several batches of MWCNT's were donated to this research. Dr. Shen's MWCNT's are produced by the Chemical Vapor Deposition method, or (CVD). They are grown on a Quartz substrate with Ferracene and Xylene acting as chemical growth precursors. The nature of their development and subsequent harvesting lead to a rather unique physical property, Dr. Shen's MWCNT's have a small Iron ball attached to the base of each carbon nanotube. This is caused by their growth from the substrate and leads to their secondary elemental components to consist primarily of Iron. This could explain some of their highly unique properties, observed throughout this research. Because these particular MWCNT's were grown for specific research purposes and not for commercial distribution, there is quite a bit unknown about them, most notably the lack of a true density. This will necessitate that their density be experimentally approximated as similar to the purchased NanoAmor nanoparticles. What is known, is encapsulated within table 8-3.

Table 8-3. Dr. T. C. Shen MWCNT profile.

Dr. T. C. Shen's MWCNT's	
Particle Type	MWCNT
Purity	>95% Carbon
OD	20-40 nm
ID	> 5 nm
# of Walls	>10
Length	1.5-90 µm
Average Length	22.8 µm
SSA	Unknown
Bulk Density	Unknown
True Density	Unknown
Primary Color	Black

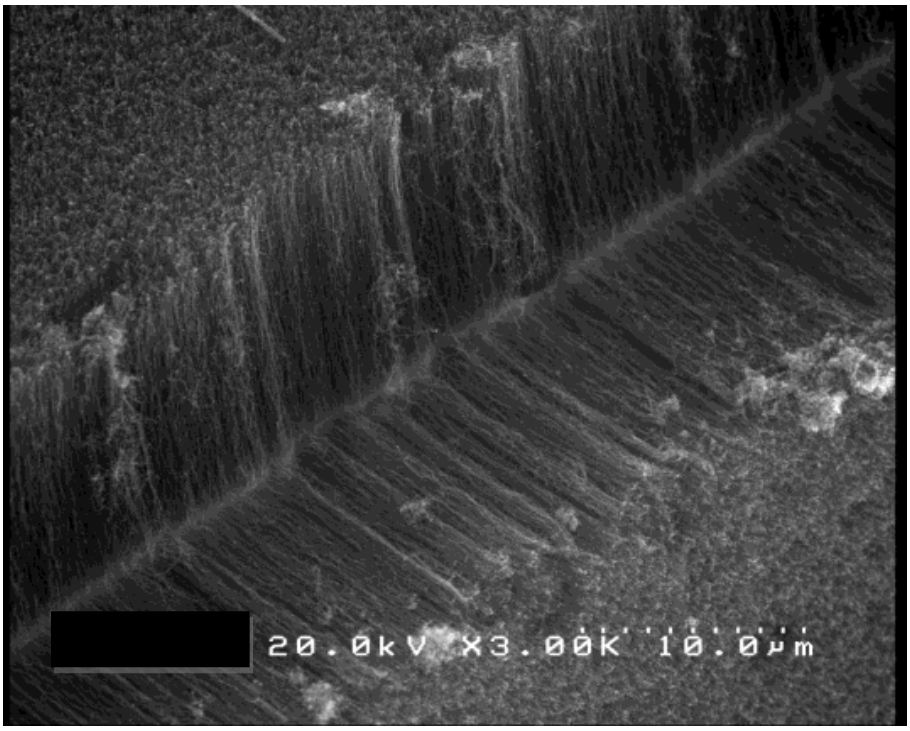

Figure 8-2. Dr. T. C. Shen MWCNT's adapted from [183].

For Dr. Shen's MWCNT's an unusual phenomenon was observed. The particles seemed to have a slightly lower density than those purchased from NanoAmor. This conclusion was made based upon the fact that the particles appeared to have more natural buoyancy when suspended in LOX and were observed to stay in suspension for a noticeably longer period of time. In addition, they appeared to tangle more easily forming visible clusters of high density. This was especially noticeable near and around the region of the hot wire. For the case of this work, it is theorized that this is due to the fact that Dr. Shen's particles have a wider range of sizes and therefore, are capable of tangling more readily. This increase in entanglement can, potentially, have two consequences, the first being that because the carbon nanotubes are locally clustered and tangled around the platinum hot wire, there could be direct contact and thus heat transfer from the wire to the carbon nanotubes. Similarly, it could cause a localized and therefore unaccounted for spike in

the particle volume concentration in the vicinity of the wire. This would be measured as an unexpected increase in thermal conductivity, due to the fact that the THW can only measure the adjacent composite fluid. Conversely, if the nanotubes are more prone to tangling and therefore create a contact based direct conduction interface, from the temperature gradient of the THW to the surrounding fluid, then a variety of the static and dynamic based theories of nanofluid science, such as percolation theory, could explain their unusually large affect on the thermal conductivity of LOX. Either way, the basic nature of Dr. Shen's MWCNT's could explain some of their truly unexpected characteristics and their ability to increase the effective thermal conductivity of LOX at low particle volume concentrations [183, 184].

8.6. Particle Volume Concentrations

The method used to calculate the particle volume percentage for each of the cryogenic nanofluids was quite simple. The true densities of the MWCNT's were divided by their measured mass, thus rendering them in terms of occupied volume. This value was than divided by the available CN volume (500 mL) and converted into a percentage. This can be seen below in terms of both the governing equation and the actual tabulated volume percentage values (table 8-4). It should be noted that there did exist some uncertainty in the calculation of these values. However, when compared to the much larger uncertainty of nanoparticle dispersion/stability, and coupled with the fact that exact numbers are not required, the following values are simply relative particle concentration comparison values for this particular research.

$$Volume\ Percentage = \left[\frac{1}{\frac{\left(\frac{\rho_{Nanoparticle}}{m_{Nanoparticle}}\right)}{V_{Total}}} \right] \cdot 100 \tag{8.1}$$

Table 8-4. MWCNT discrete particle volume fractions along with corresponding mass values.

MWCNT Particle Volume Fraction	
Particle Mass Concentrations (gm)	Particle Concentrations by Volume Percentage (%)
0.01	0.000952
0.023	0.002191
0.115	0.01095
0.230	0.0219
0.335	0.0319
0.469	0.04467
0.670	0.06381

CHAPTER 9

RESULTS

9.1. Introduction

The design, creation, and testing of an experimental thermal conductivity measurement system capable of quickly, accurately, and repeatable measuring the effective thermal conductivity of a custom made cryogenic nanofluid was completed. To this end, a theoretical base, along with numerical models was created for both preliminary design, and for post processing and comparing the resultant data. Theoretical, experimental, and numerical testing procedures were created, vetted, and practiced to provide a reliable, accurate, and consistent testing environment. The entirety of this work led to the successful measurement of three distinct MWCNT based CN's, the results of which can be seen below.

Each of the Cryogenic Nanofluids used in this work were created specifically for the testing purposes of this research. Each of the CN’s are based upon MWCNT inclusion particles, and Liquid Oxygen (LOX) as the base matrix. The LOX used in this research is medical grade and is of high enough purity to make it more than suitable for use as a host fluid. The MWCNT’s are separated by type, and include a custom made particle from Dr. T. C. Shen, along with both a long and short particle types from NanoAmor materials. The CN's were tested with variations in both MWCNT particle type and inclusion particle volume fraction. The relative effective thermal conductivity changes with respect to the reported thermal conductivity of LOX are then catalogued, and compared.

The paragraphs and figures below will detail absolute relative, percentage change, and ratio of effective thermal conductivity to baseline host fluid conductivity for each CN tested. Each plot will also show the independent measurement runs, calculated uncertainty, and total average values. Finally, comparison plots will show the total average values for each of the individual

CN's. In addition, tables summarizing the most salient details such as maximum, minimum, and averages will also be included for each individual CN. The discussion on each CN will focus on the individual curves, results and specific characteristics of each Nanofluid and measurement. Specifically, the relative magnitudes, data spreads, curve shapes, and trends will be reviewed, along with any special characteristics of the nanoparticles, nanofluid mixing, or CN itself that may have had an effect on the measurement outcomes. Hopefully, this will give the reader some additional details about each CN and shed some light onto the experimental and theoretical behavior that caused the subsequent curves.

Because each CN varies in its type, physical characteristics, and particle volume fraction, each of which obviously has great effect on the final thermal conductivity values, some conclusions on what physics are causing these enhancements can only be speculated upon. To this end, specific conclusions as to the physics and fundamental nature of CN’s will not be given in this text due to the fact that it is beyond the scope of the current research to say with certainty what exact characteristics of the MWCNT’s , used in this research, have on the effective thermal conductivity of a CN. The measured effective thermal conductivities of these three unique CN's will be presented only. It is up to the reader to form conclusions, or to conduct future research or investigation into this new branch of science.

9.2. Results: NanoAmor Stock# 1235YJS

The NanoAmor MWCNT particles (Stock #: 1235YJS) are a match for its longer tailed counterpart. It has the same rough density, number of walls, and diameters. It is, however, noticeably shorter in length than either of the other two particles used in this research. This particular particle was chosen for these very features. Some of the current research in nanofluid behavior theorizes that smaller nanoparticles have better suspension properties and inherently cause a greater increase in the effective thermal conductivity of a nanofluid. Therefore, this

MWCNT along with its longer counterpart provided a unique chance to study how nanotube lengths contribute to the effective thermal conductivity of CN's. For the purposes of this research, this particular MWCNT will be referred to as the short tailed (ST) MWCNT. This is due to the fact that it is the geometrically shorter of the two NanoAmor purchased nanoparticles.

This CN showed the lowest overall effective thermal conductivity increase of any tested. The salient values can be seen above in table 9-1. As can be seen in figures 9-1 through 9-3, the conductivity values seem to generally be on the rise and are, for the most part, measurably above the baseline effective thermal conductivity. However, the values do tend to fluctuate substantially. In addition, some discrepancies exist between the two distinct days of testing. This implies that either variations in the experimental processes or CN creation existed.

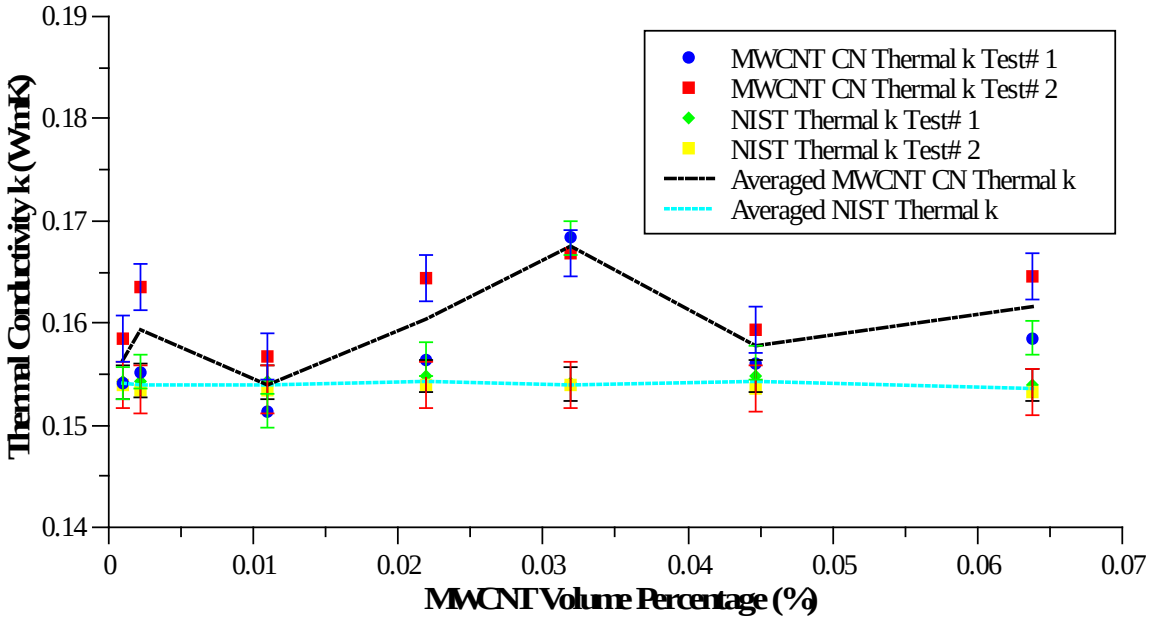

Figure 9-1. Short length NanoAmor (Stock # 1235YJS) MWCNT based cryogenic nanofluid effective thermal conductivity vs. nanoparticle concentration compared to base LOX calibration values.

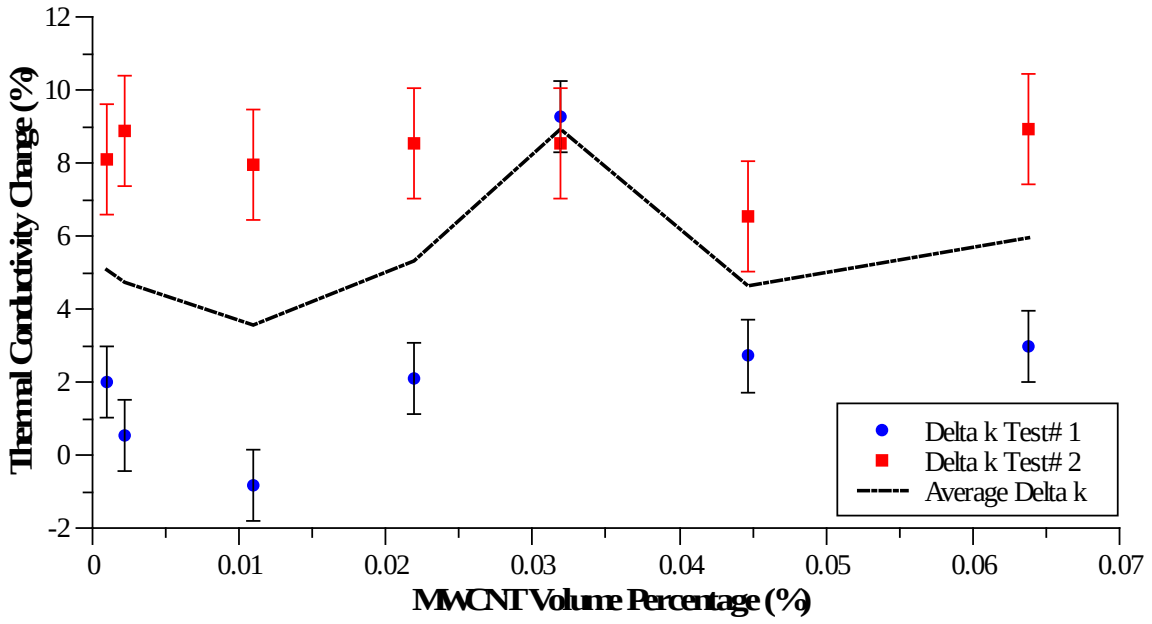

Figure 9-2. Short length NanoAmor (Stock # 1235YJS) MWCNT based cryogenic nanofluid effective thermal conductivity percent change vs. nanoparticle concentration.

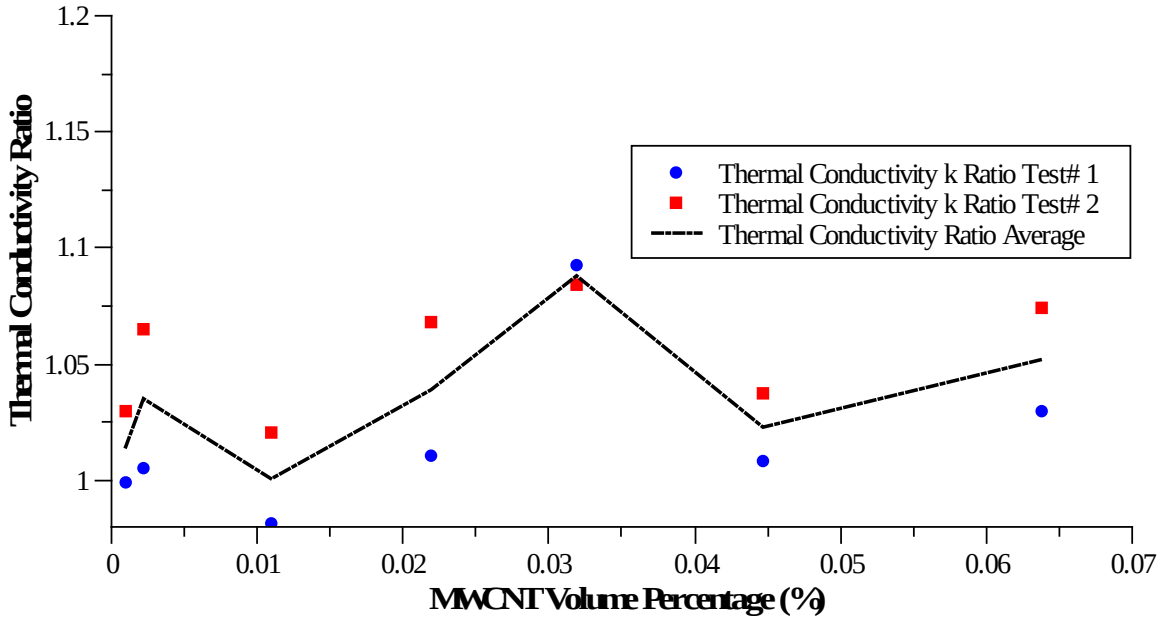

Figure 9-3. Short length NanoAmor (Stock # 1235YJS) MWCNT based cryogenic nanofluid effective thermal conductivity ratio vs. nanoparticle concentration.

Table 9-1. Tabulated effective thermal conductivity values for the CN based upon the NanoAmor stock # 1235YJ MWCNT's.

NanoAmor Stock # 1235YJS	Effective Thermal Conductivity W/mK	Effective Thermal Conductivity Change (%)
Maximum Value	**0.1676**	**8.909**
Minimum Value	**0.1593**	**4.7176**
Total Average Value	**0.1595**	**5.4485**
Total Average Base LOX Value	**0.1544**	N/A

These variations could also be explained by some of the leading theories and might be completely in line with current research. These include that smaller particles can tend to have greater attraction and can therefore tend to agglomerate faster, or that these particles did not upon inspection show as much particle entanglement and therefore would not demonstrate the leading theory of percolation, or direct particle to particle heat transfer. In addition, visual inspection at the time of this particular CN's creation and testing indicated that somewhat poorer dispersion and subsequent stabilization of the CN occurred. This could explain the curvatures and values of the above plots. However, it should be noted from the results, and the calculated uncertainty ranges a measurable and definite increase in the effective thermal conductivity occurred for the majority of the data points.

9.3. Results: NanoAmor Stock# 1204YJ

NanoAmor particle (Stock# 1204YJ) is the longer nanotube counterpart to the previous short tailed nanoparticle. It once again has the same rough number of walls, density and diameters as the previous nanotube. This particle is of a much greater length and provides insight into how length, general susceptibility to entanglement and particle to particle interactions affect the behavior of CN's. It should be noted that this particular particle was tested an additional two times for two of its intermediate values. This was due to some additional experimental factors

which led to testing inaccuracies on the first two days. These long-tailed MWCNT's showed a similar amount of tangling to their short tailed counterparts; this is not surprising, considering that they are identical in every way but length. Once again, they did not seem (by inspection) to have a great deal of stability.

This particular long tailed MWCNT based CN shows a significant effective thermal conductivity increase over its shorter counterpart (figure 9-4 through 9-6, table 9-2). This would imply that length effects do play an important role in effective thermal conductivity change. In addition, this particular CN shows a much smoother and generally increasing curve as MWCNT particle concentration increases. The individual data points from each testing day are also very close and in general agree quite well with each other and the overall trends descried in the plots above.

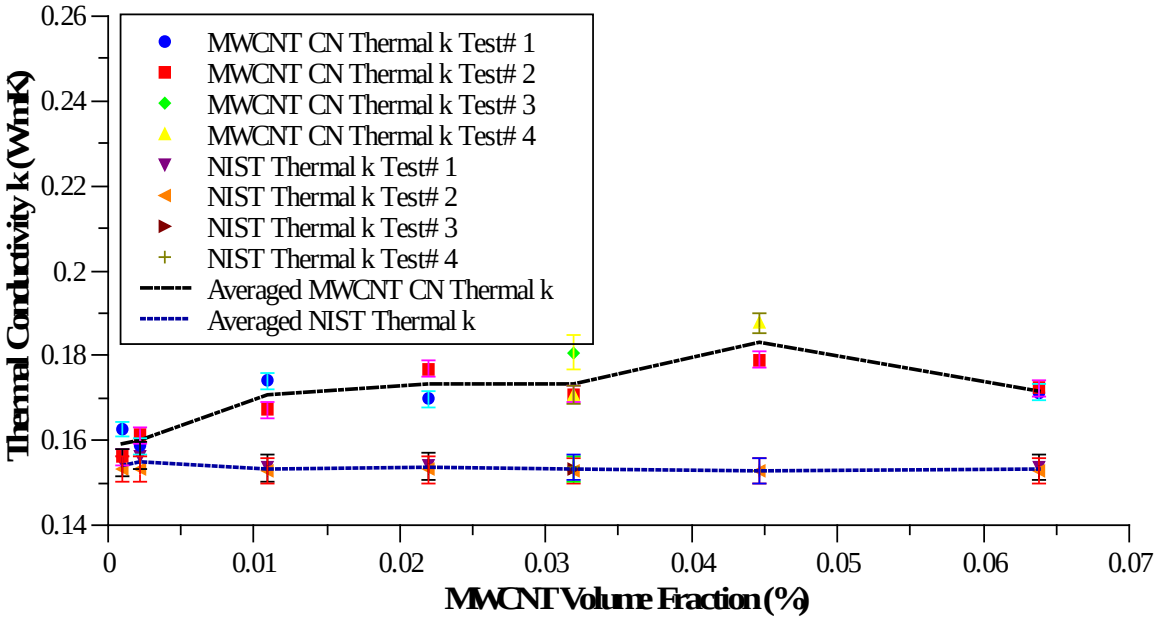

Figure 9-4. Long length NanoAmor (Stock # 1204YJ) MWCNT based cryogenic nanofluid effective thermal conductivity vs. nanoparticle concentration compared to base LOX calibration values.

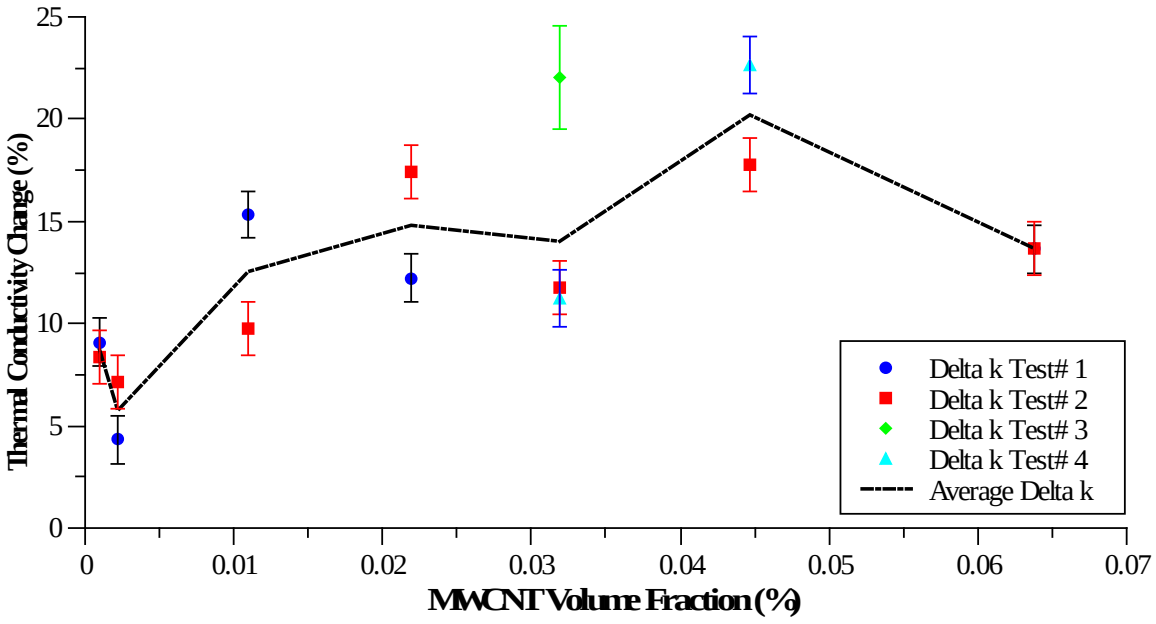

Figure 9-5. Long length NanoAmor (Stock # 1204YJ) MWCNT based cryogenic nanofluid effective thermal conductivity percent change vs. nanoparticle concentration.

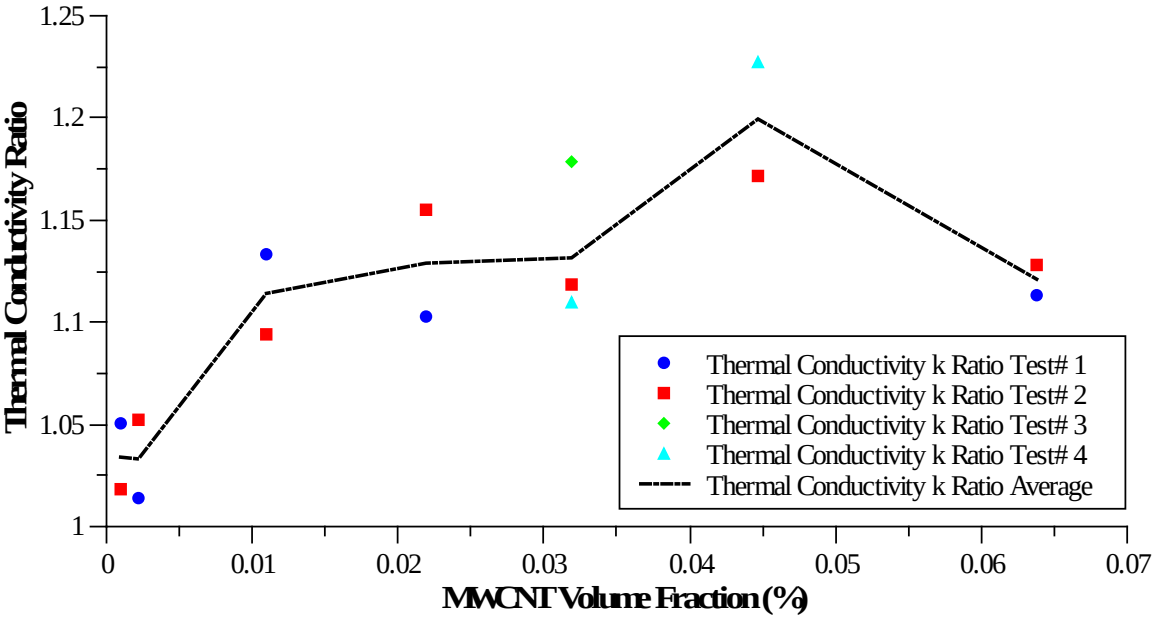

Figure 9-6. Long length NanoAmor (Stock # 1204YJ) MWCNT based cryogenic nanofluid effective thermal conductivity ratio vs. nanoparticle concentration.

Table 9-2. Tabulated effective thermal conductivity values for the CN based upon the NanoAmor stock # 1204YJ MWCNT's.

NanoAmor Stock # 1204YJ	Effective Thermal Conductivity W/mK	Effective Thermal Conductivity Change (%)
Maximum Value	**0.1836**	**20.0375**
Minimum Value	**0.1599**	**5.7246**
Total Average Value	**0.1702**	**12.6715**
Total Average Base LOX Value	**0.1535**	**N/A**

This implies a good deal of repeatability. The figures above also indicate that there is a distinct point at which the anomalous thermal conductivity enhancement provided by the MWCNT's no longer increases the overall conductivity and a plateau of conductivity increase is reached. This trend towards a plateau is once again in agreement with some of the current theories on nanofluid behavior, however, this particular effect could once again be caused by experimental factors, or be a natural artifact of nanofluid/CN behavior. However, it is quite obvious from the results above and from table 9-2. that a great deal of positive change occurred in the baseline thermal conductivity of LOX upon the insertion of the long tailed MWCNT's.

9.4. Results: Dr. T.C. Shen

These nanoparticles are something of an enigma and provided some of the most exciting effective thermal conductivity characteristics measured throughout this work. They were designed and grown by Dr. T. C. Shen of Utah State Universities Physics department .These MWCNT's were chosen due to their availability, their unique physical characteristics and the fact that they offered an interesting and exciting counterpart to the NanoAmor particles. Indeed, as can be seen in the nanoparticle profile chapter a great deal is yet unknown about them, which makes exact comparisons difficult. However, they vary significantly in terms of length, number of walls, density and diameters from the other particles tested in this work. In addition, several

batches of MWCNT's were created by Dr. Shen and measured throughout this research. These MWCNT's seemed to, in general, have a lower density than the other particles and tended to suspend much better in LOX. In addition, they appeared to entangle very easily and were attracted to the platinum Hot Wire suspended in the host liquid. This could account for some of their unusual and exciting properties. For instance, the fact that they entangled so thoroughly throughout the test could imply that direct contact conduction was occurring through nanotube clumps, and that percolation theory, or ballistic/phonon conduction accounted for a great deal of the observed results. It should be noted, that the nanotubes seemed to cluster around the platinum THW, this would create a zone of artificially high concentration around the wire and could account for some small part of the results below. However, despite the unusual nature of these particles it can simply not be argued that they provided the most stunning effective thermal conductivity increases and results throughout this research (figure 9-7 through 9-9, table 9-3).

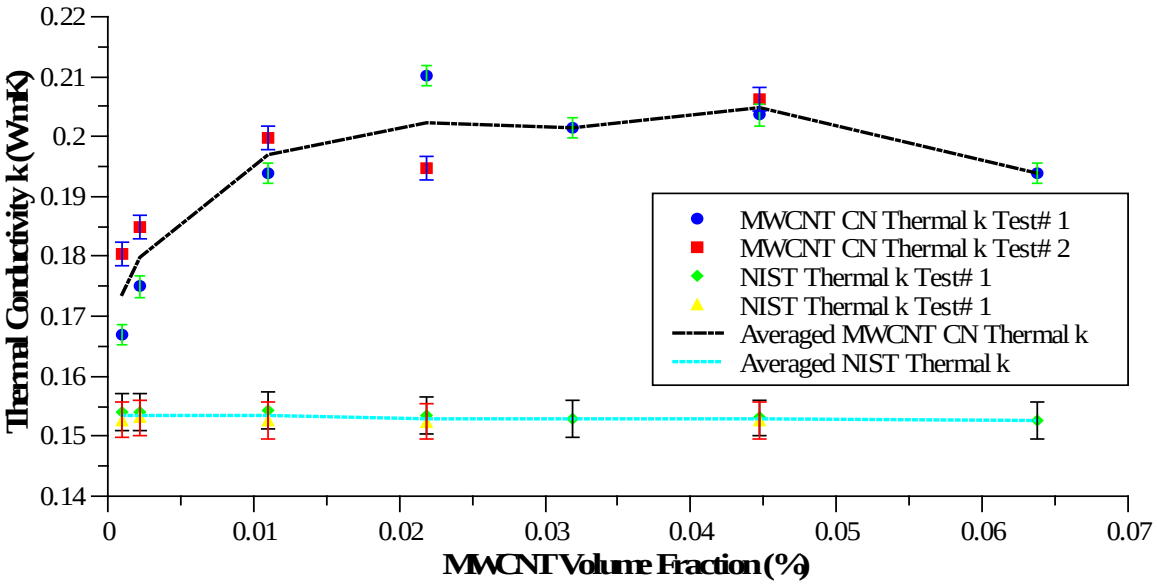

Figure 9-7. Dr. T. C. Shen MWCNT based cryogenic nanofluid effective thermal conductivity vs. nanoparticle concentration compared to base LOX calibration values.

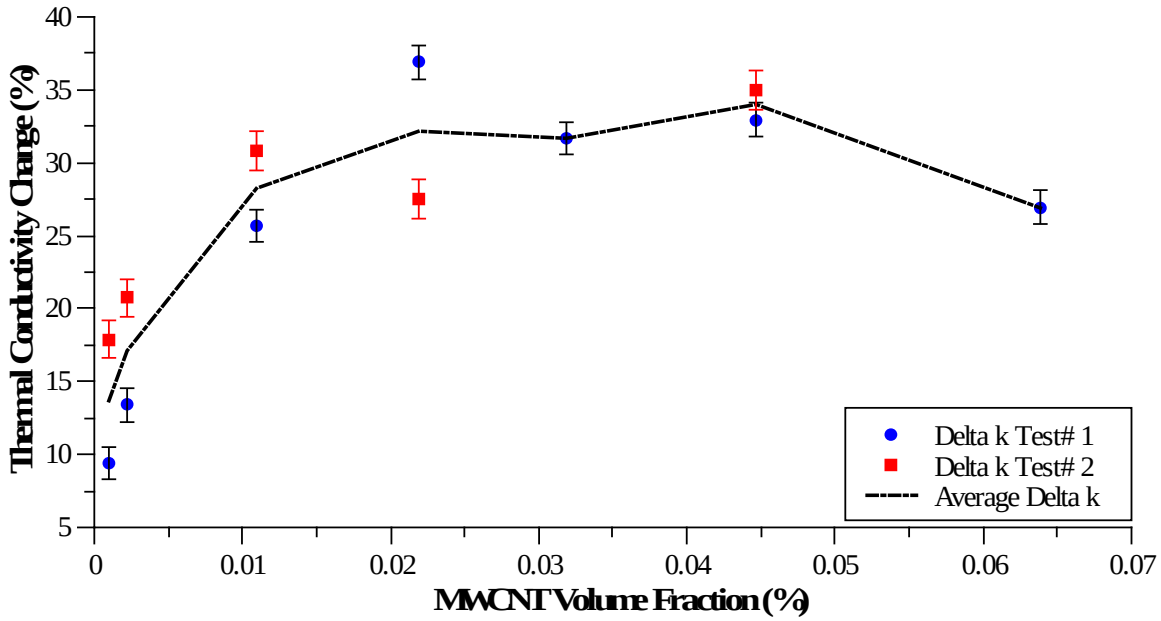

Figure 9-8. Dr. T. C. Shen MWCNT based cryogenic nanofluid effective thermal percent change vs. nanoparticle concentration.

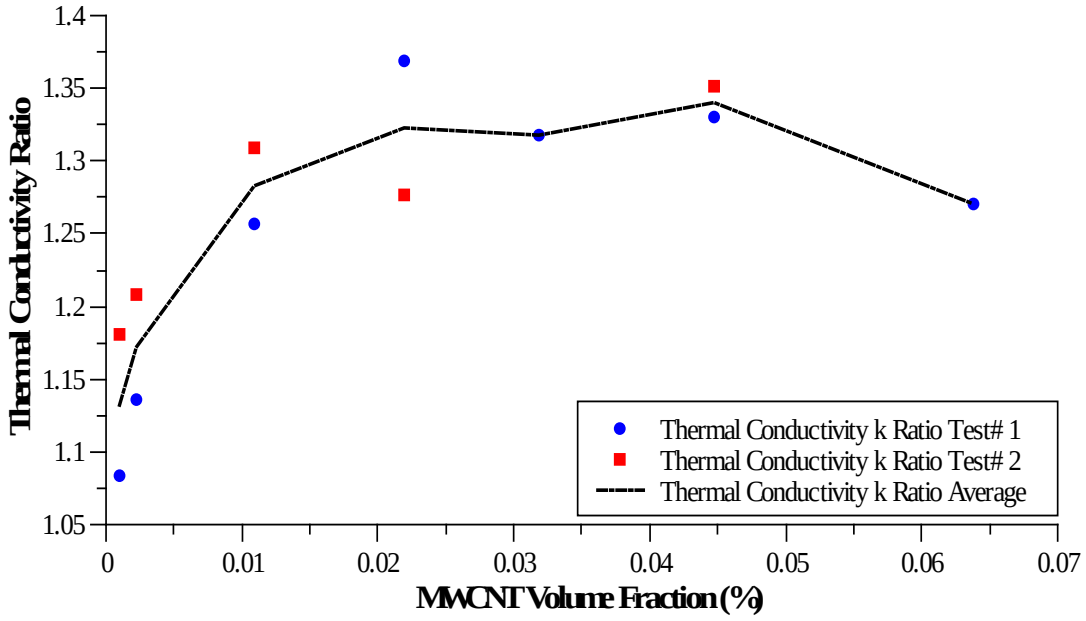

Figure 9-9. Dr. T. C. Shen MWCNT based cryogenic nanofluid effective thermal conductivity ratio vs. nanoparticle concentration.

Table 9-3. Tabulated effective thermal conductivity values for the CN based upon Dr. T. C. Shen MWCNT's

Dr. T. C. Shen MWCNT	Effective Thermal Conductivity W/mK	Effective Thermal Conductivity Change (%)
Maximum Value	**0.20488**	**33.8635**
Minimum Value	**0.1736**	**13.6186**
Total Average Value	**0.19332**	**26.1851**
Total Average Base LOX Value	**0.1531**	**N/A**

Dr. Shen's MWCNT based CN's were tested early on in this research, and provided much of the excitement and some of the impetus for this research . They showed the greatest anomalous increase in effective thermal conductivity measured throughout this research. As can be seen in table 9-3 above, they show a great deal of effective thermal conductivity increase over the baseline values even at surprisingly low MWCNT concentration values. This is demonstrated by figure 9-7, where even near the low end of tested concentration values, an increase of roughly 10-15% was measured. This was greater than the maximum measured value of the short tailed CN, and near the total average value measured for the long tailed. This implies a truly unique series of either physical properties/characteristics or phenomena that caused such an increase. Once again, the curve is generally increasing, with small deviations and fluctuations. The two different day's worth of testing implies good repeatability in the measurements and the overall slope and shape of the curve is generally smooth and increasing. Near the higher end of the tested concentration values, this CN shows a decrease in conductivity which is in line with the other CN's tested and in all likelihood, is caused by the same features. It is quite obvious, that Dr. Shen's MWCNT's created a truly impressive CN.

9.5. Results: Data Comparison

The total unsmoothed averages for each of the tested MWCNT based CN's are compared and displayed below in single plot format. These plots demonstrate how the various CN's compare to each other in terms of total effective thermal conductivity increase with respect to pure base LOX values (figure 9-10) as well as the relative differences in effective thermal conductivity, line curvature, slope, and general shape. The total comparative percent/ratio changes in conductivity are also shown (figure 9-11, 9-12).

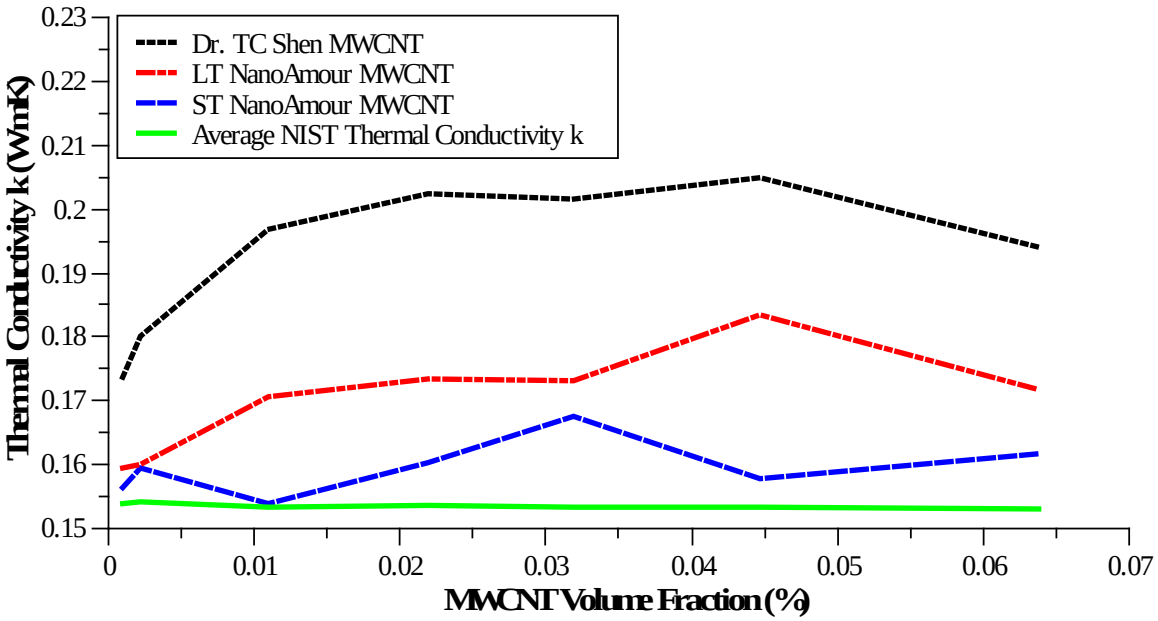

Figure 9-10. Comparison of the total average effective thermal conductivity values for all of the CN's tested in this work.

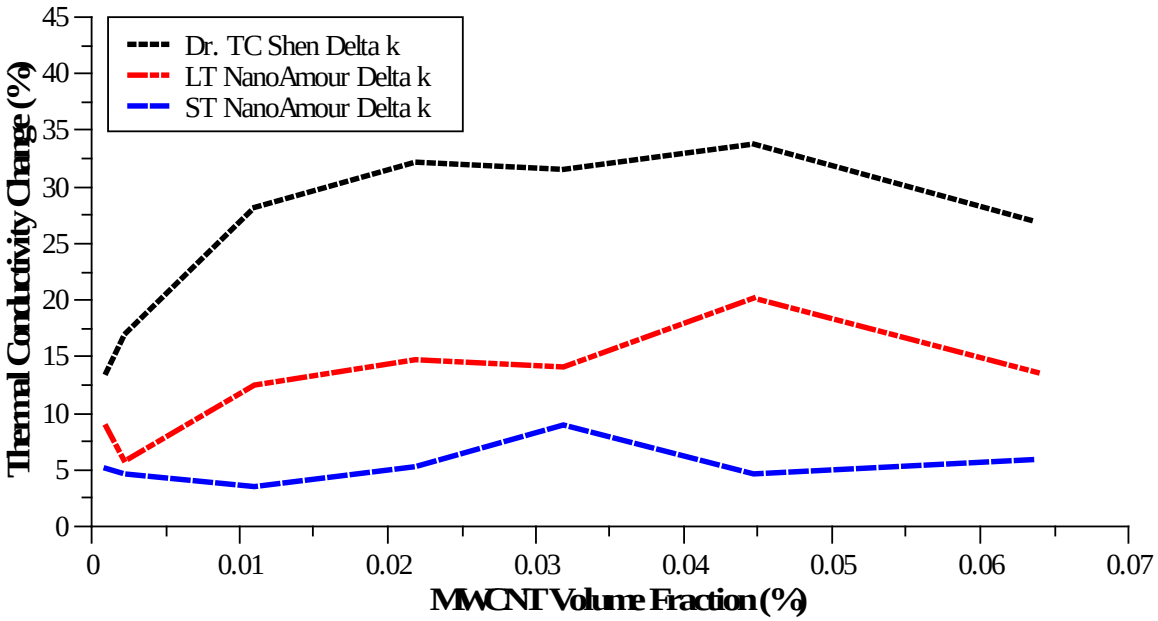

Figure 9-11. Comparison of the total average percentage change of the effective thermal conductivity for all of the CN's tested in this work.

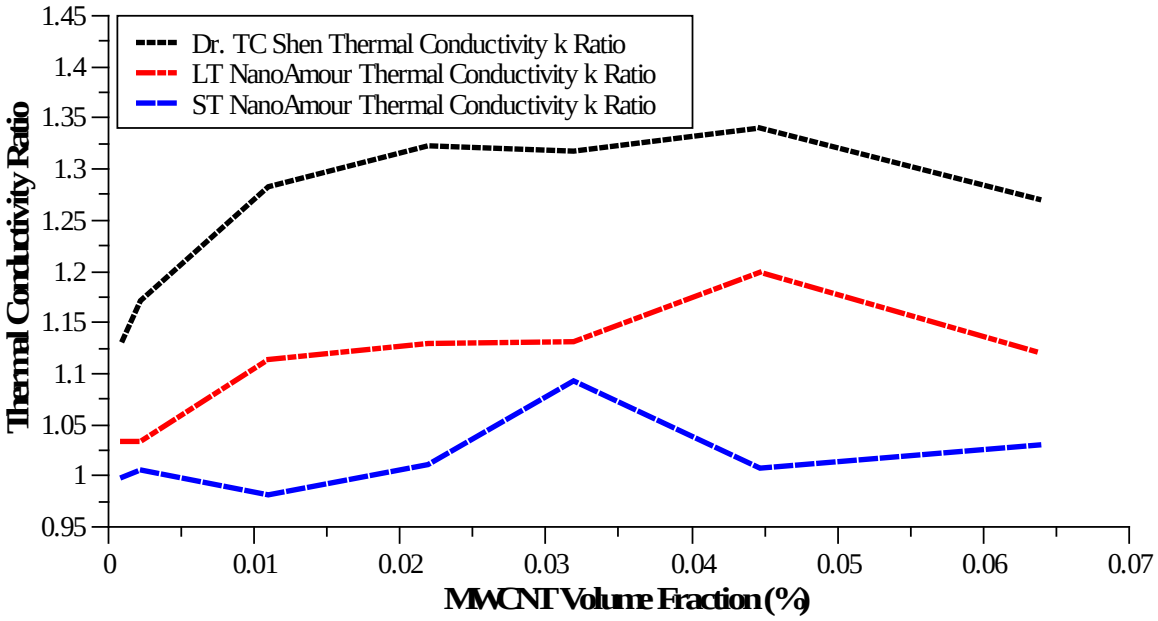

Figure 9-12. Comparison of the total average effective thermal conductivity ratio for all of the CN's tested in this work.

It can now clearly be seen that the largest increase is caused by Dr. Shen's MWCNT's with the long tailed NanoAmor MWCNT's slightly below and the short tailed NanoAmor particles detailing the smallest increase in effective thermal conductivity. Each curve, however, shows a great deal of increase over the base value of LOX. It can therefore be concluded that a noticeable change was observed for each of the CN's tested and that particle concentration played a key role in the enhancement of effective thermal conductivity. In addition, these results demonstrate that particle type, nature and morphology are important factors when designing a CN.

An additional note is that the effective thermal conductivity curves in general show complimentary slopes and trends. This in some cases represents similar increases and inflections, while others demonstrate the opposite. An example of this is the shape/trend differences between the Dr. Shen and NanoAmor Stock # 1204YJ MWCNT based CN's and the NanoAmor Stock #1235YJS CN's.

From these observations, it can be concluded that the various CN's tested in this work are similar enough to each other to allow comparison. The validity of these conclusions can be seen above and, indeed, can be compared to more traditional nanofluids and current static mixture models (Appendix C).

9.6. Effective Thermal Conductivity Data Range

An aspect of this research which bears further study is that of the range of measured effective thermal conductivity values. As with any measurement an assortment of factors can have an effect on the final calculated value. These factors can influence individual measurements in a variety of ways, and can lead to two seemingly identical measurements differing in their final value. It should be noted that this data scattering effect is not the same as the random uncertainty inherent within a measurement. Instead, it is the observation and realization of real world transient behavior within the system, and must be treated and quantified as such.

For the present work, the measured effective thermal conductivity of the assorted cryogenic nanofluids did indeed possess a wide data spread, sometimes on the order of 50% of the total value or more. This range of values could be caused by numerous theoretical, experimental, numerical, or environmental factors such as relative fluid motion, or could in fact be caused by the dynamic and highly complicated nature of the cryogenic nanofluids themselves. It is this last possibility which seems the most likely to the authors for explaining the data scattering within the current study. Nanofluids in general are dynamic system, their internal fluid matrix and suspended particles are in a constant state of flux. This transient behavior, combined with incompatibilities between the inclusion phase and the fluid phase often lead to dispersion and subsequent stability problems. Because, the current work deals with MWCNT's, which tend to clump/tangle, and can form much larger macro sized objects, and LOX, which has a sub-optimal density and low viscosity, it is entirely plausible, that the inclusion MWCNT nanoparticles settle with time. This agglomeration and subsequent settling would lower the volume fraction of inclusion nanoparticles and thus lower the effective thermal conductivities of the cryogenic nanofluids, according to the literature. This theory as to the cause of the measured data ranges is supported by noticing that the intermediate effective thermal conductivity values for each cryogenic nanofluid (see Appendix A) tend to get smaller with test number and time. In addition, the researchers observed settling in the cryogenic nanofluids as individual tests progressed.

Data that contains scattering is still valid. This is demonstrated by the calibration LOX tests, which prove that the experimental system measured the effective thermal conductivity accurately. It is however, important to catalogue and report the overall measured data scatter. This ensures that future reviewers are aware of the fact that a range of values exist, and what those ranges are. The following tables offer the maximum, average, minimum, and subsequent ranges of each of the separate cryogenic nanofluids, and their individual testing days.

Table 9-4. Effective thermal conductivity data range for the cryogenic nanofluids based upon Dr. T. C. Shen's MWCNT's. Test day # 1 (3/16/12).

MWCNT Volume Fraction (%)	Maximum Value (W/mK) Percentage (%)	Average Value (W/mK) Percentage (%)	Minimum Value (W/mK) Percentage (%)	Total Range (W/mK) Percentage (%)
0.000952	0.181021 18.931	0.167011 9.37286	0.157821 5.0966	0.0232 13.8344
0.002191	0.178021 16.951	0.174961 13.384	0.172421 10.276	0.0056 6.675
0.01095	0.219621 42.981	0.193871 25.6085	0.173721 12.02	0.0459 30.961
0.0219	0.229121 50.621	0.210171 36.785	0.193721 23.851	0.0354 26.77
0.0319	0.214921 41.251	0.201461 31.583	0.190521 22.931	0.0244 18.32
0.0446	0.226821 49.101	0.203591 32.829	0.195721 26.261	0.0311 22.84
0.06381	0.204121 34.131	0.193971 26.889	0.181821 18.381	0.0223 15.75

Table 9-5. Effective thermal conductivity data range for the cryogenic nanofluids based upon Dr. T. C. Shen's MWCNT's. Test day # 2 (3/26/12).

MWCNT Volume Fraction (%)	Maximum Value (W/mK) Percentage (%)	Average Value (W/mK) Percentage (%)	Minimum Value (W/mK) Percentage (%)	Total Range (W/mK) Percentage (%)
0.000952	0.1866 22.591	0.18036 17.8645	0.1711 12.4	0.0155 10.191
0.002191	0.1948 27.991	0.18499 20.6869	0.1762 15.702	0.0056 6.675
0.01095	0.2127 39.761	0.19984 30.759	0.1889 22.991	0.0459 30.961
0.0219	0.207 36.011	0.19464 27.459	0.1861 20.131	0.0354 26.77
0.0319	N/A	N/A	N/A	N/A
0.0446	0.218 43.291	0.20618 34.898	0.1961 27.701	0.0311 22.84
0.06381	N/A	N/A	N/A	N/A

Table 9-6. Effective thermal conductivity data range for the cryogenic nanofluids based upon NanoAmor Stock # 1235YJS MWCNT's. Test day # 4 (4/3/12).

MWCNT Volume Fraction (%)	Maximum Value (W/mK) Percentage (%)	Average Value (W/mK) Percentage (%)	Minimum Value (W/mK) Percentage (%)	Total Range (W/mK) Percentage (%)
0.000952	0.164053 8.0047	0.154113 2.00111	0.142053 -1.2355	0.022 9.2402
0.002191	0.159453 4.4577	0.155203 0.53621	0.149953 -2.0049	0.0095 6.4626
0.01095	0.157153 1.3267	0.151333 -0.83128	0.144953 -2.09028	0.0122 3.41698
0.0219	0.161953 5.4017	0.156433 2.09598	0.143753 -1.7215	0.0182 7.1232
0.0319	0.190953 25.6747	0.168323 9.26	0.158753 1.5237	0.0322 24.151
0.0446	0.168353 8.7147	0.156083 2.71008	0.144153 -1.3915	0.0242 10.1062
0.06381	0.163453 7.5637	0.158553 2.98002	0.152153 -1.2321	0.0113 8.7958

Table 9-7. Effective thermal conductivity data range for the cryogenic nanofluids based upon NanoAmor Stock # 1235YJS MWCNT's. Test day # 5 (4/4/12).

MWCNT Volume Fraction (%)	Maximum Value (W/mK) Percentage (%)	Average Value (W/mK) Percentage (%)	Minimum Value (W/mK) Percentage (%)	Total Range (W/mK) Percentage (%)
0.000952	0.16421 11.298	0.1585 8.1086	0.15011 6.335	0.0141 4.963
0.002191	0.18691 23.003	0.1635 8.89889	0.15551 5.243	0.0314 17.76
0.01095	0.16241 11.213	0.1567 7.96717	0.15021 5.09273	0.0122 6.12027
0.0219	0.17531 15.333	0.16439 8.51313	0.15841 5.8251	0.0169 9.5079
0.0319	0.17241 12.404	0.1669 8.55883	0.16041 5.5751	0.012 6.8289
0.0446	0.16371 8.312	0.15941 6.54112	0.15461 5.1646	0.0091 3.1474
0.06381	0.17371 14.32	0.16463 8.94022	0.15661 5.4692	0.0171 8.8508

Table 9-8. Effective thermal conductivity data range for the cryogenic nanofluids based upon NanoAmor Stock # 1204YJ MWCNT's. Test day # 5-8 (4/6-12/12).

MWCNT Volume Fraction (%)	Maximum Value (W/mK) Percentage (%)	Average Value (W/mK) Percentage (%)	Minimum Value (W/mK) Percentage (%)	Total Range (W/mK) Percentage (%)
0.000952	0.184499 21.886	0.162629 9.09451	0.147699 2.15307	0.0368 19.73293
0.002191	0.165099 8.17	0.158579 4.31281	0.148399 2.18451	0.0167 5.98549
0.01095	0.212599 41.516	0.173989 15.336	0.153099 3.795	0.0595 37.721
0.0219	0.211799 40.976	0.169799 12.217	0.155199 2.4841	0.0566 38.4919
0.0319	0.171199 14.246	0.161059 7.19304	0.151399 2.9557	0.0198 11.2903
0.0446	0.175699 17.216	0.162059 7.8276	0.150399 5.277	0.0253 11.939
0.06381	0.222399 47.966	0.171209 13.66	0.147499 4.489	0.0749 43.477

Table 9-9. Effective thermal conductivity data range for the cryogenic nanofluids based upon NanoAmor Stock # 1204YJ MWCNT's. Test day # 6 (4-9-12).

MWCNT Volume Fraction (%)	Maximum Value (W/mK) Percentage (%)	Average Value (W/mK) Percentage (%)	Minimum Value (W/mK) Percentage (%)	Total Range (W/mK) Percentage (%)
0.000952	0.165996 11.3381	0.156096 8.39357	0.150196 4.9308	0.0158 6.4073
0.002191	0.166896 9.7391	0.161246 7.13653	0.154396 5.1646	0.0125 4.5745
0.01095	0.173596 14.1181	0.167126 9.74653	0.157096 4.65545	0.0165 9.46265
0.0219	0.243396 60.0831	0.176776 17.387	0.149896 4.7739	0.0935 55.3092
0.0319	0.185596 22.0231	0.170826 11.7966	0.158496 4.9761	0.0271 17.047
0.0446	0.243296 60.0331	0.179016 17.791	0.155296 5.5058	0.088 54.5273
0.06381	0.188196 23.7631	0.172356 13.6661	0.155896 5.2347	0.0323 18.5284

Table 9-10. Effective thermal conductivity data range for the cryogenic nanofluids based upon NanoAmor Stock # 1204YJ MWCNT's. Test day # 7 (4-10-12).

MWCNT Volume Fraction (%)	Maximum Value (W/mK) Percentage (%)	Average Value (W/mK) Percentage (%)	Minimum Value (W/mK) Percentage (%)	Total Range (W/mK) Percentage (%)
0.000952	N/A	N/A	N/A	N/A
0.002191	N/A	N/A	N/A	N/A
0.01095	N/A	N/A	N/A	N/A
0.0219	N/A	N/A	N/A	N/A
0.0319	0.208824 40.5585	0.180714 22.0427	0.151424 4.9632	0.0574 35.5953
0.0446	N/A	N/A	N/A	N/A
0.06381	N/A	N/A	N/A	N/A

Table 9-11. Effective thermal conductivity data range for the cryogenic nanofluids based upon NanoAmor Stock # 1204YJ MWCNT's. Test day # 8 (4-12-12).

MWCNT Volume Fraction (%)	Maximum Value (W/mK) Percentage (%)	Average Value (W/mK) Percentage (%)	Minimum Value (W/mK) Percentage (%)	Total Range (W/mK) Percentage (%)
0.000952	N/A	N/A	N/A	N/A
0.002191	N/A	N/A	N/A	N/A
0.01095	N/A	N/A	N/A	N/A
0.0219	N/A	N/A	N/A	N/A
0.0319	0.208556 35.7061	0.171706 10.4546	0.151156 -0.9459	0.0574 36.652
0.0446	0.275256 79.6661	0.188666 21.8917	0.159856 1.6511	0.1154 78.015
0.06381	N/A	N/A	N/A	N/A

9.7. Analysis of Variance

In addition to cataloging and reporting data scatter the variance of the data must be analyzed via a statistical method to determine if the spread in data represents definite and significant values/trends. To accomplish this, a series of Analysis of Variance (ANOVA) tests were performed on the individual effective thermal conductivity data sets for each type of studied

cryogenic nanofluids. Specifically, the variance between the base LOX thermal conductivity, and the measured effective thermal conductivity for each CN was analyzed with a standard F-test in excel. In each case and for each day's testing, the F value surpassed the $F_{critical}$ value. Therefore, the null hypothesis can be rejected, and it can be concluded that, with 95% confidence, the effective thermal conductivity vary significantly from the base value as the MWCNT volume fraction changes. The ANOVA test was then used to compare the variance within each type of cryogenic nanofluid, specifically, whether the variations between individual volume fraction measurements and test days were so significant that similarity conclusions could not be drawn. For this case, the F values were smaller than the $F_{critical}$ values, thus implying that the null hypothesis should be accepted, and therefore demonstrating that the individual days of testing when compared to each other at each concentration value were not significantly different.

By performing these analyses, we have concluded that the measured data varies significantly with respect to MWCNT volume fraction type, and do not vary significantly between individual measurements. The specifics of the ANOVA analysis can be reviewed upon request of the authors.

CHAPTER 10

CONCLUSIONS

The primary objective of this work was to determine whether a cryogenic nanofluid would exhibit thermal conductivity enhancements similar to those observed with traditional nanofluids. This goal can be restated as to whether the effective thermal conductivity of a cryogenic nanofluid will change with the presence of inclusion nanoparticles and what absolute effective thermal conductivity value will this change represent. To accomplish this objective, several not insubstantial preliminary steps were required. These included the entirety of the theoretical, experimental, numerical, etc. details listed in this thesis along with the creation of the cryogenic nanofluids themselves which are, to the best of the author's knowledge, the first of their kind.

Some of the conclusions that were drawn from this research include the following.

Conclusions on the THW experimental technique:

- The transient hot wire method can be modified to measure the effective thermal conductivity of cryogenic nanofluids.
- The THW technique provides enough accuracy to quantify the effective thermal conductivity values of MWCNT based cryogenic nanofluids despite their dynamic nature and transient instability. Experimental Bias's were found to be on the order of 3-5% with random experimental uncertainties of roughly 1-2%.

Conclusions on the creation of cryogenic nanofluids:

- The world's first cryogenic nanofluids have been created. Three distinct MWCNT based cryogenic nanofluids were created in the laboratory with LOX acting as the host material.
- Liquid Oxygen and MWCNT's can be combined to form a cryogenic nanofluid.
- Liquid Oxygen and MWCNT's when combined form a colloidal mixture which is, by visual observation, stable and dispersed within the specified testing time of this research (10-20 min).
- The mixing technique of sonication is viable and effective in the creation/fabrication of the cryogenic nanofluids studied in this research.

Conclusions on the measurement of the effective thermal conductivity of cryogenic nanofluids:

- Cryogenic nanofluids exhibit an increase in their effective thermal conductivities above the base line value of pure liquid Oxygen.
- The effective thermal conductivities of the cryogenic nanofluids studied in this research vary with total nanoparticle inclusion volume fraction. This trend is observed to be generally increasing with an eventual plateau.
- MWCNT physical characteristics such as size, number of walls, diameters, density, etc play an important role in the overall thermal transport behavior of cryogenic nanofluids, specifically in the enhancement of effective thermal conductivity. It was observed that the MWCNT's with larger lengths cause greater increases in the effective thermal conductivity.
- Dr. T. C. Shen's MWCNT's when combined with LOX produced effective thermal conductivity enhancements of between (13-30%) with nanoparticle volume concentration below 0.1%.
- NanoAmor (Stock #1204YJ) MWCNT's when combined with LOX produced effective thermal conductivity enhancements of between (5-20%) with nanoparticle volume concentration below 0.1%.
- NanoAmor (Stock #1235YJS) MWCNT's when combined with LOX produced effective thermal conductivity enhancements of between (4-8%) with nanoparticle volume concentration below 0.1%.
- The MWCNT's created by Dr. T. C. Shen produced the greatest overall enhancement in effective thermal conductivity.
- Data ranges exist within the measurements of the effective thermal conductivity of each of the cryogenic nanofluids. This scattering is most likely attributable to the dynamic nature and inherent instability of these cryogenic nanofluids.
- Results are statistically relevant wt. 95% confidence according to ANOVA
- The observed effective thermal conductivity values show good agreement with similar traditional nanofluids when unofficially compared. Similar observations are made with respect to the potentially anomalous behavior of cryogenic nanofluids when compared to traditional models.

Notes on cryogenic nanofluid stability

- The overall dispersion and stability characteristics of nanofluids are a key parameter in their study, and should be further explored and improved upon. Ultimately, creation methodologies which produce well dispersed and stabilized cryogenic nanofluids should be found.

Therefore, it can be concluded that with the information presented in this thesis, along with the future work presented below that cryogenic nanofluids are indeed not only possible and equally deserving of study as traditional nanofluids, but are potentially viable as next generation coolants.

CHAPTER 11

CRYOGENIC NANOFLUIDS: FUTURE WORK

Because cryogenic nanofluids have been, until now, an unexplored class of super-coolants, the research that needs to be done is extensive and fundamentally groundbreaking.

The current research, which explored the effective thermal conductivity enhancements of LOX with inclusion phase MWCNT's should be expanded upon in the form of further thermal conductivity research. This research should explore the effects of nanoparticle material type, nanoparticle morphology and thermo-physical characteristics, particle loading, type of host fluid, temperature and other environmental effects, as well as dispersants and mixing/fabrication techniques etc on the effective thermal conductivity of cryogenic nanofluids.

In addition, the other fundamental forms of heat transfer such as convection and boiling should be studied for similar parameters. Ultimately, all of the salient thermo-physical properties of cryogenic nanofluids should be studied, cataloged and analyzed. Fundamentally, the primary goal of classifying any new type of material is to better understand its basic nature and behavior. This should eventually be accomplished through the development of theoretical models and theories.

An aspect of cryogenic nanofluids which will require a great deal of future attention is that of creating stable, well dispersed mixtures with little or no agglomeration and subsequent settling. This will prove to be of the utmost importance when it comes to the practical applications of cryogenic nanofluids. The future research into the fabrication of cryogenic nanofluids can also study the effect of the creation process, one step vs. two step methods, and time on their overall thermal transport behavior.

It should finally be noted that many of the future research topics described above will require extensive redesigns of existing experimental methods and techniques, and quite a few might

require new experimental methods to be developed. Finally, cryogenic nanofluids have tremendous potential as next generation coolants and are well worth studying.

REFERENCES

[1] Das S. K., Choi, S. U. S., Yu, W., and Pradeep, T., 2008 *Nanofluids Science and Technology*, John Wiley & Sons, Hoboken, NJ.

[2] Das S. K., Choi S. U., and Patel, H. E., 2006, "Heat Transfer In Nanofluids—A Review," Heat Transfer Eng., **27**(10), pp. 3–19.

[3] Keblinski P., Eastman J. A., and Cahill D. G., 2005, "Nanofluids for Thermal Transport," Mater. Today, **8**(6), pp. 36–44.

[4] Keblinski P., Prasher R., and Eapen J., 2008, "Thermal Conductance Of Nanofluids: Is the Controversy Over?," J. Nanopart. Res., **10**(7), pp. 1089–1097.

[5] Feynman, R. P., 1959, "There's Plenty of Room at the Bottom," Talk at Annual Meeting of American Physical Society, December 26; California Institute of Technology Archives, (2001), from http://www.its.caltech.edu/~feynman/plenty.html

[6] Choi, S. U., 2009, "Nanofluids: From Vision to Reality Through Research," J. Heat Transfer, **131**, p. 033106.

[7] Eastman J. A., Phillpot S., Choi S., and Keblinski, P., 2004, "Thermal Transport in Nanofluids 1," Annu. Rev. Mater. Res., **34**, pp. 219–246.

[8] Ding Y., Chen H., Wang L., Yang C., He Y., Yang W., Lee W. P., Zhang L., and Huo, R., 2007, "Heat Transfer Intensification Using Nanofluids," Kona, **25**(25), pp. 23–38.

[9] Burr, A. C., 1933, "Notes on the History of the Concept of Thermal Conductivity," Isis, **20**(1), pp. 246–259.

[10] Taylor, R., Edited by Richardson, M., Maglic, K., Cezairliyan, A., and Peletsky, V., 1992, *In Compendium of Thermophysical Property Measurement Methods, Vol. 1, Survey of Measurement Techniques,* Plenum Press, New York.

[11] Taylor, R., Edited by Richardson, M., Maglic, K., Cezairliyan, A., and Peletsky, V., 1992, In *Compendium of Thermophysical Property Measurement Methods, Vol. 2 Recommended Measurement Techniques and Practices,* Plenum Press, New York.

[12] Richards, J. D., 1988, "Transient Method for Measuring Thermal Conductivity," IEEE Electr. Insul. Mag., IEEE, **4**(1), pp. 23–32.

[13] Vadasz, P., 2010, "Rendering the Transient Hot Wire Experimental Method for Thermal Conductivity Estimation to Two-Phase Systems—Theoretical Leading Order Results," J. Heat Transfer, **132**, p. 081601.

[14] Franco, A., 2007, “An Apparatus for the Routine Measurement of Thermal Conductivity of Materials for Building Application Based on a Transient Hot-wire Method,” Appl. Therm. Eng., **27**(14), pp. 2495–2504.

[15] Xie, H., Gu, H., Fujii, M., and Zhang, X., 2005, “Short Hot Wire Technique for Measuring Thermal Conductivity and Thermal Diffusivity of Various Materials,” Meas. Sci. and Technol., **17**(1), p. 208.

[16] de Sylos Cintra Jr, J., and Nunes dos Santos, W., 2000, “Numerical Analysis of Sample Dimensions in Hot Wire Thermal Conductivity Measurements,” J. Eur. Ceram. Soc., **20**(11), pp. 1871–1875.

[17] Codreanu, C., Codreanu, N.-I., and Obreja, V. V. N., 2006, “An Experimental Approach of the Hot Wire Method for Measurement of the Thermal Conductivity,” International Semiconductor Conference, 2006, **2**, pp. 359–362.

[18] Sassi, M. B., Dos Santos, C. A., Da Silva, Z. E., Gurgel, J. M., and Junior, J. P., 2009, “Heat Conduction Models for the Transient Hot Wire Technique,” High Temperatures-High Pressures, **38**, pp. 97–117.

[19] Bleazard, J. G., and Teja, A. S., 1995, “Thermal Conductivity of Electrically Conducting Liquids by the Transient Hot-wire Method,” J. Chem. Eng. Data, **40**(4), pp. 732–737.

[20] Trump, W. N., Luebke, H. W., Fowler, L., and Emery, E. M., 1977, “Rapid Measurement of Liquid Thermal Conductivity by the Transient Hot-wire Method,” Rev. Sci. Instrum., **48**(1), pp. 47–51.

[21] Fox, J., Gaggini, N., and Wangsani, R., 1987, “Measurement of the Thermal Conductivity of Liquids Using a Transient Hot Wire Technique,” Am. J. Phys., **55**, p. 272.

[22] Fairbrother, J., 2002, “Ratio of Convection to Conduction Loss from a Hot Wire Stretched Along the Axis of a Vertical Cylindrical Tube,” Br. J. Appl. Phys., **4**(7), p. 204.

[23] dos Santos, W. N., 2008, “Advances on the Hot Wire Technique,” J. Eur. Ceram. Soc., **28**(1), pp. 15–20.

[24] Nagasaka, Y., and Nagashima, A., 2000, “Absolute Measurement of the Thermal Conductivity of Electrically Conducting Liquids by the Transient Hot-wire Method,” J. Phys. E: Sci. Instrum., **14** (12), p. 1435.

[25] ASTM Standard D2717, 95, "Standard Test method for Thermal Conductivity of Liquids," ASTM International, West Conshohocken, PA, 2009, DOI: 10.1520/D2717-95R09, from www.astm.org.

[26] ASTM Standard C1113, 99, "Standard Test method for Thermal Conductivity of Refractories by Hot Wire (Platinum Resistance Thermometer Technique)," ASTM International, West Conshohocken, PA, 2004, DOI: 10.1520/C1113_C1113M-09, from www.astm.org.

[27] ASTM Standard D5334, 05, "Standard Test method for Determination of Thermal Conductivity of Soil and Soft Rock by Thermal Needle Probe Procedure," ASTM International, West Conshohocken, PA, 2004, DOI: 10.1520/D5334-08, from www.astm.org.

[28] Manohar, K., Yarbrough, D. W., and Booth, J. R., 2000, “Measurement of Apparent Thermal Conductivity by the Thermal Probe Method,” J. Test. Eval., **28**(5), pp. 345–351.

[29] Waite, W. F., Gilbert, L. Y., Winters, W. J., and Mason, D. H., 2006, “Estimating Thermal Diffusivity and Specific Heat from Needle Probe Thermal Conductivity Data,” Rev. Sci. Instrum., **77**(4), pp. 044904–044904.

[30] ASTM Standard E1952, 06, "Standard Test method for Thermal conductivity and Thermal Diffusivity by Modulated Temperature Differential Scanning Calorimetry," ASTM International, West Conshohocken, PA, 2006, DOI: 10.1520/E1952-06, from www.astm.org.

[31] Sheffield, G. S., and Schorr, J. R., 1991, “Comparison of Thermal Diffusivity and Thermal Conductivity Methods,” Am. Ceram. Soc. Bull.; (United States), **70**(1), pp. 102-107.

[32] Parr, G., Santagata-Iervolino, E., Van Herwaarden, A. W., Wien, W., and Vellekoop, M. J., 2009, “Thermal Characterization of Microliter Amounts of Liquids by a Micromachined Calorimetric Transducer,” Micro Electro Mechanical Systems, 2009. MEMS 2009. IEEE 22nd International Conference on, pp. 535–538.

[33] Wang, C. Y., and Yang, M. L., 1995, “A New Calorimeter for Measuring Rapidly the Thermal Conductivity of Liquids,” Thermochim. Acta, **255**, pp. 365–370.

[34] Griffiths, E., 2002, “A Survey of Heat Conduction Problems,” Proc. Phys. Soc.. London, **41**(1), p. 151.

[35] Cerdeiriña, C., M\íguez, J., Carballo, E., Tovar, C., De la Puente, E., and Roman\í, L., 2000, “Highly Precise Determination of the Heat Capacity of Liquids by DSC: Calibration and Measurement,” Thermochim. Acta, **347**(1), pp. 37–44.

[36] Diedrichs, A., and Gmehling, J., 2006, “Measurement of Heat Capacities of Ionic Liquids by Differential Scanning Calorimetry,” Fluid Phase Equilib., **244**(1), pp. 68–77.

[37] ASTM Standard E1461, 07, "Standard Test method for Thermal Diffusivity by the Flash Method," ASTM International, West Conshohocken, PA, 2006, DOI: 10.1520/E1461-07, from www.astm.org.

[38] Shaikh, S., Lafdi, K., and Ponnappan, R., 2007, “Thermal Conductivity Improvement in Carbon Nanoparticle Doped PAO Oil: An Experimental Study,” J. App. Phys., **101**(6), pp. 064302–064302.

[39] Gaal, P., Thermitus, M.-A., and Stroe, D. E., 2004, “Thermal Conductivity Measurements Using the Flash Method,” J. Thermal Anal. Calorim., **78**(1), pp. 185–189.

[40] Baba, T., and Ono, A., 2001, “Improvement of the Laser Flash Method to Reduce Uncertainty in Thermal Diffusivity Measurements,” Meas. Sci. Tech., **12**(12), p. 2046.

[41] Parker, W., Jenkins, R., Butler, C., and Abbott, G., 1961, “Flash Method of Determining Thermal Diffusivity, Heat Capacity, and Thermal Conductivity,” J. App. Phys., **32**(9), pp. 1679–1684.

[42] Kubicar, L., and Bohac, V., 1999, “Review of Several Dynamic Methods of Measuring Thermophysical Parameters,” Thermal Conductivity, **24**, pp. 135–149.

[43] Gustafsson, S. E., Karawacki, E., and Khan, M. N., 1981, “Determination of the Thermal-conductivity Tensor and the Heat Capacity of Insulating Solids with the Transient Hot-strip Method,” J. App. Phys., **52**(4), pp. 2596–2600.

[44] Gustafsson, S. E., and Karawacki, E., 1983, “Transient Hot-strip Probe for Measuring Thermal Properties of Insulating Solids and Liquids,” Rev. Sci. Instrum., **54**(6), pp. 744–747.

[45] Gustafsson, S., Karawacki, E., and Khan, M. N., 2001, “Transient Hot-strip Method for Simultaneously Measuring Thermal Conductivity and Thermal Diffusivity of Solids and Fluids,” J. Phys. D: App. Phys., **12**(9), p. 1411.

[46] Gustafsson, S. E., Ahmed, K., Hamdani, A. J., and Maqsood, A., 1982, “Transient Hot-strip Method for Measuring Thermal Conductivity and Specific Heat of Solids and Fluids: Second Order Theory and Approximations for Short Times,” J. App. Phys., **53**(9), pp. 6064–6068.

[47] Log, T., and Metallinou, M. M., 1992, “Thermal Conductivity Measurements Using a Short Transient Hot-strip Method,” Rev. Sci. Instrum., **63**(8), pp. 3966–3971.

[48] Coquard, R., Baillis, D., and Quenard, D., 2008, “Experimental and Theoretical Study of the Hot-ring Method Applied to Low-density Thermal Insulators,” Int. J. Therm. Sci., **47**(3), pp. 324–338.

[49] Gustafsson, S. E., 1991, “Transient Plane Source Techniques for Thermal Conductivity and Thermal Diffusivity Measurements of Solid Materials,” Rev. Sci. Instrum., **62**(3), pp. 797–804.

[50] Cahill, D. G., and Pohl, R. O., 1987, “Thermal Conductivity of Amorphous Solids above the Plateau,” Phys. Rev. B, **35**(8), p. 4067.

[51] Heyd, R., Hadaoui, A., Fliyou, M., Koumina, A., Ameziane, L. E. H., Outzourhit, A., and Saboungi, M.-L., 2010, “Development of Absolute Hot-wire Anemometry by the 3-Omega Method,” Rev. Sci. Instrum., **81**(4), pp. 044901–044901.

[52] Chirtoc, M., Henry, J., Turgut, A., Sauter, C., Tavman, S., Tavman, I., and Pelzl, J., 2008, “Modulated Hot Wire Method for Thermophysical Characterization of Nanofluids,” Proceedings of the 5th European Thermal Sciences Conference, Eindhoven.

[53] Turgut, A., Sauter, C., Chirtoc, M., Henry, J., Tavman, S., Tavman, I., and Pelzl, J., 2008, “AC Hot Wire Measurement of Thermophysical Properties of Nanofluids with 3-Omega Method,” Eur. Phys. J.-Spec. Top., **153**(1), pp. 349–352.

[54] Lu, L., Yi, W., and Zhang, D., 2001, “3-Omega Method for Specific Heat and Thermal Conductivity Measurements,” Rev. Sci. Instrum., **72**(7), pp. 2996–3003.

[55] Chirtoc, M., Henry, J., Turgut, A., Tavman, I., Hadjov, K., Schuchmann, H., Sauter, C., Antoniow, J., Fudym, O., and Tavman, S., 2010, “Assessment of Modulated Hot Wire Method for Thermophysical Characterization of Fluid and Solid Matrices Charged with (nano) Particle Inclusions,” J. Phys.: Conf. Ser., **214**(1), p, 012135.

[56] ASTM Standard E 177, 04, "Standard Test method for Steady-State Heat Flux Measurements and Thermal Transmission Properties by Means of the Guarded-Hot-Plate Apparatus," ASTM International, West Conshohocken, PA, 2006, DOI: 10.1520/C0177-10, from www.astm.org.

[57] ASTM Standard E 1044, 07, "Standard Practice for Using a Guarded-Hot-Plate Apparatus or Thin-Heater Apparatus in the Single-Sided Mode," ASTM International, West Conshohocken, PA, 2006, DOI: 10.1520/C1044-07, from www.astm.org.

[58] ASTM Standard E 1043, 06, "Standard Practice for Guarded-Hot-Plate Design Using Circular Line-Heat Sources," ASTM International, West Conshohocken, PA, 2006, DOI: 10.1520/C1043-06R10, from www.astm.org.

[59] ASTM Standard E 1530, 06, "Standard Test Method for Evaluating the Resistance to Thermal Transmission of Materials by the Guarded Heat Flow Meter Technique," ASTM International, West Conshohocken, PA, 2006, DOI: 10.1520/E1530-11, from www.astm.org.

[60] ASTM Standard E 1225, 04, "Standard Test Method for Thermal Conductivity of Solids by Means of the Guarded-Comparative-Longitudinal Heat Flow Technique," ASTM International, West Conshohocken, PA, 2006, DOI: 10.1520/E1225-09, from www.astm.org.

[61] ASTM Standard D 6744, 06, "Standard Test Method for Determination of the Thermal Conductivity of Anode Carbons by the Guarded Heat Flow Meter Technique," ASTM International, West Conshohocken, PA, 2006, DOI: 10.1520/D6744-06R11E01, from www.astm.org.

[62] Stradomskiy, M., Maksimov, Y., Malyarov, V., and Plita, A., 1985, “Determination of the Thermophysical Properties of Materials by the Heat-wave Method,” Heat Transfer: Sov. Res., **17**(4), pp. 140–144.

[63] Czarnetzki, W., and Roetzel, W., 1995, “Temperature Oscillation Techniques for Simultaneous Measurement of Thermal Diffusivity and Conductivity,” Int. J. Thermophys., **16**(2), pp. 413–422.

[64] Jensen, C, "TRISO Fuel Thermal Conductivity Measurement Instrument Development," 2010, *All Graduate Theses and Dissertations.* Paper 838, from http://digitalcommons.usu.edu/etd/838

[65] Laubitz, M., and McElroy, D., 2005, “Precise Measurement of Thermal Conductivity at High Temperatures (100-1200 K),” Metrologia, **7**(1), p. 1.

[66] Powell, R., 2002, “A Realistic Approach to Laboratory Thermal Conductivity Experiments with Solids,” Physics Educ., **4**(4), p. 199.

[67] Wang, Y., Sun, L., Yi, S., Huang, Y., Lenaghan, S. C., and Zhang, M., 2012, “Naturally Occurring Nanoparticles from Arthrobotrys Oligospora as a Potential Immunostimulatory and Antitumor Agent,” Adv. Funct. Mater., **23**(17), pp. 2175–2184.

[68] Puntes V., and Cavalle J. S., 2013 *Nanoparticles Before Nanotechnology*, Nanowiki, Epublication.

[69] Poole, Jr, C. P., and Owens, F. J., 2003, *Introduction to Nanotechnology*, Wiley-Interscience, New York,

[70] Kreuter, J., 2007, “Nanoparticles—a Historical Perspective,” Int. J. Pharm., **331**(1), pp. 1–10.

[71] Faraday, M., 1857, “The Bakerian Lecture: Experimental Relations of Gold (and Other Metals) to Light,” Philos. Trans. R. Soc. Lond., **147**, pp. 145–181.

[72] Pradhan, N. R., 2010, “Thermal Conductivity of Nanowires, Nanotubes and Polymer-Nanotube Composites,” M.S. thesis, Physics, Worcester Polytechnic Institute.

[73] Han, Z., and Fina, A., 2011, “Thermal Conductivity of Carbon Nanotubes and Their Polymer Nanocomposites: a Review,” Prog. Polym. Sci., **36**(7), pp. 914–944.

[74] Kim, P., Shi, L., Majumdar, A., and McEuen, P., 2001, “Thermal Transport Measurements of Individual Multiwalled Nanotubes,” Phyas. Rev. Lett., **87**(21), p. 215502.

[75] Hone, J., 2004, “Carbon Nanotubes: Thermal Properties,” Dekker Encyclopedia of Nanoscience and Nanotechnology, pp. 603–610.

[76] Maruyama, H., Tomita, K., Kariya, R., and Arai, F., 2011, “Evaluation Method of Thermal Conductivity of Single Carbon Nanotube in Liquid Using Quantum Dot Hydrogel Sensor,” Nanotechnology (IEEE-NANO) Conf., 2011, pp. 1755–1758.

[77] Behabtu, N., Young, C. C., Tsentalovich, D. E., Kleinerman, O., Wang, X., Ma, A. W., Bengio, E. A., ter Waarbeek, R. F., de Jong, J. J., Hoogerwerf, R. E., and others, 2013, “Strong, Light, Multifunctional Fibers of Carbon Nanotubes with Ultrahigh Conductivity,” Sci., **339**(6116), pp. 182–186.

[78] Choi, T.-Y., Poulikakos, D., Tharian, J., and Sennhauser, U., 2006, “Measurement of the Thermal Conductivity of Individual Carbon Nanotubes by the Four-point 3-Omega Method,” Nano. Lett., **6**(8), pp. 1589–1593.

[79] Choi, T. Y., Poulikakos, D., Tharian, J., and Sennhauser, U., 2005, “Measurement of Thermal Conductivity of Individual Multiwalled Carbon Nanotubes by the 3-Omega Method,” Appl. Phys. Lett., **87**(1), pp. 013108–013108.

[80] Fujii, M., Zhang, X., Xie, H., Ago, H., Takahashi, K., Ikuta, T., Abe, H., and Shimizu, T., 2005, “Measuring the Thermal Conductivity of a Single Carbon Nanotube,” Phys. Rev. Lett., **95**(6), p. 65502.

[81] Wang, X., Choi, S. U., Xu, X., and Wang, X., 2012, “Thermal Conductivity of Nanoparticle-fluid Mixture,” J. Thermophys. Heat Transfer, **13**(4), pp. 478–480.

[82] Walvekar, R., Faris, I. A., and Khalid, M., 2012, “Thermal Conductivity of Carbon Nanotube nanofluid—Experimental and Theoretical Study,” Heat Transfer—Asian Res., pp. 145–163.

[83] Choi, S., Zhang, Z., Yu, W., Lockwood, F., and Grulke, E., 2001, “Anomalous Thermal Conductivity Enhancement in Nanotube Suspensions,” Appl. Phys. Lett., **79**(14), pp. 2252–2254.

[84] Ebrahimi, S., Sabbaghzadeh, J., Lajvardi, M., and Hadi, I., 2007, “Nanolayer Effects in Thermal Conductivity of Nanofluids Containing Cylindrical Nanoparticles,” Nanotechnology (IEEE-NANO), 2007, Conf., pp. 1195–1198.

[85] Townsend, J. Kenvarg, A. Swartz, E. and Christianson, R., 2010, “The Applicability and Accuracy of Thermal Conductivity Measurement Techniques for the Characterization of Nanofluids,”Presented 2009. Paper in consideration. International J. Thermophysics.

[86] Buongiorno, J., Venerus, D. C., Prabhat, N., McKrell, T., Townsend, J., Christianson, R., Tolmachev, Y. V., Keblinski, P., Hu, L., Alvarado, J. L., and others, 2009, “A Benchmark Study on the Thermal Conductivity of Nanofluids,” J. Appl. Phys., **106**(9), pp. 094312–094312.

[87] Maxwell, J. C., 1881, *A Treatise on Electricity and Magnetism*, Clarendon Press, Oxford, England.

[88] Nan, C.-W., Birringer, R., Clarke, D. R., and Gleiter, H., 1997, “Effective Thermal Conductivity of Particulate Composites with Interfacial Thermal Resistance,” J. Appl. Phys., **81**(10), pp. 6692–6699.

[89] Eastman, J., Choi, S., Li, S., Yu, W., and Thompson, L., 2001, “Anomalously Increased Effective Thermal Conductivities of Ethylene Glycol-based Nanofluids Containing Copper Nanoparticles,” Appl. Phys. Lett., **78**(6), pp. 718–720.

[90] Murshed, S., Leong, K., and Yang, C., 2005, "Enhanced Thermal Conductivity of TiO_2—water Based Nanofluids," Int. J. Thermal Sciences, **44**(4), pp. 367–373

[91] Murshed, S., Leong, K., and Yang, C., 2008, "Investigations of Thermal Conductivity and Viscosity of Nanofluids," Int. J. Therm. Sci., **47**(5), pp. 560–568.

[92] Hong, T.-K., Yang, H.-S., and Choi, C., 2005, "Study of the Enhanced Thermal Conductivity of Fe Nanofluids," J. Appl. Phys., **97**(6), pp. 064311–064311.

[93] Hong, K., Hong, T.-K., and Yang, H.-S., 2006, "Thermal Conductivity of Fe Nanofluids Depending on the Cluster Size of Nanoparticles," Appl. Phys. Lett., **88**(3), pp. 031901–031901.

[94] Shaikh, S., Lafdi, K., and Ponnappan, R., 2007, "Thermal Conductivity Improvement in Carbon Nanoparticle Doped PAO Oil: An Experimental Study," J. Appl. Phys., **101**(6), pp. 064302–064302.

[95] Kleinstreuer, C., and Feng, Y., 2011, "Experimental and Theoretical Studies of Nanofluid Thermal Conductivity Enhancement: A Review," Nanoscale Res. Lett., **6**(1), pp. 1–13.

[96] Xie, H., Wang, J., Xi, T., Liu, Y., Ai, F., and Wu, Q., 2002, "Thermal Conductivity Enhancement of Suspensions Containing Nanosized Alumina Particles," J. Appl. Phys., **91**(7), pp. 4568–4572.

[97] Patel, H. E., Das, S. K., Sundararajan, T., Sreekumaran Nair, A., George, B., and Pradeep, T., 2003, "Thermal Conductivities of Naked and Monolayer Protected Metal Nanoparticle Based Nanofluids: Manifestation of Anomalous Enhancement and Chemical Effects," Appl. Phys. Lett., **83**(14), pp. 2931–2933.

[98] Assael, M., Metaxa, I., Arvanitidis, J., Christofilos, D., and Lioutas, C., 2005, "Thermal Conductivity Enhancement in Aqueous Suspensions of Carbon Multi-walled and Double-walled Nanotubes in the Presence of Two Different Dispersants," Int. J. Thermophys., **26**(3), pp. 647–664.

[99] Buongiorno, J., 2006, "Convective Transport in Nanofluids," J. Heat Transfer, **128**, p. 240.

[100] Khanafer, K., Vafai, K., and Lightstone, M., 2003, "Buoyancy-driven Heat Transfer Enhancement in a Two-dimensional Enclosure Utilizing Nanofluids," Int. J. Heat Mass Transfer, **46**(19), pp. 3639–3653.

[101] Ma, K.-Q., and Liu, J., 2007, "Nano Liquid-metal Fluid as Ultimate Coolant," Phys. Lett. A, **361**(3), pp. 252–256.

[102] Miner, A., and Ghoshal, U., 2004, "Cooling of High-power-density Microdevices Using Liquid Metal Coolants," Appl. Phys. Lett., **85**(3), pp. 506–508.

[103] Bleazard, J. G., and Teja, A. S., 1995, "Thermal Conductivity of Electrically Conducting Liquids by the Transient Hot-wire Method," J. Chem. Eng. Data, **40**(4), pp. 732–737.

[104] Wikipedia The Free Encyclopedia, 2013, “Cryogenics,” from http://en.wikipedia.org/wiki/Cryogenics.

[105] National Institute of Standards and Testing, 2013, “Thermophysical Properties of Fluid Systems,” from http://webbook.nist.gov/chemistry/fluid/.

[106] Scurlock R. G., 2008, “History of Cryogenics,” from http://www.cryogenicsociety.org/resources/cryo_central/history_of_cryogenics/

[107] Hall, L. A., 1963, “Thermal Conductivity of Ten Cryogenic Liquids-a Bibliography,” National Bur. Stand., Bolulder, Colorado.

[108] Laesecke, A., Krauss, R., Stephan, K., and Wagner, W., 1990, “Transport Properties of Fluid Oxygen,” J. Phys. Chem. Ref., **19**(5), pp. 1089–1274 .

[109] Younglove, B. A., 1982, “Thermophysical Properties of Fluids. I. Argon, Ethylene, Parahydrogen, Nitrogen, Nitrogen Trifluoride, and Oxygen,”National Stand. Ref. Data System.

[110] Richards, R. J., Steward, W., and Jacobs, R., 1961, “A Survey of the Literature on Heat Transfer from Solid Surfaces to Cryogenic Fluids,” DTIC Doc.

[111] Giauque, W., and Johnston, H., 1929, “The Heat Capacity of Oxygen from 12 K. to Its Boiling Point and Its Heat of Vaporization. The Entropy from Spectroscopic Data,” J. Am. Chem. Soc., **51**(8), pp. 2300–2321.

[112] Celik, D., and Van Sciver, S., 2005, “Thermal Conductivity of Subcooled Liquid Oxygen,” Cryogenics, **45**(9), pp. 620–625.

[113] Ziebland, H., and Burton, J., 2002, “The Thermal Conductivity of Liquid and Gaseous Oxygen,” Br. J. Appl. Phys., **6**(12), p. 416.

[114] Jacobsen, R. T., Stewart, R. B., and Jahangiri, M., 1986, “Thermodynamic Properties of Nitrogen from the Freezing Line to 2000 K at Pressures to 1000 MPa,” J. Phys. Chem. Ref. Data, **15**, p. 735.

[115] Span, R., Lemmon, E., Jacobsen, R., and Wagner, W., 1998, “A Reference Quality Equation of State for Nitrogen,” Int. J. Thermophys., **19**(4), pp. 1121–1132.

[116] Polupan, A., 2004, “Boiling Crisis in Oxygen-Nitrogen Mixtures,” Chem. Pet. Eng., **40**(7), pp. 394–400.

[117] Brentari, E., Giarratano, P., and Smith, R. V., 1965, *Boiling Heat Transfer for Oxygen, Nitrogen, Hydrogen, and Helium*, US National Bureau of Standards: For Sale by the Supt. of Docs., US Govt. Print. Off., **317**. Gaithersburg, Maryland.

[118] Wang, P., 2008, “Thermal Bubble Behaviour in Liquid Nitrogen Under Electric Fields,” IEEE Trans. Dielectr. Electr Insul., **15**(3), pp. 626–634.

[119] Yuan, K., 2006, “Cryogenic Boiling and Two-phase Chilldown Process Under Terrestrial and Microgravity Conditions,”Ph. D. thesis, Mechanical and Aerospace Engineering, University of Florida.

[120] Kosky, P., and Lyon, D., 1968, “Pool Boiling Heat Transfer to Cryogenic Liquids; I. Nucleate Regime Data and a Test of Some Nucleate Boiling Correlations,” AIChE J., **14**(3), pp. 372–379.

[121] Ekin, J., 2006, *Experimental Techniques for Low-temperature Measurements: Cryostat Design, Material Properties and Superconductor Critical-Current Testing*, Oxford University Press, Oxford, England.

[122] Cahill, D. G., 1990, “Thermal Conductivity Measurement from 30 to 750 K: The 3 Omega Method,” Rev. Sci. Instrum., **61**(2), pp. 802–808.

[123] Ziebland, H., and Burton, J., 2002, “The Thermal Conductivity of Liquid and Gaseous Oxygen,” Br. J. Appl. Phys., **6**(12), p. 416.

[124] Carslaw, H. S., Jaeger, J. C., 1959 *Conduction of Heat in Solids*, 2nd Ed., Oxford University Press, Oxford, England.

[125] Jiji, L. M., 2009 *Heat Conduction*, 3rd Ed., Scientific Publishing Services, Chennai, India.

[126] Kakac S., Yener, Y., 1993 *Heat Conduction*, 3rd Ed., CRC Press, Tyler and Francis Group, Boca Raton, FL.

[127] Vadasz, P., 2010, “Rendering the Transient Hot Wire Experimental Method for Thermal Conductivity Estimation to Two-Phase Systems—Theoretical Leading Order Results,” J. Heat Transfer, **132**, p. 081601.

[128] Kluitenberg, G., Ham, J., and Bristow, y K., 1993, “Error Analysis of the Heat Pulse Method for Measuring Soil Volumetric Heat Capacity,” Soil Sci. Soc. Am. J., **57**(6), pp. 1444–1451.

[129] Zeng, H., Diao, N., and Fang, Z., 2002, “A Finite Line-source Model for Boreholes in Geothermal Heat Exchangers,” Heat Transfer—Asian Res., **31**(7), pp. 558–567.

[130] Bandos, T. V., Montero, Á., Fernández, E., Santander, J. L. G., Isidro, J. M., Pérez, J., Córdoba, P. J., and Urchuegu’\ia, J. F., 2009, “Finite Line-source Model for Borehole Heat Exchangers: Effect of Vertical Temperature Variations,” Geothermics, **38**(2), pp. 263–270.

[131] Wikipedia The Free Encyclopedia, “Cryogenics,” from http://en.wikipedia.org/wiki/Cryogenics.

[132] Measurement Computing, “USB 1608FS,” from http://www.mccdaq.com/usb-data-acquisition/USB-1608FS.aspx.

[133] Automatic Components, Inc., “Temperature Sensing and Transmitting,” from http://workaci.com/pdf/technotes/temp_technical_notes.pdf.

[134] Honeywell Sensors, “Platinum RTD Resistances vs. Temperature Function,” from http://www.honeywell-sensor.com.cn/prodinfo/sensor_temperature/technical/c15_136.pdf.

[135] PRelectronics, “The Callendar – Van Dusen Coefficients,” from http://www.prelectronics.dk/filer/CvD_UK.pdf.

[136] National Physics Laboratory, “What is a Platinum Resistance Thermometer?,” from http://www.npl.co.uk/reference/faqs/what-is-a-platinum-resistance-thermometer-(faq-thermal).

[137] PGM Database, “Platinum,” from http://www.pgmdatabase.com/jmpgm/index.jsp.

[138] Berry, R., 1963, “Relationship Between the Real and Ideal Resistivity of Platinum,” Can. J. Phys., **41**(6), pp. 946–982.

[139] Richards, R. J., Steward, W., and Jacobs, R., 1961, “A Survey of the Literature on Heat Transfer from Solid Surfaces to Cryogenic Fluids,” DTIC Doc., Ft. Belvoir, Virginia.

[140] Wang, P., 2008, “Thermal Bubble Behaviour in Liquid Nitrogen Under Electric Fields,” Ph.D. thesis, School of Electronics and Computer Science, University of Southhampton.

[142] Qsonica,“How Does a Sonicator Work,” from http://www.sonicator.com/pdf/Howdoesitwork.pdf.

[143] Dukhin, A., and Goetz, P., 2005, “Ionic Properties of So-called ‘non-ionic’ Surfactants in Non-polar Liquids,” Dispersion Technology Inc, Bedford Hills, New York, **15**, pp. 151–157.

[144] Nielsen, L. E., 1978, *Predicting the Properties of Mixtures*, Mixture Rules in Science and Engineering, Marcel Dekker, New York.

[145] Nan, C. W., 1993, “Physics of inhomogeneous inorganic materials,” Prog, Mater, Sci., **37**, pp. 1-116.

[146] Rayleigh, L., 1892, “On the Influence of Obstacles Arranged in Rectangular Order Upon the Properties of a Medium,” Philo. Mag., **34**, pp. 481-502.

[147] Meredith, R. E., and C. W. Tobias, 1960, “Resistance to Potential Flow Through a Cubical Array of Spheres,” J. Appl. Phys., **31**, pp. 1270-1273.

[148] Jeffrey, D. J., 1973, “Conduction Through a Random Suspension of Spheres,” Proc. R. Soc., London A, **335**, pp. 355-367.

[149] Davis, R. H., 1986, "The Effective Thermal Conductivity of a Composite Material with Spherical Inclusions," Int. J. Thermophys., **7**, pp. 609-620.

[150] Cheng, S. C., and Vachon, R. I., 1969, "The Predictions of the Thermal Conductivity of Two and Three Phase Solid Heterogeneous Mixtures," Int. J. Heat Mass Transfer, **12**, pp. 249-264.

[151] Tsao, G. T. N., 1961, "Thermal Conductivity of Two-Phase Materials," Ind. Eng. Chem., **53**, pp. 395-397.

[152] Yu, W., and Choi, S. U. S., 2005, "An Effective Thermal Conductivity Model of Nanofluids with a Cubic Arrangement of Spherical Particles," J. Nanosci. Nanotechnol., **5**, pp. 580-586.

[153] Nan, C. W., Shi, Z., and Lin, Y., 2003, "A Simple Model for Thermal Conductivty of Carbon Nanotube-Based Compsoites," Chem. Phys. Lett., **375**, pp. 666-669

[154] Fricke, H., 1924, "A Mathematical Treatment of the Electric Conductivity and Capacity of Disperse Systems: I. The Electric Conductivity of a Suspension of Homogeneous Spheroids," Phsy. Rev., **24**, pp. 575-587.

[155] Fricke, H., 1959, "The Maxwell-Wagner Dispersion in a Suspension of Ellipsoids," J. Phys. Chem., **57**, pp. 934-937.

[156] Wang, X., Xu, X., and Choi, S. U. S., 1999, "Thermal Conductivity of Nanoparticle-Fluid Mixture," J. Thermophys. Heat Trasnfer, **13**(4), pp. 474-480.

[157] Xuan, Y., and Li, Q., 2000, "Heat Transfer Enhancement of nano-Fluids," Int. J. Heat Fluid Flow, **21**, pp. 58-64.

[158] Keblinski, P., and Cahill, D. G., 2005, "Comment on Model for Heat Conduction in Nanofluids," Phys. Rev. lett., **95**(20), p. 209401.

[159] Das, S. K., Putra, N., Thiesen, P., and Roetzel W., 2003, "Temperature Dependence of Thermal conductivity enhancement for nanofluids," J. Heat Transfer, **125**, pp. 567-574.

[160] Patel, H. E., Das, S. K., Sundararajan, T., Sreekumaran, N. A., George, B., and Pradeep, T., 2003, "Thermal Conductivity of Naked and Monolayer Protected Metal nanoparticle Based Nanofluids: Manifestation of Anomalous Enhancement and Chemical Effects," Appl. Phys. Lett., **83**(14), pp. 2931-2933.

[161] Xuan, Y., Li, Q., and Hu, W., 2003, "Aggregation Structure and Thermal Cnoductivity of Nanfluids," AIChE J., **49**(4), pp. 1038-1043.

[162] Yu, W., and Choi, S. U. S., 2003, The Role of Interfacial Layers in the Enhanced Thermal Conductivity of Nanofluids: A Renovated Maxwell Model," J. Nanopart. Res., **5**, pp. 167-171.

[163] Jang, S. P., and Choi, S. U. S., " 2004, "Role of Brownian Motion in the Enhanced Thermal Conductivity of Nanofluids," Appl. Phys. Lett., **84**(21):, pp. 4316-4318.

[164] Kumar, D. H., Patel, H. E., Kumar, V. R. R., Sundararajan T., Pradeep, T., and Das, S. K., 2004, "Model for Heat Conduction in Nanofluids," Phys. Rev. Lett., **93**(14), p. 144301.

[165] Koo, J., and Kleinstreuer C., 2004, "A New Thermal Conductivity Model for Nanofluids," J. Nanopart. Res., **6**(6), pp. 577-588.

[166] Koo, J., and Kleinstreuer C., 2005, "Impact Analysis of Nanoparticle Motion Mechanisms on the Thermal Conductivity of Nanofluids," Int. Commun. Heat Mass Trasnfer, **32**(9), pp. 1111-1118.

[167] Prasher, R., Bhattacharya, P., and Phelan, P. E., 2005, "Thermal Conductivity of Nanoscale Colloidal Solutions (nanofluids)," Phys. Rev. Lett., **94**(2), p. 025901.

[168] Prasher, R., Bhattacharya, P., and Phelan, P. E., 2006, "Brownian-Motion-Based Convective-Conductive Model for the Effective Thermal Conductivity of Nanofluids," J. Heat Transfer, **128**, pp. 588-595.

[169] Ren, Y., Xie, H., and Cai, A., 2005, "Effective Thermal Conductivity of nanofluids Containing Spherical Nanoparticles," J. Phys. D Appl. Phys., **38**: 3958-3961.

[170] Patel, H. E., Sundararajan, T., Pradeep, T., Dasgupta, A., Dasgupta, N., and Das, S.k., 2005, "A Micro-Convection Model for Thermal Conductivity of Nanofluids," Pramana J. Phys., **65**, pp. 863-869:

[171] Chon, C. H., Kihm, K. D., Lee, S. P., and Choi, S. U. S., 2005, "Empirical Correlation Finding the Role of Temperaure and Particle Size for Nanofluid (Al^2O^3) Thermal Conductivity Enhancement," Appl. Phys. Lett., **87**(15), p. 153107.

[172] Xue, Q. Z., 2006, "Model for the Effective Thermal Conductivity of carbon Nanotubes Composites," Nanotechnol., **17**, pp. 1655-1660.

[173] Wang, B.-X., Zhou, L.-P., and Peng, X.-F., 2003, "A Fractal Model for Predicting the Effective Thermal Conductivity of Liquid with Suspension of Nanoparticles," International J. Heat and Mass Transfer, **46**(14), pp. 2665–2672.

[174] Evans, W., Fish, J., and Keblinski, P., 2006, "Role of Brownian Motion Hydrodynamics on Nanofluid Thermal Conductivity," Appl. Phys. Lett., **88**(9), pp. 093116–093116.

[175] Prasher, R., Phelan, P. E., and Bhattacharya, P., 2006, "Effect of Aggregation Kinetics on the Thermal Conductivity of Nanoscale Colloidal Solutions (nanofluid)," Nano Lett., **6**(7), pp. 1529–1534.

[176] Domingues, G., Volz, S., Joulain, K., and Greffet, J.-J., 2005, "Heat Transfer Between Two Nanoparticles Through Near Field Interaction," Phys. Rev. Lett., **94**(8), p. 85901.

[177] TDK-Lambda Corporation,“ZUP Series,” from http://www.tdk-lambda.com/products/sps/catalog/eng/zup.pdf.

[178] Newark, “Stop the Noise: The Importance of Being (Properly) Shielded,” from http://www.newark.com/pdfs/techarticles/Stop_the_Noise_The_Importance_of_Being_Properly_Shielded_FINAL_2-20-07.pdf.

[179] Tyco Electronics Division, “DC Shunts,” from http://www.cromptonusa.com/DC%20Shunts%20Theory.pdf.

[180] Coleman H. W., and Steele, W. G., 2008 *Experimentation, Validation, and Uncertainty Analysis for Engineers,* 3rd Ed., John Wiley & Sons, Hoboken, NJ.

[181] Nanostructured & Amorphous Materials, Inc., “Short MWNT (95+%, OD 8-15 nm),” from http://www.nanoamor.com/inc/pdetail?v=1&pid=4017.

[182] Nanostructured & Amorphous Materials, Inc., “Regular MWNT (95+%, OD 8-15 nm),” from http://www.nanoamor.com/inc/pdetail?v=1&pid=1846.

[183] Call, R. W., 2011, “Carbon Nanotube Growth Via Spray Pyrolysis,”.Dept. Honors, Dept. Phys., Utah State University.

[184] Call, R. W., 2012, “The Effect of Growth Parameters on the Height and Density of Carbon Nanotube Forests,”.M.S. thesis, Dept. Phsy., Utah State Unversity.

APPENDICES

APPENDIX A: INTERMEDIATE CRYOGENIC NANOFLUID RESULTS

A.1. Introduction

The following figures will detail the intermediate cryogenic nanofluid results. The effective thermal conductivity values will be compared to their base LOX values as each varies by test number (i.e. testing time). The total average values will also be included, along with figures depicting the effective thermal conductivity increase in percentage, along with the total average percentage increase for each test. The intermediate results will be presented for each CN for each complete test run. Base LOX calibration results will be detailed first, followed by the results for each nanoparticle volume concentration value. At the end of each subsection, figures depicting that cryogenic nanofluids data scatter will be presented in terms of both the effective thermal conductivity value, and the overall percentage change.

A.2 Intermediate Results for Dr. T. C. Shen's MWCNT based CN Test Run #1

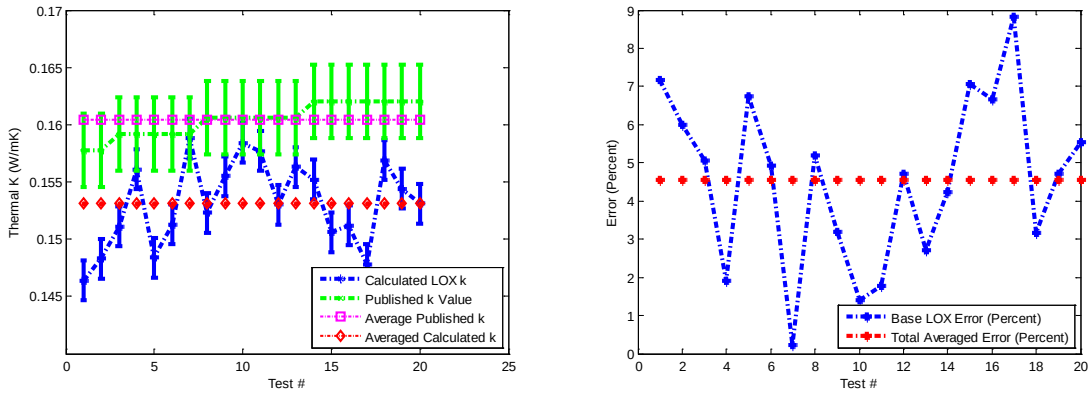

Figure A-1.Base LOX calibration for Dr. T. C. Shen MWCNT based cryogenic nanofluid. Test day #1 (3/16/12). Effective thermal conductivity vs. reported LOX values along with test value error in percent.

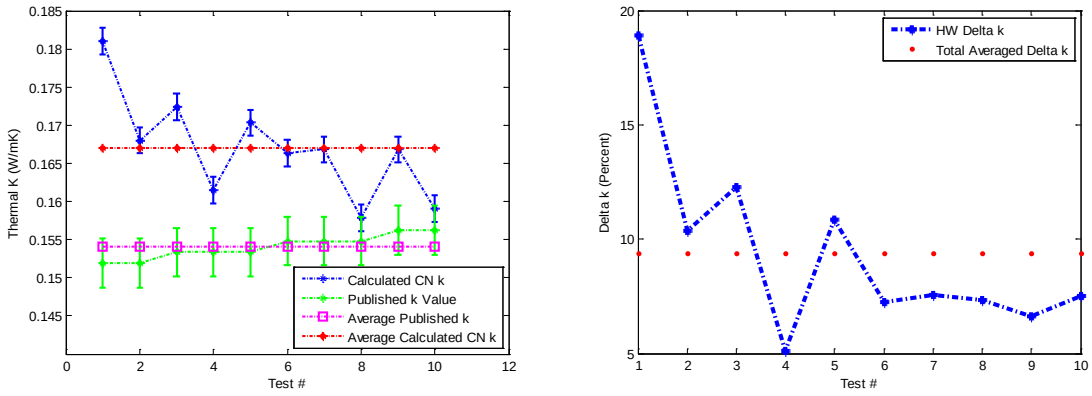

Figure A-2. Effective thermal conductivity vs. base lox values including conductivity increase in percent for Dr. T. C. Shen's MWCNT based cryogenic nanofluid. Test day #1 (3/16/12) for a particle concentration of 0.01 gm (0.000952% by volume concentration).

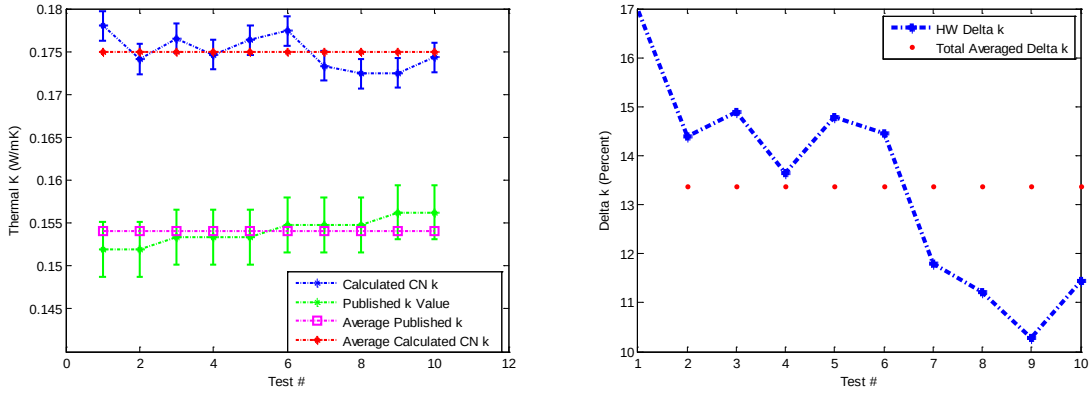

Figure A-3. Effective thermal conductivity vs. base lox values including conductivity increase in percent for Dr. T. C. Shen's MWCNT based cryogenic nanofluid. Test day #1 (3/16/12) for a particle concentration of 0.023 gm (0.00219% by volume concentration).

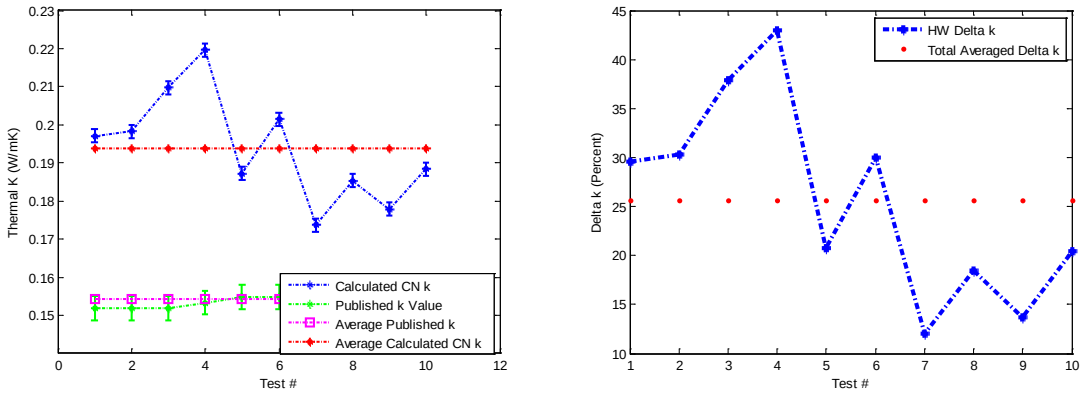

Figure A-4. Effective thermal conductivity vs. base lox values including conductivity increase in percent for Dr. T. C. Shen's MWCNT based cryogenic nanofluid. Test day #1 (3/16/12) for a particle concentration of 0.115 gm (0.01095% by volume concentration).

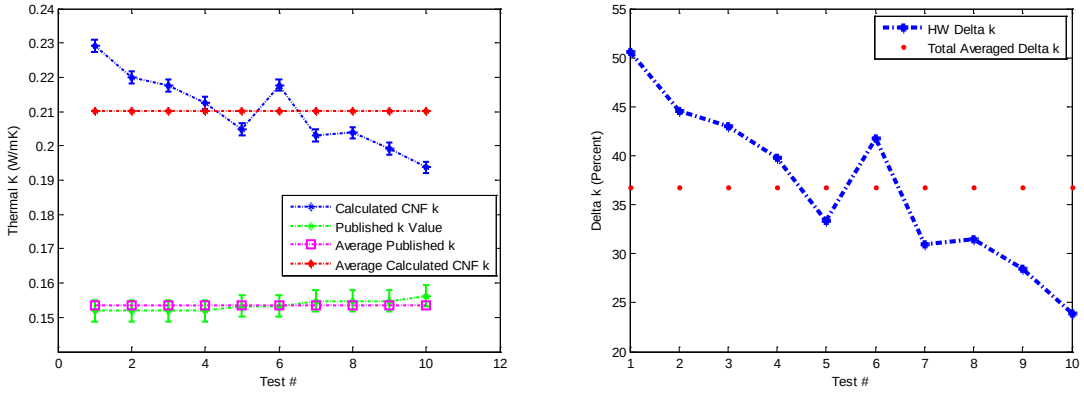

Figure A-5. Effective thermal conductivity vs. base lox values including conductivity increase in percent for Dr. T. C. Shen's MWCNT based cryogenic nanofluid. Test day #1 (3/16/12) for a particle concentration of 0.230 gm (0.0219% by volume concentration).

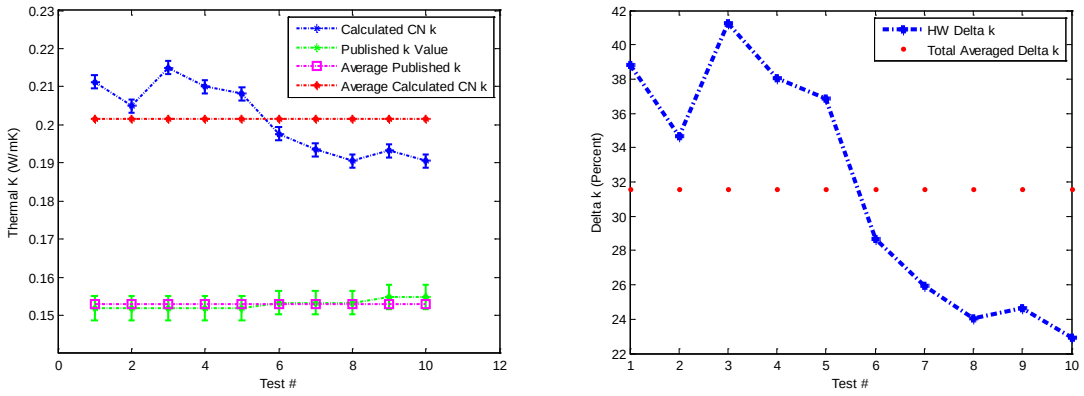

Figure 12-6. Effective thermal conductivity vs. base lox values including conductivity increase in percent for Dr. T. C. Shen's MWCNT based cryogenic nanofluid. Test day #1 (3/16/12) for a particle concentration of 0.335 gm (0.0319% by volume concentration).

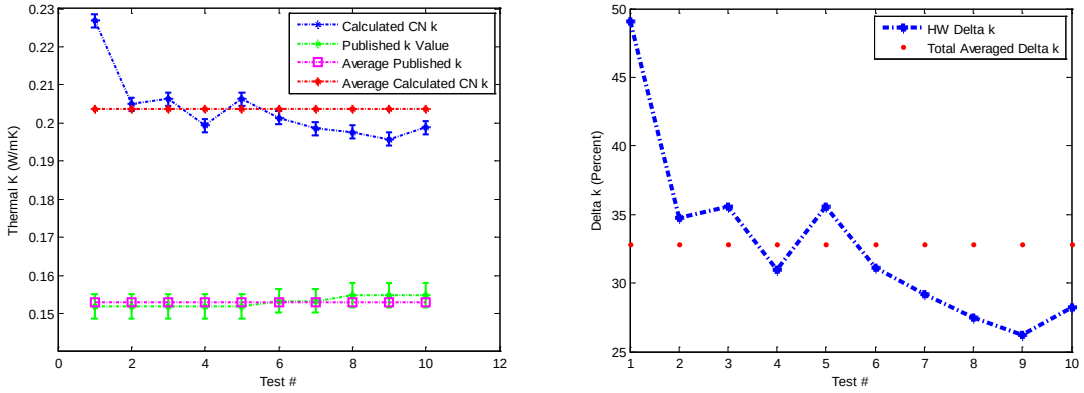

Figure 12-7. Effective thermal conductivity vs. base lox values including conductivity increase in percent for Dr. T. C. Shen's MWCNT based cryogenic nanofluid. Test day #1 (3/16/12) for a particle concentration of 0.469 gm (0.0447% by volume concentration).

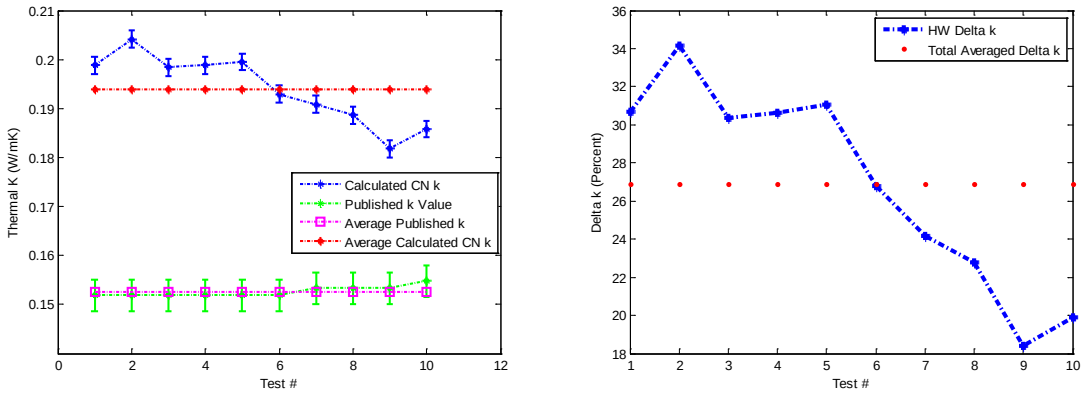

Figure A-8. Effective thermal conductivity vs. base lox values including conductivity increase in percent for Dr. T. C. Shen's MWCNT based cryogenic nanofluid. Test day #1 (3/16/12) for a particle concentration of 0.670 gm (0.0638% by volume concentration).

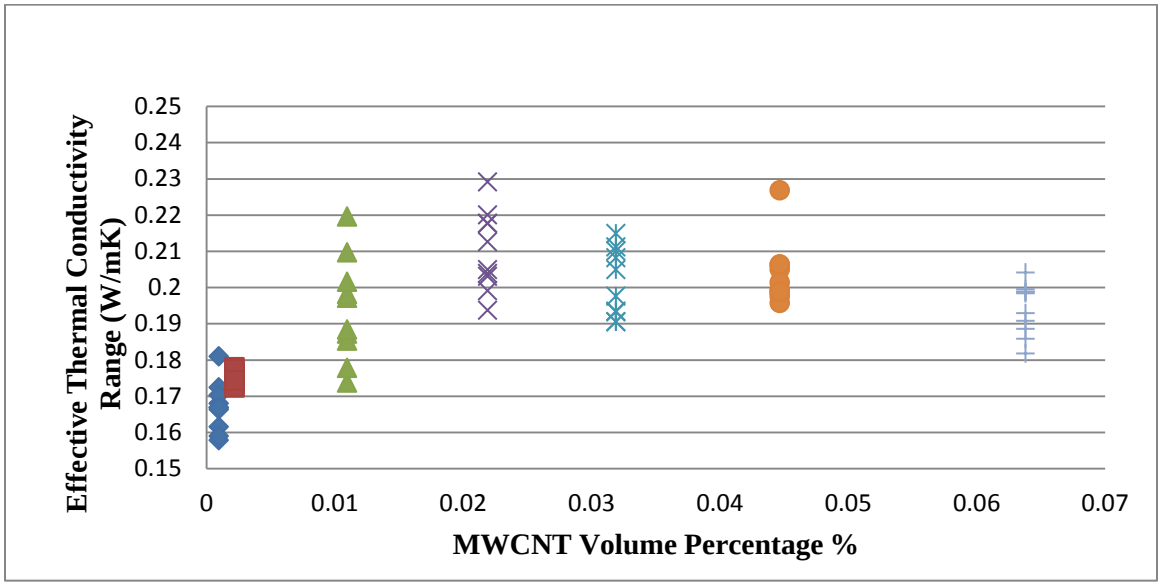

Figure A-9. Effective thermal conductivity data range for Dr. T. C. Shen's MWCNT based cryogenic nanofluids. Test day # 1 (3/16/12)

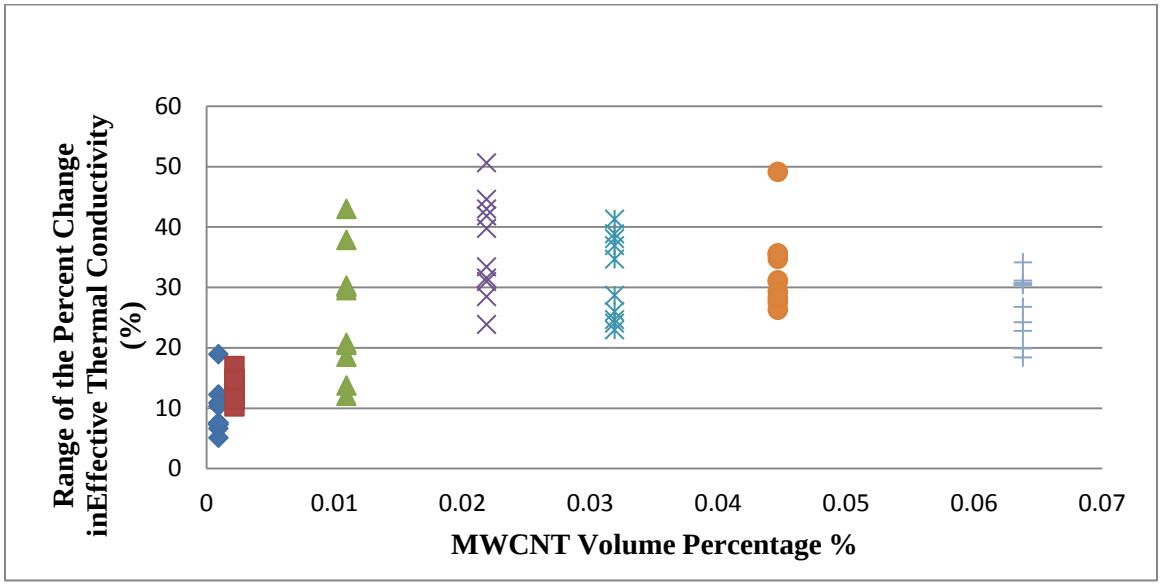

Figure A-10. Effective thermal conductivity (percent change) data range for Dr. T. C. Shen's MWCNT based cryogenic nanofluids. Test day # 1 (3/16/12)

A.3 Intermediate Results for Dr. T. C. Shen's MWCNT based CN Test Run #2

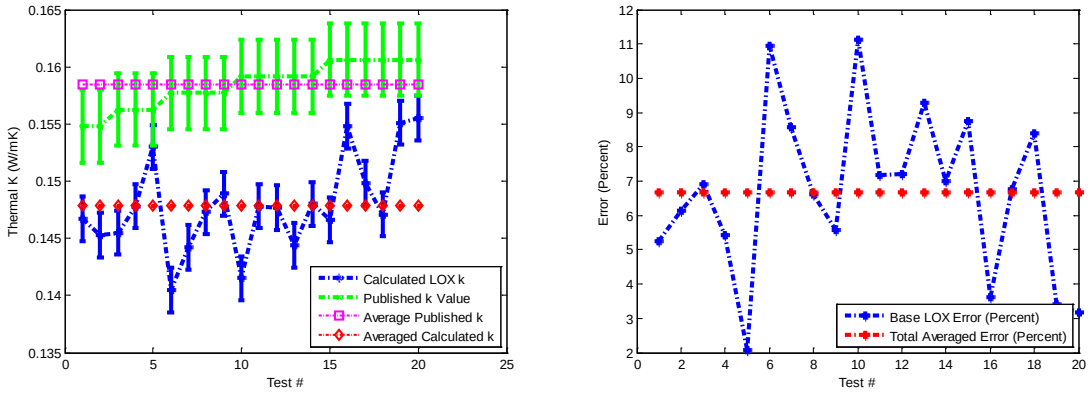

Figure A-11. Base LOX calibration for Dr. T. C. Shen MWCNT based cryogenic nanofluid. Test day #2 (3/26/12). Effective thermal conductivity vs. reported LOX values along with test value error in percent.

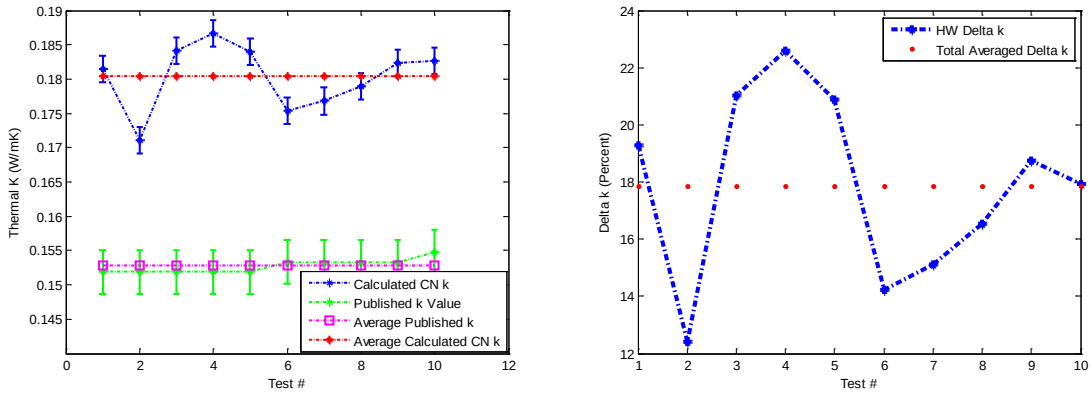

Figure A-12. Effective thermal conductivity vs. base lox values including conductivity increase in percent for Dr. T. C. Shen's MWCNT based cryogenic nanofluid. Test day #2 (3/26/12) for a particle concentration of 0.01 gm (0.000952% by volume concentration).

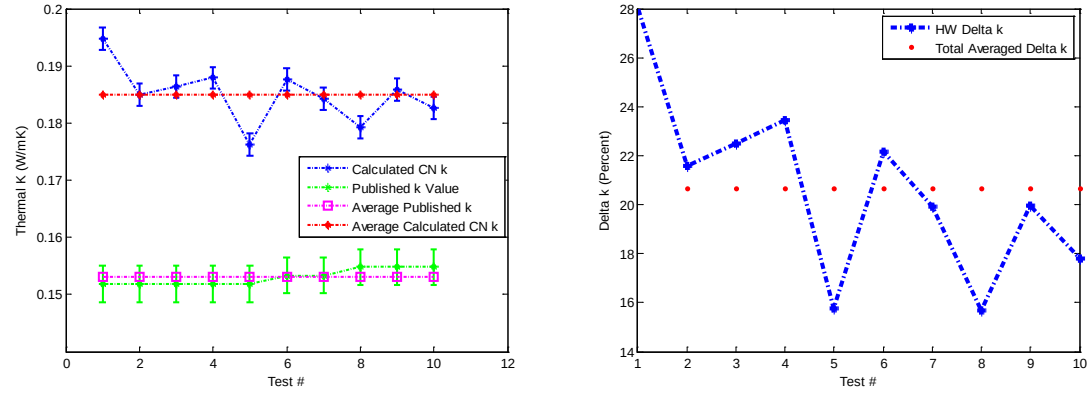

Figure A-13. Effective thermal conductivity vs. base lox values including conductivity increase in percent for Dr. T. C. Shen's MWCNT based cryogenic nanofluid. Test day #2 (3/26/12) for a particle concentration of 0.023 gm (0.00219% by volume concentration).

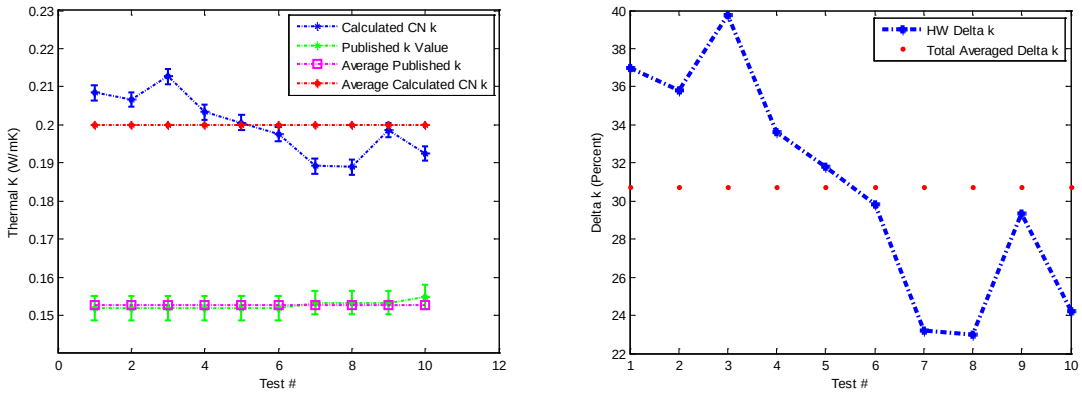

Figure A-14. Effective thermal conductivity vs. base lox values including conductivity increase in percent for Dr. T. C. Shen's MWCNT based cryogenic nanofluid. Test day #2 (3/26/12) for a particle concentration of 0.115 gm (0.01095% by volume concentration).

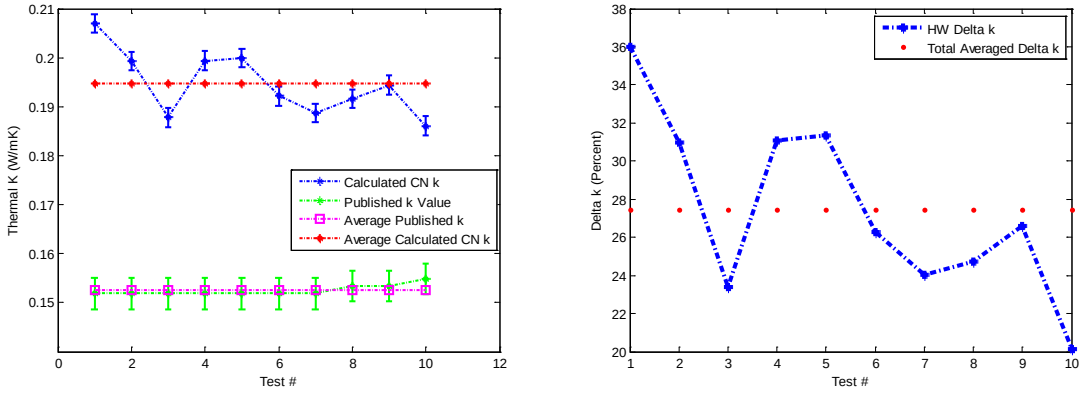

Figure A-15. Effective thermal conductivity vs. base lox values including conductivity increase in percent for Dr. T. C. Shen's MWCNT based cryogenic nanofluid. Test day #2 (3/26/12) for a particle concentration of 0.230 gm (0.0219% by volume concentration).

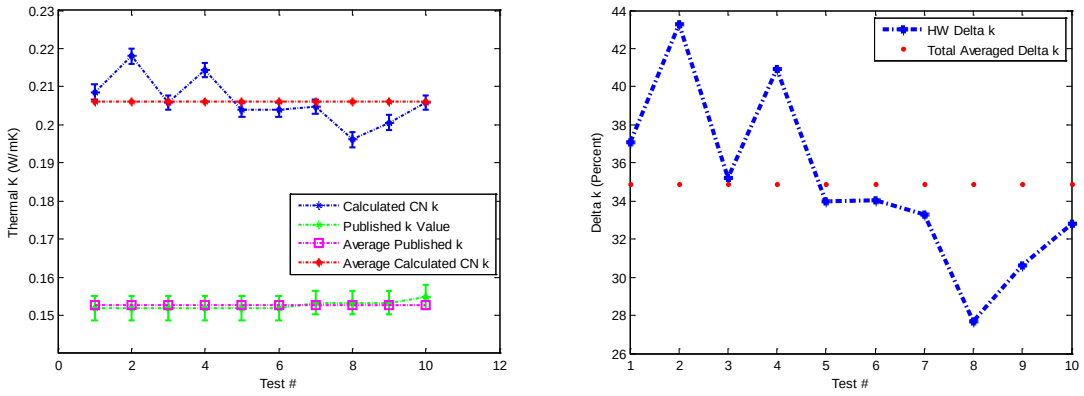

Figure A-16. Effective thermal conductivity vs. base lox values including conductivity increase in percent for Dr. T. C. Shen's MWCNT based cryogenic nanofluid. Test day #2 (3/26/12) for a particle concentration of 0.469 gm (0.0447% by volume concentration).

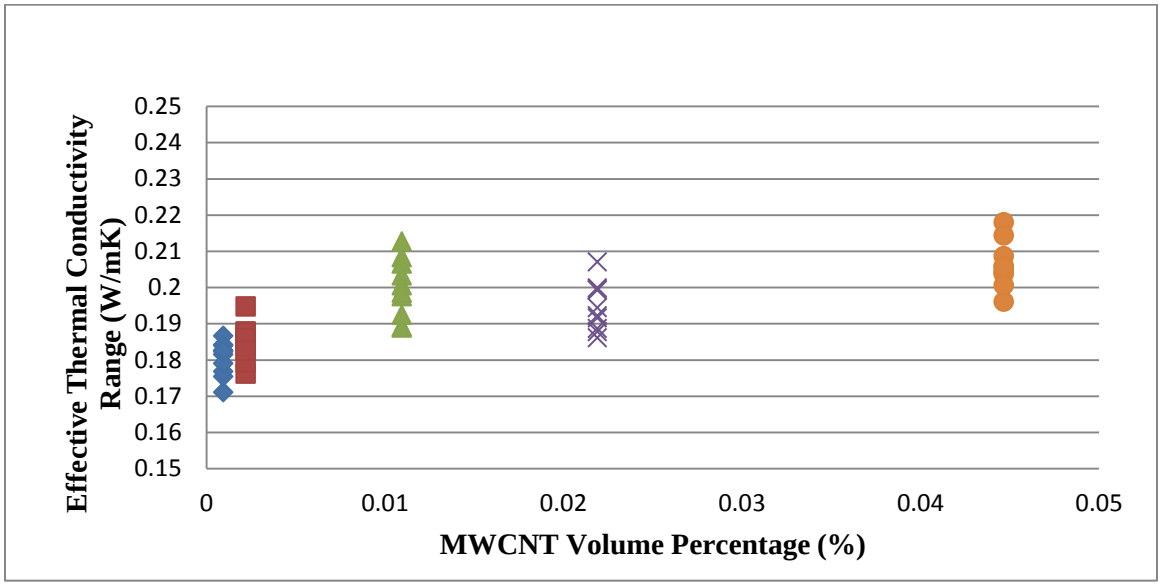

Figure A-17. Effective thermal conductivity data range for Dr. T. C. Shen's MWCNT based cryogenic nanofluids. Test day # 1 (3/26/12)

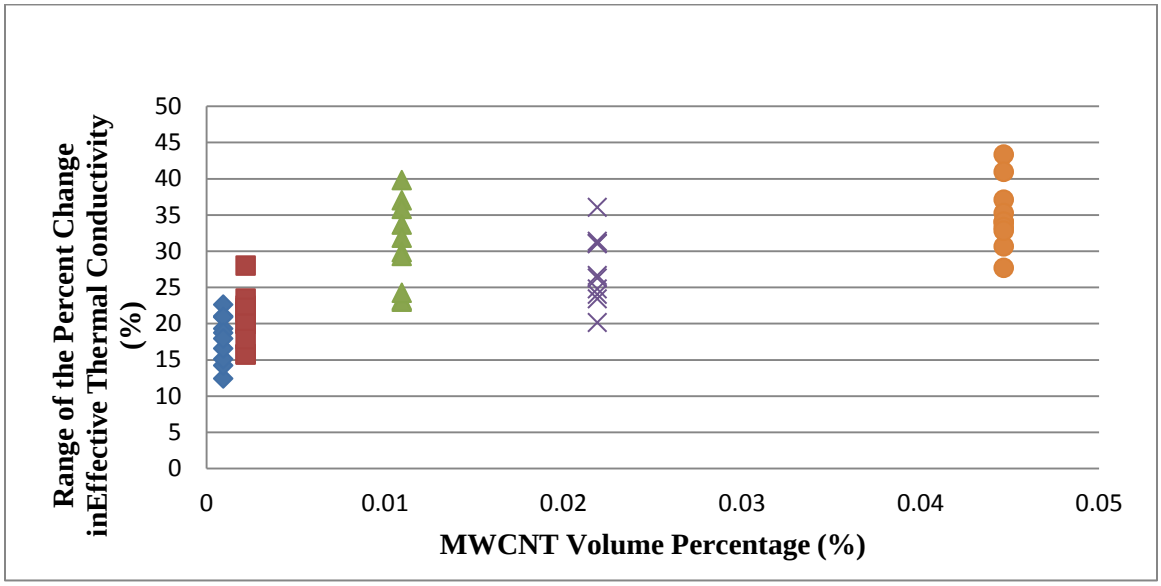

Figure A-18 Effective thermal conductivity (percent change) data range for Dr. T. C. Shen's MWCNT based cryogenic nanofluids. Test day # 2 (3/26/12)

A.4 Intermediate Results for NanoAmor Short Tailed (Stock #1235YJS) MWCNT based CN Test Run #1

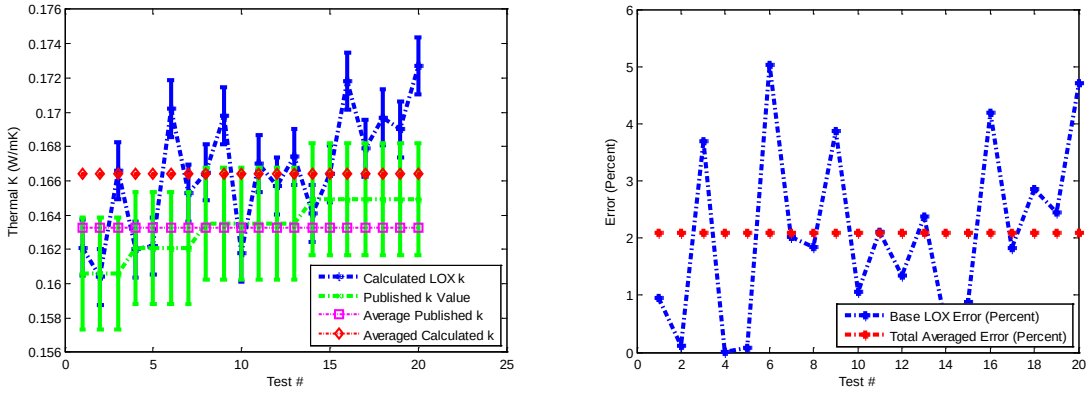

Figure A-19. Base LOX calibration for NanoAmor Short Tailed (Stock #1235YJS) MWCNT based cryogenic nanofluid. Test day #1 (4/3/12). Effective thermal conductivity vs. reported LOX values along with test value error in percent.

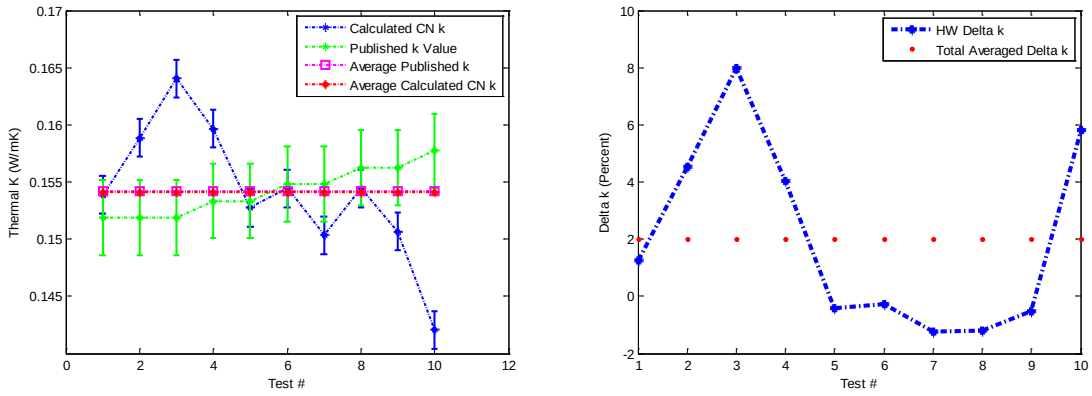

Figure A-20. Effective thermal conductivity vs. base lox values including conductivity increase in percent for NanoAmor Short Tailed (Stock #1235YJS) MWCNT based cryogenic nanofluid. Test day #1 (4/3/12) for a particle concentration of 0.01 gm (0.000952% by volume concentration)

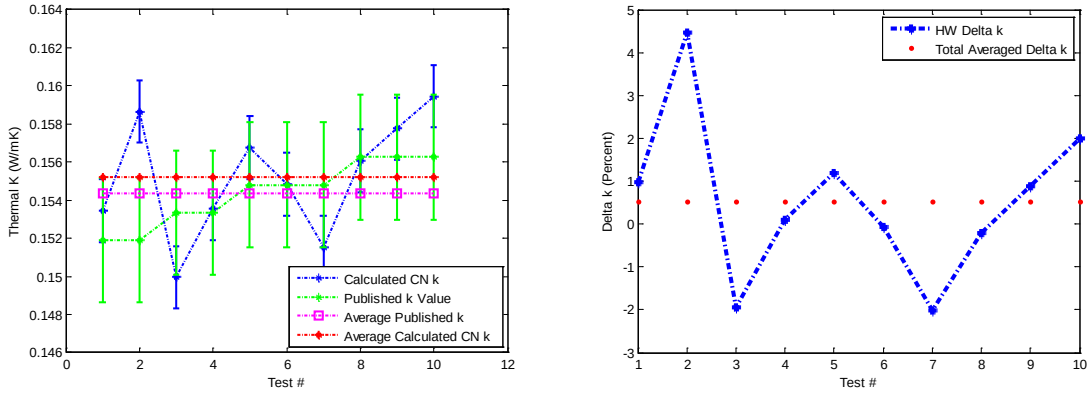

Figure A-21. Effective thermal conductivity vs. base lox values including conductivity increase in percent for NanoAmor Short Tailed (Stock #1235YJS) MWCNT based cryogenic nanofluid. Test day #1 (4/3/12) for a particle concentration of 0.023 gm (0.00219% by volume concentration)

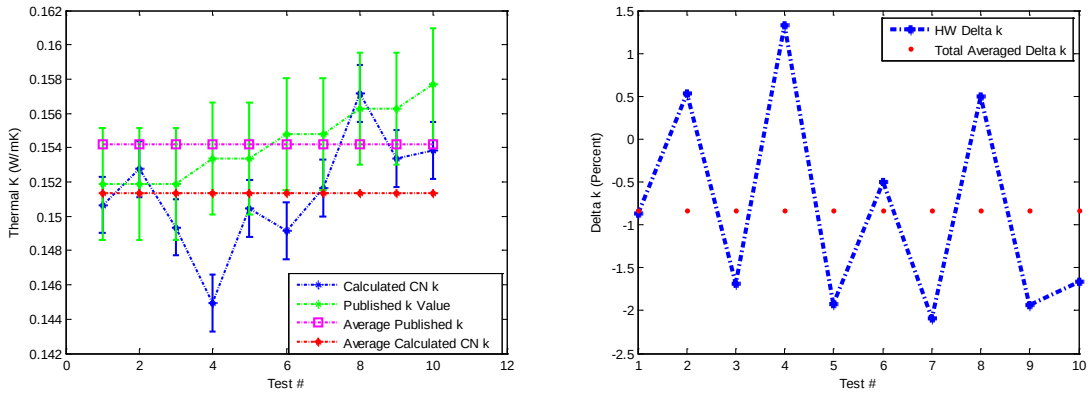

Figure A-22. Effective thermal conductivity vs. base lox values including conductivity increase in percent for NanoAmor Short Tailed (Stock #1235YJS) MWCNT based cryogenic nanofluid. Test day #1 (4/3/12) for a particle concentration of 0.115 gm (0.0109% by volume concentration)

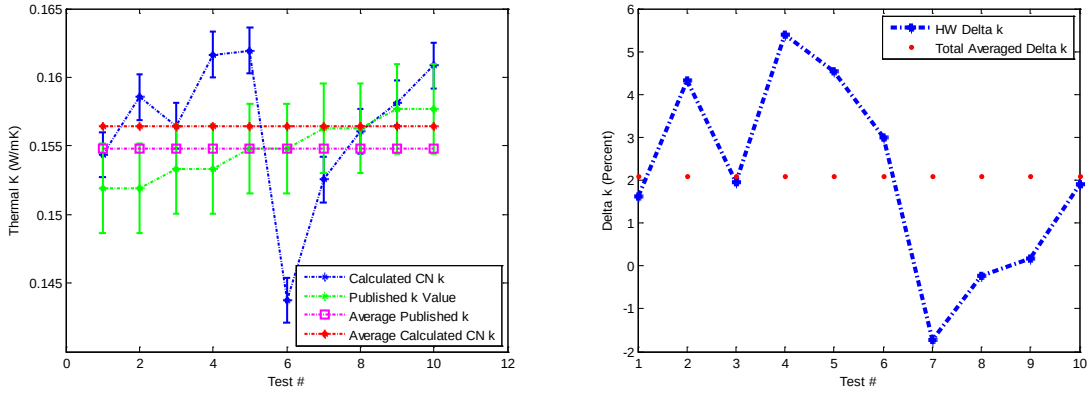

Figure A-23. Effective thermal conductivity vs. base lox values including conductivity increase in percent for NanoAmor Short Tailed (Stock #1235YJS) MWCNT based cryogenic nanofluid. Test day #1 (4/3/12) for a particle concentration of 0.230 gm (0.0219% by volume concentration)

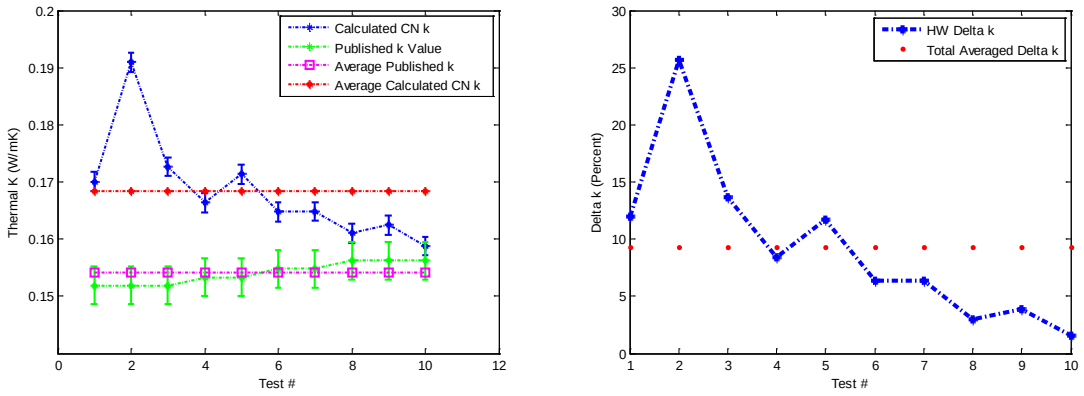

Figure A-24. Effective thermal conductivity vs. base lox values including conductivity increase in percent for NanoAmor Short Tailed (Stock #1235YJS) MWCNT based cryogenic nanofluid. Test day #1 (4/3/12) for a particle concentration of 0.335 gm (0.0319% by volume concentration).

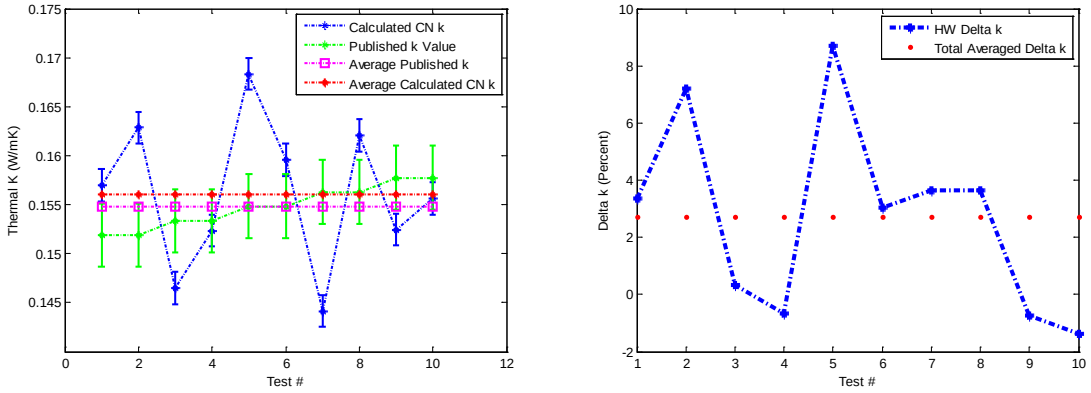

Figure A-25. Effective thermal conductivity vs. base lox values including conductivity increase in percent for NanoAmor Short Tailed (Stock #1235YJS) MWCNT based cryogenic nanofluid. Test day #1 (4/3/12) for a particle concentration of 0.469 gm (0.0447% by volume concentration).

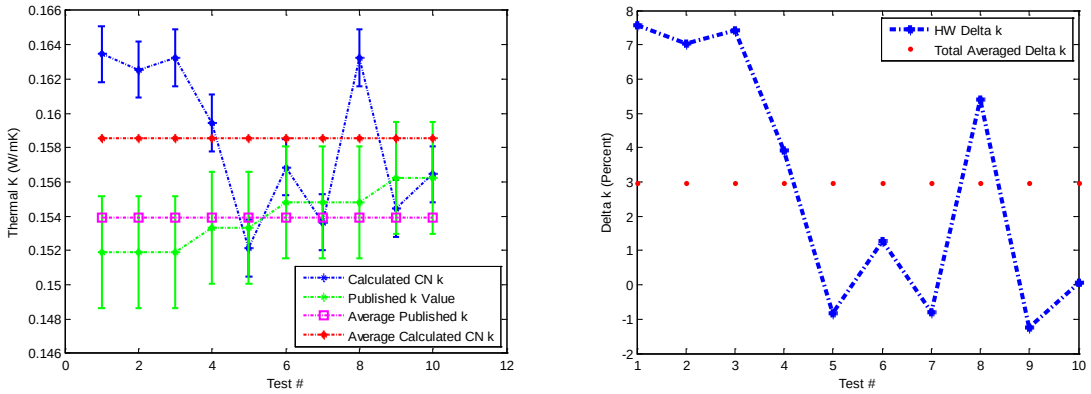

Figure A-26. Effective thermal conductivity vs. base lox values including conductivity increase in percent for NanoAmor Short Tailed (Stock #1235YJS) MWCNT based cryogenic nanofluid. Test day #1 (4/3/12) for a particle concentration of 0.670 gm (0.0638% by volume concentration).

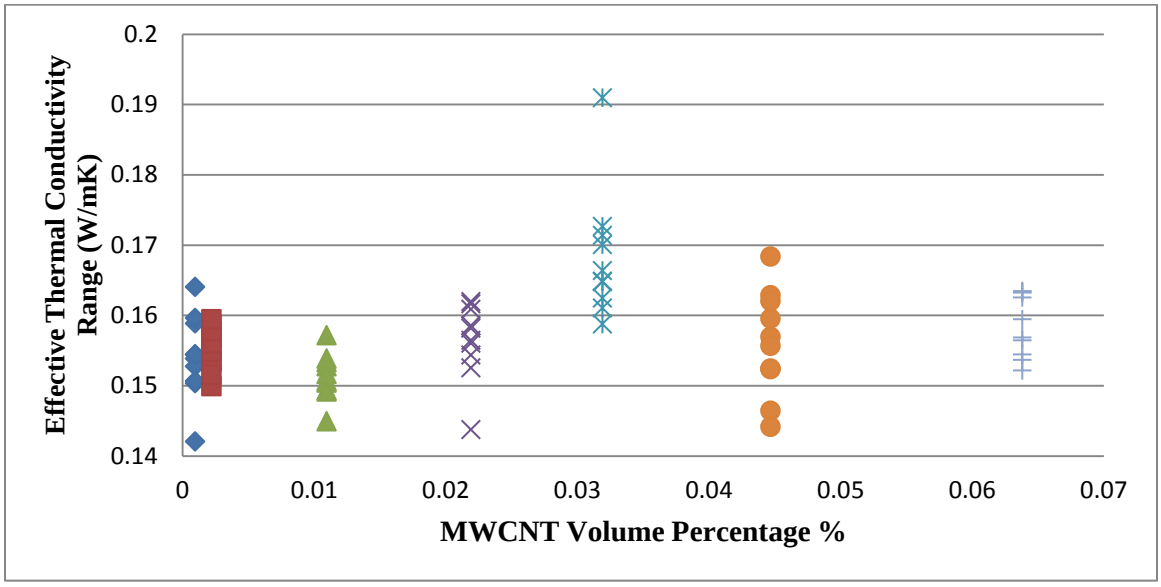

Figure A-27. Effective thermal conductivity data range for NanoAmor Short Tailed (Stock # 1235YJS) MWCNT based cryogenic nanofluids. Test day # 3 (4/3/12).

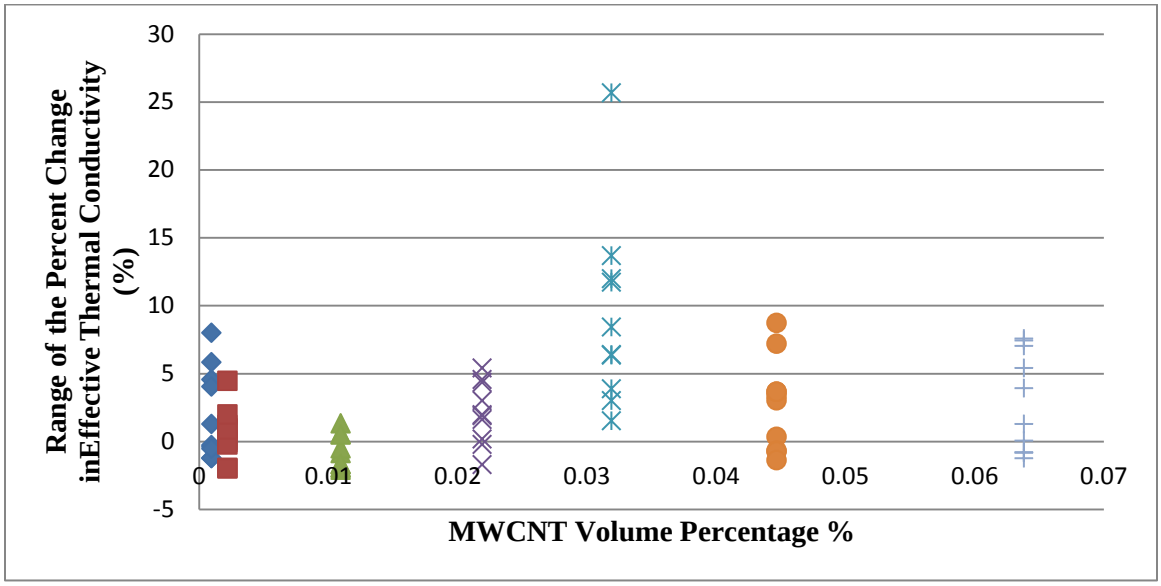

Figure A-28. Effective thermal conductivity (percent change) data range for NanoAmor Short Tailed (Stock # 1235YJS) MWCNT based cryogenic nanofluids. Test day # 3 (4/3/12).

A.5 Intermediate Results for NanoAmor Short Tailed (Stock #1235YJS) MWCNT based CN Test Run #2

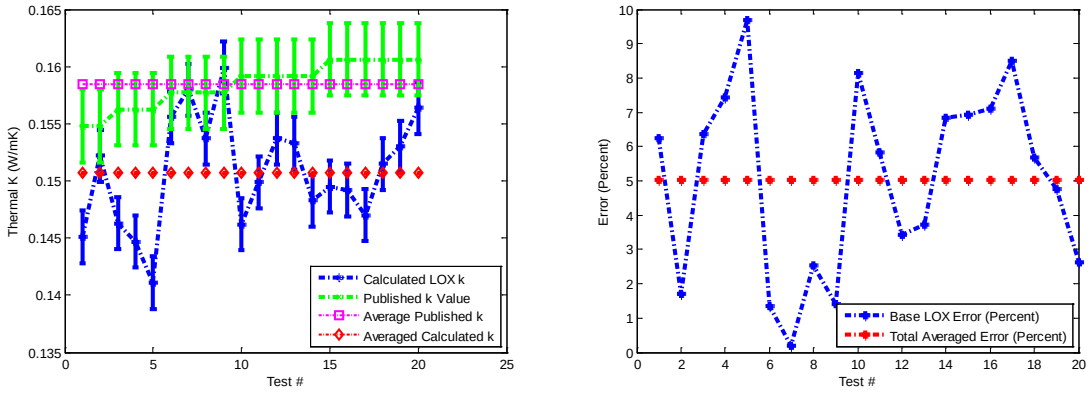

Figure A-29. Base LOX calibration for NanoAmor Short Tailed (Stock #1235YJS) MWCNT based cryogenic nanofluid. Test day #2 (4/4/12). Effective thermal conductivity vs. reported LOX values along with test value error in percent.

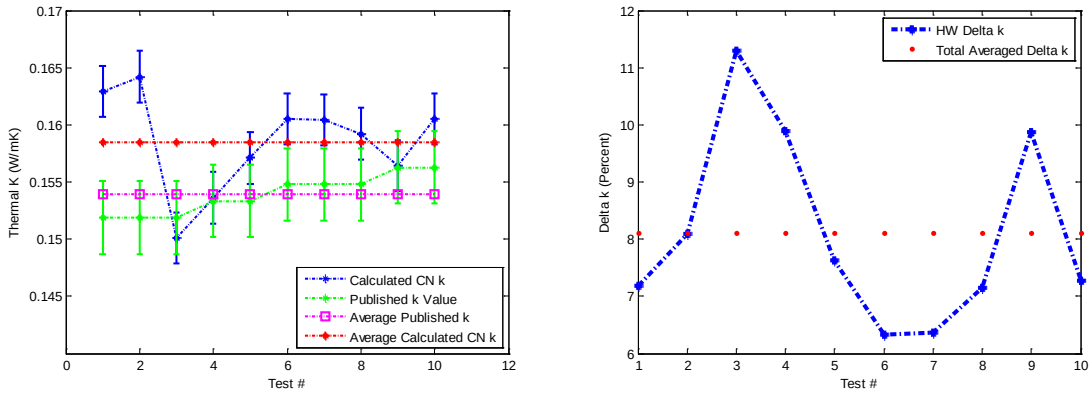

Figure A-30. Effective thermal conductivity vs. base lox values including conductivity increase in percent for NanoAmor Short Tailed (Stock #1235YJS) MWCNT based cryogenic nanofluid. Test day #2 (4/4/12) for a particle concentration of 0.01 gm (0.000952% by volume concentration).

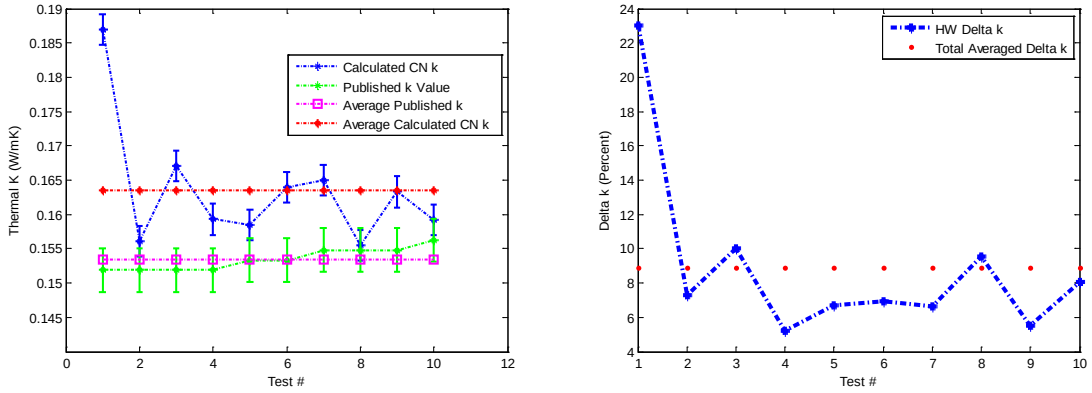

Figure A-31. Effective thermal conductivity vs. base lox values including conductivity increase in percent for NanoAmor Short Tailed (Stock #1235YJS) MWCNT based cryogenic nanofluid. Test day #2 (4/4/12) for a particle concentration of 0.023 gm (0.00219% by volume concentration).

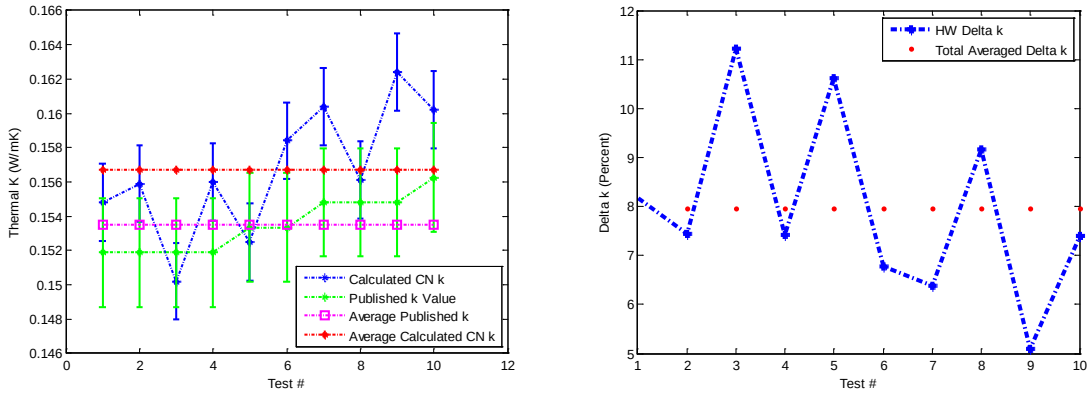

Figure A-32. Effective thermal conductivity vs. base lox values including conductivity increase in percent for NanoAmor Short Tailed (Stock #1235YJS) MWCNT based cryogenic nanofluid. Test day #2 (4/4/12) for a particle concentration of 0.115 gm (0.01095% by volume concentration).

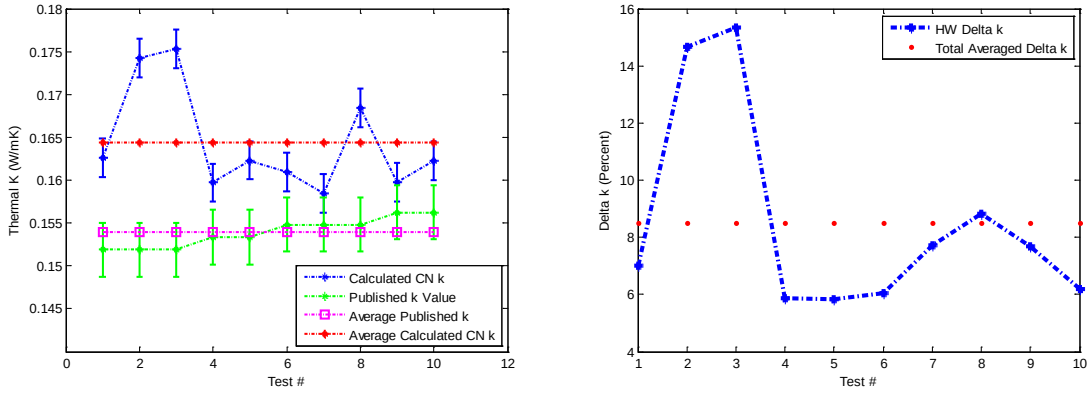

Figure A-33. Effective thermal conductivity vs. base lox values including conductivity increase in percent for NanoAmor Short Tailed (Stock #1235YJS) MWCNT based cryogenic nanofluid. Test day #2 (4/4/12) for a particle concentration of 0.230 gm (0.0219% by volume concentration).

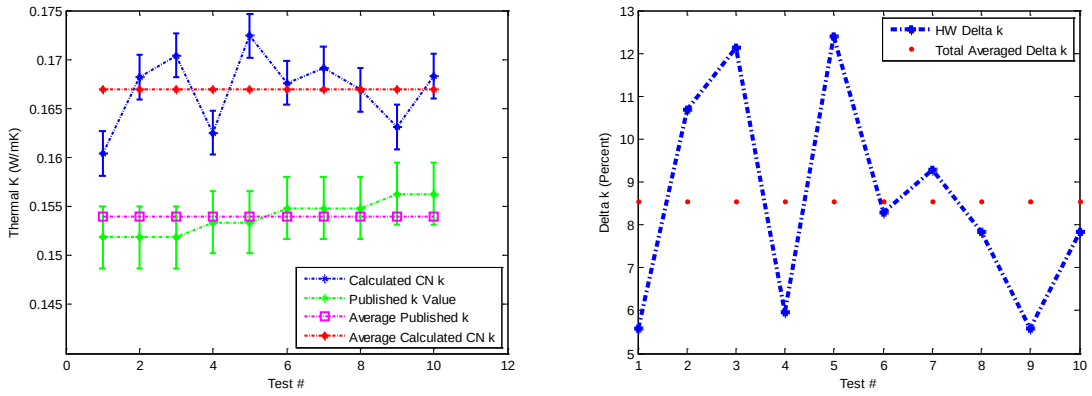

Figure A-34. Effective thermal conductivity vs. base lox values including conductivity increase in percent for NanoAmor Short Tailed (Stock #1235YJS) MWCNT based cryogenic nanofluid. Test day #2 (4/4/12) for a particle concentration of 0.335 gm (0.0319% by volume concentration).

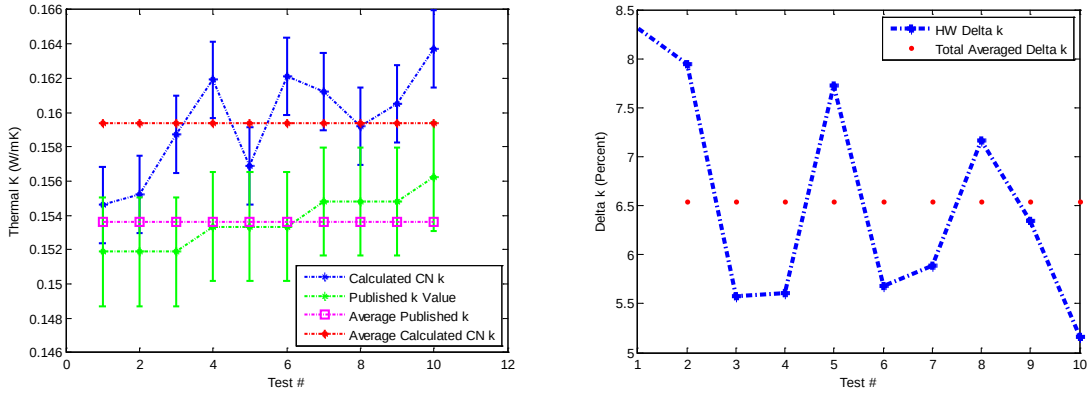

Figure A-35. Effective thermal conductivity vs. base lox values including conductivity increase in percent for NanoAmor Short Tailed (Stock #1235YJS) MWCNT based cryogenic nanofluid. Test day #2 (4/4/12) for a particle concentration of 0.469 gm (0.0447% by volume concentration).

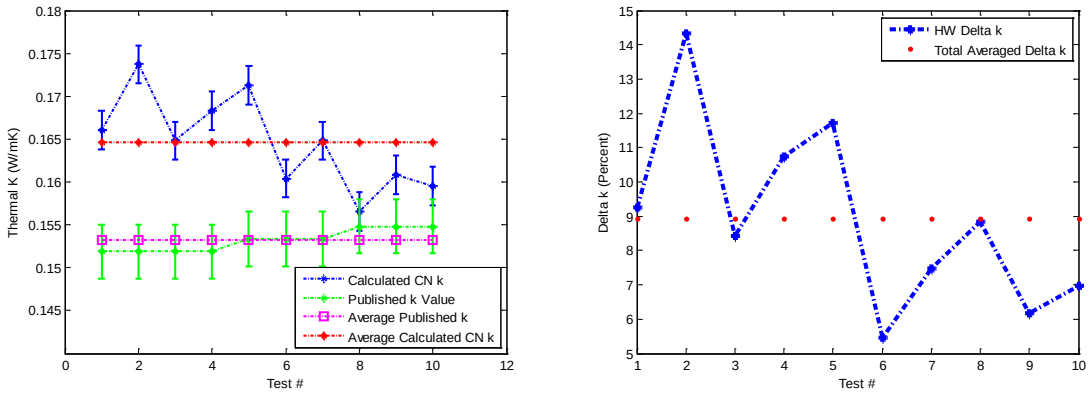

Figure A-36. Effective thermal conductivity vs. base lox values including conductivity increase in percent for NanoAmor Short Tailed (Stock #1235YJS) MWCNT based cryogenic nanofluid. Test day #2 (4/4/12) for a particle concentration of 0.670 gm (0.0638% by volume concentration).

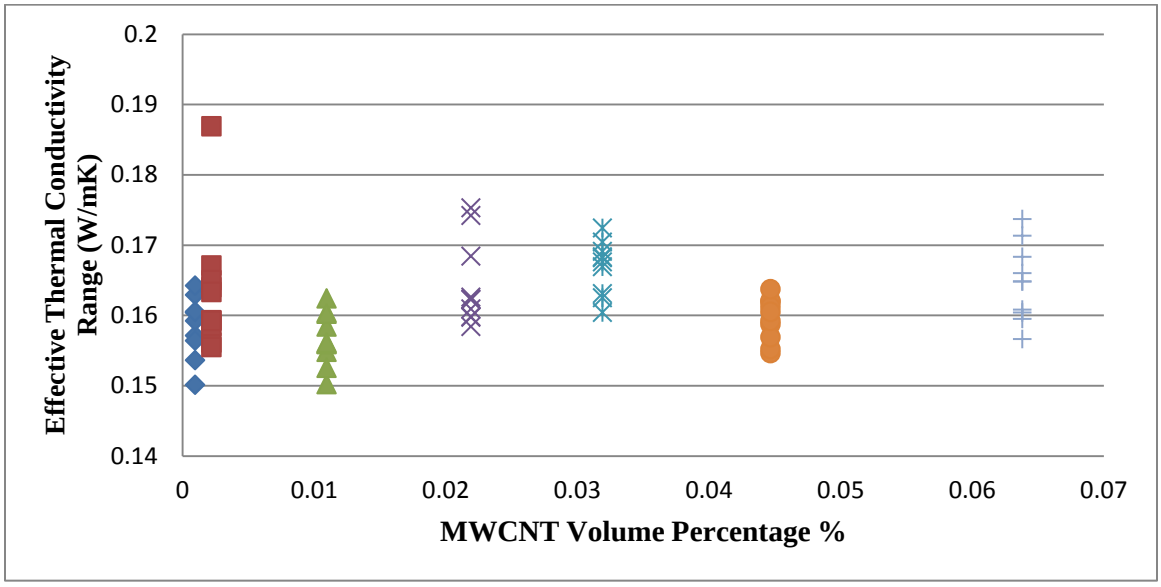

Figure A-37. Effective thermal conductivity data range for NanoAmor Short Tailed (Stock # 1235YJS) MWCNT based cryogenic nanofluids. Test day # 4 (4/4/12).

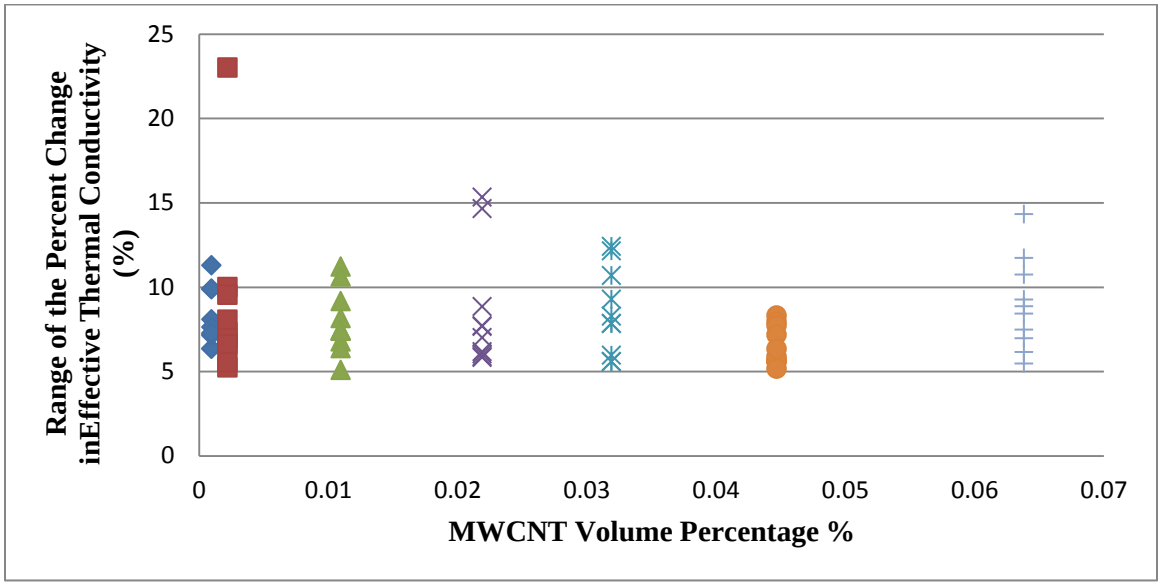

Figure A-38. Effective thermal conductivity (percent range) data range for NanoAmor Short Tailed (Stock # 1235YJS) MWCNT based cryogenic nanofluids. Test day # 4 (4/4/12).

A.6 Intermediate Results for NanoAmor Long Tailed (Stock #1204YJ) MWCNT based CN Test Run #1

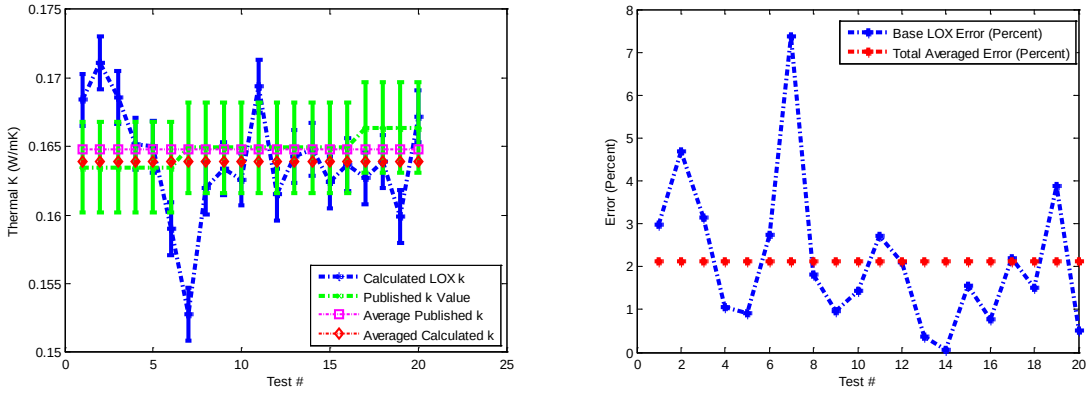

Figure A-39. Base LOX calibration for NanoAmor Long Tailed (Stock #1204YJ) MWCNT based cryogenic nanofluid. Test day #1 (4/6/12). Effective thermal conductivity vs. reported LOX values along with test value error in percent.

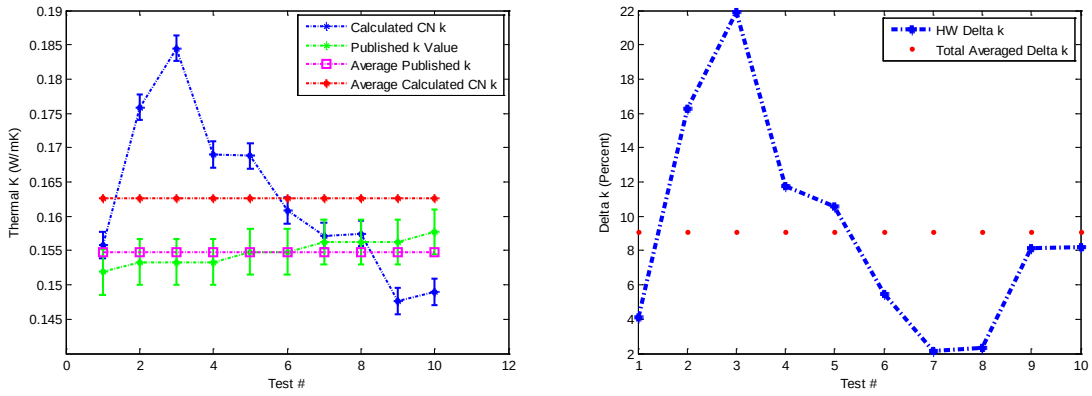

Figure A-40. Effective thermal conductivity vs. base lox values including conductivity increase in percent for NanoAmor Long Tailed (Stock #1204YJ) MWCNT based cryogenic nanofluid. Test day #1 (4/6/12) for a particle concentration of 0.01 gm (0.000952% by volume concentration).

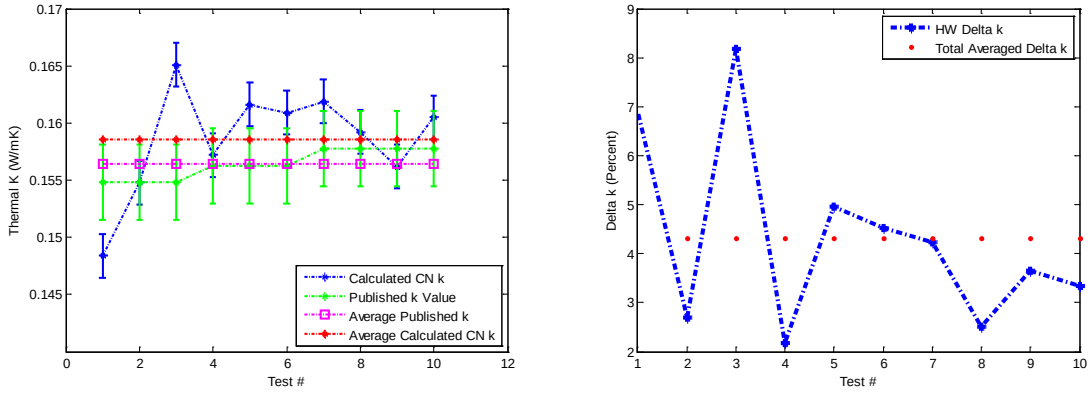

Figure A-41. Effective thermal conductivity vs. base lox values including conductivity increase in percent for NanoAmor Long Tailed (Stock #1204YJ) MWCNT based cryogenic nanofluid. Test day #1 (4/6/12) for a particle concentration of 0.023 gm (0.00219% by volume concentration).

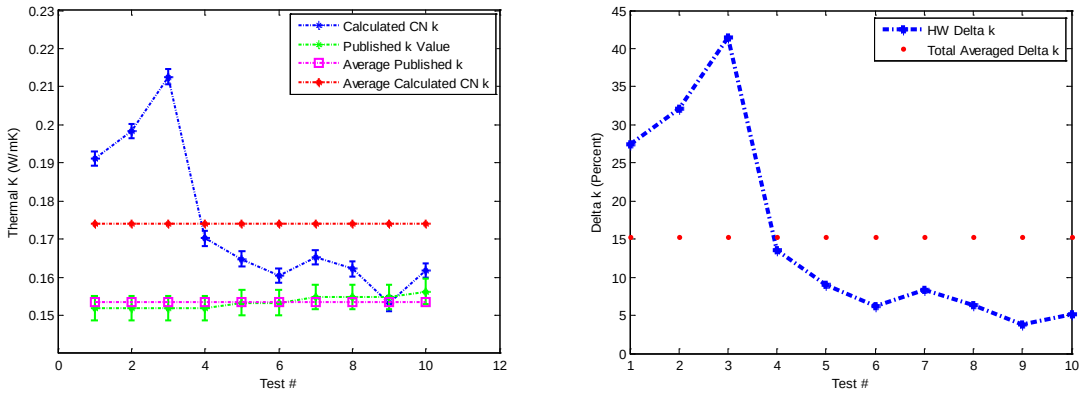

Figure A-42. Effective thermal conductivity vs. base lox values including conductivity increase in percent for NanoAmor Long Tailed (Stock #1204YJ) MWCNT based cryogenic nanofluid. Test day #1 (4/6/12) for a particle concentration of 0.115 gm (0.01095% by volume concentration).

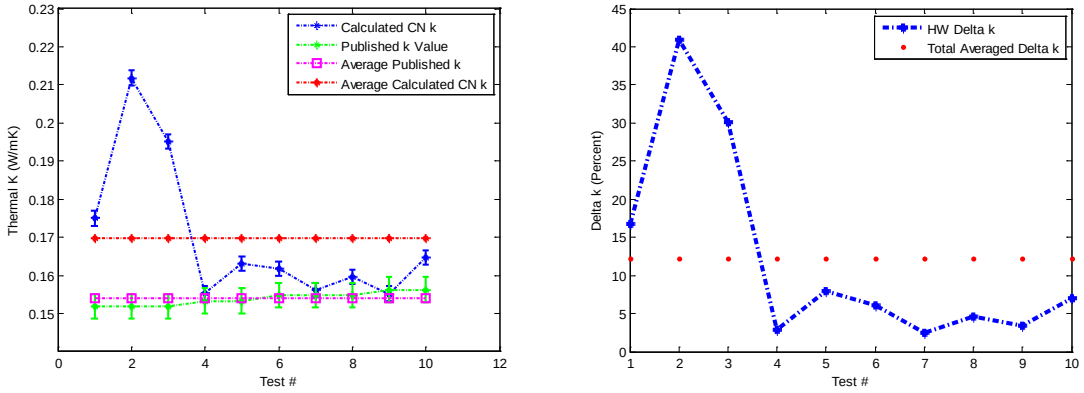

Figure A-43. Effective thermal conductivity vs. base lox values including conductivity increase in percent for NanoAmor Long Tailed (Stock #1204YJ) MWCNT based cryogenic nanofluid. Test day #1 (4/6/12) for a particle concentration of 0.230 gm (0.0219% by volume concentration).

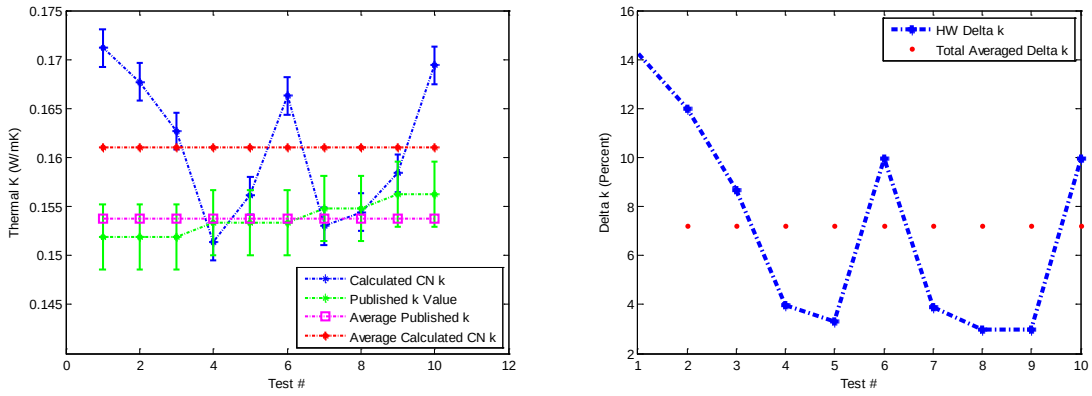

Figure A-44. Effective thermal conductivity vs. base lox values including conductivity increase in percent for NanoAmor Long Tailed (Stock #1204YJ) MWCNT based cryogenic nanofluid. Test day #1 (4/6/12) for a particle concentration of 0.335 gm (0.0319% by volume concentration).

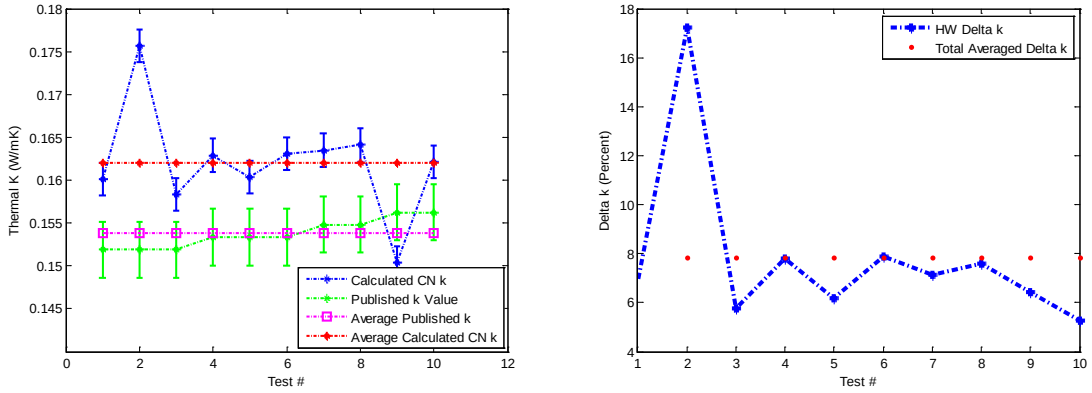

Figure A-45. Effective thermal conductivity vs. base lox values including conductivity increase in percent for NanoAmor Long Tailed (Stock #1204YJ) MWCNT based cryogenic nanofluid. Test day #1 (4/6/12) for a particle concentration of 0.469gm (0.0447% by volume concentration).

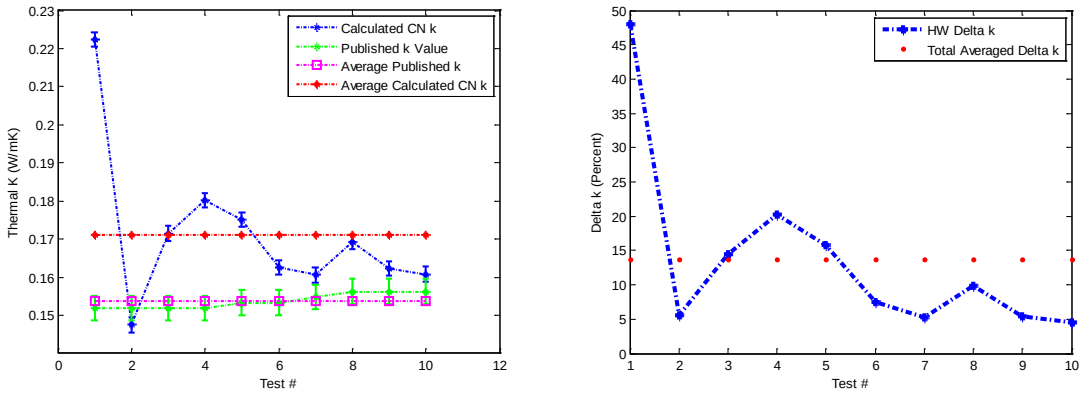

Figure A-46. Effective thermal conductivity vs. base lox values including conductivity increase in percent for NanoAmor Long Tailed (Stock #1204YJ) MWCNT based cryogenic nanofluid. Test day #1 (4/6/12) for a particle concentration of 0.670 gm (0.06381% by volume concentration).

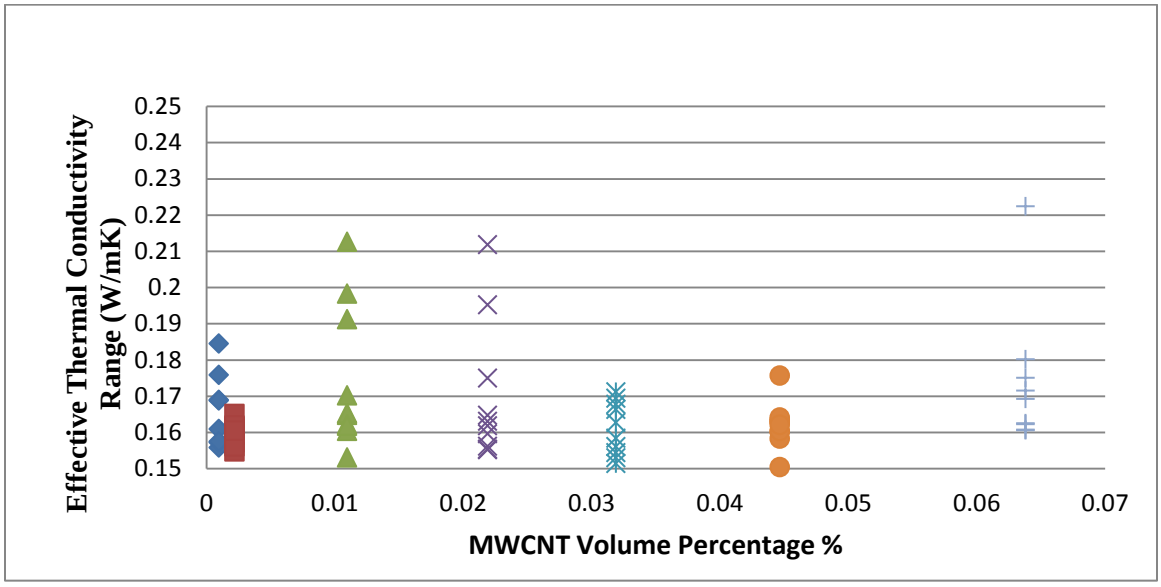

Figure A-47. Effective thermal conductivity data range for NanoAmor Long Tailed (Stock # 1204YJ) MWCNT based cryogenic nanofluids. Test day # 5 (4/6/12).

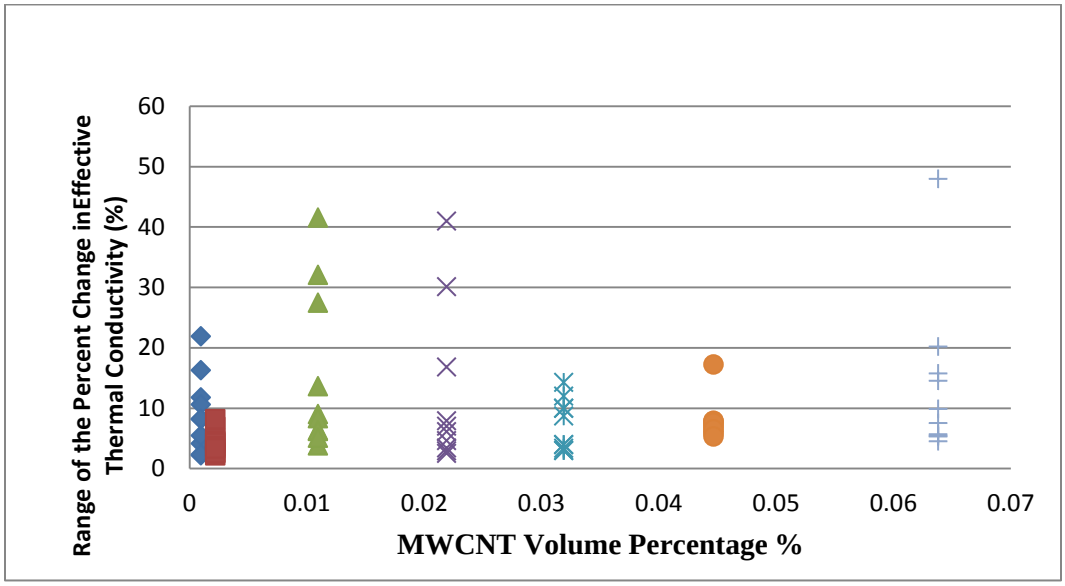

Figure A-48. Effective thermal conductivity (percent change) data range for NanoAmor Long Tailed (Stock # 1204YJ) MWCNT based cryogenic nanofluids. Test day # 5 (4/6/12).

A.7 Intermediate Results for NanoAmor Long Tailed (Stock #1204YJ) MWCNT based CN Test Run #2

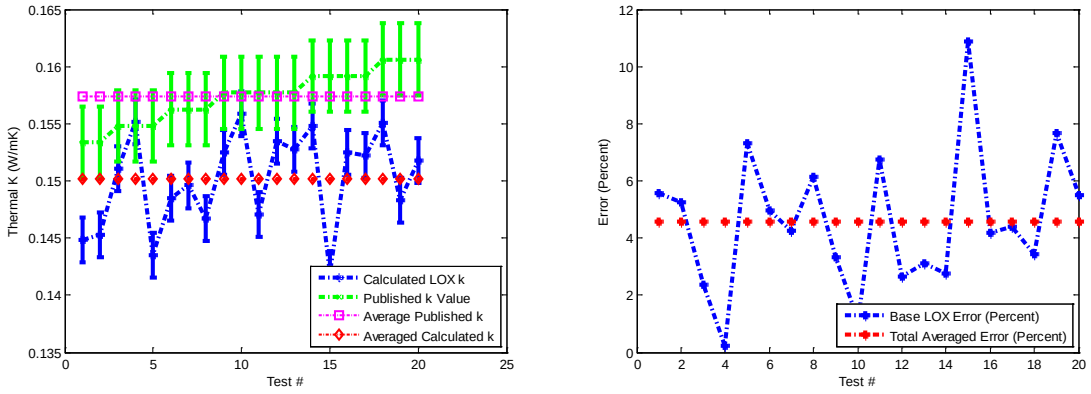

Figure A-49. Base LOX calibration for NanoAmor Long Tailed (Stock #1204YJ) MWCNT based cryogenic nanofluid. Test day #2 (4/9/12). Effective thermal conductivity vs. reported LOX values along with test value error in percent.

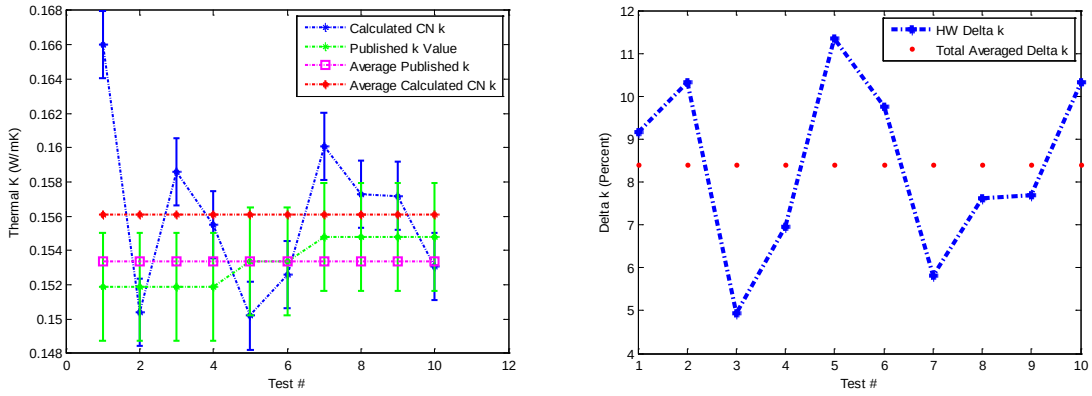

Figure A-50. Effective thermal conductivity vs. base lox values including conductivity increase in percent for NanoAmor Long Tailed (Stock #1204YJ) MWCNT based cryogenic nanofluid. Test day #2 (4/9/12) for a particle concentration of 0.01 gm (0.000952% by volume concentration).

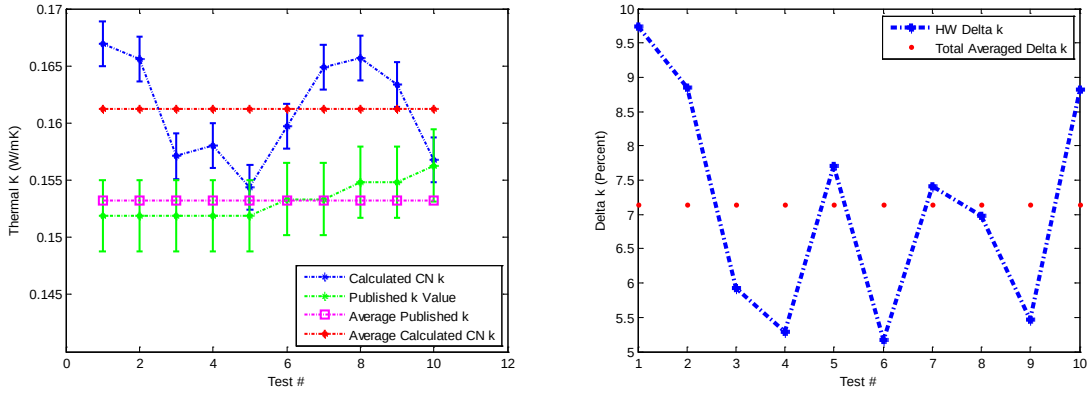

Figure A-51. Effective thermal conductivity vs. base lox values including conductivity increase in percent for NanoAmor Long Tailed (Stock #1204YJ) MWCNT based cryogenic nanofluid. Test day #2 (4/9/12) for a particle concentration of 0.023 gm (0.00219% by volume concentration).

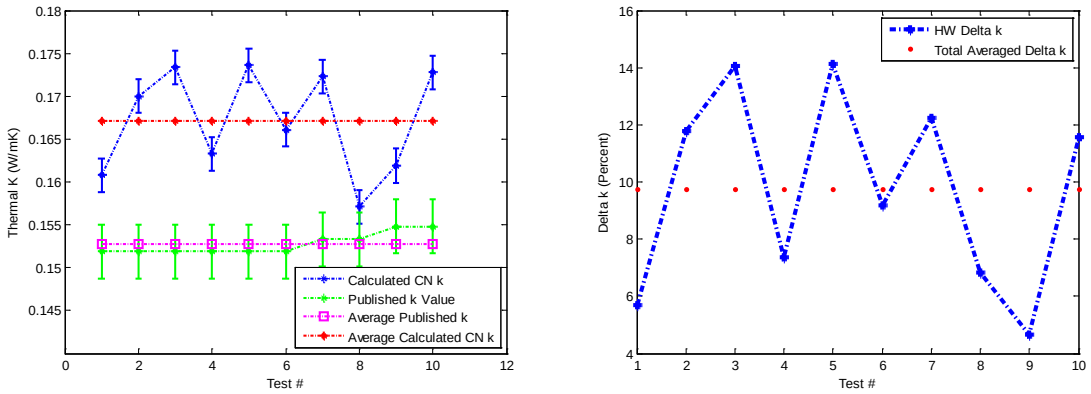

Figure A-52. Effective thermal conductivity vs. base lox values including conductivity increase in percent for NanoAmor Long Tailed (Stock #1204YJ) MWCNT based cryogenic nanofluid. Test day #2 (4/9/12) for a particle concentration of 0.115 gm (0.01095% by volume concentration).

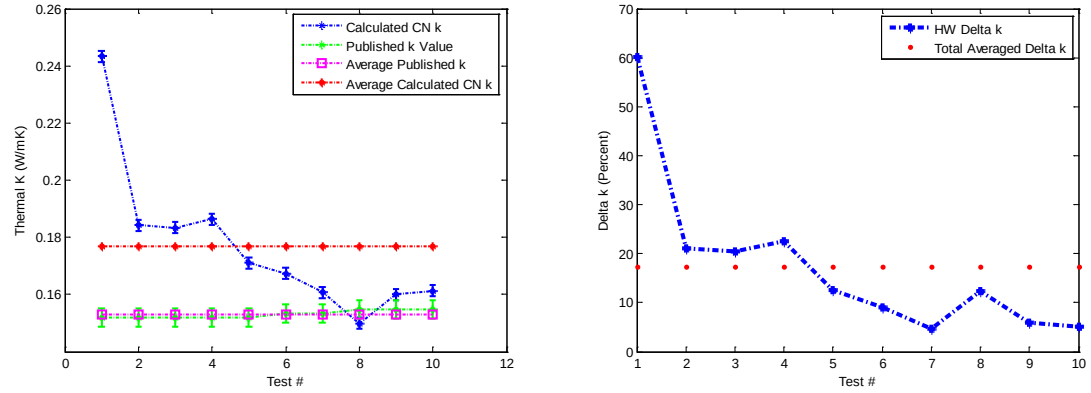

Figure A-53. Effective thermal conductivity vs. base lox values including conductivity increase in percent for NanoAmor Long Tailed (Stock #1204YJ) MWCNT based cryogenic nanofluid. Test day #2 (4/9/12) for a particle concentration of 0.230 gm (0.0219% by volume concentration).

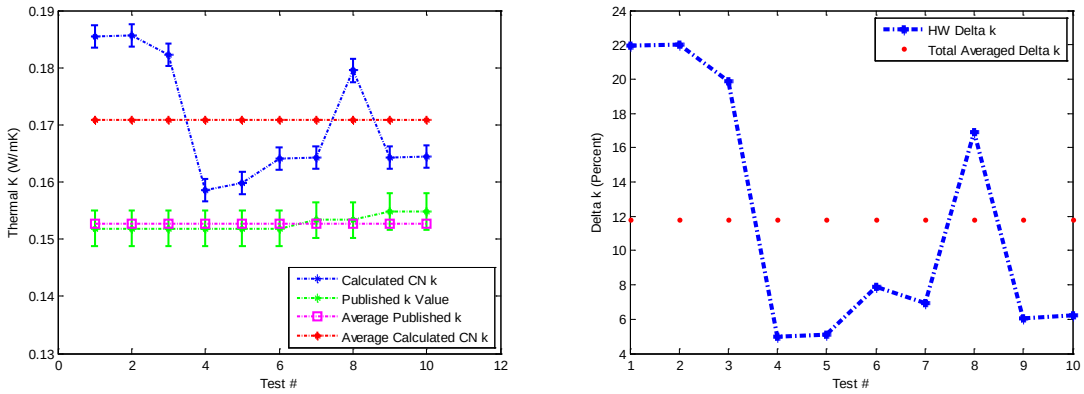

Figure A-54. Effective thermal conductivity vs. base lox values including conductivity increase in percent for NanoAmor Long Tailed (Stock #1204YJ) MWCNT based cryogenic nanofluid. Test day #2 (4/9/12) for a particle concentration of 0.335 gm (0.0319% by volume concentration).

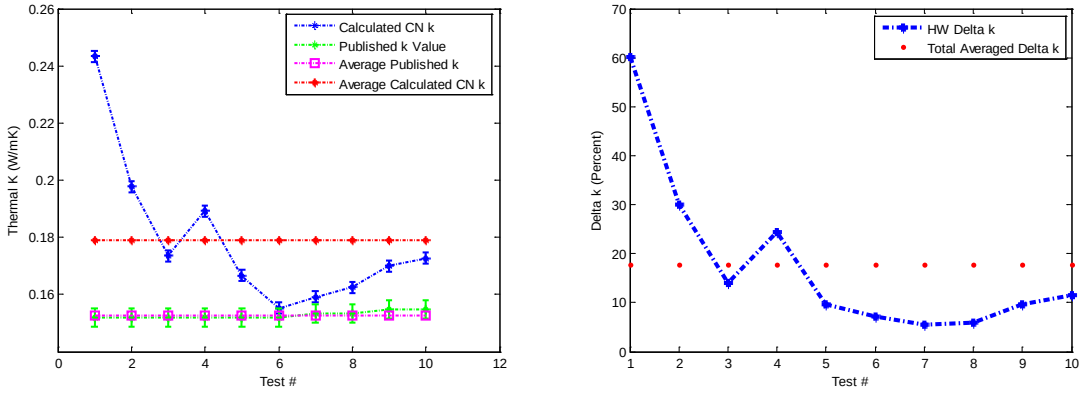

Figure A-55. Effective thermal conductivity vs. base lox values including conductivity increase in percent for NanoAmor Long Tailed (Stock #1204YJ) MWCNT based cryogenic nanofluid. Test day #2 (4/9/12) for a particle concentration of 0.469 gm (0.0447% by volume concentration).

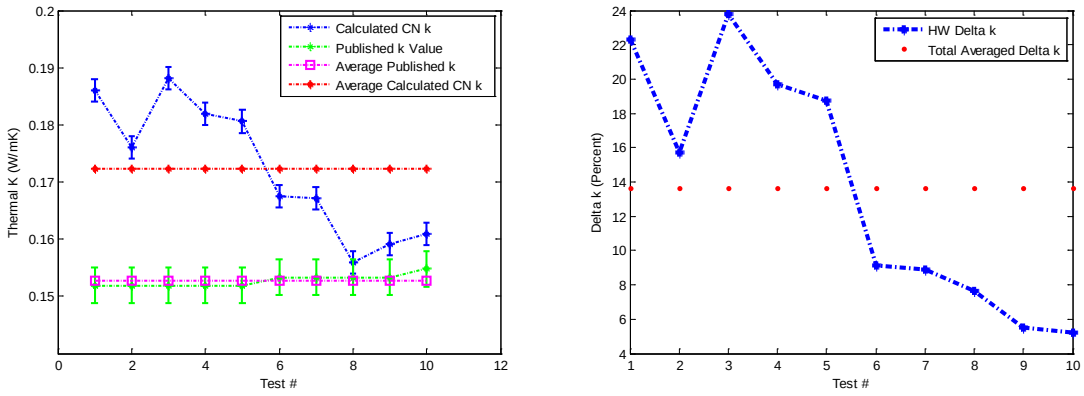

Figure A-56. Effective thermal conductivity vs. base lox values including conductivity increase in percent for NanoAmor Long Tailed (Stock #1204YJ) MWCNT based cryogenic nanofluid. Test day #2 (4/9/12) for a particle concentration of 0.670 gm (0.0638% by volume concentration).

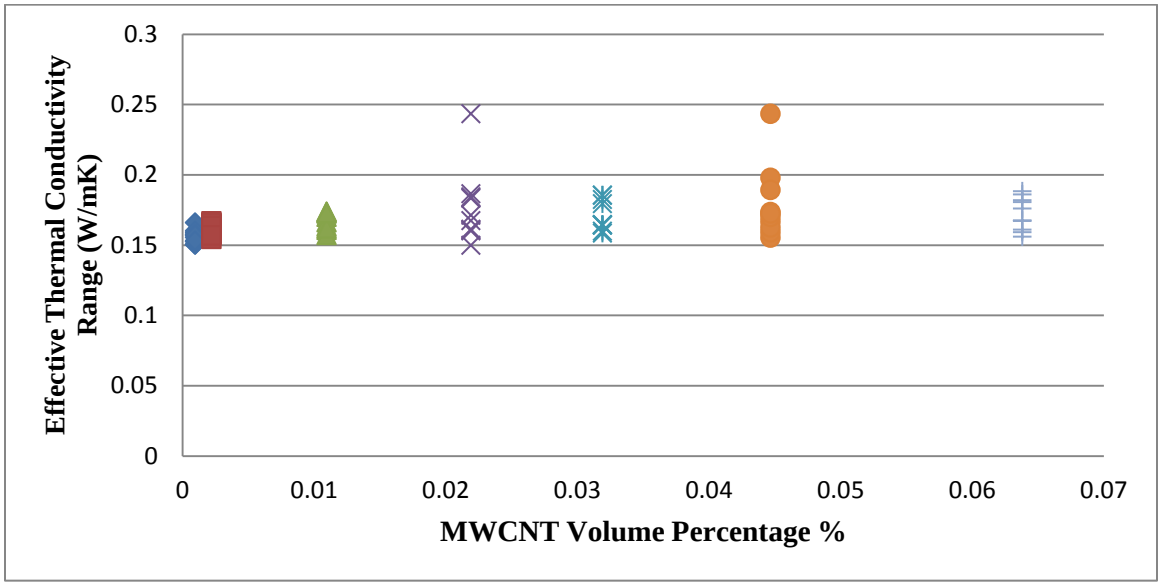

Figure A-57. Effective thermal conductivity data range for NanoAmor Long Tailed (Stock # 1204YJ) MWCNT based cryogenic nanofluids. Test day # 6 (4/9/12).

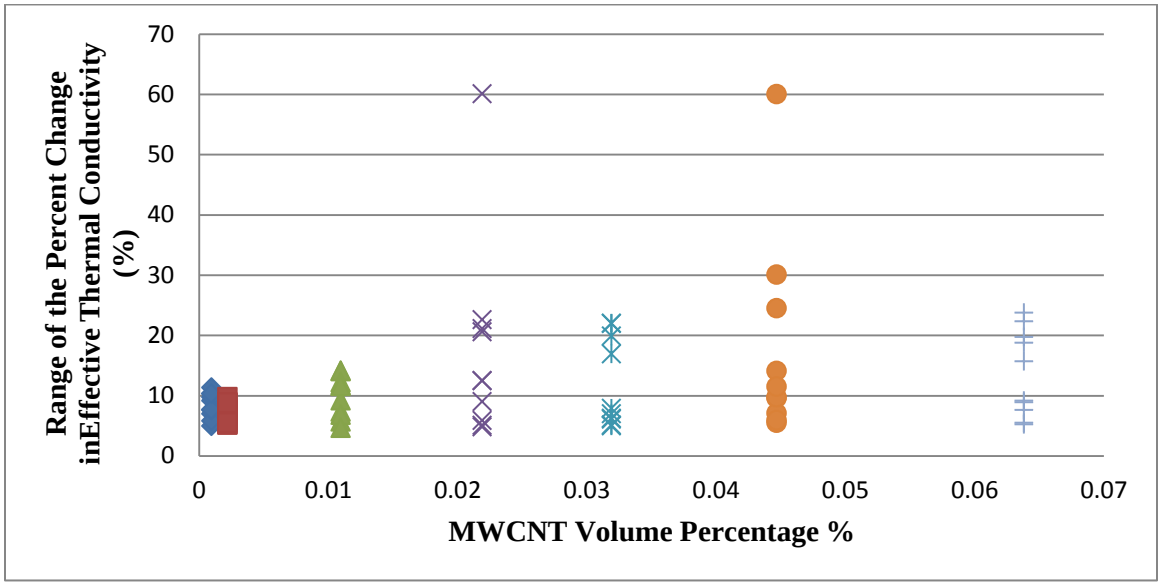

Figure A-58. Effective thermal conductivity (percent change) data range for NanoAmor Long Tailed (Stock # 1204YJ) MWCNT based cryogenic nanofluids. Test day # 6 (4/9/12).

A.8 Intermediate Results for NanoAmor Long Tailed (Stock #1204YJ) MWCNT based CN Test Run #3

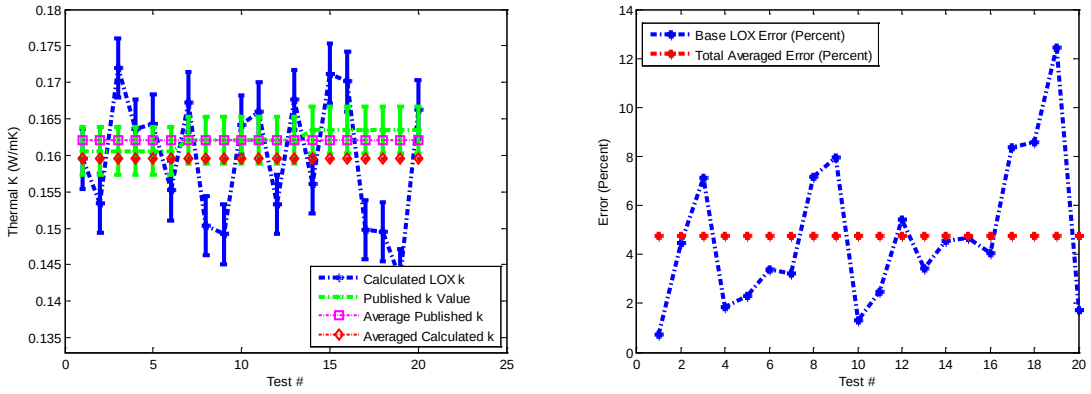

Figure A-59. Base LOX calibration for NanoAmor Long Tailed (Stock #1204YJ) MWCNT based cryogenic nanofluid. Test day #3 (4/10/12). Effective thermal conductivity vs. reported LOX values along with test value error in percent.

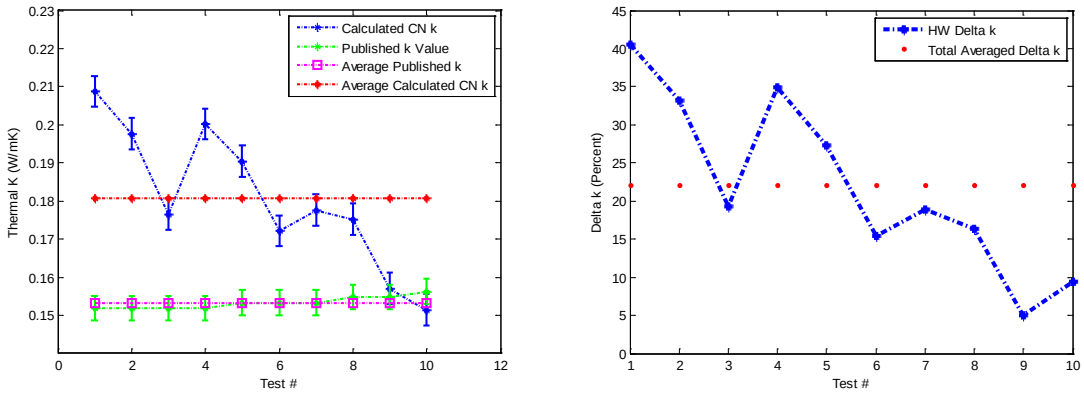

Figure A-60. Effective thermal conductivity vs. base lox values including conductivity increase in percent for NanoAmor Long Tailed (Stock #1204YJ) MWCNT based cryogenic nanofluid. Test day #3 (4/10/12) for a particle concentration of 0.335 gm (0.0319% by volume concentration).

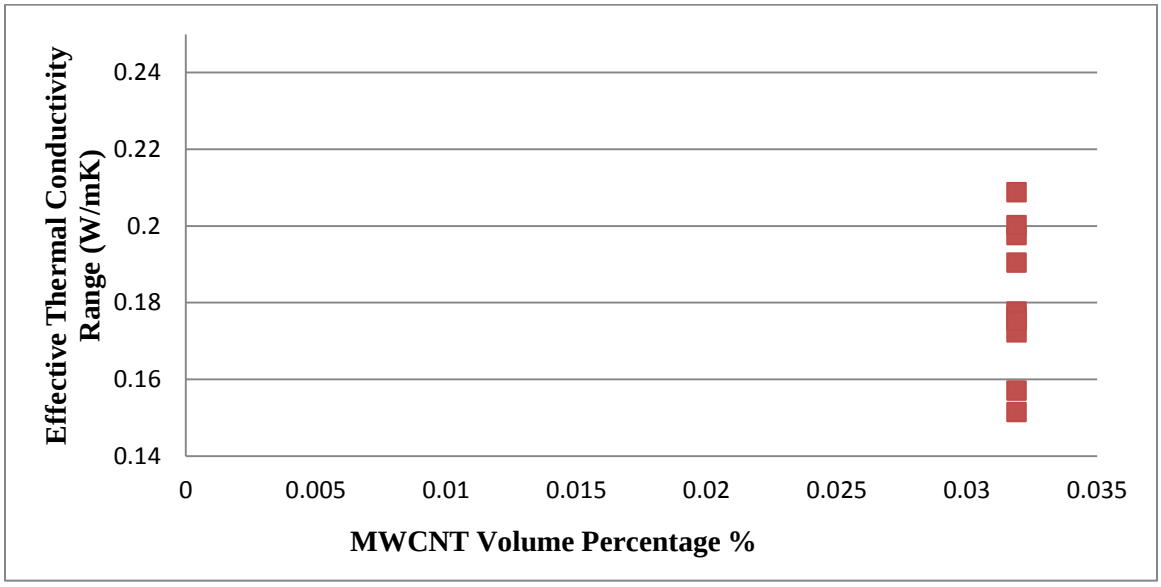

Figure A-61. Effective thermal conductivity data range for NanoAmor Long Tailed (Stock # 1204YJ) MWCNT based cryogenic nanofluids. Test day # 7 (4/10/12).

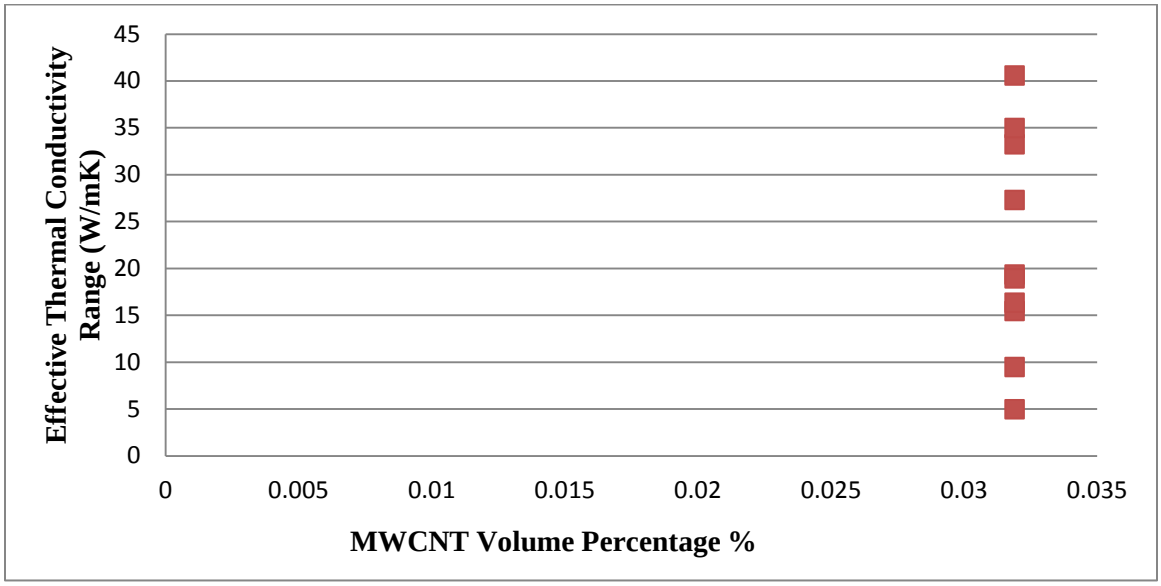

Figure A-62. Effective thermal conductivity (percent change) data range for NanoAmor Long Tailed (Stock # 1204YJ) MWCNT based cryogenic nanofluids. Test day # 7 (4/10/12).

A.9 Intermediate Results for NanoAmor Long Tailed (Stock #1204YJ) MWCNT based CN Test Run #4

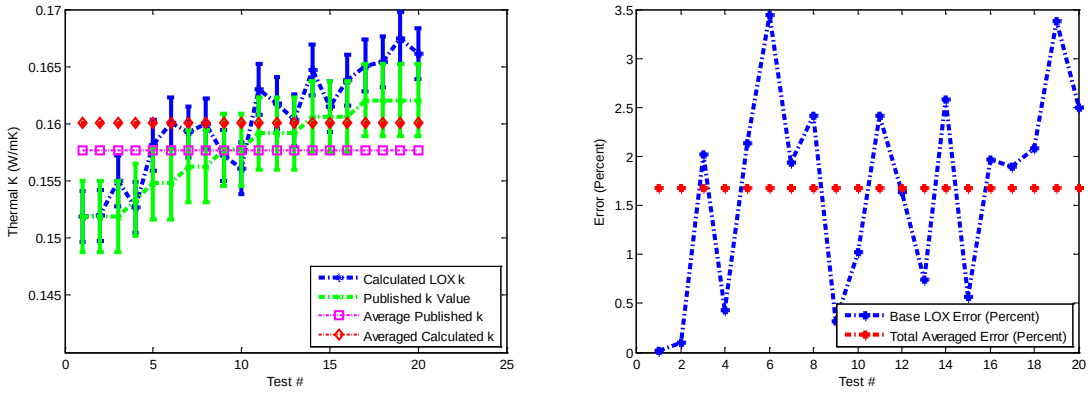

Figure A-63. Base LOX calibration for NanoAmor Long Tailed (Stock #1204YJ) MWCNT based cryogenic nanofluid. Test day #4 (4/12/12). Effective thermal conductivity vs. reported LOX values along with test value error in percent.

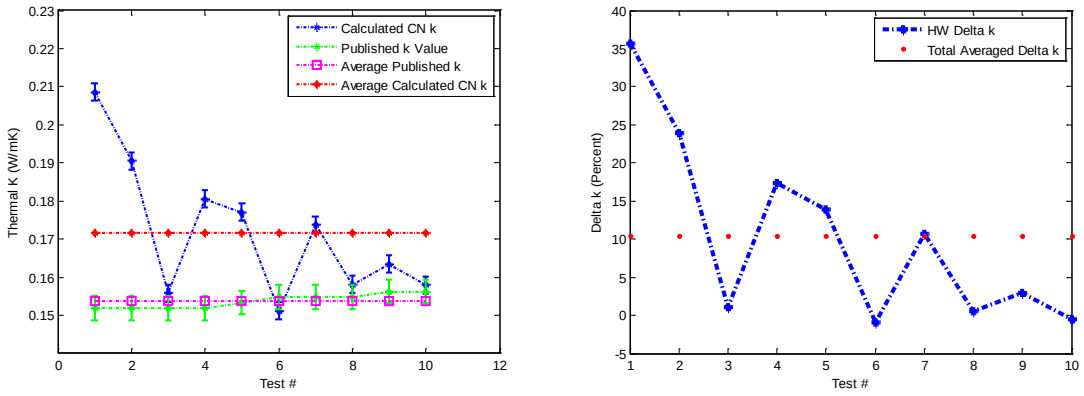

Figure A-64. Effective thermal conductivity vs. base lox values including conductivity increase in percent for NanoAmor Long Tailed (Stock #1204YJ) MWCNT based cryogenic nanofluid. Test day #4 (4/12/12) for a particle concentration of 0.335 gm (0.0319% by volume concentration).

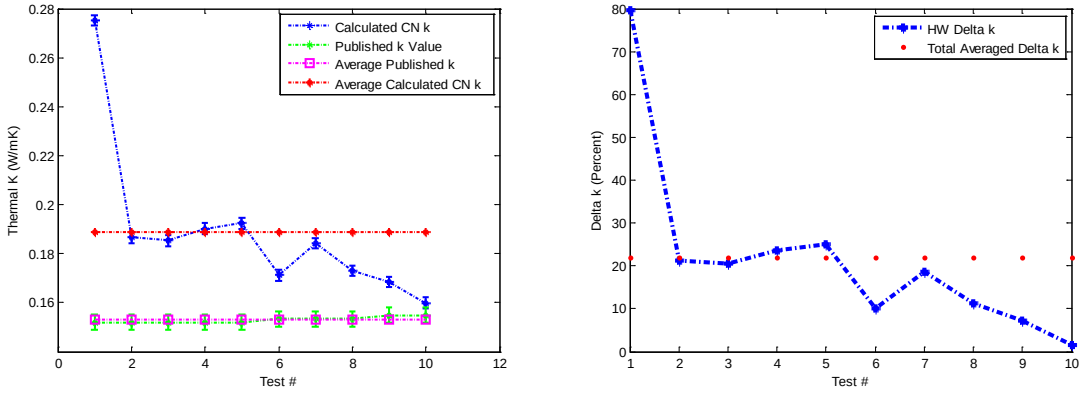

Figure A-65. Effective thermal conductivity vs. base lox values including conductivity increase in percent for NanoAmor Long Tailed (Stock #1204YJ) MWCNT based cryogenic nanofluid. Test day #4 (4/12/12) for a particle concentration of 0.469 gm (0.0447% by volume concentration).

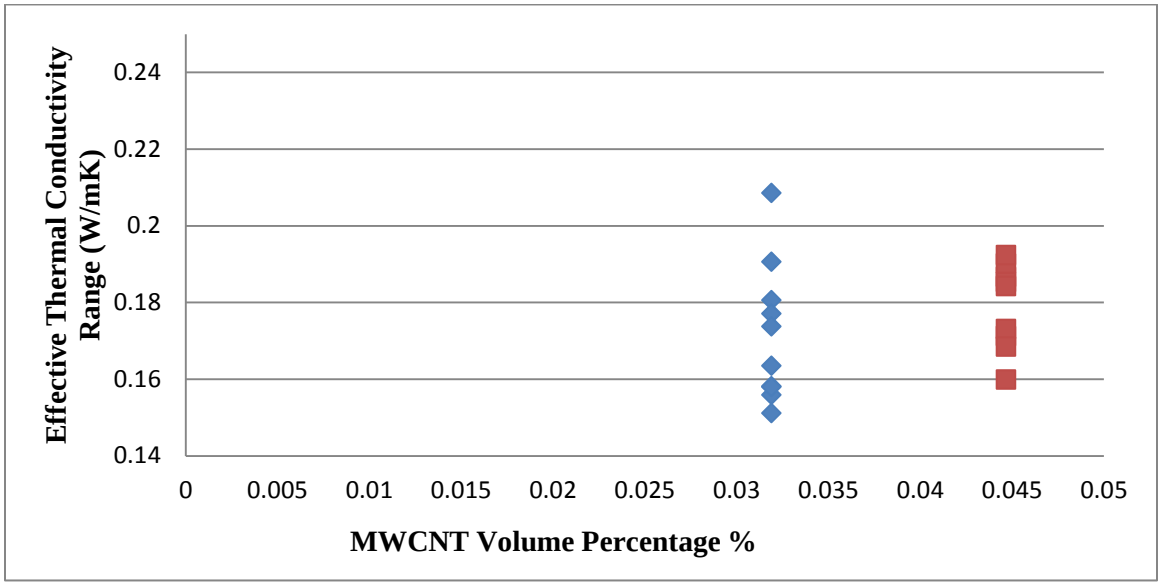

Figure A-66. Effective thermal conductivity data range for NanoAmor Long Tailed (Stock # 104YJ) MWCNT based cryogenic nanofluids. Test day # 8 (4/12/12).

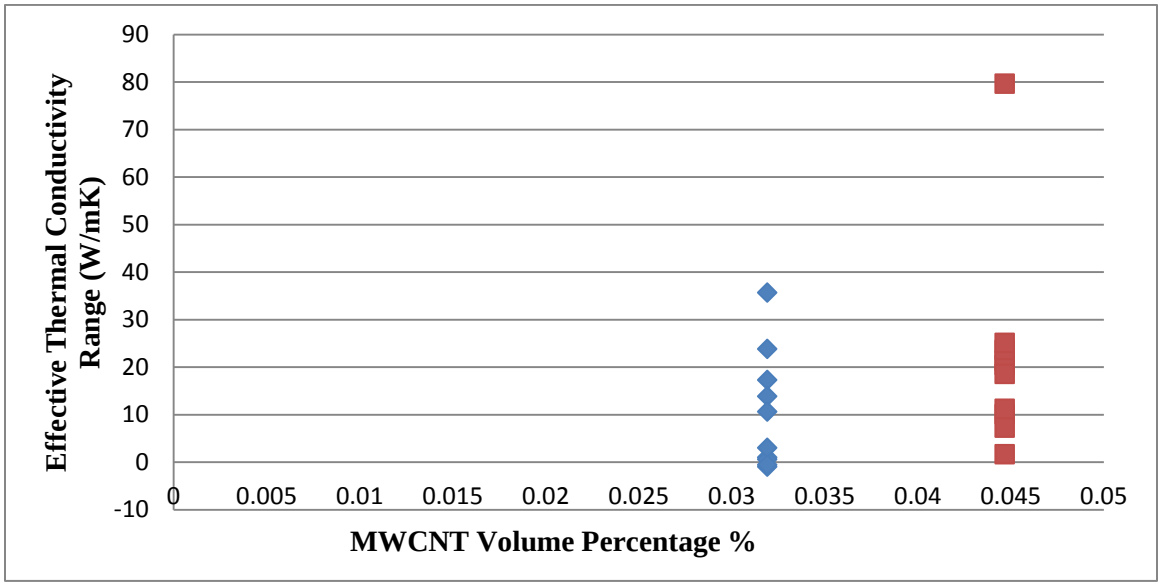

Figure A-67. Effective thermal conductivity (percent change) data range for NanoAmor Long Tailed (Stock # 1204YJ) MWCNT based cryogenic nanofluids. Test day # 8 (4/12/12).

APPENDIX B: NUMERICAL ANALYSIS PROGRAMS

B.1. Fast Data Loader: Base LOX

```
%Cryogenic Nano-Fluid Research
%Lucas Anderson
%Hot Wire thermal Conductivity Fast Data loader code
%MAE Thesis 2013

%-------------------------Fast Data Loader-----------------------------
----

clc         %Clear command window
clear all   %Clear all data
close all   %Close all figures

%Hot Wire data path
path = 'I:\MAE Masters Research\Luke Anderson Masters Thesis 2012\MAE
Thesis 2012\Results Chapter\Results\Data\Dr. Shen MWCNT\Base LOX +
MWCNT Shen 3-26-12\Base LOX\';

%Hot Wire data loader
%-------------------------------------------------------------------------
----

for A = 5:5%14

    %Set current folder path
    current = 0.3 + (A-1)*0.1;

    %Hot Wire data path
    Data.path = [path,num2str(current),' Amp\'];

    %Allow variation in current folder name
    if current < 1.0
        current_str = ['point',num2str(10*current)];
    else
        current_str = ['1point',num2str(10*(current-1))];
    end

    %Determine data set analysis range
    for data_set = 1:20%5
        for data_method = 3:3%3
            if data_method == 1
                method_str = 'start_twothirds';
            elseif data_method == 2
                method_str = 'start_onethird';
            else
                method_str = 'middle';
            end

            %Display filename and data path
            for run = 1:1%3
```

```
                disp('Data_Set'),data_set
                disp('Data Range Included'),method_str
                disp('Data Run #'),run
                Data.f_name = ['BaseLOXTest#',num2str(data_set),...
                    current_str,'A','_','3_26_12.txt'];
                Data.fig3 = ['analytic_fit#',num2str(data_set),'_',...
                    current_str,'_run',num2str(run),'_',method_str,...
                    '_','3_16_12.fig'];
                Data.fig4 =
['conductivity_error#',num2str(data_set),...
                    '_',current_str,'_run',num2str(run),'_',...
                    method_str,'_','3_26_12.fig'];
                Data.txt = ['LOXTest#',num2str(data_set),'_',...
                    current_str,'_run',num2str(run),'_',...
                    method_str,'_','3_26_12_data.mat'];
                disp(' ')
                disp(Data.f_name)

                %Call Analytical model solver
                FastDataAquisitionSimplifiedResistivity_CryoTemp(Data)
            end
        end
    end
end

%Send data to processor function
FastDataProcessorBaseLox()
```

B.2. Fast Data Loader: MWCNT Based CN

```
%Cryogenic Nano-Fluid Research
%Lucas Anderson
%Hot Wire thermal Conductivity Fast Data loader code
%MAE Thesis 2013

%-------------------------Fast Data Loader-----------------------------
----

clc         %Clear command window
clear all   %Clear all data
close all   %Close all figures

path = 'I:\MAE Masters Research\Luke Anderson Masters Thesis 2012\MAE
Thesis 2012\Results Chapter\Results\Data\Dr. Shen MWCNT\Base LOX +
MWCNT Shen 3-26-12\TC Shen MWCNT\';
%Number of carbon concentrations
NumberofCarbonTests=7;

%Hot Wire data loader
%-----------------------------------------------------------------------
----
```

```
for A = 5:5%14

    %Set current folder path
    current = 0.3 + (A-1)*0.1;


    for CarbonTests=1:NumberofCarbonTests;

        if CarbonTests==1
                VolumePercent=0.01;
                Percentstring='Point01gm';
            elseif CarbonTests==2
                VolumePercent=0.023;
                Percentstring='Point023gm';
            elseif CarbonTests==3
                VolumePercent=0.115;
                Percentstring='Point115gm';
            elseif CarbonTests==4
                VolumePercent=0.230;
                Percentstring='Point230gm';
            elseif CarbonTests==5;
                VolumePercent=0.335;
                Percentstring='Point335gm';
            elseif CarbonTests==6;
                VolumePercent=0.469;
                Percentstring='Point469gm';
            else
                VolumePercent=0.670;
                Percentstring='Point670gm';
        end

        %Hot Wire data path
        Data.path = [path,num2str(VolumePercent),' gm\'];

        %Allow variation in current folder name
        if current < 1.0
            current_str = ['Point',num2str(10*current)];
        else
            current_str = ['1point',num2str(10*(current-1))];
        end

        %Determine data set analysis range
        for data_set = 1:10

            for data_method = 3:3%3
                if data_method == 1
                    method_str = 'start_twothirds';
                elseif data_method == 2
                    method_str = 'start_onethird';
                else
                    method_str = 'middle';
                end
```

```
                %Display filename and data path
                for run = 1:1%3
                    disp('Data_Set'),data_set
                    disp('Data Range Included'),method_str
                    disp('Data Run #'),run
                    Data.f_name = ['MWCNT',...
                        Percentstring,current_str,...

'A','Test#',num2str(data_set),'_','3_26_12.txt'];
                    Data.fig3 = ['analytic_fit#',num2str(data_set)...
                        ,'_',current_str,'_run',num2str(run),'_',...
                        method_str,'_','3_26_12.fig'];
                    Data.fig4 = ['conductivity_error#',...
                        num2str(data_set),'_',current_str,'_run',...
                        num2str(run),'_',method_str,'_','3_26_12.fig'];
                    Data.txt = ['MWCNTTest#',num2str(data_set),'_',...
                        current_str,'_run',num2str(run),'_',...
                        method_str,'_','3_26_12_data.mat'];
                    disp(' ')
                    disp(Data.f_name)

                    %Call Analytical model solver

FastDataAquisitionSimplifiedResistivity_CryoTemp(Data)

                end
            end
        end

    end
end

%Send data to processor function
FastDataProcessorMWCNT()
```

B.3. Fast Data Acquisition System

```
%Cryogenic Nano-Fluid Research
%Lucas Anderson
%Hot Wire thermal Conductivity Modeling and Analysis Code
%MAE Thesis 2013

function FastDataAquisitionSimplifiedResistivity_CryoTemp(Data)

%-------------Hot Wire Thermal Conductivity Analysis Code--------------
----

% clear all                   %Clear all variables
% close all                   %Close all existing plots
% clc                         %Clear command window
```

```
% Request the text file name from the user
% disp('Please input the data text file name')

% Use uigent file to open file from GUI interface
%[f,p]=uigetfile('.txt')

%Assign file name and path to corresponding variables
f = Data.f_name;
p = Data.path;

%Read the text file name into Matlab
text_file_name=[p,f];

%Open the given file and extract the data
[Time,Col1,Col2,Col3] = textread(text_file_name,'%f%f%f%f',...
    'headerlines',22);
%------------------------------------------------------------------------
----

%Data Dictionary
%------------------------------------------------------------------------
----
%Set the given column's of data to specific channels
Ch0=Col1;
Ch1=Col2;
Ch2=Col3;

%Set Wire properties
Diameter=1.27*10^-4;                            %(Meter)
Length=0.161;                                   %(Meter)
Area=(pi()*(Diameter^2))/4;                     %(Meter^2)

%Shunt Voltage
ShuntVoltage=Ch2;                               %(Volts)

%Shunt Current
ShuntCurrent=1.0*(Ch2/0.01);                    %(Amps)

%Hot Wire Current
HWCurrent=mean(ShuntCurrent(25000:35000));      %(Amps) Mean Shunt
Value

%Hot Wire Voltage
HWVoltage=Ch0-Ch1;                              %(volts)

%Hot Wire Resistance
HWResistance=HWVoltage/HWCurrent;               %(Ohms)

%Hot Wire Power
HWPower=HWVoltage*HWCurrent;                    %(Watts)
```

```
%-------------------------------------------------------------------------
----

%Post Process Data
%-------------------------------------------------------------------------
----
%Smooth Hot Wire Resistance
WsmoothResistance=smooth(HWResistance,300,'moving');            %(Ohms)

%Calculate the Hot Wire Resistivity
HWResistivity=(HWResistance)*((pi()*((Diameter^2)/4))/Length);
%(Ohm*Meter)

%Calculate the Log of Time
logtime=log(Time);
%(Seconds)
%-------------------------------------------------------------------------
----

%Plot the Hot Wire Current & Pick out possible time shift region
%-------------------------------------------------------------------------
----
figure(1)
plot(Time,ShuntCurrent)
title('Shunt Current')
xlabel('Time (Seconds)'), ylabel('Current (Amps)')
legend('Shunt Current',2)
%-------------------------------------------------------------------------
----

%HW Power Transition Point
%-------------------------------------------------------------------------
----

%Determine the time value and location of the transient power up
[ShuntCurrentSizeOfArray offaxis]=size(ShuntCurrent);

for ShuntCurrentCounter=1:(ShuntCurrentSizeOfArray)/2;

    ShuntCurrentDifference=(ShuntCurrent(ShuntCurrentCounter+25))...
        -(ShuntCurrent(ShuntCurrentCounter));

    if
(ShuntCurrentDifference>(abs(ShuntCurrent(ShuntCurrentCounter))*5.))
        break

    else

    end
end
```

```
%Set the minimum and maximum allowed time shifts
xpos(1)=Time(ShuntCurrentCounter-1000);
xpos(2)=Time(ShuntCurrentCounter+1000);
jcount=xpos(1);
icount=xpos(2);

%Calculate the array locations that correspond to the given mouse
clicks
[min_difference1, array_position1] = min(abs(Time-jcount));
[min_difference2, array_position2] = min(abs(Time-icount));
jcount=array_position1;
icount=array_position2;
%-------------------------------------------------------------------------
----


%Calculate the platinum wire's resistivity based upon Berry's Method
%-------------------------------------------------------------------------
----

%Berry's Resistivity
[BerryTemperature,BerryResistivity] = ...
    textread('BerryResistivity.txt','%f%f');
%(Ohm*Meter)

%Berry's Resistance
BerryResistance=BerryResistivity*(Length/Area);             %(Ohms)

%Hot Wire Temperature Calculation
%(Interpolated from R. J. Berry's resistivity data)
HWTemperature=interp1(BerryResistance,BerryTemperature,...
    HWResistance,'cubic');                                  %(Kelvin)

%Smooth the raw/rough data
Wsmooth=smooth(HWTemperature,300,'moving');
SplineFitTemperature=spline(BerryResistance,...
    BerryTemperature,WsmoothResistance);                    %(Kelvin)
%-------------------------------------------------------------------------
----

%Plot the Hot Wire Temperature & pick area to be analytically curve
fitted
%-------------------------------------------------------------------------
----

figure(2)
plot(logtime(jcount:size(Time)),HWTemperature...
    (jcount:size(HWTemperature)),'b')
hold on
plot(logtime(jcount:size(Time)),...
    SplineFitTemperature(jcount:size(Wsmooth)),'r')
title('Hot Wire Temperature')
```

```
xlabel('Time (Seconds)'), ylabel('Temperature (Kelvin)')
legend('HW Temperature',2)
%-------------------------------------------------------------------
----

%Calculate the start and end points of the analytical temperature curve
fit
%-------------------------------------------------------------------
----

%Determine the analytical model start time
HotWireTemperatureStartposition=ShuntCurrentCounter+500;

%Determine the array position of the maximum temperature
[HWTemperatureMaxValue,MAXTempPosition]=...
    max(SplineFitTemperature(ShuntCurrentCounter+500:end-500));

%Determine the analytical model end time
HotWireTemperatureEndposition=nearest((1./2.)*...
    (MAXTempPosition+ShuntCurrentCounter+500+500));

%Determine the array positions of the model start and end times
position1=logtime(HotWireTemperatureStartposition);
position2=logtime(HotWireTemperatureEndposition);

%Calculate the array positions of the start and end times
[min_difference1, array_position1] = min(abs(logtime-position1));
[min_difference2, array_position2] = min(abs(logtime-position2));

%Set the final array positions for analytical model start and end times
position1=array_position1;
position2=array_position2;
Position1=array_position1;
Position2=array_position2;
%-------------------------------------------------------------------
----

%------------------General Hot Wire PlotsPlotting-------------------
----

%Query the user about plotting intermediate plots
%answer=input('Would you like to plot intermediate values--
Yes=1,No=2');

%Possible pause for user decision
%pause

%Default user answer
answer=2;

%Plot the intermediate figures
```

```
if (answer==1)

    %Shunt Current
    %-------------------------------------------------------------------
----
    figure(3)
    hold on
    plot(Time,ShuntCurrent)
    title('Shunt Current')
    xlabel('Time (Seconds)'), ylabel('Current (Amps)')
    legend('Shunt Current',2)
    %-------------------------------------------------------------------
----

    %Hot Wire voltage
    %-------------------------------------------------------------------
----
    figure(4)
    hold on
    plot(Time,HWVoltage)
    title('Hot Wire Voltage')
    xlabel('Time (Seconds)'), ylabel('Voltage (Volts)')
    legend('HW Voltage',2)
    %-------------------------------------------------------------------
----

    %Hot Wire Resistance
    %-------------------------------------------------------------------
----
    figure(5)
    hold on
    plot(Time,HWResistance)
    title('Hot Wire Resistance')
    xlabel('Time (Seconds)'), ylabel('Resistance (Ohms)')
    legend('HW Resistance',2)
    %-------------------------------------------------------------------
----

    %Hot Wire Power
    %-------------------------------------------------------------------
----
    figure(6)
    hold on
    plot(Time,HWPower)
    title('Hot Wire Power')
    xlabel('Time (Seconds)'), ylabel('Power (Watts)')
    legend('HW Power',2)
    %-------------------------------------------------------------------
----

    %Hot Wire Temperature
```

```
    %-------------------------------------------------------------------
----
    figure(7)
    plot(Time(icount:size(Time)),HWTemperature...
        (icount:size(HWTemperature)),'b')
    hold on
    plot(Time(icount:size(Time)),SplineFitTemperature...
        (icount:size(SplineFitTemperature)),'g')
    title('Hot Wire Temperature')
    xlabel('Time (Seconds)'), ylabel('Temperature (Kelvin)')
    legend('HW Temperature','Moving Average',2)
    %-------------------------------------------------------------------
----

    %Bery's Resistivity
    %-------------------------------------------------------------------
----
    figure(8)
    hold on
    plot(BerryTemperature,BerryResistivity)
    title('Temperature vs. Resistivity')
    xlabel('Temperature (Kelvin)'), ylabel('Resistivity (Ohms Meters)')
    legend('HW Resistivity',2)
    %-------------------------------------------------------------------
----

    %Bery's Resistance
    %-------------------------------------------------------------------
----
    figure(9)
    hold on
    plot(BerryTemperature,BerryResistance)
    title('Temperature vs. Resistance')
    xlabel('Temperature (Kelvin)'), ylabel('Resistivity (Ohms)')
    legend('HW Resistance',2)
    %-------------------------------------------------------------------
----

elseif (answer==2)
    %Skip intermediate plotting
    'You have chosen not to plot intermediate values'

end
%-----------------------------------------------------------------------
----

%Hot Wire Power Calculation
%-----------------------------------------------------------------------
----

%Calculate the smoothed power
```

```
smoothedpower=smooth(HWPower,300,'moving');
%(Watts)

%Calculate the average power value within the model time period
SystemPower=(mean(smoothedpower(position1:position2)))/Length;
%(Watts)
%-------------------------------------------------------------------------
----

%Analytical Model Solution
%-------------------------------------------------------------------------
----

%Determine the appropriate LOX properties based on temperature
[LOXTemperature,LOXK,LOXDensity,LOXCP] = textread...
    ('LOXProperties.txt','%f%f%f%f');

%Determine the average temperature
MidRangeTemperature=round(((SplineFitTemperature(position2)...
    -SplineFitTemperature(position1))/2.0)+...
    SplineFitTemperature(position1));

%Determine the fluid properties that correspond to the average
temperature
[PropertyMin,PropertyArrayPosition]=min...
    (abs(MidRangeTemperature-LOXTemperature));

%Set the material properties
KLOX=LOXK(PropertyArrayPosition);
fluiddensity=LOXDensity(PropertyArrayPosition);
fluidCp=LOXCP(PropertyArrayPosition);

%Calculate the materials thermal diffusivity
alphaf=KLOX/(fluiddensity*fluidCp);

%Calcuate the materials initial temperature
InitialTemp=(mean(HWTemperature(icount:icount+1000)));

%Set the analytical models parameters and initial values
stepsize=30;
loopcounter=0;
ShiftedTime=Time;                                    %(Seconds)
Xshiftedtime=(ShiftedTime(:)+Time(jcount));          %(Seconds)
KLOXguess=.1;
%(Watts/Meter*Kelvin)
%-------------------------------------------------------------------------
----

%Use lsqnonlin to curve fit the analytical hot wire solution to the
given
%hot wire data
```

```
%-------------------------------------------------------------------------
----

TimeShiftingArraySize=floor((icount-(nearest(jcount/2.)))/stepsize);

%Preallocate model arrays
conductivityarray(1:TimeShiftingArraySize)=NaN;
InitialTemparray(1:TimeShiftingArraySize)=NaN;
XTimearraystartingtime(1,1:TimeShiftingArraySize)=NaN;
resnormarray(1:TimeShiftingArraySize)=NaN;
uncertainty(1:TimeShiftingArraySize)=NaN;

%Begin iterative time shifting loop
for shift=nearest(jcount/2):stepsize:icount

        %Keep track of loop iterations
        i=position1;
        loopcounter=loopcounter+1;

        %Shifted time array
        shiftarray(loopcounter)=shift;

        %Analytical model time array
        X=(Time((position1:position2)))-Time(shift);    %(Seconds)

        %Analytical model temperature array
        Y=SplineFitTemperature(position1:position2);    %(Kelvin)

        %Send material properties and model parameters to analytical
model
        X0=[KLOXguess InitialTemp SystemPower fluiddensity fluidCp];

        options = optimset('Largescale','off');

        % Calculate new analytical model coefficients using LSQNONLIN.
        [x, resnorm, residual]=lsqnonlin(@fit_simp,X0,[],[],...
            options,X,Y,SystemPower,Diameter,fluiddensity,fluidCp);


        %Calculate the uncertainty in percent
        conductivityarray(loopcounter)=x(1);
        InitialTemparray(loopcounter)=x(2);
        XTimearray(:,loopcounter)=X;

XTimearraystartingtime(1,loopcounter)=XTimearray(1,loopcounter);
        resnormarray(loopcounter)=resnorm;
        Errorfinal=abs((x(1)-KLOX)/KLOX)*100;
        uncertainty(loopcounter)=Errorfinal;

        %Check for NAN numbers
        NANcheck=isnan(resnorm);
```

```
        if NANcheck==1;

            break

        else

       end

    %end

end
%-------------------------------------------------------------------------
----

%Calculate final answer and minimum uncertainty
%-------------------------------------------------------------------------
----

%Calculate the time shift with the smallest residual of the normes
[minimumresnorm, Indexresnorm]=min(resnormarray);

%Calculate the final minimum uncertainty
[minimumuncertainty,Index]=min(uncertainty);

%Determine the solved for analytical model coefficients
x(1)=conductivityarray(Indexresnorm);
x(2)=InitialTemparray(Indexresnorm);
X=XTimearray(:,Indexresnorm);

startposition=i;

%Resolve the analytical Hot Wire temperature model with new
coefficients
interior=((1./X*((Diameter/2)^2)/(4*(x(1)/(x(4)*x(5))))));
firstbit=((x(3))/(4*pi()*x(1)));
diffnew=(firstbit*real(EXPINT(interior)))+x(2);
%-------------------------------------------------------------------------
----

%Test the fit of the data.
Percentfit=((Y-diffnew)./Y)*100;

%Plot the smoothed hot wire temperature
%-------------------------------------------------------------------------
----
figure(10)
plot(logtime,SplineFitTemperature,'r','linewidth',6)
title('Smoothed Hot Wire Temperature vs Log of Time')
xlabel('LogTime (Seconds)'),ylabel('HW Temperature (Kelvin)')
legend('HW Temperature',2)
```

```
%-------------------------------------------------------------------------
----

%Plot analytical solution superimposed on given data
%-------------------------------------------------------------------------
----
fig_handle = figure(11);
[AX,H1,H2]=plotyy(Time(startposition:position2),...
    HWTemperature(startposition:position2),...
    Time(startposition:position2),Percentfit,'plot');
hold on
plot(Time(startposition:position2),HWTemperature...
    (startposition:position2),'b','linewidth',1)
hold on
plot(Time(startposition:position2),diffnew(:),'y','linewidth',3)
hold on
plot(Time(startposition:position2),Percentfit(:),'r','linewidth',3)
title('Hot Wire Temperature Analytical Curve Fit')
set(get(AX(1),'Ylabel'),'String','Temperature (Kelvin)') ;
set(get(AX(2),'Ylabel'),'String',...
    'Analytical Fit Percent Difference (Percent)');
xlabel('Time (Seconds)'), ylabel('Temperature (Kelvin)')
legend('HW Temperature',2)
saveas(fig_handle,[Data.path,Data.fig3]);
%-------------------------------------------------------------------------
----

%Plot residual of the norms and overall uncertainty
%-------------------------------------------------------------------------
----
fig_handle = figure(12);
plot(XTimearraystartingtime,resnormarray,'r','linewidth',3)
hold on
plot(XTimearraystartingtime,uncertainty,'y','linewidth',3)
title('HW Goodness of Fit Model')
xlabel('Time (Seconds)'), ylabel('Fit (Percent)')
legend('Residual of the Norm',2)
saveas(fig_handle,[Data.path,Data.fig4]);

%fid = fopen([Data.path,Data.txt]);

%Print solution data to screen
strFileName=sprintf('File Name= %33s',f);
%fprintf(fid,strFileName,'%c');
disp(strFileName)

strminuncertainty=sprintf...
    ('The Absolute Minimum Uncertainty ...is %8.4g Percent'...
    ,minimumuncertainty);
%fprintf(fid,strminuncertainty,'%c');
disp(strminuncertainty)
```

```
strBestFitUncertainty=sprintf...
    ('The Best Fit Uncertainty is %8.4g Percent',uncertainty...
    (Indexresnorm));
%fprintf(fid,strBestFitUncertainty,'%c');
disp(strBestFitUncertainty)

strBestFitConductivity=sprintf...
    ('The Best Fit Thermal Conductivity is %8.4g W/mK',...
    conductivityarray(Indexresnorm));
%fprintf(fid,strBestFitConductivity,'%c');
disp(strBestFitConductivity)

strBestFitTimeShift=sprintf...
    ('The Best Fit Time Shift is %8.4g Seconds',...
    Time(shiftarray(Indexresnorm)));
%fprintf(fid,strBestFitTimeShift,'%c');
disp(strBestFitTimeShift)

strBestFitStartTime=sprintf...
    ('The Best Fit Start Time is %8.4g Seconds',...
    XTimearraystartingtime(Indexresnorm));
%fprintf(fid,strBestFitStartTime,'%c');
disp(strBestFitStartTime)

%fprintf(fid,x,'%10.6f %10.6f %10.6f %10.6f %10.6f %10.6f');
save([Data.path,Data.txt],...
    'strFileName','strminuncertainty','strBestFitUncertainty',...
    'strBestFitConductivity','strBestFitTimeShift',...
    'strBestFitStartTime','x')

%Save all Data from current workspace
save([Data.path,Data.txt])

disp(KLOX)

%User pause Function
%pause

clc, clear all, close all
```

B.4. Least Squares Nonlinear Curve Fit Subroutine

```
function diff = fit_simp(x,X,Y,SystemPower,Diameter,...
    fluiddensity,fluidCp)
% This function is called by lsqnonlin.
% x is a vector which contains the coefficients of the
% equation.  X and Y are the option data sets that were
% passed to lsqnonlin.
```

```
%Model Coefficients
A=x(1);
B=x(2);

%Analytical Hot Wire temperature model
diff = ((SystemPower/(4.0*pi()*A))*real(expint((1./(X))*...
    (((Diameter/2)^2)/((4.0*A)/(fluiddensity*fluidCp)))))+B)-Y;

end
```

B.5. Fast Data Processor: Base LOX

```
%%Cryogenic Nano-Fluid Research
%Lucas Anderson
%Hot Wire thermal Conductivity Fast Data loader code
%MAE Thesis 2013

%function FastDataProcessor()

%-------------------------Fast Data Processor-------------------------
----

clc         %Clear command window
clear all   %Clear all data
close all   %Close all figures

%Preallocate arrays
error(1,1:10,1,1:3) = NaN;
k(1,1:10,1,1:3) = NaN;

%Set Hot Wire data file path
path = 'I:\MAE Masters Research\Luke Anderson Masters Thesis 2012\MAE
Thesis 2012\Results Chapter\Results\Data\Dr. Shen MWCNT\Base LOX +
MWCNT Shen 3-26-12\Base LOX\';

%Initialize the Current value
A=1;

%Student T uncertainty coefficient
t95=2.093;

%Select data analysis method
data_method=1;

%Assign testing current value
current = 0.7;

%Create Hot Wire data file path
Path = [path,num2str(current),' Amp\'];
```

```
%Set the current folder path
current_str = ['Point',num2str(10*current)];

%File Directory Information
Date='3/26/12';
Filename='BaseLOXData_3_26_12.txt';
FileAddress= [Path,Filename];
fileID = fopen(FileAddress,'wt');

%------------------------------------------------------------------------
----

%----------------------Read in Hot Wire data sets----------------------
----

    %Data set loop
    for data_set = 1:20

            %Data set analysis method
            method_str = 'middle';

            %Data run loop
            for run = 1:1
                Fname =
['LOXTest#',num2str(data_set),'_',current_str,...
                    '_run',num2str(run),'_',method_str,...
                    '_','3_26_12_data.mat'];

                %Create temporary path and filename
                temp = open([Path,Fname]);

                %Create an error array
                error(A,data_set,data_method,run) = str2double...
                    (temp.strBestFitUncertainty(28:36));

                %Create a conductivity array
                k(A,data_set,data_method,run) = str2double...
                    (temp.strBestFitConductivity(37:46));

                %Create an expected (NIST) conductivity array
                ExpectedKArray(data_set,run)=temp.KLOX;


            end

    end
%------------------------------------------------------------------------
----
```

```
%Create Variables For Potential Base LOX Analysis
%-------------------------------------------------------------------------
----
%Read in possible Hot Wire current values
[HWCurrents] = textread('HWCurrents.txt','%f');

%Read in fluid properties
[LOXTemperature,LOXK,LOXDensity,LOXCP] = textread...
    ('LOXProperties.txt','%f%f%f%f');
%-------------------------------------------------------------------------
----

%----------------------Post process Hot Wire Data----------------------
----
     %Determine total test average conductivities and errors
     for data_set=1:20

         for run=1:1

                %Create a temporary error array
                Temprunserror(run)=error(A,data_set,data_method,run);

                %Create a temporary conductivity array

Temprunsconductivity(run)=k(A,data_set,data_method,run);

         end

                %Average the calculated errors
                Tempaveragerunserror(data_set)=mean(Temprunserror);

                %Average the calculated conductivity values
                Tempaveragerunsconductivity(data_set)=mean...
                    (Temprunsconductivity);

     end


%Calculate the total averages for the calculated thermal conductivity
%-------------------------------------------------------------------------
----
%Calculate the total average error
ErrorTotalAverage=mean(Tempaveragerunserror);

%Calculate the total average conductivity
ConductivityTotalAverage=mean(Tempaveragerunsconductivity);
%-------------------------------------------------------------------------
----

%Create a testnumber matrix
testnumber=[1, 2, 3, 4, 5, 6, 7, 8, 9, 10, 11, 12, 13, 14, 15,...
```

```
    16, 17, 18, 19, 20];

%Determine the size and shape of the test matrix
[Rows SampleSize]=size(testnumber(1,:));

%Preallocate the outlier test
Outliersize(SampleSize)=0.;

%Chauvenets criteria coefficient
SampleCriterion=2.24;

%Chauvenents criteria
Chauvenets=SampleCriterion*(std(Tempaveragerunsconductivity));

%Test for outliers
for counter=1:SampleSize



   if
((Tempaveragerunsconductivity(counter)>ConductivityTotalAverage...
           +Chauvenets) || (Tempaveragerunsconductivity...
           (counter)<ConductivityTotalAverage-Chauvenets))

        Outlier(counter)=Tempaveragerunsconductivity(counter);
        OutlierDataSet=counter;

       fprintf('Outliers Detected')
       pause
   else

      fprintf('No Outliers exist')

   end

end


%Calculate the array total mean values of error and conductivity
%-------------------------------------------------------------------------
----
ArrayErrorTotalAveragePercent(1:data_set,1)=mean...
    (Tempaveragerunserror);
ArrayConductivityTotalAverage(1:data_set,1)=mean...
    (Tempaveragerunsconductivity);
%-------------------------------------------------------------------------
----
%Calculate the total NIST uncertainty and average NIST conductivity
Expectedk=mean(ExpectedKArray);
AverageExpectedkArray(testnumber)=Expectedk;
```

```
NISTUncertainty=Expectedk*.02;

%Calculate the Standard Deviation
%-------------------------------------------------------------------------
----
StandardDeviationError=std(Tempaveragerunserror);
StandardDeviationConductivity=std(Tempaveragerunsconductivity);

%Calculate the Random Standard Deviation
RandomStandardDeviationConductivity=StandardDeviationConductivity/...
    sqrt(SampleSize);
%-------------------------------------------------------------------------
----

%Calculate the average Bias Value
%-------------------------------------------------------------------------
----
%Final Average Bias Value
BiasThermalkFinal=abs(ConductivityTotalAverage-Expectedk);

%Calculate the total uncertainty with bias
BiasTotalUncertainty=(t95.*(sqrt((BiasThermalkFinal.^2)+...
    (RandomStandardDeviationConductivity^2)))./2.;

%Calculate the total uncertainty with bias (Percent)
BiasTotalUncertaintyPercent=(t95.*(sqrt((BiasThermalkFinal.^2)...
    +(RandomStandardDeviationConductivity^2))./...
    ConductivityTotalAverage).*100;

AverageBiasTotalUncertaintyPercent=mean(BiasTotalUncertaintyPercent);

%Create a total bias matrix
BiasTotalUncertaintyMatrix=BiasTotalUncertainty;
%-------------------------------------------------------------------------
----

%Calculate the random uncertainties (w/t bias)
%-------------------------------------------------------------------------
----
%Random uncertainties
TotalUncertaintyhigh=(t95*(StandardDeviationConductivity/...
    sqrt(SampleSize)));
TotalUncertaintylow=(t95*(StandardDeviationConductivity/...
    sqrt(SampleSize)));

%Random uncertainties (Percent)
TotalUncertaintyhighlowPercent=(TotalUncertaintyhigh/ConductivityTotalA
verage)*100;

%Total random uncertainty matrices
TotalUncertaintyhighMatrix(1:SampleSize)=TotalUncertaintyhigh;
```

```
TotalUncertaintylowMatrix(1:SampleSize)=TotalUncertaintylow;
%-------------------------------------------------------------------------
----

%NIST uncertainty matrix
NISTUncertaintyMatrix(1:SampleSize)=NISTUncertainty;

%Figure Save File Directory
Data.path = [path,num2str(current),' Amp\'];

%Plot the callibration error
fig_handle = figure(1);
plot(testnumber,Tempaveragerunserror,'-.b*','linewidth',3)
hold on
plot(testnumber,ErrorTotalAverage,'-.r*','linewidth',3)
title({'Base LOX k Error (Percent)'; Date})
xlabel('Test #'), ylabel('Error (Percent)')
legend('Base LOX Error (Percent)','Total Averaged Error (Percent)',4)
saveas(fig_handle,[Data.path,'PercentError']);

%Plot the calculated thermal conductivity vs. NIST conductivity
fig_handle = figure(2);
errorbar(testnumber,Tempaveragerunsconductivity,...
    TotalUncertaintylowMatrix,TotalUncertaintyhighMatrix,...
    '-.b*','linewidth',3)
hold on
errorbar(testnumber,ExpectedKArray,NISTUncertaintyMatrix,...
    NISTUncertaintyMatrix,'-.gx','linewidth',3)
hold on
plot(testnumber,AverageExpectedkArray,'-.ms','linewidth',2)
hold on
plot(testnumber,ConductivityTotalAverage,'-.rd','linewidth',2)
title({'Base LOX Thermal Conductivity';Date});
xlabel('Test #'), ylabel('Thermal K (W/mK)')
legend...
   ('Calculated LOX k','Published k Value',...
   'Average Published k','Averaged Calculated k',4)
saveas(fig_handle,[Data.path,'ConductivityError']);

%Write Salient data to text file
str1='Total Averaged Conductivity Error=';
str2='Total Averaged Conductivity Error(Percent)=';
str3='Thermal Conductivity Bias';
str4='Thermal Conductivity Bias (Percent)';
str5='Student T Random Uncertainty';
str6='Student T Random Uncertainty (Percent)';
str7='NIST Uncertainty';
str8='Average Expected k';

%Write data
fprintf(fileID,'%40s %10.6g \n',str1,ConductivityTotalAverage)
fprintf(fileID,'%40s %10.6g \n',str2,ErrorTotalAverage)
```

```
fprintf(fileID,'%40s %10.6g \n',str3,BiasThermalkFinal)
fprintf(fileID,'%40s %10.6g \n',str4,ErrorTotalAverage)
fprintf(fileID,'%40s %10.6g \n',str5,TotalUncertaintylow)
fprintf(fileID,'%40s %10.6g \n',str6,TotalUncertaintyhighlowPercent)
fprintf(fileID,'%40s %10.6g \n',str7,NISTUncertainty)
fprintf(fileID,'%40s %10.6g \n',str8,Expectedk)

%Close File ID
fclose(fileID);

%Send job completion and results script
% %Matlab Send E-mail when Job Complete
% setpref('Internet', 'E_mail', 'l.s.anderson@aggiemail.usu.edu');
% setpref('Internet', 'SMTP_Username',
'l.s.anderson@aggiemail.usu.edu');
% setpref('Internet', 'SMTP_Password', 'lsloveNB#21');
% setpref('Internet', 'SMTP_Server', 'smtp.gmail.com');
% props = java.lang.System.getProperties;
% props.setProperty('mail.smtp.auth','true');
% props.setProperty('mail.smtp.socketFactory.class',...
%'javax.net.ssl.SSLSocketFactory');
% props.setProperty('mail.smtp.socketFactory.port', '465');
% sendmail('l.s.anderson@aggiemail.usu.edu','JOB complete.',...
%'Calculation Complete',{'ThermalConductivityError.jpg',...
%'PercentError.jpg','BaseLOXData.txt'})
```

B.6. Fast Data Processor: MWCNT Based CN

```
%Cryogenic Nano-Fluid Research
%Lucas Anderson
%Hot Wire thermal Conductivity Fast Data loader code
%MAE Thesis 2013

%function FastDataProcessorMWCNT()

%-------------------------Fast Data Processor-------------------------
----

clc         %Clear command window
clear all   %Clear all data
close all   %Close all figures


%--------------------Fast Precessor Variables-------------------------
---
%--------------------------------------------------------------------
---
Date='3/26/12';

%Set the NIST uncertainty based upon callibration data
LOXTotalUncertainty=0.001939;
```

```
%Set the NIST bias based upon callibration data
BaseLOXFinalBias=.0105;

BaseLOXFinalBiasPercent=6.671;

%Set the NIST total uncertainty based upon callibration data
NISTTotalUncertainty=0.003168;
%-------------------------------------------------------------------------
----
%-------------------------------------------------------------------------
----

%Preallocate arrays
error(1,1:10,1,1:3) = NaN;
k(1,1:10,1,1:3) = NaN;

%Set Hot Wire data file path
path = 'I:\MAE Masters Research\Luke Anderson Masters Thesis 2012\...
MAE Thesis 2012\Results Chapter\Results\Data\Dr. Shen MWCNT\...
    Base LOX + MWCNT Shen 3-26-12\TC Shen MWCNT\';

%Initialize the test number matrix
testnumber=[1; 2; 3; 4; 5; 6; 7; 8; 9; 10;];

%Specify number of carbon tests
NumberofCarbonTests=5;

%Create a loop to run through the various particle concentrations
for CarbonTests=1:5;%NumberofCarbonTests;

    %Initialize the Current value
    A=1;

    %Select data analysis method
    data_method=1;

    %Assign testing current value
    current = 0.7;

        %Select carbon test value
        if CarbonTests==1
                MWCNTMass=0.01;
                Percentstring='Point01gm';
                str='Volume Percent=0.00149% (0.01gm)';
                VolumePercent='By Volume 0.000952 %';
            elseif CarbonTests==2
                MWCNTMass=0.023;
                Percentstring='Point023gm';
                str='Volume Percent=0.00343% (0.023gm)';
                VolumePercent='By Volume 0.00219 %';
```

```
            elseif CarbonTests==3
                MWCNTMass=0.115;
                Percentstring='Point115gm';
                str='Volume Percent=0.017% (0.115gm)';
                VolumePercent='By Volume 0.01095 %';
             elseif CarbonTests==4
                MWCNTMass=0.230;
                Percentstring='Point230gm';
                VolumePercent='By Volume 0.0219 %';
            elseif CarbonTests==5
                MWCNTMass=0.469;
                Percentstring='Point469gm';
                VolumePercent='By Volume 0.0447 %';
%                 MWCNTMass=0.335;
%                 Percentstring='Point335gm';
%                 MassPercent='By Mass 0.0319 %';
            elseif CarbonTests==6;
                MWCNTMass=0.469;
                Percentstring='Point469gm';
                VolumePercent='By Volume 0.0447 %';
            else
                MWCNTMass=0.670;
                Percentstring='Point670gm';
                VolumePercent='By Mass 0.0638 %';
        end

%Percent string
Percentstring='Percent';

%Create Hot Wire data file path
Path = [path,num2str(MWCNTMass),' gm\'];
TitleExtension=['MWCNT Mass=',num2str(MWCNTMass),' gm'];

%File directory information
Filename='MWCNTData_3_26_12.txt';
FileAddress= [Path,Filename];
fileID = fopen(FileAddress,'wt');

%Set the current folder path
current_str = ['Point',num2str(10*current)];

    %Data set loop
    for data_set = 1:10

                method_str = 'middle';

            %Data set run loop
            for run = 1:1

                %Hot Wire data filename
                Fname = ['MWCNTTest#',num2str(data_set),'_',...
                    current_str,'_run',num2str(run),'_',...
```

```
                    method_str,'_','3_26_12_data.mat'];

                %Filename and data path variable
                temp = open([Path,Fname]);

                %Create an error array
                error(A,data_set,data_method,run) = str2double...
                    (temp.strBestFitUncertainty(28:36));

                %Create a conductivity array
                k(A,data_set,data_method,run) = str2double...
                    (temp.strBestFitConductivity(37:46));

                %Create an expected (NIST) conductivity array
                ExpectedKArray(data_set,run)=temp.KLOX;


            end

    end


%Create Variables For Potential Base LOX Analysis
%-------------------------------------------------------------------------
----
%Read in possible Hot Wire current values
[HWCurrents] = textread('HWCurrents.txt','%f');

%Read in fluid properties
[LOXTemperature,LOXK,LOXDensity,LOXCP] = textread...
    ('LOXProperties.txt','%f%f%f%f');
%-------------------------------------------------------------------------
----


%----------------------Post process Hot Wire Data----------------------
----

            %Determine total test average conductivities and errors
         for data_set=1:10

            for run=1:1

                %Create a temporary error array
                Temprunserror(run)=error(A,data_set,data_method,run);

                %Create a temporary conductivity array

Temprunsconductivity(run)=k(A,data_set,data_method,run);
```

```
            end

                %Average the calculated errors
                Tempaverageerunserror(data_set)=mean(Temprunserror);

                %Average the calculated conductivity values
                Tempaverageerunsconductivity(data_set)=mean...
                    (Temprunsconductivity);

        end

%Calculate the total averages for the calculated thermal conductivity
%-------------------------------------------------------------------------
----
%Calculate the total average thermal conductivty percent change
AverageTotalIncreasekPercent=mean(Tempaverageerunserror);

%Calculate the total average thermal conductivity change
TotalAveragekchange=mean(Tempaverageerunsconductivity);
%-------------------------------------------------------------------------
----

%Calculate the array total mean values of conductivity change
%-------------------------------------------------------------------------
----
AverageConductivityArray(testnumber)=TotalAveragekchange;

%Total Average Conductivity (Percent)
AverageConductivityArrayPercent(testnumber)=...
    AverageTotalIncreasekPercent;
%-------------------------------------------------------------------------
----

%Add in the base LOX bias values calculated previously
%-------------------------------------------------------------------------
----

%Add in the calculated final bias value to the Delta k value
TotalAveragekchangeBias=TotalAveragekchange+BaseLOXFinalBias;

%Add in the calculated final bias value to the Delta k value (Percent)
AverageTotalIncreasekPercentBias=AverageTotalIncreasekPercent+...
    BaseLOXFinalBiasPercent;

%Account for bias in array variables
AverageConductivityArray(testnumber)=TotalAveragekchange+...
    BaseLOXFinalBias;

AverageConductivityArrayPercent(testnumber)=...
    AverageTotalIncreasekPercent+...
    BaseLOXFinalBiasPercent;
```

```
%Update temporary calculated k change arrays
TempaveragerunsconductivityBias=Tempaveragerunsconductivity+...
    BaseLOXFinalBias;

TempaveragerunserrorBias=Tempaveragerunserror+BaseLOXFinalBiasPercent;
%-------------------------------------------------------------------------
----
%-------------------------------------------------------------------------
----

%Convert the NIST Uncertainty, and the Random uncertainty to array
values
%-------------------------------------------------------------------------
----
%Random uncertainty
LOXTotalUncertaintyMatrix(testnumber)=LOXTotalUncertainty;

%NIST uncertainty
NISTTotalUncertaintyMatrix(testnumber)=NISTTotalUncertainty;
%-------------------------------------------------------------------------
----

%Determine the size and shape of the test matrix
[Rows SampleSize]=size(testnumber(1,:));

%Preallocate the outlier test
Outliersize(testnumber)=0.;

%Account for possible outliers within the data
%-------------------------------------------------------------------------
----
%Chauvenets criteria coefficient
SampleCriterion=2.24;

%Chauvenents criteria
Chauvenets=SampleCriterion*(std(TempaveragerunsconductivityBias));

%Test for outliers
for counter=1:SampleSize

   if
((TempaveragerunsconductivityBias(counter)>TotalAveragekchangeBias...
          +Chauvenets) || (TempaveragerunsconductivityBias(counter)...
          <TotalAveragekchangeBias-Chauvenets))

        Outlier(counter)=Tempaveragerunsconductivity(counter);
        OutlierDataSet=counter;

        fprintf('Outliers Detected')
```

```
    else

        fprintf('No Outliers exist')

    end

end
%-------------------------------------------------------------------------
----

%Calculate the Standard Deviation
StandardDeviationError=std(TempaveragerunserrorBias);
StandardDeviationConductivity=std(TempaveragerunsconductivityBias);

%Create a NIST expected conductivity array
AverageExpectedk=mean(ExpectedKArray);

%Average Expected k Array
AverageExpectedkArray(1:data_set,1)=mean(ExpectedKArray);

%Calculate The Final Total Average Magnitude Change In Delta k
AverageCNFMWCNTDeltak=abs(AverageExpectedk-TotalAveragekchangeBias);

%Figure Save File Directory
Data.path = [path,num2str(MWCNTMass),' gm\'];

%Plot the nanofluid thermal conductivity percent change
fig_handle = figure(1);
plot(testnumber,TempaveragerunserrorBias,'-.b*','linewidth',3)
hold on
plot(testnumber,AverageTotalIncreasekPercentBias,'.r','linewidth',3)
title({'MWCNT Delta k (Percent)'; Date; TitleExtension; VolumePercent})
xlabel('Test #'), ylabel('Delta k (Percent)')
legend('HW Delta k','Total Averaged Delta k',1)
saveas(fig_handle,[Data.path,'Delta k (Percent)'])

%Plot the nanofluid thermal conductivity change
fig_handle = figure(2);
errorbar(testnumber,TempaveragerunsconductivityBias,...
    LOXTotalUncertaintyMatrix,LOXTotalUncertaintyMatrix,...
    '-.b*','linewidth',2)
hold on
errorbar(testnumber,ExpectedKArray,NISTTotalUncertaintyMatrix,...
    NISTTotalUncertaintyMatrix,'-.g*','linewidth',2)
hold on
plot(testnumber,AverageExpectedkArray,'-.ms','linewidth',2);
hold on
plot(testnumber,AverageConductivityArray','-.r*','linewidth',2)
title({'MWCNT Delta k'; Date; TitleExtension; VolumePercent})
xlabel('Test #'), ylabel('Thermal K (W/mK)')
```

```
legend('Calculated CN k','Published k Value',...
    'Average Published k','Average Calculated CN k',4)
saveas(fig_handle,[Data.path,'Delta k'])

%Calculate the data range and scatter
%Maximum/Minimum Conductivity Value
ThermalkMax=max(TempaveragerunsconductivityBias);
ThermalkMin=min(TempaveragerunsconductivityBias);

%Maximum/Minimum Conductivity Value (Percent)
ThermalkMaxPercent=max(TempaveragerunserrorBias);
ThermalkMinPercent=min(TempaveragerunserrorBias);

%Display thermal conductivity range
ThermalkRange=TempaveragerunsconductivityBias;
ThermalkRangePercent=TempaveragerunserrorBias;


%Write Salient data to text file
str1='Total Averaged Conductivity Value=';
str2='Total Averaged Conductivity Change=';
str3='Total Averaged Conductivity Value (Percent)=';
str4='Average Expected k';
str5='Maximum Thermal k Value';
str6='Minimum Thermal k Value';
str7='Maxium Thermal k Value Percent';
str8='Minimum Thermal k Value Percent';
str9='Random Uncertainty';
str10='Bias';
str11='Bias Percent';

% %Write data
fprintf(fileID,'%40s %10.6g \n',str1,TotalAveragekchangeBias)
fprintf(fileID,'%40s %10.6g \n',str2,AverageCNFMWCNTDeltak)
fprintf(fileID,'%40s %10.6g \n',str3,AverageTotalIncreasekPercentBias)
fprintf(fileID,'%40s %10.6g \n',str4,AverageExpectedk)
fprintf(fileID,'%40s %10.6g \n',str5,ThermalkMax)
fprintf(fileID,'%40s %10.6g \n',str6,ThermalkMin)
fprintf(fileID,'%40s %10.6g \n',str7,ThermalkMaxPercent)
fprintf(fileID,'%40s %10.6g \n',str8,ThermalkMinPercent)
fprintf(fileID,'%40s %10.6g \n',str9,LOXTotalUncertainty)
fprintf(fileID,'%40s %10.6g \n',str10,BaseLOXFinalBias)
fprintf(fileID,'%40s %10.6g \n',str11,BaseLOXFinalBiasPercent)

%Data range and scatter directory information
FilenameScatterRange='MWCNTData_3_16_12Scater&Range.txt';
FileAddressScatterRange= [Path,FilenameScatterRange];
fileIDScatterRange = fopen(FileAddressScatterRange,'wt');

%Data range and scatter directory information
FilenameScatterRangePercent='MWCNTData_3_16_12Scater&RangePercent.txt';
FileAddressScatterRangePercent= [Path,FilenameScatterRangePercent];
```

```
fileIDScatterRangePercent = fopen(FileAddressScatterRangePercent,'wt');

%Print data to file
fprintf(fileIDScatterRange,'%10.6g\n ',ThermalkRange)
fprintf(fileIDScatterRangePercent,'%10.6g \n',ThermalkRangePercent)

%Close File ID
fclose(fileID);

%Close File ID
fclose(fileIDScatterRange);

%Close File ID
fclose(fileIDScatterRangePercent);

%Send job completion and results script
%Matlab Send E-mail when Job Complete
% setpref('Internet', 'E_mail', 'l.s.anderson@aggiemail.usu.edu');
% setpref('Internet', 'SMTP_Username',
'l.s.anderson@aggiemail.usu.edu');
% setpref('Internet', 'SMTP_Password', 'lsloveNB#21');
% setpref('Internet', 'SMTP_Server', 'smtp.gmail.com');
% props = java.lang.System.getProperties;
% props.setProperty('mail.smtp.auth','true');
% props.setProperty('mail.smtp.socketFactory.class',...
%'javax.net.ssl.SSLSocketFactory');
% props.setProperty('mail.smtp.socketFactory.port', '465');
% sendmail('l.s.anderson@aggiemail.usu.edu','JOB complete.',...
%'Calculation Complete',{'str2.jpg','str1.jpg'})

%Begin fresh calculations
close all


end
```

B.7. Cryogenic Nanofluid Data Comparison

```
%Cryogenic Nano-Fluid Research
%Lucas Anderson
%Nanofluid Static Modeling vs. Cryogenic Nanofluid Thermal k Data
%comparison
%MAE Thesis 2013

%Clear data, close active windows, clear workspace
close all
clear all
clc
```

```
%MWCNT Volume Fractions-------------------------------------------------
----

%Continuous Volume Fraction Values
VPContinuous=9.5238*10^-6:.0000001:6.38095*10^-4;

[sizeD1 sizeD2]=size(VPContinuous);

%Discrete Volume Fraction Values
VPDiscrete=[9.52381*10^-6, 2.19048*10^-5, 1.09524*10^-4, 2.19048*10^-
4,...
    3.19048*10^-4, 4.46667*10^-4, 6.38095*10^-4];

%Calculated MWCNT Effective Thermal Conductivities---------------------
----

%Dr. T. C. Shen's MWCNT's
kpTCShen=571.658571;

%NanoAmor Stock #1204YJ: Long Tailed
kpshorttailed=132.378403;

%NanoAmor Stock #1235YJS: Short Tailed
kplongtailed=3.177082*10^3;

%Measured Cryogenic Nanofluid Effective Thermal Conductivities---------
----
kTCSheneffectivediscrete=[0.1736855, 0.1799755, 0.1968555,
0.2024055,...
    0.201461, 0.2048855, 0.193971];

kSTeffectivediscrete=[0.156306, 0.159351, 0.154016, 0.160411,
0.167611,...
    0.157746, 0.161591];

kLTeffectivediscrete=[0.1593625, 0.1599125, 0.1705575, 0.1732875,...
    0.17326125, 0.1833275, 0.1717825];


%Base LOX Expected Effective Thermal Conductiviites--------------------
----
kmatrix=0.1663;

LOXbasevalues=[0.153859, 0.154102, 0.153470, 0.153616,...
    0.15336, 0.15330, 0.1531545];

kmatrix=mean(LOXbasevalues);

%Static Models----------------------------------------------------------
----
```

```
for x=1:1:sizeD2;

%Parallel mixture rule
kparallelTCShen(1,x)=kmatrix+VPContinuous(1,x)*(kpTCShen-kmatrix);

kparallelST(1,x)=kmatrix+VPContinuous(1,x)*(kpshorttailed-kmatrix);

kparallelLT(1,x)=kmatrix+VPContinuous(1,x)*(kplongtailed-kmatrix);

%Series mixture rule
kseriesTCShen(1,x)=kmatrix+VPContinuous(1,x)*((kpTCShen-kmatrix)/...
(kpTCShen+VPContinuous(1,x)*(kpTCShen-kmatrix)))*kmatrix;

kseriesST(1,x)=kmatrix+VPContinuous(1,x)*((kpshorttailed-kmatrix)/...
    (kpshorttailed+VPContinuous(1,x)*(kpshorttailed-kmatrix)))*kmatrix;

kseriesLT(1,x)=kmatrix+VPContinuous(1,x)*((kplongtailed-kmatrix)/...
    (kplongtailed+VPContinuous(1,x)*(kplongtailed-kmatrix)))*kmatrix;

%Simple Mixture Models
ksimplemixtureTCShen(1,x)=kmatrix+3*VPContinuous(1,x)*...
    ((kpTCShen-kmatrix)/(2*kmatrix+kpTCShen))*kmatrix;

ksimplemixtureST(1,x)=kmatrix+3*VPContinuous(1,x)*...
    ((kpshorttailed-kmatrix)/(2*kmatrix+kpshorttailed))*kmatrix;

ksimplemixtureLT(1,x)=kmatrix+3*VPContinuous(1,x)*...
    ((kplongtailed-kmatrix)/(2*kmatrix+kplongtailed))*kmatrix;

%Regular Symmetric MWCNT Distribution Models
kregTCShenint1(1,x)=(1-1.227*(VPContinuous(1,x)^7/3)*((kpTCShen-
kmatrix)...
    /(4*kmatrix+3*kpTCShen)));
kregTCShenint2(1,x)=(1+1.227*(VPContinuous(1,x)^4/3)*...
    (((2*kmatrix+kpTCShen)+2.215*VPContinuous(1,x)*...
    (kpTCShen-kmatrix))/(4*kmatrix+3*kpTCShen)))*(kpTCShen-kmatrix);
kregTCShenint2b(1,x)=((kpTCShen-kmatrix)/(2*kmatrix+kpTCShen-...
    VPContinuous(1,x)*(kregTCShenint2(1,x))))*kmatrix;
kregTCShentotal(1,x)=kmatrix+3*VPContinuous(1,x)*kregTCShenint1(1,x)*..
.
    kregTCShenint2b(1,x);

kregSTint1(1,x)=(1-1.227*(VPContinuous(1,x)^7/3)*((kpshorttailed-
kmatrix)...
    /(4*kmatrix+3*kpshorttailed)));
kregSTint2(1,x)=(1+1.227*(VPContinuous(1,x)^4/3)*...
    (((2*kmatrix+kpshorttailed)+2.215*VPContinuous(1,x)*...
    (kpshorttailed-
kmatrix))/(4*kmatrix+3*kpshorttailed)))*(kpshorttailed-kmatrix);
kregSTint2b(1,x)=((kpshorttailed-kmatrix)/(2*kmatrix+kpshorttailed-...
    VPContinuous(1,x)*(kregSTint2(1,x))))*kmatrix;
```

```
kregSTtotal(1,x)=kmatrix+3*VPContinuous(1,x)*kregSTint1(1,x)*...
    kregSTint2b(1,x);

kregLTint1(1,x)=(1-1.227*(VPContinuous(1,x)^7/3)*((kplongtailed-
kmatrix)...
    /(4*kmatrix+3*kplongtailed)));
kregLTint2(1,x)=(1+1.227*(VPContinuous(1,x)^4/3)*...
    (((2*kmatrix+kplongtailed)+2.215*VPContinuous(1,x)*...
    (kplongtailed-kmatrix))/(4*kmatrix+3*kplongtailed)))*...
    (kplongtailed-kmatrix);
kregLTint2b(1,x)=((kplongtailed-kmatrix)/(2*kmatrix+kplongtailed-...
    VPContinuous(1,x)*(kregLTint2(1,x))))*kmatrix;
kregLTtotal(1,x)=kmatrix+3*VPContinuous(1,x)*kregLTint1(1,x)*...
    kregLTint2b(1,x);

%Random MWCNT Distribution Models
FaTCShen=log((kpTCShen/kmatrix));
FaST=log((kpshorttailed/kmatrix));
FaLT=log((kplongtailed/kmatrix));

krandomTCShen(1,x)=(1+((3*((kpTCShen/kmatrix)-
1))/((kpTCShen/kmatrix)...
    +2-((kpTCShen/kmatrix)-1)*VPContinuous(1,x)))*...
    (VPContinuous(1,x)+FaTCShen*(VPContinuous(1,x)^2)))*kmatrix;

krandomST(1,x)=(1+((3*((kpshorttailed/kmatrix)-1))/...
    ((kpshorttailed/kmatrix)+2-((kpshorttailed/kmatrix)-1)*...

VPContinuous(1,x)))*(VPContinuous(1,x)+FaST*(VPContinuous(1,x)^2)))...
    *kmatrix;

krandomLT(1,x)=(1+((3*((kplongtailed/kmatrix)-1))/...
    ((kplongtailed/kmatrix)+2-((kplongtailed/kmatrix)-1)*...

VPContinuous(1,x)))*(VPContinuous(1,x)+FaLT*(VPContinuous(1,x)^2)))...
    *kmatrix;

%Combination MWCNT Distribution Models
kcombint1TCShen(1,x)=2.-(((nthroot((16./(9.*pi()*VPContinuous(1,x)^2)),
3))...
    *kmatrix)/((sqrt(kpTCShen-kmatrix))*(sqrt((nthroot(((16./...
    (9.*pi()*VPContinuous(1,x).^2))),3)*kmatrix)+(kpTCShen-
kmatrix)))));
kcombint2TCShen(1,x)=(sqrt((nthroot(((16./...
    (9.*pi()*VPContinuous(1,x).^2))),3)*kmatrix)+(kpTCShen-
kmatrix))+...
    (sqrt(kpTCShen-kmatrix)))/...
    (sqrt((nthroot(((16./(9.*pi()*VPContinuous(1,x).^2))),3)...
    *kmatrix)+(kpTCShen-kmatrix))-(sqrt(kpTCShen-kmatrix)));
kcombtotalTCShen(1,x)=(1-nthroot(((3*VPContinuous(1,x))/(4*pi())),
3)...
    *(kcombint1TCShen(1,x)*log(kcombint2TCShen(1,x))))^-1*kmatrix;
```

```
kcombint1ST(1,x)=2.-(((nthroot((16./(9.*pi()*VPContinuous(1,x)^2)),
3))...
    *kmatrix)/((sqrt(kpshorttailed-kmatrix))*(sqrt((nthroot(((16./...
    (9.*pi()*VPContinuous(1,x).^2))),3)*kmatrix)+(kpshorttailed-
kmatrix)))));
kcombint2ST(1,x)=(sqrt((nthroot(((16./...
    (9.*pi()*VPContinuous(1,x).^2))),3)*kmatrix)+(kpshorttailed-
kmatrix))+...
    (sqrt(kpshorttailed-kmatrix)))/...
    (sqrt((nthroot(((16./(9.*pi()*VPContinuous(1,x).^2))),3)...
    *kmatrix)+(kpshorttailed-kmatrix))-(sqrt(kpshorttailed-kmatrix)));
kcombtotalST(1,x)=(1-nthroot(((3*VPContinuous(1,x))/(4*pi())), 3)...
    *(kcombint1ST(1,x)*log(kcombint2ST(1,x))))^-1*kmatrix;

kcombint1LT(1,x)=2.-(((nthroot((16./(9.*pi()*VPContinuous(1,x)^2)),
3))...
    *kmatrix)/((sqrt(kplongtailed-kmatrix))*(sqrt((nthroot(((16./...
    (9.*pi()*VPContinuous(1,x).^2))),3)*kmatrix)+(kplongtailed-
kmatrix)))));
kcombint2LT(1,x)=(sqrt((nthroot(((16./...
    (9.*pi()*VPContinuous(1,x).^2))),3)*kmatrix)+(kplongtailed-
kmatrix))+...
    (sqrt(kplongtailed-kmatrix)))/...
    (sqrt((nthroot(((16./(9.*pi()*VPContinuous(1,x).^2))),3)...
    *kmatrix)+(kplongtailed-kmatrix))-(sqrt(kplongtailed-kmatrix)));
kcombtotalLT(1,x)=(1-nthroot(((3*VPContinuous(1,x))/(4*pi())), 3)...
    *(kcombint1LT(1,x)*log(kcombint2LT(1,x))))^-1*kmatrix;

%MWCNT Geometry Based Models
keffectgeometrybasedTCShen(1,x)=kmatrix+(1/3)*...
    (VPContinuous(1,x))*(kpTCShen);

keffectgeometrybasedST(1,x)=kmatrix+(1/3)*(VPContinuous(1,x))...
    *(kpshorttailed);

keffectgeometrybasedLT(1,x)=kmatrix+(1/3)*(VPContinuous(1,x))...
    *(kplongtailed);


end

%Comparison plots----------------------------------------------------
----
figure(1)
plot(VPDiscrete, kTCSheneffectivediscrete,'-o','color','b')
hold on
plot(VPDiscrete, kSTeffectivediscrete,':s', 'color','g')
hold on
plot(VPDiscrete, kLTeffectivediscrete,'--+','color','r')
hold on
plot(VPContinuous,kparallelTCShen,'-','color','b','linewidth',3)
```

```
hold on
plot(VPContinuous,kparallelST,'-','color','g','linewidth',3)
hold on
plot(VPContinuous,kparallelLT,'-','color','r','linewidth',3)
hold on
plot(VPDiscrete, LOXbasevalues,'k.','linewidth',2)
xlabel('Volume Fraction'), ylabel('Thermal K (W/mK)')
legend('Modeled CN k: T. C. Shen', 'Modeled CN k: NanoAmor 1235YJS'...
    , 'Modeled CN k: NanoAmor 1204YJ', 'Measured CN k: T. C. Shen',...
    'Measured CN k: NanoAmor 1235YJS', 'Measured CN k: NanoAmor
1204YJ',...
    'Pure LOX', 2)

figure(2)
plot(VPDiscrete, kTCSheneffectivediscrete,'-o','color','b')
hold on
plot(VPDiscrete, kSTeffectivediscrete,':s', 'color','g')
hold on
plot(VPDiscrete, kLTeffectivediscrete,'--+','color','r')
hold on
plot(VPContinuous,kseriesTCShen,'-','color','b','linewidth',3)
hold on
plot(VPContinuous,kseriesST,'-','color','g','linewidth',3)
hold on
plot(VPContinuous,kseriesLT,'-','color','r','linewidth',3)
hold on
plot(VPDiscrete, LOXbasevalues,'k.','linewidth',2)
xlabel('Volume Fraction'), ylabel('Thermal K (W/mK)')
legend('Modeled CN k: T. C. Shen', 'Modeled CN k: NanoAmor 1235YJS'...
    , 'Modeled CN k: NanoAmor 1204YJ', 'Measured CN k: T. C. Shen',...
    'Measured CN k: NanoAmor 1235YJS', 'Measured CN k: NanoAmor
1204YJ',...
    'Pure LOX', 2)

figure(3)
plot(VPDiscrete, kTCSheneffectivediscrete,'-o','color','b')
hold on
plot(VPDiscrete, kSTeffectivediscrete,':s', 'color','g')
hold on
plot(VPDiscrete, kLTeffectivediscrete,'--+','color','r')
hold on
plot(VPContinuous,ksimplemixtureTCShen,'-','color','b','linewidth',3)
hold on
plot(VPContinuous,ksimplemixtureST,'-','color','g','linewidth',3)
hold on
plot(VPContinuous,ksimplemixtureLT,'-','color','r','linewidth',3)
hold on
plot(VPDiscrete, LOXbasevalues,'k.','linewidth', 2)
xlabel('Volume Fraction'), ylabel('Thermal K (W/mK)')
legend('Modeled CN k: T. C. Shen', 'Modeled CN k: NanoAmor 1235YJS'...
    , 'Modeled CN k: NanoAmor 1204YJ', 'Measured CN k: T. C. Shen',...
    'Measured CN k: NanoAmor 1235YJS', 'Measured CN k: NanoAmor
1204YJ',...
```

```
    'Pure LOX', 2)

figure(4)
plot(VPDiscrete, kTCSheneffectivediscrete,'-o','color','b')
hold on
plot(VPDiscrete, kSTeffectivediscrete,':s','color','g')
hold on
plot(VPDiscrete, kLTeffectivediscrete,'--+','color','r')
hold on
plot(VPContinuous,kregTCShentotal,'-','color','b','linewidth',3)
hold on
plot(VPContinuous,kregSTtotal,'-','color','g','linewidth',3)
hold on
plot(VPContinuous,kregLTtotal,'-','color','r','linewidth',3)
hold on
plot(VPDiscrete, LOXbasevalues,'k.','linewidth',2)
xlabel('Volume Fraction'), ylabel('Thermal K (W/mK)')
legend('Modeled CN k: T. C. Shen', 'Modeled CN k: NanoAmor 1235YJS'...
    , 'Modeled CN k: NanoAmor 1204YJ', 'Measured CN k: T. C. Shen',...
    'Measured CN k: NanoAmor 1235YJS', 'Measured CN k: NanoAmor
1204YJ',...
    'Pure LOX', 2)

figure(5)
plot(VPDiscrete, kTCSheneffectivediscrete,'-o','color','b')
hold on
plot(VPDiscrete, kSTeffectivediscrete, ':s', 'color','g')
hold on
plot(VPDiscrete, kLTeffectivediscrete,'--+','color','r')
hold on
plot(VPContinuous,krandomTCShen,'-','color','b','linewidth',3)
hold on
plot(VPContinuous,krandomST,'-','color','g','linewidth',3)
hold on
plot(VPContinuous,krandomLT,'-','color','r','linewidth',3)
hold on
plot(VPDiscrete, LOXbasevalues,'k.', 'linewidth',2)
xlabel('Volume Fraction'), ylabel('Thermal K (W/mK)')
legend('Modeled CN k: T. C. Shen', 'Modeled CN k: NanoAmor 1235YJS'...
    , 'Modeled CN k: NanoAmor 1204YJ', 'Measured CN k: T. C. Shen',...
    'Measured CN k: NanoAmor 1235YJS', 'Measured CN k: NanoAmor
1204YJ',...
    'Pure LOX', 2)

figure(6)
plot(VPDiscrete, kTCSheneffectivediscrete,'-o','color','b')
hold on
plot(VPDiscrete, kSTeffectivediscrete,':s','color','g')
hold on
plot(VPDiscrete, kLTeffectivediscrete,'--+','color','r')
hold on
plot(VPContinuous,kcombtotalTCShen,'-','color','b','linewidth',3)
hold on
```

```
plot(VPContinuous,kcombtotalST,'-','color','g','linewidth',3)
hold on
plot(VPContinuous,kcombtotalLT,'-','color','r','linewidth',3)
hold on
plot(VPDiscrete, LOXbasevalues,'k.','linewidth',2)
xlabel('Volume Fraction'), ylabel('Thermal K (W/mK)')
legend('Modeled CN k: T. C. Shen', 'Modeled CN k: NanoAmor 1235YJS'...
    , 'Modeled CN k: NanoAmor 1204YJ', 'Measured CN k: T. C. Shen',...
    'Measured CN k: NanoAmor 1235YJS', 'Measured CN k: NanoAmor
1204YJ',...
    'Pure LOX', 2)

figure(7)
plot(VPDiscrete, kTCSheneffectivediscrete,'-o','color','b')
hold on
plot(VPDiscrete, kSTeffectivediscrete, ':s', 'color','g')
hold on
plot(VPDiscrete, kLTeffectivediscrete, '--+','color','r')
hold on
plot(VPContinuous,keffectgeometrybasedTCShen,'-
','color','b','linewidth',3)
hold on
plot(VPContinuous,keffectgeometrybasedST,'-','color','g','linewidth',3)
hold on
plot(VPContinuous,keffectgeometrybasedLT,'-','color','r','linewidth',3)
hold on
plot(VPDiscrete, LOXbasevalues,'k.','linewidth',2)
xlabel('Volume Fraction'), ylabel('Thermal K (W/mK)')
legend('Modeled CN k: T. C. Shen', 'Modeled CN k: NanoAmor 1235YJS',...
    'Modeled CN k: NanoAmor 1204YJ', 'Measured CN k: T. C. Shen',...
    'Measured CN k: NanoAmor 1235YJS', 'Measured CN k: NanoAmor
1204YJ',...
    'Pure LOX', 2)
```

APPENDIX C: NANOFLUID MODELING

C.1. Introduction

The following theoretical models for the behavior of nanofluid effective thermal conductivity are a sampling of the current work being done in the field. These theories vary from classical to modern and will focus on the following categories of static nanofluid modeling.

- Simple Mixture
- Variable Particle Distribution
- Variable Particle Geometries

Numerous other nanofluid models exist, and are discussed at further length within the theory chapter, and the provided references. It should be noted that the following discussions are provided to give the reader a better understanding of the current work through demonstrations of the actual calculations made and the values used. Therefore, the given equations, values, and ultimate plots are presented without fanfare or elaboration. For a more detailed discussion of the work, see the nanofluid theory chapter of this thesis.

C.2. Background

All material properties are taken at the average cryogenic testing temperature of roughly 80 K. The approximate Thermal Conductance of an individual MWCNT's at 80 K is shown below. Value referenced from Nanoparticle literature review.

$$\text{ThermalConductance}_{\text{MWCNT}} := 1.1 \cdot 10^{-8} \frac{\text{W}}{\text{K}} \tag{C.1}$$

Convert material thermal conductance to corresponding thermal conductivity:

$$Thermal\ conductivity\ of\ a\ given\ material = \frac{Conductance * Length}{Area} \tag{C.2}$$

Host fluid material (LOX) thermal conductivity referenced at 80 K.

$$k_m := .1536 \frac{W}{m \cdot K} \tag{C.3}$$

C.3. Individual MWCNT Thermal Conductivity and Inclusion Particle Volume Fraction

C.3.1. Inclusion Particle thermal conductivity: Dr. T. C. Shen's, MWCNT's.

Particle geometry and subsequent calculated cross sectional area are displayed below along with the calculated MWCNT thermal conductivity. Calculations based upon specific material conductivity and inverse relationship between conductivity and thermal resistance.

$$\begin{aligned} \text{Approximate}_{\text{LengthTCShen}} &:= 50\mu m \\ \text{Approximate}_{\text{DiameterTCShen}} &:= 35nm \\ \text{Approximate}_{\text{AreaTCShen}} &:= \pi \cdot \frac{\left(\text{Approximate}_{\text{DiameterTCShen}}\right)^2}{4} = 9.621 \times 10^{-16} m^2 \end{aligned} \tag{C.4}$$

$$k_{pTCShen} := \frac{\left(\text{ThermalConductance}_{MWCNT} \cdot \text{Approximate}_{\text{LengthTCShen}}\right)}{\text{Approximate}_{\text{AreaTCShen}}} = 571.658571 \cdot \frac{W}{m \cdot K} \tag{C.5}$$

C.3.2. Inclusion Particle thermal conductivity: NanoAmor Stock #1204YJ, MWCNT's.

Particle geometry and subsequent calculated cross sectional area are displayed below along with the calculated MWCNT thermal conductivity. Calculations based upon specific material conductivity and inverse relationship between conductivity and thermal resistance.

$$\begin{aligned} \text{Approximate}_{\text{LengthLTailed}} &:= 30\mu m \\ \text{Approximate}_{\text{DiameterLTailed}} &:= 11.5nm \\ \text{Approximate}_{\text{AreaLTailed}} &:= \pi \cdot \frac{\left(\text{Approximate}_{\text{DiameterLTailed}}\right)^2}{4} = 1.039 \times 10^{-16} m^2 \end{aligned} \tag{C.6}$$

$$k_{pLTailed} := \frac{\left(\text{ThermalConductance}_{MWCNT} \cdot \text{Approximate}_{\text{LengthLTailed}}\right)}{\text{Approximate}_{\text{AreaLTailed}}} = 3.177082 \times 10^{3} \cdot \frac{W}{m \cdot K} \tag{C.7}$$

C.3.3. Inclusion Particle thermal conductivity: NanoAmor Stock #1235YJS, MWCNT's.

Particle geometry and subsequent calculated cross sectional area are displayed below along with the calculated MWCNT thermal conductivity. Calculations based upon specific material conductivity and inverse relationship between conductivity and thermal resistance.

$$\text{Approximate}_{\text{LengthSTailed}} := 1.25\mu\text{m}$$

$$\text{Approximate}_{\text{DiameterSTailed}} := 11.5\text{nm}$$

$$\text{Approximate}_{\text{AreaSTailed}} := \pi \cdot \frac{\left(\text{Approximate}_{\text{DiameterSTailed}}\right)^2}{4} = 1.039 \times 10^{-16}\,\text{m}^2 \tag{C.8}$$

$$k_{\text{pSTailed}} := \frac{\left(\text{ThermalConductance}_{\text{MWCNT}} \cdot \text{Approximate}_{\text{LengthSTailed}}\right)}{\text{Approximate}_{\text{AreaSTailed}}} = 132.378403 \cdot \frac{\text{W}}{\text{m}\cdot\text{K}} \tag{C.9}$$

C.3.4. Calculated Inclusion Particle Volume Fractions

The inclusion particles volume fractions are calculated based upon the methods described in the nanoparticle profile chapter of this thesis. Primarily, they are calculated from dividing the densities of the inclusion MWCNT's by their measured bulk masses. This number is than inverted and divided by the total available volume. The nanoparticle volume fraction ranges and densities utilized in this work can be seen below.

$$\textit{Dr. T. C. Shen MWCNT assumed density: } 1.34 - 2.1\,\frac{gm}{cm^3}$$

$$\textit{NanoAmor Stock \#1204YJ, 1235YJS MWCNT assumed density: } 2.1\,\frac{gm}{cm^3} \tag{C.10}$$

$$\textit{Inclusion nanoparticle volume percentage range} \sim \textit{0.000952-0.0638\%}$$

C.4. Nanofluid Thermal Conductivity Mixture Models

Note: All equations and information presented within this appendix are referenced back to the literature provided in chapter 4 of this thesis.

C.4.1. Parallel and Series Mixture Models

Parallel mixture model

$$k_{eparallel}(\nu_p, k_p) := k_m + \nu_p \cdot (k_p - k_m)$$

Series mixture model

$$k_{eseries}(\nu_p, k_p) := k_m + \nu_p \cdot \left[\frac{(k_p - k_m)}{k_p - \nu_p \cdot (k_p - k_m)} \right] \cdot k_m \qquad \text{(C.11)}$$

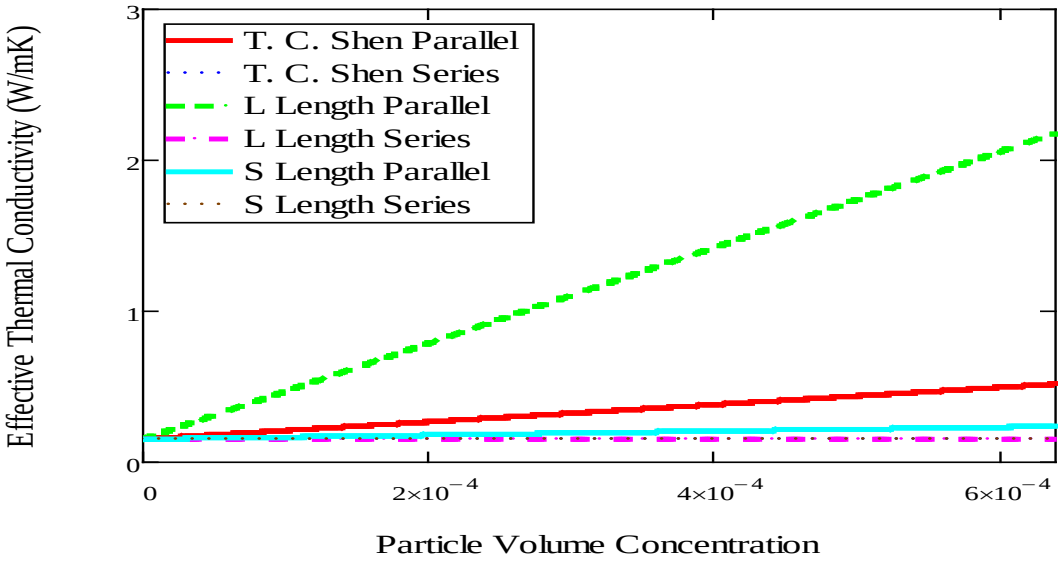

Figure C-1. Series and parallel mixture laws applied to the CN's used in this research.

C.4.2. Simple Nanofluid Mixture Models

$$k_{eSimpleMixture}(\nu_p, k_p) := k_m + 3 \cdot \nu_p \cdot \frac{(k_p - k_m)}{(2 \cdot k_m + k_p)} \cdot k_m \qquad \text{(C.12)}$$

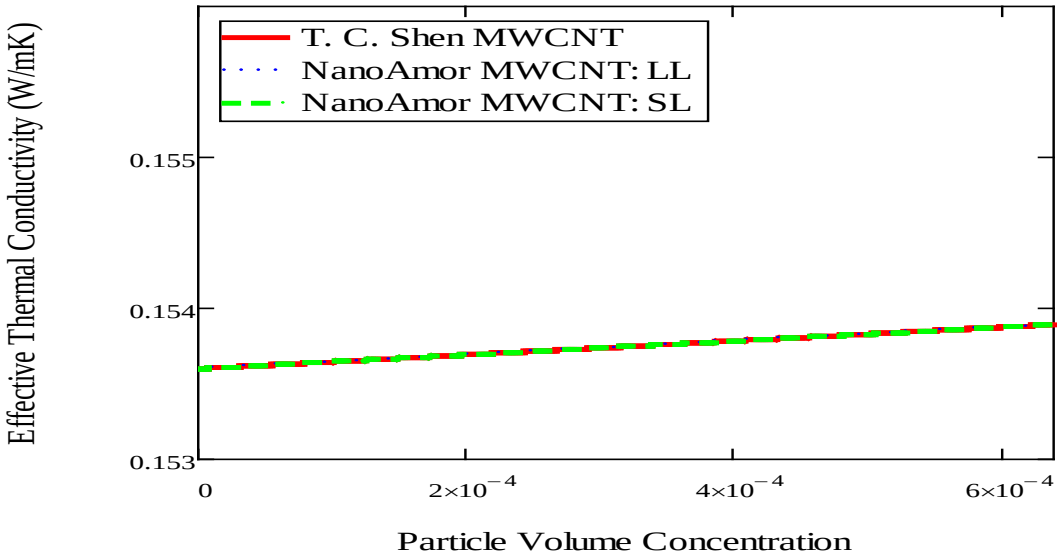

Figure C-2. Simplified Maxwell's mixture model applied to the CN's used in this research.

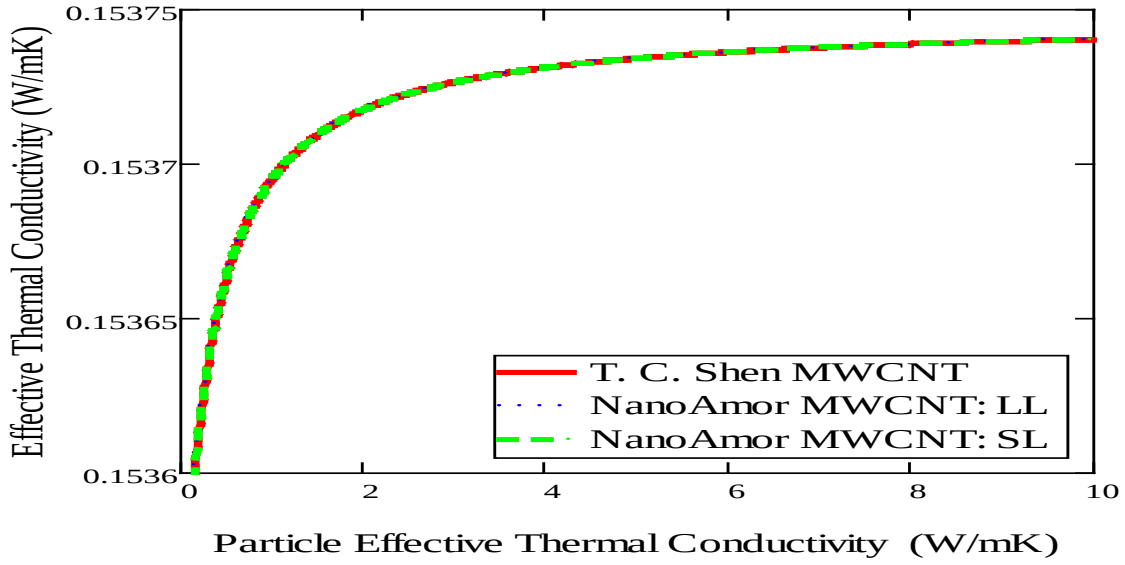

Figure C-3. Maxwell's mixture model demonstrating the theoretical limit of increase in mixture effective thermal conductivity compared to inclusion particle thermal conductivity.

C.4.3. Nanofluid models For Regular/Symmetric Nanoparticle Distributions

Note: Due to the length of the regular distribution equation, it has been broken up into more manageable pieces.

$$k_{einterior1}(\nu_p, k_p) := \left[1 - 1.1227\cdot\left(\nu_p^{\frac{7}{3}}\right)\cdot\frac{(k_p - k_m)}{(4\cdot k_m + 3\cdot k_p)}\right]$$

$$k_{einterior2b}(\nu_p, k_p) := \left[1 + 1.227\cdot\nu_p^{\frac{4}{3}}\cdot\frac{(2\cdot k_m + k_p) + 2.215\cdot\nu_p\cdot(k_p - k_m)}{4\cdot k_m + 3\cdot k_p}\right]\cdot(k_p - k_m) \qquad \text{(C.13)}$$

$$k_{einterior2}(\nu_p, k_p) := \frac{(k_p - k_m)}{2\cdot k_m + k_p - \nu_p\cdot k_{einterior2b}(\nu_p, k_p)}\cdot k_m$$

$$k_{eRegularDistribution}(\nu_p, k_p) := k_m + 3\cdot\nu_p\cdot k_{einterior1}(\nu_p, k_p)\cdot k_{einterior2}(\nu_p, k_p)$$

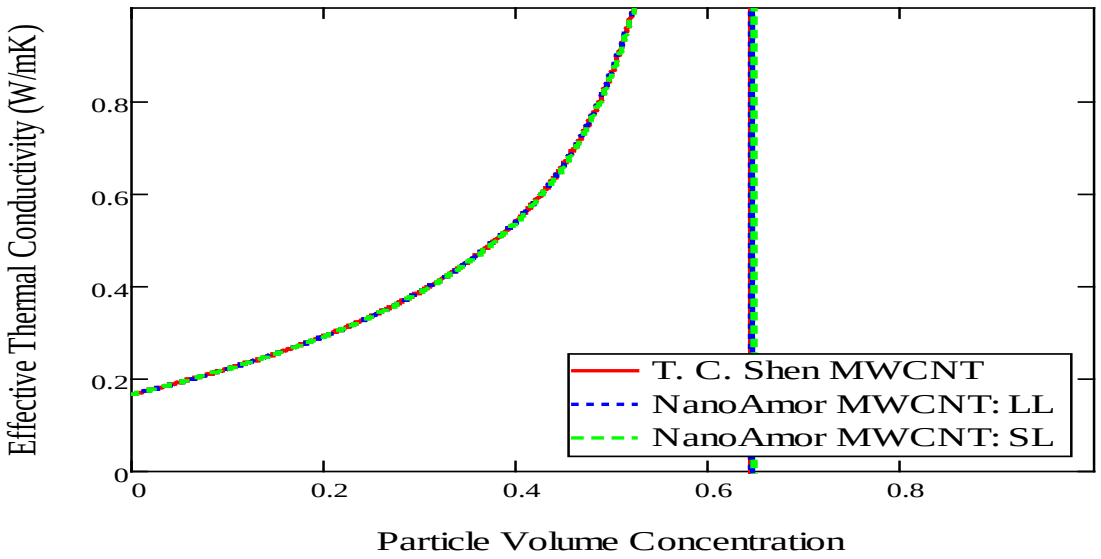

Figure C-4. Regular inclusion particle distribution mixture model applied to the CN's created in this research. Demonstration of asymptotic behavior included.

C.4.4. Nanofluid models For Random Nanoparticle Distributions

The solution to the graphically represented f(α) variable from the nanofluid chapter, for the random distribution equation, is presented below for the CN's created in this research.

$$\log_{10}\alpha TCShen := \log\left(\left(\frac{k_{pTCShen}}{k_m}\right)\right) = 3.570746$$

$$\log_{10}\alpha STailed := \log\left(\left(\frac{k_{pLTailed}}{k_m}\right)\right) = 4.315637 \qquad \text{(C.14)}$$

$$\log_{10}\alpha LTailed := \log\left(\left(\frac{k_{pSTailed}}{k_m}\right)\right) = 2.935426$$

$$k_{eRandomDistribution}(\nu_p, k_p) := \left[1 + \left[\frac{\left[3\cdot\left[\left(\frac{k_p}{k_m}\right) - 1\right]\right]}{\left(\frac{k_p}{k_m}\right) + 2 - \left[\left(\frac{k_p}{k_m}\right) - 1\right]\cdot\nu_p}\right]\cdot\left(\nu_p + .504\cdot\nu_p^{\,2}\right)\right]\cdot k_m \qquad \text{(C.15)}$$

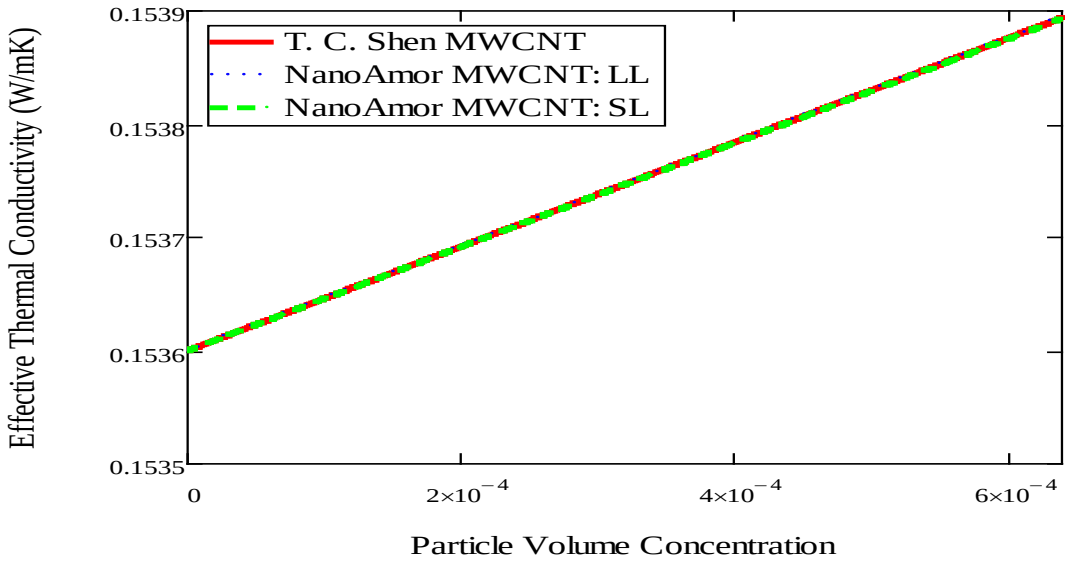

Figure C-5. Random inclusion particle distribution mixture model applied to the CN's created in this research.

C.4.5. Nanofluid models For Combination (Random + Structured) Nanoparticle Distributions

$$k_{eRand1}(\nu_p, k_p) := 2 - \frac{\left[\sqrt[3]{\left[\frac{16}{\left(9\cdot\pi\cdot\nu_p^{\,2}\right)}\right]}\right]\cdot k_m}{\sqrt{k_p - k_m}\cdot\sqrt{\left[\sqrt[3]{\left[\frac{16}{\left(9\cdot\pi\cdot\nu_p^{\,2}\right)}\right]}\right]\cdot k_m + \left(k_p - k_m\right)}}$$

$$k_{eRand2}(\nu_p, k_p) := \frac{\sqrt{\left[\sqrt[3]{\left[\frac{16}{\left(9\cdot\pi\cdot\nu_p^{\,2}\right)}\right]}\right]\cdot k_m + \left(k_p - k_m\right)} + \sqrt{k_p - k_m}}{\sqrt{\left[\sqrt[3]{\left[\frac{16}{\left(9\cdot\pi\cdot\nu_p^{\,2}\right)}\right]}\right]\cdot k_m + \left(k_p - k_m\right)} - \sqrt{k_p - k_m}} \qquad \text{(C.16)}$$

$$k_{eCombinationDistribution}(\nu_p, k_p) := \left[1 - \sqrt[3]{3\cdot\frac{\nu_p}{4\cdot\pi}}\cdot\left(k_{eRand1}(\nu_p, k_p)\cdot\ln\left(k_{eRand2}(\nu_p, k_p)\right)\right)\right]^{-1}\cdot k_m \qquad \text{(C.17)}$$

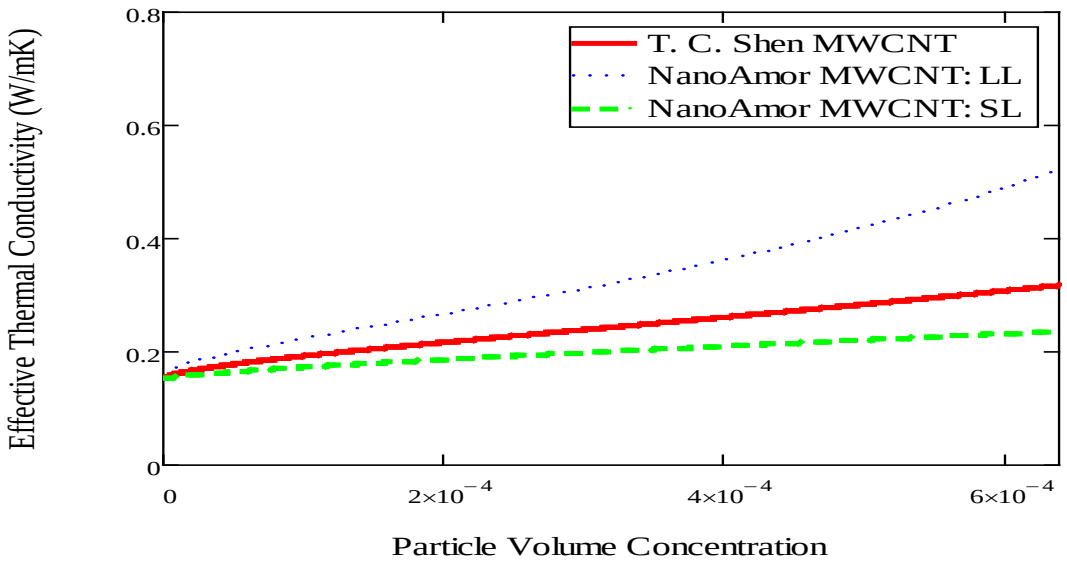

Figure C-6. Combination inclusion particle distribution mixture model applied to the CN's created in this research. Axes ranges modified to show additional information.

C.4.6. Nanofluid models For Particle Geometry Distributions

$$k_{eGeometryConsidered}(v_p, k_p) := k_m + \left(\frac{1}{3}\right) \cdot v_p \cdot k_p \tag{C.18}$$

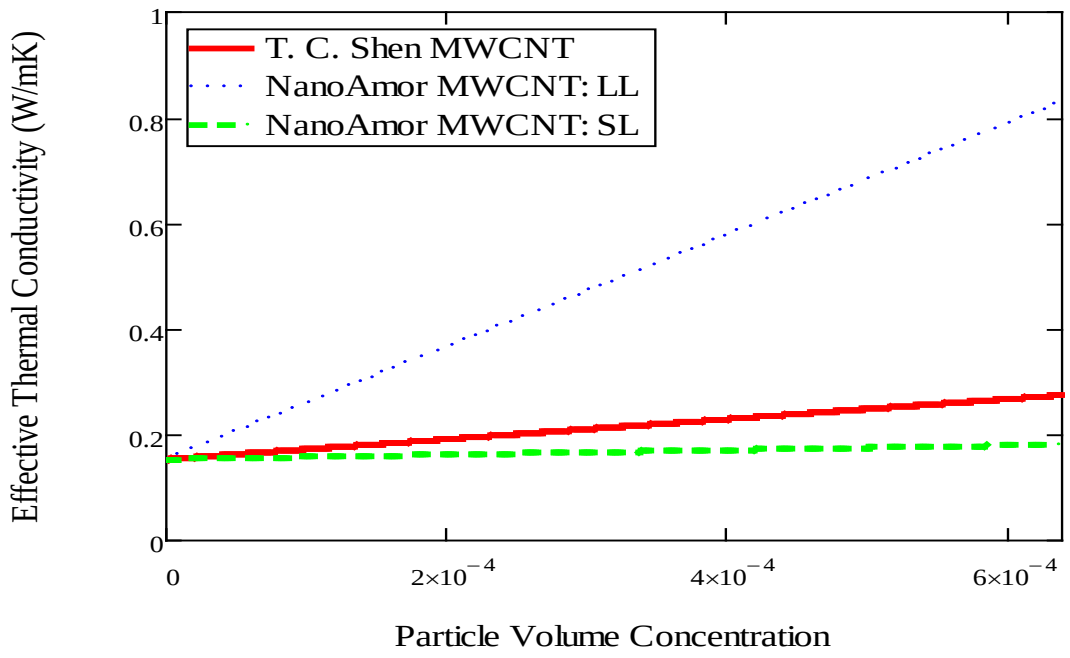

Figure C-7. Inclusion particle geometry based distribution mixture model applied to the CN's created in this research.

C.5. Model/Data Comparison

The following figures compare the static nanofluid models from (1) to the measured effective thermal conductivity values for the three cryogenic nanofluids studied in this work. It should be noted that the models require an assumed matrix thermal conductivity value, which is given as the measured averaged value of pure LOX. The conductivity values for the assorted MWCNT's are taken as constants and calculated based upon the literature. Several of the presented models predict effective thermal conductivity increases on the order of the measured values, but only at

larger nanoparticle volume fractions. The models also depict the maximum volume fractions available due to spherical packing fractions (roughly 0.62). It is clear that many of the models do not accurately predict the behavior of the studied cryogenic nanofluids, and in fact represent them so poorly that direct comparisons are difficult. However, it should be noted that the combination and geometry based static models represents the measured data to a degree, thus proving the importance and viability of modeling for cryogenic nanofluids.

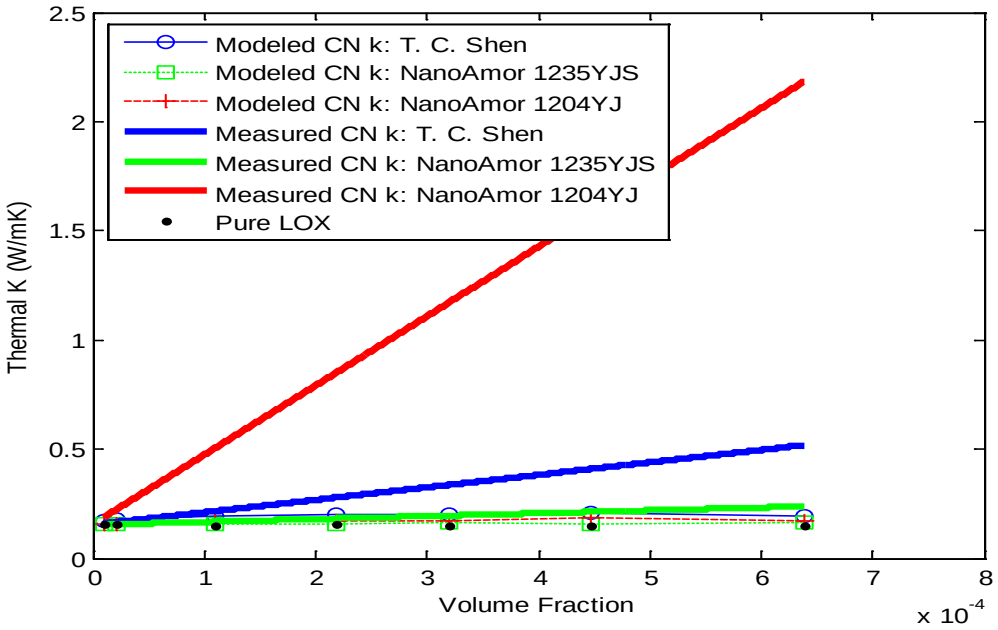

Figure C-8. Parallel mixture laws compared to the studied Cryogenic Nanofluids.

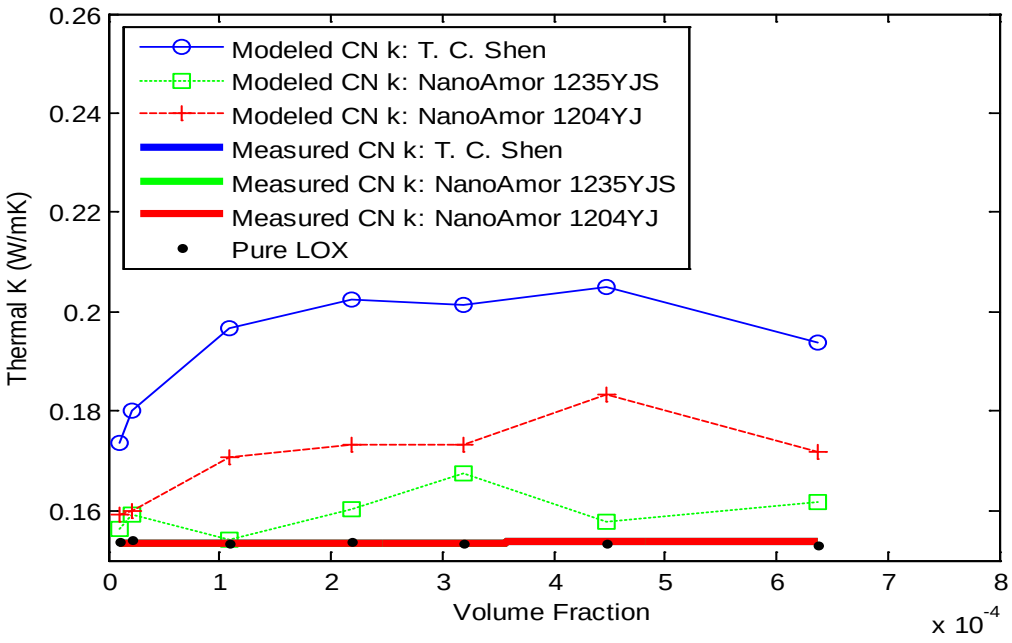

Figure C-9. Series mixture laws compared to the studied Cryogenic Nanofluids.

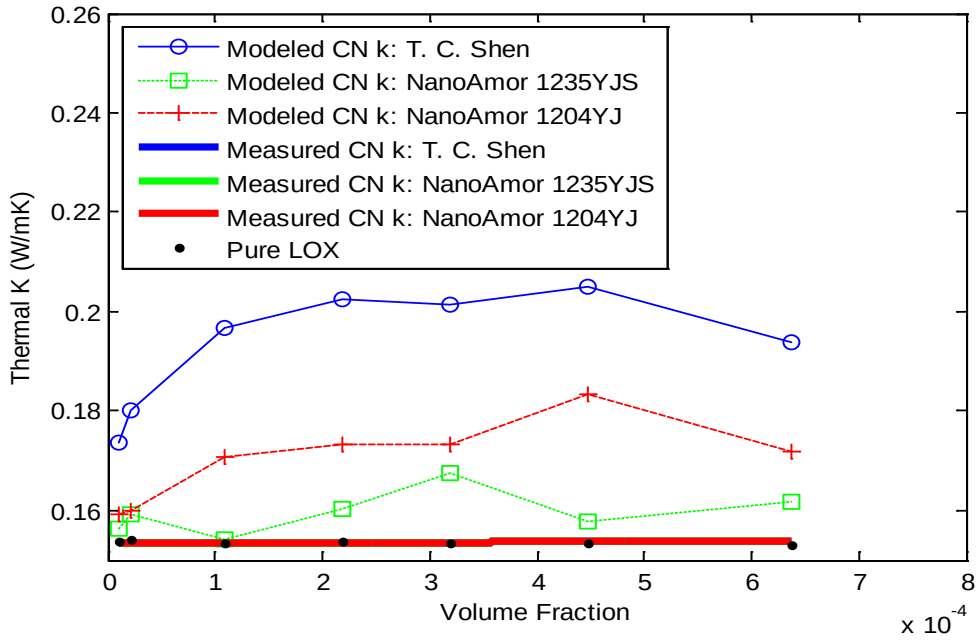

Figure C-10. Simplified Maxwell models compared to the studied Cryogenic Nanofluids.

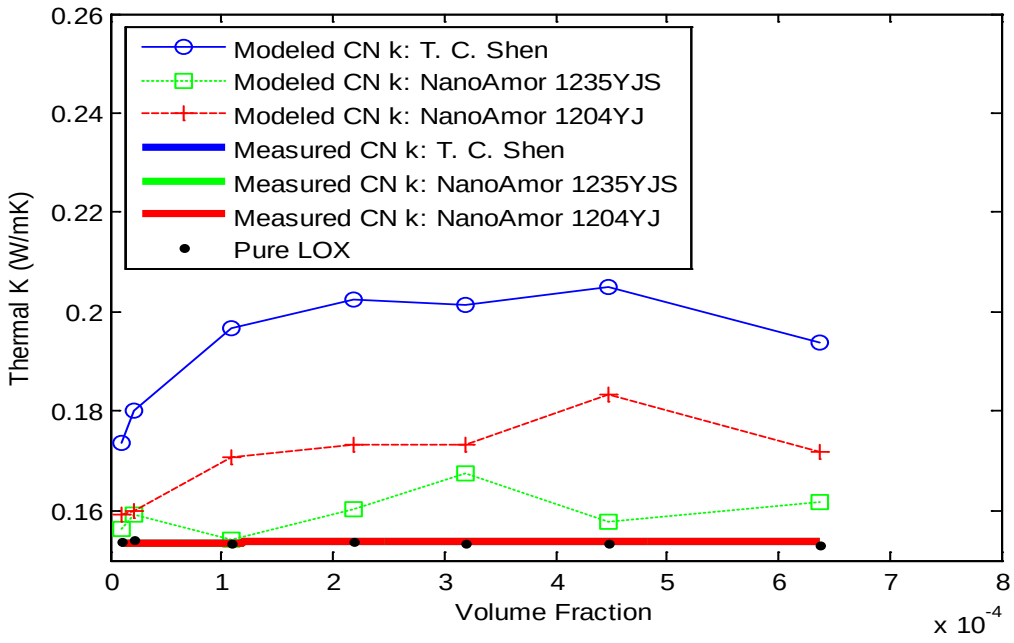

Figure C-11. Regular distribution static models compared to the studied Cryogenic Nanofluids.

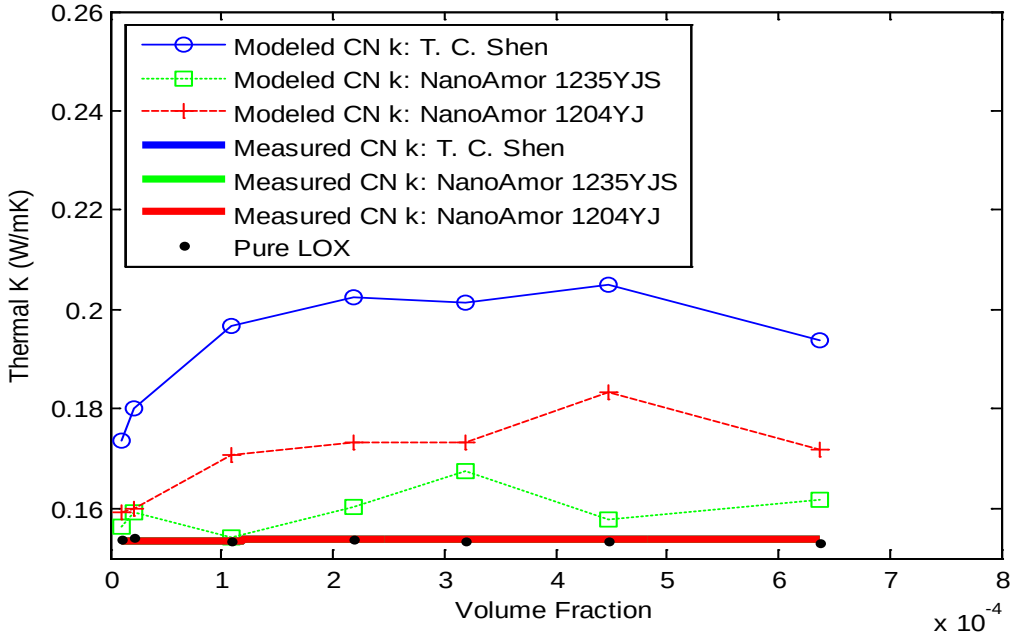

Figure C-12. Random distribution static models compared to the studied Cryogenic Nanofluids.

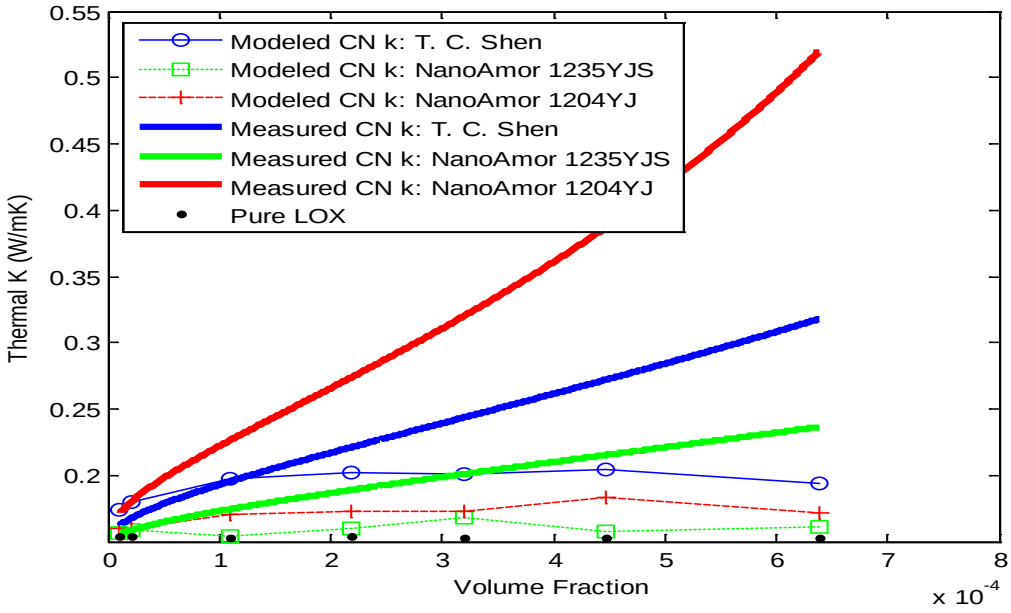

Figure C-13. Combination distribution static models compared to the studied Cryogenic Nanofluids.

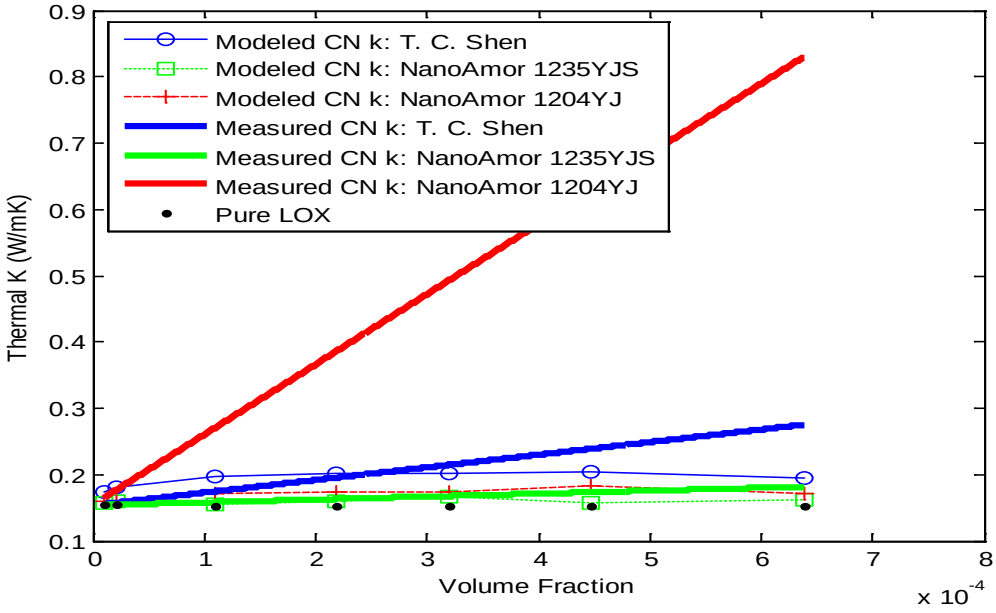

Figure C-14. Nanoparticle geometry based static models compared to the studied Cryogenic Nanofluids.

APPENDIX D: TRANSIENT HOT WIRE TEMPERATURE MODELING

D.1. Introduction

It is the hope of the authors that by publicizing the actual equations, values and steps taken in the temperature modeling of the THW, future scientists will find this research more helpful in their own studies. The following work will present the three theoretical line heat source equations used to model the temperature behavior of the THW, as well as the actual values and intermediate steps that went into their creation.

D.2. Preliminary Work

The MTL laboratory of Utah State University is located in Logan Utah with the following environmental conditions.

$$\begin{gathered} \text{Altitude} := 4534\text{ft} \\ \textit{Atmospheric Pressures:} \\ \text{Atmospheric}_{\text{Pressure}} := 30\text{in\_Hg} \\ \text{Atmospheric}_{\text{Pressure}} = 0.102\cdot\text{MPa} \\ \text{Atmospheric}_{\text{Pressure}} = 14.735\cdot\text{psi} \end{gathered} \tag{D.1}$$

These environmental conditions dictate the thermo-physical properties of LOX. It should be noted that these values are only approximate.

$$\begin{gathered} \textit{LOX Boiling Point=90.251 K} \\ \text{Conductivity}_{\text{LOX}} := .16350\,\frac{\text{W}}{\text{m}\cdot\text{K}} \\ C_{\text{pLOX}} := 1.683\,\frac{\text{J}}{\text{gm}\cdot\text{K}} \\ \text{Density}_{\text{LOX}} := 1181.1\,\frac{\text{kg}}{\text{m}^3} \end{gathered} \tag{D.2}$$

The THW utilized in this research has the following approximate dimensions.

$$L_{HotWire} := .161m$$

$$r_{HotWire} := \frac{0.005}{2}in$$

$$A_{HotWire} := \left(\pi \cdot r_{HotWire}^{2}\right) \tag{D.3}$$

$$A_{HotWire} = 1.267 \times 10^{-8} m^2$$

The THW is made of extremely pure platinum. Therefore, its resistivity at the cryogenic temperatures of LOX can be used to calculate its resistance (Ω), voltage (V) and power (W). In addition, due to the fact that the optimal THW energizing power/current was not initially known for this work, a variety of potential values were studied.

Table D-1. THW energized values: current, resistance, voltage, and power.

Potential Experimental THW Current Values:		
$I_1 := .05A$ $I_2 := .1A$ $I_3 := .3A$ $I_4 := .5A$	$I_5 := .7A$ $I_6 := 1A$ $I_7 := 1.2A$	(D.4)
Platinum Resistivity at Specified Cryogenic Temperature: $\rho_{HotWire} := 2.0455 \cdot 10^{-8} ohm \cdot m$ *Approximate THW Resistance (Ω):* $R_{HotWire} := \rho_{HotWire} \cdot \frac{L_{HotWire}}{A_{HotWire}}$ $R_{HotWire} = 0.26\Omega$		(D.5)
Approximate THW Voltage (V): $V_{HotWire}(I_{HotWire}) = R_{HotWire} \cdot I_{HotWire}$		(D.6)

$V_{HotWire}(I_1) = 0.013\,V$ $V_{HotWire}(I_2) = 0.026\,V$ $V_{HotWire}(I_3) = 0.078\,V$ $V_{HotWire}(I_4) = 0.13\,V$	$V_{HotWire}(I_5) = 0.182\,V$ $V_{HotWire}(I_6) = 0.26\,V$ $V_{HotWire}(I_7) = 0.312\,V$	
Approximate THW Power (W): $q_{HotWire}(I) := R_{HotWire} \cdot I^2$		
$q_{HotWire}(I_1) = 6.499 \times 10^{-4}\,W$ $q_{HotWire}(I_2) = 2.6 \times 10^{-3}\,W$ $q_{HotWire}(I_3) = 0.023\,W$ $q_{HotWire}(I_4) = 0.065\,W$	$q_{HotWire}(I_5) = 0.127\,W$ $q_{HotWire}(I_6) = 0.26\,W$ $q_{HotWire}(I_7) = 0.374\,W$	(D.7)

The radial position of interest for the following temperature vs. time models for the THW is the theoretical limit of the inner boundary condition.

$$Radius\ of\ interest = Limit\ of\ radius\ of\ THW \tag{D.8}$$

D.3. Carslaw and Jaeger Temperature vs. Time Model

$$\Delta T_{CJ}(t, r, q_{HotWire}) := \frac{-\frac{q_{HotWire}}{L_{HotWire}}}{4 \cdot \pi \cdot Conductivity_{LOX}} \cdot Re\left(Ei\left(\frac{-r^2}{4 \cdot Thermal_{Diffusivity} \cdot t}\right)\right) \tag{D.9}$$

Where the real portion of the exponential integral function is defined below and γ is the Euler-Mascheroni constant.

$$Ei(x) = \int_{-\infty}^{x} \frac{e^t}{t}\,t$$

$$Ei(x) := \gamma + \ln(x) + \sum_{k=1}^{160} \frac{x^k}{k \cdot k!} \tag{D.10}$$

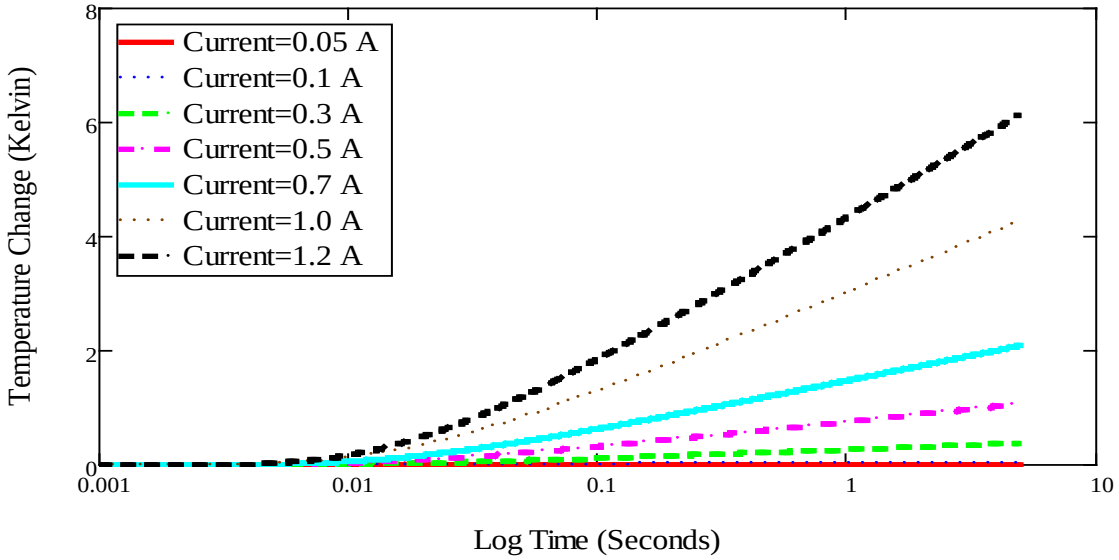

Figure D-1. Temperature vs. Time model based upon the work done by Carslaw and Jaeger.

D.4. Kluitenberg Temperature vs. Time Model

$$\Delta T_{Kluitenberg}(t,r,q) := \frac{\frac{q}{L_{HotWire}}}{4\cdot\pi\cdot Conductivity_{LOX}}\cdot Kluitenberg_{Internal}(t,r) \tag{D.11}$$

Where the internal function shown above is defined as

$$Kluitenberg_{Internal}(t,r) := \int_{\frac{r^2}{4\cdot(Thermal_{Diffusivity})\cdot t}}^{200} u^{-1}\cdot\exp(-u)\cdot erf\left(\frac{b}{r}\cdot\sqrt{u}\right)\,du \tag{D.12}$$

$$a := r_{HotWire}$$

$$b := L_{HotWire}$$

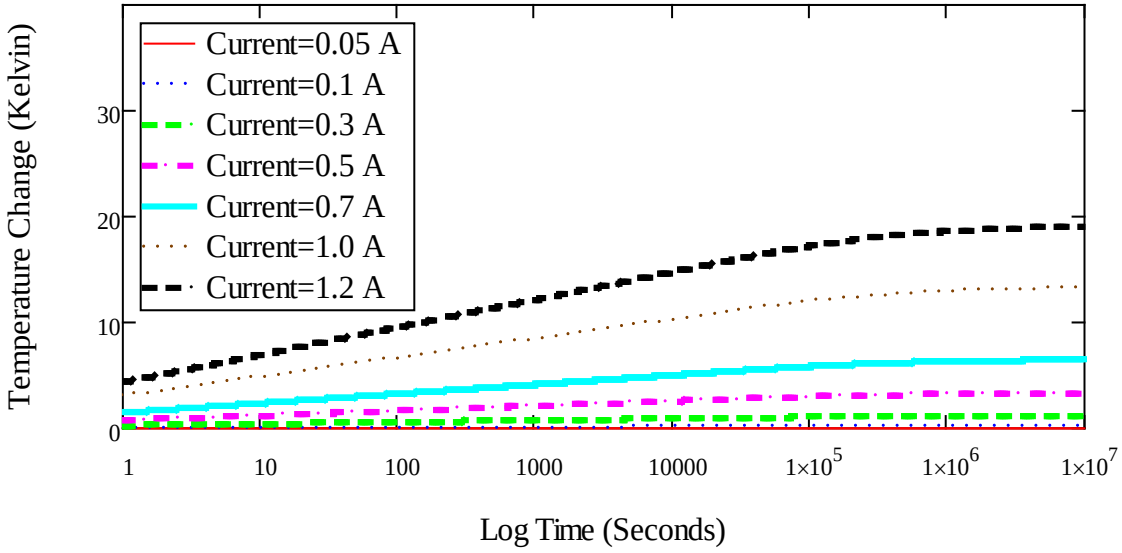

Figure D-2. Temperature vs. time model for the THW, as presented by Kluitenberg.

D.5. Borehole Temperature vs. Time Model

$$\Delta T_{\theta borehole}(t, r, q_{HotWire}) := \left[\frac{\left(\frac{q_{HotWire}}{L_{HotWire}}\right)}{\left(4\cdot\pi\cdot Conductivity_{LOX}\right)}\right]\cdot Borehole_{Internal}(t, r) \qquad (D.13)$$

$$Borehole_{Internal}(t, r) := \int_0^{L_{HotWire}} \left[\left[\frac{\operatorname{erfc}\left[\frac{\left[\sqrt{r^2+\left(\frac{L_{HotWire}}{2}-h\right)^2}\right]}{2\cdot\sqrt{Thermal_{Diffusivity}\cdot t}}\right]}{\sqrt{r^2+\left(\frac{L_{HotWire}}{2}-h\right)^2}}\right]\right] dh \qquad (D.14)$$

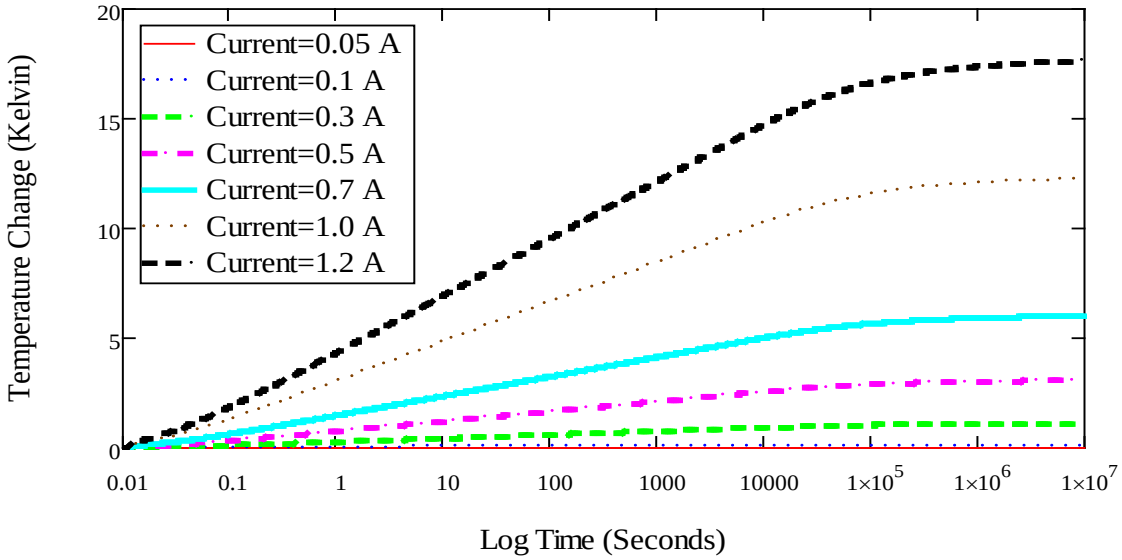

Figure D-3. Temperature vs. time model presented in the form utilized in some Borehole research.